Cosmological and Black Hole Singularities in Effective Loop Quantum Gravity and Holography

Dissertation

zur Erlangung des Doktorgrades
der Naturwissenschaften (Dr. rer. nat.)
der Fakultät für Physik
der Universität Regensburg

vorgelegt von

Johannes Münch

aus Gelnhausen

im Jahr 2020

Promotionsgesuch eingereicht am: 23. April 2020
Die Arbeit wurde angeleitet von: Dr. Norbert Bodendorfer

Cosmological and Black Hole Singularities in Effective Loop Quantum Gravity and Holography

Abstract

Singularities occurring in cosmology and black holes denote the breakdown of classical General Relativity (GR). The holographic principle and in particular the string theory based Anti-de Sitter / Conformal Field Theory (AdS/CFT) correspondence allows on the one hand to transfer the singularity problem into the language of Quantum Field Theory (QFT). On the other hand, according to this strategy, quantum gravity predictions about singularities might be tested by means of QFT simulations. Indeed, Loop Quantum Gravity (LQG), in particular the symmetry reduced Loop Quantum Cosmology (LQC), allows to describe spacetime in the vicinity of the classical singularity. Still, LQG is not formulated as a holographic theory, thus this thesis addresses how LQG can be meaningfully embedded into the AdS/CFT framework and how this embedding could be tested. Besides a possible strategy to test quantum gravitational predictions, this further allows to gain insights into the connection of different approaches, such as LQG, holography, and string theory. For this purpose, the role of cosmological singularity resolution within AdS/CFT is discussed in this thesis. In order to do so, the effect of LQC quantum corrections on finite distance poles in the dual field theory correlators is examined. As will be revealed, the divergences are resolved and an example of improved holographic behaviour due to LQC effects is found. It is argued that black holes provide a suitable framework for further tests. Consequently, effective quantum models are discussed in the last part of the thesis. As black holes are still an open research problem within LQG literature, the main focus lies on four dimensional models without cosmological constant as a starting point for further investigations. Quantum corrections are introduced along the lines of LQC. Herein, as new strategy, two sets of variables related to the Kretschmann scalar are introduced, allowing to constrain the onset of quantum effects in the high curvature regime. Physical properties as the singularity resolution, the causal structure, and the unique curvature bound are discussed in detail. Finally, an outlook is given on the possible generalisation of these models to arbitrary dimensions and to negative cosmological constant, placing them in the context of AdS/CFT.

Singularitäten in der Kosmologie und schwarzen Löchern innerhalb von effektiver Schleifenquantengravitation und Holographie

Zusammenfassung

Singularitäten, die in der Kosmologie und in schwarzen Löchern auftreten, bedeuten den Zusammenbruch der klassischen Allgemeinen Relativitätstheorie. Das holographische Prinzip und speziell die auf String Theorie basierte Anti-de Sitter / Conformal Field Theory (AdS/CFT) Korrespondenz erlaubt auf der einen Seite, das Problem von Singularitäten in die Sprache von Quantenfeldtheorie (QFT) zu übersetzen. Auf der anderen Seite könnten nach dieser Strategie Vorhersagen der Quantengravitation über Singularitäten mittels QFT Simulationen getestet werden. Tatsächlich erlaubt die Schleifenquantengravitation (SQG), speziell die Symmetriereduzierte Schleifenquantenkosmologie (SQK), die Beschreibung der Raumzeit in der Umgebung der klassischen Singularität. Dennoch ist SQG nicht als holographische Theorie definiert und daher befasst sich diese Arbeit damit, wie SQG sinnvoll in den Rahmen von AdS/CFT eingebettet werden kann und wie diese Einbettung getestet werden könnte. Neben einer möglichen Strategie, Vorhersagen der Quantengravitation zu testen, erlaubt dieses Vorgehen Einblicke in den Zusammenhang zwischen verschiedenen Ansätzen, wie SQG, Holographie und String Theorie. Daher wird in dieser Arbeit die Rolle von behobenen kosmologischen Singularitäten innerhalb von AdS/CFT diskutiert. Folglich wird der Effekt von SQK-Quantenkorrekturen auf endliche Distanz-Pole in Korrelatoren der dualen Feldtheorie untersucht. Es stellt sich heraus, dass die Divergenzen behoben werden und somit ein Beispiel für verbessertes holographisches Verhalten durch SQK-Effekte gefunden wurde. Es wird argumentiert, inwiefern schwarze Löcher ein geeigneter Rahmen für weitere Tests sind. Folglich werden effektive Quantenmodelle im letzten Teil der Arbeit diskutiert. Da schwarze Löcher immer noch eine offene Forschungsfrage in der SQG-Literatur sind, liegt der Hauptfokus auf vierdimensionalen Modellen ohne kosmologische Konstante, die einen Startpunkt für weitere Untersuchungen liefern. Quantenkorrekturen werden im Sinne von SQK eingeführt. Hierbei werden als neue Strategie zwei Sets an Variablen eingeführt, die mit dem Kretschmannskalar zusammenhängen und so erlauben,

Quanteneffekte auf den Bereich hoher Krümmungen zu beschränken. Physikalische Eigenschaften wie die Behebung der Singularität, die kausale Struktur und die universelle obere Grenze für die Krümmung werden in Einzelheiten diskutiert. Schließlich wird ein Ausblick auf die Verallgemeinerung dieser Modelle zu beliebigen Dimensionen und negativer kosmologischer Konstante gegeben, womit diese wieder in den Kontext von AdS/CFT platziert werden.

Danksagung

An dieser Stelle möchte ich mich bei allen bedanken, die mir während meiner Promotionszeit zur Seite standen und ohne deren vielseitige Unterstützung diese Arbeit nicht möglich gewesen wäre.

Zuallererst möchte ich meinen Eltern und meiner Familie danken, die immer hinter mir standen und mich in allen Belangen unterstützt haben, um mir die Promotion zu ermöglichen. Ebenfalls möchte ich meinen Freunden und meiner Freundin Nele Bleitgen für den Beistand außerhalb der Universität danken. Danke, Nele, für deinen Rückhalt und deine Geduld, das alles mit mir durchzustehen!

Ich möchte ebenfalls all meinen Studienkollegen und Freunden danken, für zahlreiche Diskussionen über Physik und alles, was darüber hinaus geht. Auch möchte ich meinen früheren Kollegen am FIAS danken, für alles, was ich dort lernen durfte und was die Grundlage für diese Promotion geschaffen hat.

Besonderer Dank geht an meinen Betreuer Norbert Bodendorfer, der mich während der letzten drei Jahre in allen Belangen von physikalischen Inhalten bis hin zur Lebensplanung als Physiker immer unterstützt hat. Auch das offene und angenehme Arbeitsklima, das er geschaffen hat und seine ständige Erreichbarkeit für Diskussionen schätze ich sehr. Ich bin froh, von ihm als Mentor fachlich und persönlich gelernt zu haben und hoffe, auch in Zukunft noch von ihm lernen zu dürfen.

Zudem danke ich Norbert für seine Unterstützung in der Bewerbungsphase für eine Postdoc-Stelle und für seine zahllosen Gutachten und Referenzschreiben. Ich bin ihm ebenfalls dankbar für seine Geduld und seinen Beistand bei meinen wiederkehrenden Rückfragen zu seiner Meinung und nicht zuletzt seinen guten Worten. Mein Dank gilt selbstverständlich auch Jürgen Struckmeier und Andreas Schäfer für ihre mühevoll geschriebenen Referenzschreiben.

Special thanks goes further to my colleagues and friends Fabio Mele and Stratos Pateloudis. I am happy about the time we shared in our office, discussing about physics and other things. I enjoyed each discussion about coffee and “hate rice”, and I am happy

to have explored the Regensburg nightlife with you! In particular I would like to thank Fabio for three years of collaboration and fruitful discussions where — I guess both of us — learned a lot from each other. Furthermore I would like to thank all my new gained friends and colleagues I met on all the conferences during the past three years. I am happy for each physics discussion and fun we had in this time. Ich möchte auch Andreas Rabenstein für die schöne gemeinsame Zeit an der Uni Regensburg und außerhalb danken. Auch für seine Geduld für meine Rückfragen zu der Bürokratie und Formatierung dieser Arbeit bin ich ihm dankbar.

Zudem gilt besonderer Dank Stratos Pateloudis und Andreas Rabenstein für das Lesen der ersten Version dieser Arbeit und ihr nützliches Feedback. Ich danke ganz besonders Hannah Niederbuchner und Nele Bleitgen als Ansprechpartnerinnen für alle sprachlichen Belange dieser Arbeit und ihre Mühe beim Lektorat.

Meine Doktorandenstelle wurde finanziell durch das Elitenetzwerk Bayern ermöglicht.

Ohne die Unterstützung von all diesen Seiten wäre diese Arbeit nicht möglich gewesen. Vielen Dank euch allen!

Publications

This thesis is based on the following publications:

1. N. Bodendorfer, F. M. Mele, and J. Münch, "Holographic signatures of resolved cosmological singularities II: numerical investigations", *Classical and Quantum Gravity* **36** (2019) 245013, arXiv:1804.01387 [hep-th].

2. N. Bodendorfer, F. M. Mele, and J. Münch, "Is limiting curvature mimetic gravity an effective polymer quantum gravity?", *Classical and Quantum Gravity* **35** (2018) 225001, arXiv:1806.02052 [gr-qc].

3. N. Bodendorfer, F. M. Mele, and J. Münch, "Effective quantum extended spacetime of polymer Schwarzschild black hole", *Classical and Quantum Gravity* **36** (2019) 195015, arXiv:1902.04542 [gr-qc].

4. N. Bodendorfer, F. M. Mele, and J. Münch, "A note on the Hamiltonian as a polymerisation parameter", *Classical and Quantum Gravity* **36** (2019) 187001, arXiv:1902.04032 [gr-qc].

5. N. Bodendorfer, F. M. Mele, and J. Münch, "(b,v)-type variables for black to white hole transitions in effective loop quantum gravity", arXiv:1911.12646 [gr-qc].

6. N. Bodendorfer, F. M. Mele, and J. Münch, "Mass and Horizon Dirac Observables in Effective Models of Quantum Black-to-White Hole Transition", arXiv:1912.00774 [gr-qc].

Contents

1

Introduction

The modern understanding of gravitation is based on Einstein's theory of General Relativity (GR) [7, 8], which was presented already over 100 years ago. Since then, the theory has been tested repeatedly and still correctly describes the outcome of modern gravitational wave and imaging experiments [9, 10]. Nevertheless, this extremely successful theory generically predicts singularities under reasonable assumptions for matter [11, 12], which still challenges modern research. Due to these singularities and the breakdown of the predictability of GR, the origin of the universe and the behaviour inside astrophysical objects, such as black holes are not clear. This has raised much interest in the past and it is assumed that a combined description of quantum physics and GR solves the puzzles about these singularities, see e.g. [13, 14]. Hence, several approaches for a theory of quantum gravity have been developed in the past, but there is no final answer yet. Singularities have been studied in Loop Quantum Gravity (LQG) [14–18], string theory [13, 19–22], Anti-de Sitter / Conformal Field Theory (AdS/CFT) [23–28], as well as Non-Commutative Geometry (NCG) [29–32] and related contexts [33–36].

Along the lines of the semi-classical analysis of black holes, new phenomena at the interplay of gravitational and quantum physics were discovered in the past. This led in particular to the development of black hole thermodynamics [37–41] and later to the holographic principle [42–45]. Moreover, a concrete realisation of the holographic principle, the so-called AdS/CFT correspondence, was formulated by Maldacena [44], who conjec-

tured a dynamical duality between quantum gravity and Quantum Field Theory (QFT) in one spatial dimension less. Strictly speaking, the AdS/CFT correspondence assumes string theory in asymptotic Anti-de Sitter (AdS) space as quantum gravity theory and a Conformal Field Theory (CFT) as a particular kind of a QFT. Along the lines of this conjecture, quantum gravity can be equivalently formulated in terms of an ordinary QFT, which is a highly developed branch of physics. Furthermore, this duality is weak to strong, meaning that a difficult problem on one side becomes easy on the other side and vice versa. On top of that, the AdS/CFT correspondence allows for a new strategy to analyse the fate of a singularity: The gravitational problem can be translated into the dual QFT and computations can be performed there by using the well-developed tools known in quantum physics. Nevertheless, this strategy is not developed extensively enough to produce satisfactory answers. On the one hand, this correspondence is so far only a conjecture, though well-motivated and with a high amount of evidence. On the other hand, the precise formulation and the evidence holds only in the so-called weak regime, where gravity is effectively classical. As there is no independent non-perturbative definition of string theory [44, 46, 47], it is difficult to formulate the so-called strong conjecture, which includes the quantum gravity regime, and thus the problem of singularities can only be addressed partially.

Besides string theory, there are many other approaches to a quantum theory of gravity, one of them being LQG. As a non-perturbative and background independent approach, it is assumed that LQG resolves the classical singularities and has the potential to answer the mysteries of the beginning of the universe and of the inside of black holes. Although several formulations of LQG exist, such as in the Hamiltonian framework [48, 49], via path integrals [50] and also in terms of group field theory [51], no concluding progress has been made on the level of the full theory. In contrast, in the context of symmetry reduced models [52–64], progress has been made and moreover, qualitative consensus has been reached in the context of cosmology. The symmetry reduced Loop Quantum Cosmology (LQC) models the behaviour of the universe close to the big bang singularity and replaces it with a big bounce. Even more, conceptual problems could be resolved, see e.g. [65] and phenomenological effects were worked out [66, 67]. Nevertheless, there are many assumptions and ambiguities in constructing the quantum cosmological models and the field is still part of active research as recent discussions show [68]. Despite the symmetry reduced setup of cosmology paving the way for possible observations, there is no evidence that quantum gravity effects can be measured in the near future and thus there is no experimental data supporting or ruling out individual models.

At this point, the approaches of string theory and LQG might profit from an exchange of techniques. On the one hand, LQG can answer the question of singularities in the symmetry reduced context, which is difficult within string theory. On the other hand, the

AdS/CFT correspondence gives an opportunity to test quantum gravity predictions. If the conjecture holds true, the gravitational prediction about singularities can be translated into the dual QFT and tested there with an independent computation [69, 70]. This allows at least hypothetically to support or rule out certain approaches. Nevertheless, string theory and LQG are independent approaches and their relation is not clear. Moreover, it is not clear if LQG and the result of singularity resolution can be meaningfully embedded into the context of the AdS/CFT correspondence. In fact, there are considerations of a No Transmission Principle (NTP) [27, 28], which argue against singularity resolution within the AdS/CFT correspondence. The aim of this thesis is exactly to address the question of how LQG and its feature of singularity resolution is compatible with the principles of AdS/CFT, and how this can be tested.

This problem is approached in three parts. In the first part, introductory material is presented. In chapter 2, AdS space and different interpretations are recalled. Further in section 2.2, properties of AdS space are worked out, which are central for the realisation of the holographic principle. The chapter closes with a discussion of the boundary space of AdS space in section 2.3, which will be relevant for later considerations. The following chapter 3 gives a motivation for the holographic principle at the example of black holes. As further black holes will be central in the third part of the thesis, section 3.1 recalls properties of classical black holes as the horizon and the curvature singularity. Based on this overview of classical black holes, semi-classical considerations are added in section 3.2, leading to the laws of black hole thermodynamics and the formulation of the holographic principle. The central statements and the mathematical formulation of the AdS/CFT correspondence, a particular realisation of the holographic principle, are collected in section 3.3. Furthermore, the different regimes and approximations of the AdS/CFT conjecture are put into context, which leads to the notion of weak and strong duality. The chapter closes with an outlook on the more general notion of gauge/gravity duality in section 3.4, where the possible relation to LQG is discussed. As already stated above, particular progress in LQG has been made in the context of symmetry reduced models, strictly speaking in the framework of cosmology, which is reviewed in chapter 4. The chapter begins with an introduction to the canonical formulation of classical cosmology in section 4.1. Further, the analysis of constraints, solution strategies for constrained systems, and the classical big bang singularity are examined, which sets the grounds for the later discussions of black holes. As next step, classical polymerisation is introduced and discussed in section 4.2. Herein, central focus lies on the polymerisation strategies, the singularity resolution, and the discussion of this kind of approximation. The concept of polymerisation becomes more natural in the discussion of the full quantum theory of cosmology, which is presented in section 4.3. It is presented how the quantum theory can be constructed and to which extend the approximation of classical polymerisation

can be justified. Apart from that, these considerations are put in context to full LQG in section 4.4, where the central ideas of LQG are reviewed and a connection to the previous construction of LQC can be made. It is demonstrated how the techniques of polymerisation are motivated by LQG and it is discussed in which sense LQC is related to LQG. This closes the first part of the thesis and finishes the review of introductory material.

New research is first presented in the second part of the thesis, where in chapter 5 the holographic signatures of resolved cosmological singularities are studied. The chapter is based on the preceding work [71, 72] and a companion paper [73], whose setup is reviewed in section 5.1. Using the AdS/CFT correspondence, the equal-time two-point correlator of the dual field theory can be computed on the gravitational side by determining the length of a spacelike geodesic attached to the boundary of the anisotropic version of AdS space, also used in the preceding work [71, 72]. Moreover, it is argued that the classical singularity in this anisotropic Kasner-AdS cosmology is holographically dual to a finite distance pole in the equal-time two-point correlator of the dual CFT. Further, in section 5.2, the result of [73] is reviewed, where the metric is quantum corrected by means of LQC, and the singularity, as well as the two-point correlator finite distance pole are both resolved in this case. The simplifications of this previous work are discussed in section 5.3. In addition, it is argued why in a first step the scale of quantum effects should be adjusted and why in a second step, also so-called Kasner transitions should be taken into account to gain more evidence in the preceding work [73]. Furthermore, it is discussed that omitting these simplifications does not allow an analytical computation of the geodesic length any more, and the numerical solution strategy is discussed in detail in section 5.4. The particular improved metrics for each of the steps to make the model more realistic are separately discussed in section 5.5. Furthermore, a detailed discussion of Kasner transition models and their limitations is presented in section 5.5.2. Using numerical techniques, the results of the gravitational computation for the two-point correlator are presented and analysed. The chapter concludes in section 5.6 with a discussion of the achievements and limitations of this framework.

Analysing the limitations of the previous framework in detail, the conclusion is drawn that black holes in higher dimension and with negative cosmological constant are a better suited framework to study holographic signatures of resolved singularities, which leads to the third part of the thesis. Even though previously a lot of effort has been put into describing black holes consistently within LQG [18, 74–88], no consensus has been achieved so far. Because of this, a step back is taken and the focus is shifted to four dimensional black hole models without cosmological constant in chapter 6. In a first instance, previous models of so-called polymer black holes, inspired by LQG techniques already discussed in section 4, are reviewed in section 6.1. On top of that, it is examined which requirements a quantum black hole model should satisfy to lead to reasonable phenomenology. It is argued

that a central criterion is an unique upper bound of the curvature invariants. As a first step, the canonical formulation of spherically symmetric and static black holes is presented in section 6.2, where new variables are introduced to approach the problem of polymer black holes in a next step. Besides, the new variables are interpreted and it is argued that the application of the polymerisation technique could allow to meet the initially defined criteria. Consequently, the model is constructed and solved in section 6.3. The resulting effective spacetime is discussed, its causal structure worked out, and it is assessed if an unique upper curvature bound can be achieved. The limitations of this model are discussed and it is argued that they might be overcome by using the polymerisation scheme defined by the second set of new variables introduced in section 6.4. This second polymerised model is constructed and solved. This is followed by a detailed discussion of the causal structure of the resulting spacetime and of the boundedness of the curvature invariants in sections 6.4.1 and 6.4.2. In the conclusions, section 6.5, achievements and limitations, as well as further directions are discussed. Finally, an outlook is given in section 7 on how the previously introduced black hole models could be generalised to arbitrary dimensions and negative cosmological constant. This way the models are generalised so that they are suitable for a holographic analysis. Therefore, it is examined how the two generalisation steps, higher dimensions and inclusion of a non-zero cosmological constant, can possibly be done by pointing out obstructions, as well as possible solution strategies. The thesis concludes in chapter 8 by summarising the results, discussing achievements and limitations, and giving an outlook on future research directions. This includes the critical examination of the initial question, to which extent LQG techniques can be applied to the framework of AdS/CFT and how this can be tested.

Additional material is presented in the Appendix. Conventions and notations used throughout this thesis are collected in appendix A. Supplementary definitions are recalled in appendix B.

Part I

Introductory Material

2

Anti-de Sitter-Space and its Boundary

One of the most important developments of modern theoretical physics is the holographic principle. The most concrete realisation thereof is the AdS/CFT correspondence (cfr. Sec. 3.3) introduced by Maldacena [44]. In this section AdS space is introduced and its properties, which make it suitable for holographic considerations are discussed.

2.1 Anti-de Sitter-Space

AdS can be viewed from different perspectives. First, the embedding picture is discussed. Consider the smooth metric manifold $(\mathcal{M}_{q+1,p}, \eta)$ where $\mathcal{M}_{q+1,p} \simeq_{\text{diff}} \mathbb{R}^{p+q+1}$ and it is equipped with the flat Minkowski metric η of signature $(q+1, p)$. $\mathcal{M}_{q+1,p}$ is maximally symmetric and has the isometry group $SO(q+1, p)$. Then $AdS(q, p)$ of radius L can be defined as (cfr. [89])

$$AdS(q,p) := \left\{ x \in \mathcal{M}_{q+1,p} \mid -(x^0)^2 - \sum_{i=1}^{q} (x^i)^2 + \sum_{i=q+1}^{q+p} (x^i)^2 = -L^2 \right\} . \tag{2.1.1}$$

As such $AdS(q, p)$ is an orbit (see Def. B.1 in App. B) of $SO(q+1, p)$. Further, $SO(q+1, p)$

acts freely and transitive on each orbit, $AdS(q,p)$ is isomorphic to this group. For physics the relevant case is $q = 1$, $p = d$, which has $d+1$ spacetime dimensions. Further the abbreviation

$$AdS(d+1) := AdS(1,d)$$

is defined. Given an embedding $e : AdS(d+1) \longrightarrow \mathcal{M}_{2,d}$ a metric can be induced on $AdS(d+1)$ via the pull back $g_{AdS} = e^*\eta$. The $AdS(d+1)$ condition (2.1.1) can be rephrased as

$$\sum_{i=1}^{d}(x^i)^2 + L^2 = (x^0)^2 + (x^{d+1})^2 \,, \tag{2.1.2}$$

which shows that the two timelike coordinates (x^0, x^{d+1}) have the geometry of a circle of radius $\sqrt{\sum_{i=1}^{d}(x^i)^2 + L^2}$. Further, the spatial coordinates lie on a $d-1$-sphere of radius $\sqrt{(x^0)^2 + (x^{d+1})^2 - L^2}$. This makes explicit that $AdS(d+1)$ is fully connected. Another rewriting of the embedding condition is

$$-(x^0)^2 - (x^{d+1})^2 + \sum_{i=1}^{d}(x^i)^2 = -L^2 \,. \tag{2.1.3}$$

Parametrising the timelike coordinates by means of their radius R and the angle τ, i.e. $x^0 = R\sin(\tau)$ and $x^{d+1} = R\cos(\tau)$ (see later Eq. (2.1.5)), this condition becomes

$$-R^2 + \sum_{i=1}^{d}(x^i)^2 = -L^2 \,. \tag{2.1.4}$$

For each $\tau = const.$ slice this is nothing else than the embedding condition of hyperbolic space $\mathbb{H}^d$ in $\mathcal{M}_{1,d}$ (see [90] and Def. B.2 in App. B). Further, the hyperbolic radius of each $\tau = const.$-slice is L and τ independent. This is discussed and shown explicitly in more details below (cfr. Eq. (2.1.5) and Fig. 2.2 (b)).

To make this geometry explicit, several useful coordinates are introduced in the following. Of particular interest is the static slicing, which provides a set of global coordinates $(t, r, \theta_1, \ldots \theta_{d-1})$ of $AdS(d+1)$ defined by

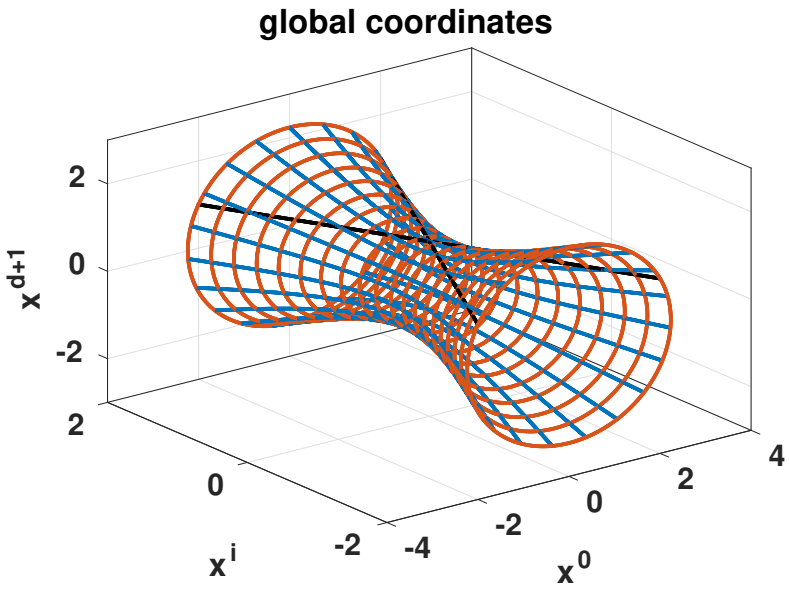

FIGURE 2.1: *AdS space parametrised by global coordinates* (τ, ρ, θ_i)*. Red circles are constant* ρ*-slices, while blue lines are constant* τ*-slices. Each blue line is a copy of hyperbolic space with hyperbolic radius* $L = 1$*. At each point a* $d-1$*-sphere is attached. The black lines show lightlike geodesics.*

$$\begin{aligned} x^0 &= \sqrt{L^2 - r^2}\sin\left(\frac{t}{L}\right) \ , \\ x^{d+1} &= \sqrt{L^2 - r^2}\cos\left(\frac{t}{L}\right) \ , \\ x^i &= r z^i(\theta_1, \ldots, \theta_{d-1}) \quad , \quad 1 \leq i \leq d \ , \end{aligned} \tag{2.1.5}$$

where z^i are the components of a parametrisation of the unit sphere $\mathbb{S}^{d-1}$. The line element of the induced metric g_{AdS} takes the form

$$\mathrm{d}s^2 = -\left(1 + \frac{r^2}{L^2}\right)\mathrm{d}t^2 + \left(1 + \frac{r^2}{L^2}\right)^{-1}\mathrm{d}r^2 + r^2\mathrm{d}\Omega_{d-1}^2 \ , \tag{2.1.6}$$

where $\mathrm{d}\Omega_{d-1}^2$ is the line element of the round metric of $\mathbb{S}^{d-1}$. This global parametrisation makes particular use of Eq. (2.1.2) and uses the coordinate t as angle parameter of the timelike (x^0, x^{d+1})-circle. In this sense $AdS(d+1)$ allows closed timelike curves, although usually the coordinate t is de-compactified [89], i.e. the topology is changed form a circle to the real line $\mathbb{S}^1 \mapsto \mathbb{R}$. Closely related to this coordinate system are the coordinates $(\tau, \rho, \theta_1, \ldots \theta_{d-1})$

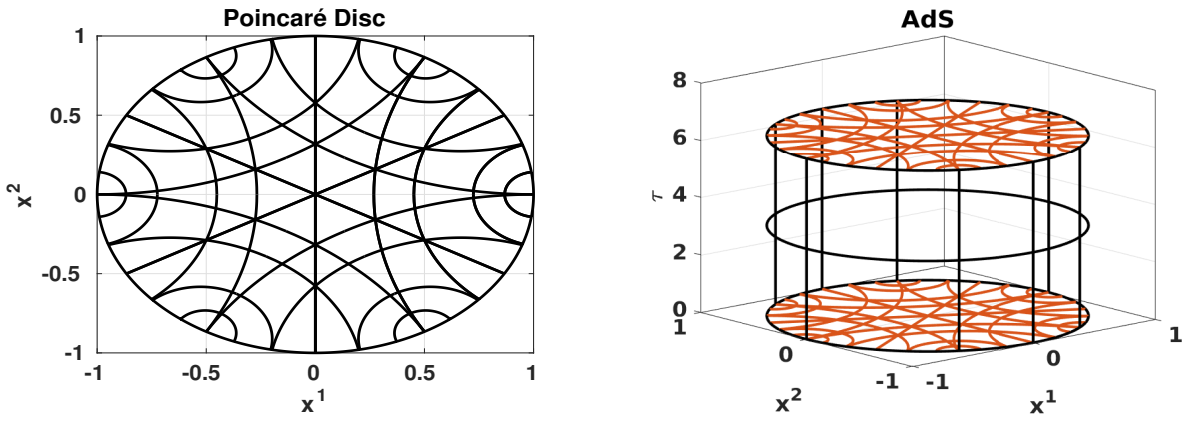

(a) (b)

FIGURE 2.2: *(a) shows the Poincaré disc, which is a realisation of* $2d$ *hyperbolic space. Via a projection* $\mathbb{H}^2$ *is mapped into the open ball* $B_L(0)$ *of radius* L*. The black lines are samples of geodesics in hyperbolic geometry. (b) visualises AdS space as a cylinder. As the hyperbolic radius* L *of the* $\tau = const.$ *surfaces remain the same for all* τ*, the radius* L *of each Poincaré disc remains the same. In the embedding picture the* τ *direction has topology* $\mathbb{S}^1$ *(*$\tau \in [0, 2\pi)$*) and the upper and lower part of the cylinder have to be identified. It is also possible to unwrap this direction and continue the cylinder infinitely, leading to the topology* $\mathbb{R} \times \mathbb{H}^d$*. For both plots it is* $L = 1$*.*

$$\begin{aligned} x^0 &= L\cosh(\rho)\sin(\tau) \ , \\ x^{d+1} &= L\cosh(\rho)\cos(\tau) \ , \\ x^i &= L\sinh(\rho) z^i(\theta_1, \ldots, \theta_{d-1}) \quad , \quad 1 \leq i \leq d \ , \end{aligned} \tag{2.1.7}$$

which are equivalent to Eqs. (2.1.5) for $\tau = {}^t/_L$ and $r = L\sinh(\rho)$. The line element then takes the form

$$\mathrm{d}s^2 = L^2\left(-\cosh(\rho)^2\mathrm{d}\tau^2 + \mathrm{d}\rho^2 + \sinh(\rho)^2\mathrm{d}\Omega_{d-1}^2\right) \ , \tag{2.1.8}$$

and makes the hyperbolic structure of $AdS(d+1)$ visible. Indeed, for $\tau = const.$ the line element reduces to the metric of hyperbolic space $\mathbb{H}^d$ and each slice has the same hyperbolic radius L. This can also be seen by inserting x^0 and x^d into Eq. (2.1.2). Fig. 2.1 visualises these coordinates.

These coordinates give rise to another visualisation of $AdS(d+1)$. As indicated above is each slice with $t, \tau = const.$ a copy of hyperbolic space $\mathbb{H}^d$, i.e. topologically it is $AdS(d+1) \simeq_{\text{top}} \mathbb{S}^1 \times \mathbb{H}^d$. As argued (cfr. [89]), the t-circle can be unwrapped and the topology $\mathbb{R} \times \mathbb{H}^d$ is achieved. One way of visualising $\mathbb{H}^d$ is the Poincaré ball model [90],

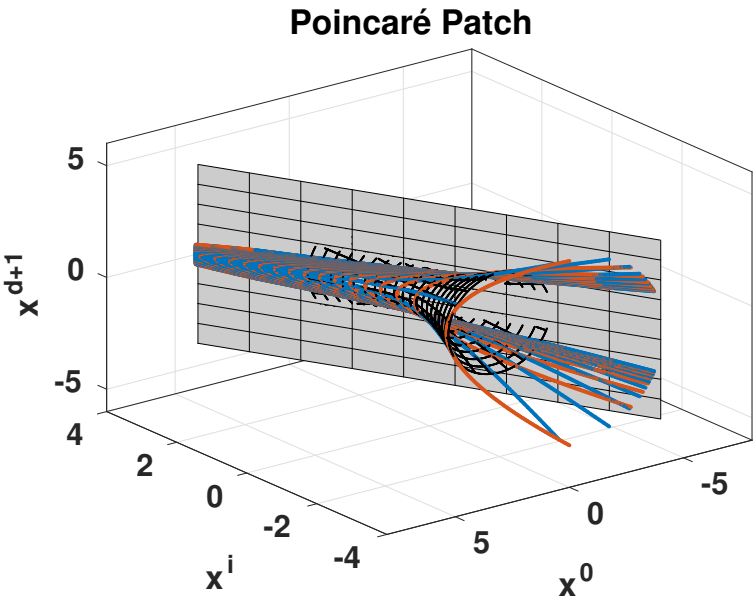

FIGURE 2.3: *AdS space parametrised by Poincaré coordinates. Red lines are constant r-slices and blue lines constant t-slices. Poincaré coordinates do not fully cover AdS space. There is a lightlike plane intersecting $AdS(d+1)$ space which is asymptotically approached for $r \to 0$. The other side is covered by negative r.*

which is the projection of a hyperboloid onto a d-dimensional ball. The Poincaré-disk ($d = 2$) is visualised in Fig. 2.2 (a). Moving from one constant t-slice to another does not change the hyperbolic radius L, nor the radius of the Poincaré ball. This leads to a cylinder depiction of $AdS(d+1)$, which is shown in Fig. 2.2 (b).

Another commonly used parametrisation of (the half of) $AdS(d+1)$ is the Poincaré patch. It is defined by

$$\begin{aligned} x^0 &= \frac{L^2}{2r}\left(1 + \frac{r^2}{L^4}\left(\sum_{i=1}^{d-1}(y^i)^2 - t^2 + L^2\right)\right) , \\ x^i &= \frac{ry^i}{L}, \quad 1 \leq i \leq d-1 , \\ x^d &= \frac{L^2}{2r}\left(1 + \frac{r^2}{L^4}\left(\sum_{i=1}^{d-1}(y^i)^2 - t^2 - L^2\right)\right) , \\ x^{d+1} &= \frac{rt}{L} , \end{aligned} \tag{2.1.9}$$

where y^i is a set of Cartesian coordinates, $t \in \mathbb{R}$ and $r > 0$. The line element in these

coordinates takes the form

$$\mathrm{d}s^2 = \frac{L^2}{r^2}\mathrm{d}r^2 + \frac{r^2}{L^2}\left(-\mathrm{d}t^2 + \sum_{i=1}^{d-1}(\mathrm{d}y^i)^2\right) \tag{2.1.10}$$

As the name suggests these coordinates cover only a patch of $AdS(d+1)$, which can be seen by computing

$$x^0 - x^d = r > 0 \ .$$

The lightlike surface $x^0 - x^d = 0$ divides $AdS(d+1)$ in the two region $r > 0$ and $r < 0$. The coordinates defined in Eq. (2.1.9) describe only the patch for positive r, whereas another patch is needed for negative r. The situation is visualised in Fig. 2.3. At $r = 0$ is a Killing Horizon (see Def. B.4 in App. B) of the metric (2.1.10). A commonly used coordinate is $z = {}^{L^2}/_r$ which brings the metric conformally in Minkowski form

$$\mathrm{d}s^2 = \frac{L^2}{z^2}\left(-\mathrm{d}t^2 + \sum_{i=1}^{d-1}(\mathrm{d}y^i)^2 + \mathrm{d}z^2\right) \ . \tag{2.1.11}$$

These coordinates will be of particular interest later on.

In the next step, further properties of $AdS(d+1)$ and its relation to GR are discussed. As argued above and as Eq. (2.1.1) shows, $AdS(d+1)$ has the isometry group $SO(2,d)$. The group $SO(2,d)$ contains $d(d-1)/2$ independent rotations (cfr. [91]), $2d$ independent boosts (d boosts for each timelike dimension) and one more rotation in the timelike directions, leading to [92]

$$\dim\left(SO(2,d)\right) = \frac{d(d-1)}{2} + 2d + 1 = \frac{(d+1)(d+2)}{2}$$

independent symmetries. This is the maximal number of symmetries, which a $d+1$-dimensional space as $AdS(d+1)$ can have (cfr. [91]). Another way to see this is computing the Riemann curvature tensor, the Ricci tensor and the Ricci scalar in any parametrisa-

tion, leading to (cfr. [89, 92])

$$R_{\mu\nu\alpha\beta} = -\frac{1}{L^2}\left(g_{\mu\alpha}g_{\nu\beta} - g_{\nu\alpha}g_{\mu\beta}\right) \ , \tag{2.1.12a}$$

$$R_{\mu\nu} = -\frac{d}{L^2}g_{\mu\nu} \ , \tag{2.1.12b}$$

$$R = -\frac{d(d+1)}{L^2} \ . \tag{2.1.12c}$$

It can be seen that the curvature is constant everywhere in spacetime. This shows again that $AdS(d+1)$ is maximally symmetric.

A last way of interpreting $AdS(d+1)$ is as a solution of vacuum Einstein equations with negative cosmological constant. The Einstein equations with cosmological constant Λ are

$$R_{\mu\nu} - \frac{R}{2}g_{\mu\nu} + \Lambda g_{\mu\nu} = 0 \ , \tag{2.1.13}$$

from which by contraction

$$R = \frac{2(d+1)}{d-1}\Lambda$$

can be deduced. This equation is exactly satisfied for $AdS(d+1)$ (cfr. Eq. (2.1.12c)) of AdS-radius

$$L^2 = -\frac{d(d-1)}{2\Lambda} \quad \Leftrightarrow \quad \Lambda = -\frac{d(d-1)}{2L^2} \ . \tag{2.1.14}$$

This can only be true for $\Lambda < 0$. Inserting the $AdS(d+1)$-metric, e.g. Eq. (2.1.6) into the Einstein equations (2.1.13) proves that these equations are solved[1] for the AdS-radius of Eq. (2.1.14).

[1] A particular interesting setting is cosmology with $\Lambda < 0$, which of course has in vacuum $AdS(d+1)$ as a solution compatible with the above discussion. In turn, a parametrisation exists of $AdS(d+1)$ starting with Eq. (2.1.1), which brings the line element in Friedmann-Lemaítre-Robertson-Walker (FLRW)-form. For hyperbolic slicing ($k = -1$) the scale factor is $a(t) = L\cos(t/L)$ with cosmological time t. As it is not important in the following, this parametrisation is not stated here.

In summary:

$AdS(d+1)$ of radius L is a maximally symmetric space with $SO(2,d)$ as isometry group and constant negative curvature. $AdS(d+1)$ solves the Einstein equations with negative cosmological constant $\Lambda = -\frac{d(d-1)}{2L^2}$.

2.2 Properties of $AdS(d+1)$

In the following it is presented in detail why this space is so special and which properties it has to make it suitable for holographic descriptions. For this purpose, the global coordinates (2.1.5) are especially useful and the metric in the form of Eq. (2.1.6) is used. The causal structure of $AdS(d+1)$ can be understood by studying radial lightlike geodesics. These satisfy

$$\mathrm{d}s^2 = 0 = -\left(1+\frac{r^2}{L^2}\right)\mathrm{d}t^2 + \left(1+\frac{r^2}{L^2}\right)^{-1}\mathrm{d}r^2 \,, \tag{2.2.1}$$

which is solved for

$$t = \pm\int^r \frac{\mathrm{d}r'}{1+\frac{r'^2}{L^2}} = \pm L\arctan\left(\frac{r}{L}\right) + C \quad \Longleftrightarrow \quad r = \pm L\tan\left(\frac{t-C}{L}\right) \,, \tag{2.2.2}$$

with integration constant C. Observe that $r \to \pm\infty$ is reached in finite coordinate time $t = \pm\frac{L\pi}{2} + C$. A lightlike geodesic is hence a straight line in $\mathcal{M}_{2,d}$ labelled by their angle in the $x^0 - x^{d+1}$-plane and the angle in $\mathbb{S}^{d-1}$ and attached to the hyperboloid (see Fig. 2.1).

Of further interest are radial timelike geodesics, which minimise the length functional

$$S[x,\dot{x}] = \int \mathrm{d}\lambda \sqrt{\left(1+\frac{r^2}{L^2}\right)\frac{\mathrm{d}t}{\mathrm{d}\lambda}^2 - \left(1+\frac{r^2}{L^2}\right)^{-1}\frac{\mathrm{d}r}{\mathrm{d}\lambda}^2} \,. \tag{2.2.3}$$

For λ the affine parameter ($\sqrt{\left(1+\frac{r^2}{L^2}\right)\frac{\mathrm{d}t}{\mathrm{d}\lambda}^2 - \left(1+\frac{r^2}{L^2}\right)^{-1}\frac{\mathrm{d}r}{\mathrm{d}\lambda}^2} = 1$) the variation of the

length functional leads to the Euler-Lagrange equations

$$\left(1+\frac{r^2}{L^2}\right)\dot{t}^2-\left(1+\frac{r^2}{L^2}\right)^{-1}\dot{r}^2=1\,, \tag{2.2.4a}$$

$$\left(1+\frac{r^2}{L^2}\right)\dot{t}=const.\,, \tag{2.2.4b}$$

$$\ddot{r}+\frac{r}{L}=0\,, \tag{2.2.4c}$$

where the dot denotes the derivative with respect to the affine parameter λ. Eq. (2.2.4c) shows that a massive particle in $AdS(d+1)$ behaves like moving in a harmonic potential. Defining $\epsilon=-\left(1+\frac{r^2}{L^2}\right)\dot{t}$ by using Eq. (2.2.4b) and inserting this into Eq. (2.2.4a) gives

$$\dot{r}^2+\frac{r^2}{L^2}=\epsilon^2-1\,, \tag{2.2.5}$$

which is the "energy" function of a classical harmonic oscillator of energy ϵ^2-1. Solutions of these equations describe in the phase space $(r/L,\dot{r})$ circles of radius $\sqrt{\epsilon^2-1}$. This shows that a massive particle, no matter how much energy it has, will never reach $r\to\pm\infty$. A particle is hence always bounded in the interior and cannot even "escape" from $AdS(d+1)$ in the limit $t\to\infty$. This is clearly different from asymptotically flat spacetimes as Minkowski space or the Schwarzschild black hole, where radii can become arbitrary large in infinite time.

This leads to the central conclusion:

> $AdS(d+1)$ behaves like a harmonic potential preventing any massive particle to escape, as this would cost infinite energy. $AdS(d+1)$ behaves naturally as a box.

Note that light can escape $AdS(d+1)$ even in finite coordinate time t. Nevertheless, this costs infinitely much energy as can be seen from the redshift (similar to [93])

$$\frac{\nu_f}{\nu_i}=\sqrt{\frac{1+\frac{r_i^2}{L^2}}{1+\frac{r_f^2}{L^2}}}\xrightarrow{r_f\to\infty}0\,, \tag{2.2.6}$$

(ν_i is the initial frequency and ν_f the final observed one) which vanishes for $r_f\to\infty$[2]. The surface $r\to\infty$ can hence be considered as infinite-redshift surface.

As a last point, the Penrose diagram of $AdS(d+1)$ will be constructed. For this

[2]Note that the redshift is defined as $z=\nu_i/\nu_f-1$ (cfr. [93]), which diverges.

purpose, global coordinates from Eq. (2.1.7) are used as the starting point. Furthermore, θ is introduced by $\tan(\theta) = \sinh(\rho)$. While $\rho \in [0, \infty)$, the range of $\theta \in [0, \pi/2)$ is bounded. The metric takes the form

$$\mathrm{d}s^2 = \frac{L^2}{\cos(\theta)^2}\left(-\mathrm{d}\tau^2 + \mathrm{d}\theta^2 + \sin(\theta)^2 \mathrm{d}\Omega_{d-1}^2\right) , \tag{2.2.7}$$

which is (up to the conformal factor) the metric of the so-called Einstein static universe [89]. This chart is still global and lightlike geodesics satisfy $\tau = \pm\theta + const.$, i.e. they are 45° lines in a (τ, θ)-plot. Plotting (τ, θ) is nothing else than the Penrose diagram of $AdS(d+1)$, which is depicted in Fig. 2.4. From the Penrose diagram it is easily visible that the conformal boundary (see next section) is located at $\theta = \pi/2$ and is timelike. This is another crucially important property making $AdS(d+1)$ suitable for holographic considerations.

2.3 The Boundary $\partial AdS(d+1)$

The metric manifold $AdS(d+1)$ is not a manifold with a boundary in the standard (topological) sense. In this section the notion of a conformal boundary is introduced and the properties of the conformal boundary of $AdS(d+1)$ are discussed.

Following the ideas of Penrose [94], the first ingredient is the *conformal embedding*

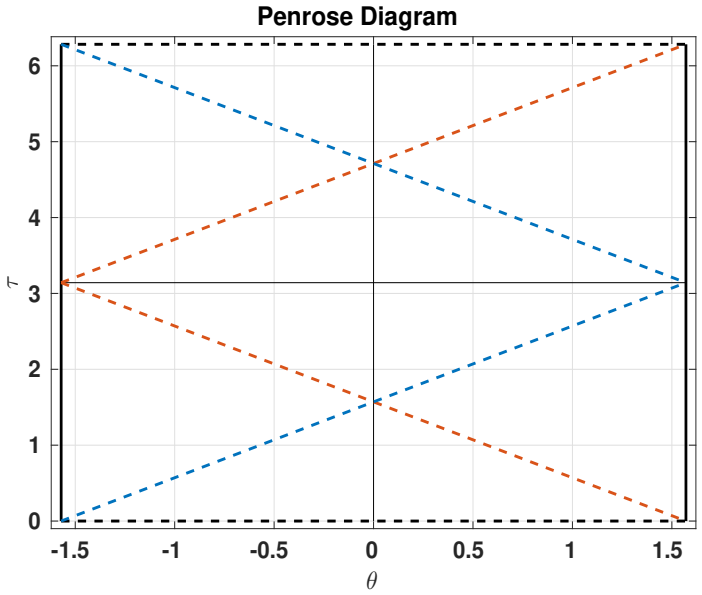

FIGURE 2.4: *Penrose diagram of $AdS(d+1)$ with $\mathbb{S}^{d-1}$ attached to each point. Negative values of θ correspond to the a parity transformation in the $\mathbb{S}^{d-1}$ part. Note that $\tau \in [0, 2\pi)$, but τ can also be considered as unwrapped, which leads to an infinite extended diagram.*

defined as:

Definition 2.3.1 (Conformal embedding)**:**
Given two Riemannian (Lorentzian) manifolds (M, g) and $(\tilde{M}, \tilde{g})$, a *conformal embedding* is a map $\Phi : M \longrightarrow \tilde{M}$, which is an embedding, i.e.

i) Φ maps into a larger manifold: $\Phi(M) \subsetneq \tilde{M}$,

ii) $\Phi : M \longrightarrow \Phi(M)$ is a diffeomorphism,

and preserves the causal structure, i.e.

$$\Phi^* \tilde{g} = \chi g \quad , \quad \chi \in C^\infty(M) \; .$$

In the case of $AdS(d+1)$, such a map is easily constructed in the coordinates of the Einstein static universe (cfr. Eq. (2.2.7)). A particular embedding can be realised by a map to $\tilde{M} = \mathbb{R} \times [-\pi, \pi] \times \mathbb{S}^{d-1}$, which is equipped with the metric $\tilde{g}_{\mu\nu} \mathrm{d}x^\mu \mathrm{d}x^\nu = -\mathrm{d}t^2 + \mathrm{d}r^2 + \sin(r)^2 \mathrm{d}\Omega^2_{d-1}$. The map is then simply defined by

$$\Phi : AdS(d+1) \longrightarrow \tilde{M} \quad , \quad (\tau, \theta, \theta_i) \longmapsto (t, r, \theta_i) \; , \tag{2.3.1}$$

and the conformal factor is $\chi = {}^{L^2}/_{\cos(\theta)^2}$. The *conformal boundary* is then defined as follows:

Definition 2.3.2 (Conformal boundary)**:**
Let (M, g), $(\tilde{M}, \tilde{g})$ be two Riemannian (Lorentzian) manifolds and $\Phi : M \to \tilde{M}$ a conformal embedding. The *conformal boundary of* M is defined as

$$\partial M := \partial \left(\Phi(M) \right) \subset \tilde{M} \; ,$$

where ∂ on the right hand side is the topological boundary in $\tilde{M}$.

Due to this definition, the conformal boundary $\partial AdS(d+1)$ is the solid black line in the Penrose diagram Fig. 2.4. $\partial AdS(d+1)$ can be naturally equipped with the induced metric of $\tilde{M}$ on that boundary. Note that this metric is only defined up to conformal transformation as the conformal embedding is not unique.

The construction of the conformal boundary depends on several choices and one has to make sure that all drawn conclusions are independent of this. More precise and independent of the explicit embedding is a definition of the boundary in terms of geodesic rays.

For hyperbolic space $\mathbb{H}^d$ this is discussed in detail in [90]. Nevertheless, in Lorenzian spacetimes this discussion does not apply, as there is no Riemann distance function. The idea is as follows: The information of the conformal boundary $\partial AdS(d+1)$ (black lines in Fig. 2.4) can be equally repharsed in terms of lightlike, spacelike and timelike geodesics. Here all geodesics terminating in the same boundary point are collected in equivalence classes, so-called *geodesics rays*.

Definition 2.3.3 (Geodesic ray)**:**
Let $\gamma_1,\ \gamma_2 : \mathbb{R} \longrightarrow M$ be two geodesics in $AdS(d+1)$. Given a conformal embedding $\Phi : M \longrightarrow \tilde{M}$, two geodesics are defined to be equivalent if

$$\gamma_1 \sim \gamma_2 \quad :\Longleftrightarrow \quad \lim_{\lambda\to\infty} \Phi\left(\gamma_1(\lambda)\right) = \lim_{\lambda\to\infty} \Phi\left(\gamma_2(\lambda)\right)$$

A *geodesic ray* is one equivalence class $[\gamma]$.

This definition is effectively independent of the conformal embedding Φ as all embedding spaces have to be related by a conformal transformation. The topological property of two points being equal is thus preserved and the equivalence classes remain preserved and well-defined for any conformal embedding.

It is possible to define further the geodesically compactified boundary.

Definition 2.3.4 (Geodesically compactified boundary[3])**:**
The *geodesically compactified boundary* of $AdS(d+1)$ is then the set of rays:

$$AdS_\infty(d+1) := \{[\gamma] \mid \gamma \text{ is a geodesic in } AdS(d+1)\} \ . \tag{2.3.2}$$

$AdS(d+1)$ has the special property that all rays have a radial lightlike representative. As discussed, timelike geodesics remain inside $AdS(d+1)$ and do not reach the boundary, i.e. have no concrete end point. Spacelike geodesics do run towards the boundary but their endpoints always coincide with a lightlike geodesic (cfr. Fig. 2.4). The points of the conformal boundary $\partial AdS(d+1)$ can thus be labelled by lightlike geodesics on $AdS(d+1)$. From this follows the conclusion

$$AdS_\infty(d+1) \simeq \partial AdS(d+1) \ .$$

Defining the boundary in terms of geodesic rays explicitly shows that the geodesically comcatified boundary is independent of the choice of the embedding. Due to the identification

[3]For hyperbolic space this definition is discussed in [90]

of both notions, also the conformal boundary is independent of the chosen embedding. The geodesic picture allows to speak about the boundary of $AdS(d+1)$ more abstractly and it is not necessary to refer to any larger manifold. The interpretation of $\partial AdS(d+1)$ as a set of geodesic rays allows further to make contact with the definition of [89] for the boundary of $AdS(d+1)$. As a ray is the full equivalence class of geodesics, it suffices to pick only one representative of each class. In fact, the boundary can simply be defined as

$$\partial AdS(d+1) :\simeq \left\{ [x]_o \subset \mathcal{M}_{2,d} \mid x \neq 0,\ -\left(x^0\right)^2 + \sum_{i=1}^{d} \left(x^i\right)^2 - \left(x^{d+1}\right)^2 = 0 \right\} , \qquad (2.3.3)$$

with the equivalence class

$$x, y \in \mathcal{M}_{2,d} :\ x \sim y \quad :\Longleftrightarrow \quad \exists \lambda \in \mathbb{R} \setminus 0 \ :\ x = \lambda y \ .$$

The equivalence classes $[x]_o$ are then lightlike geodesics rays in $\mathcal{M}_{2,d}$ crossing the origin. These rays have no intersection with $AdS(d+1)$, nevertheless, it is possible to map uniquely each $[x]_o$ to a ray in $[\gamma] \in AdS_\infty(d+1)$[4]. Eq. (2.3.3) simply states that the boundary of AdS is the projective space made of rays in the light cone of $\mathcal{M}_{2,d}$.

The topological structure of $\partial AdS(d+1)$ can be analysed further. The boundary has the dimension $\dim(\partial AdS(d+1)) = d$, as can be seen from Eq. (2.3.3). It is required that the point in $\mathcal{M}_{2,d}$ lies on the light cone, which reduces the dimension from $d+2$ to $d+1$. On this submanifold points along the same straight line are identified, which reduces the dimension further to d. As noticed above, slices of $AdS(d+1)$ with constant angles in the $x^0 - x^{d+1}$-plane are hyperbolic spaces $\mathbb{H}^d$. From this, it can be concluded that $\partial AdS(d+1) \simeq_{\text{top}} \mathbb{S}^1 \times \partial\mathbb{H}^d$. The rewriting of Eq. (2.3.3) gives further insight, as

$$\left(x^0\right)^2 + \left(x^{d+1}\right)^2 = \sum_{i=1}^{d} \left(x^i\right)^2 \ .$$

As different points are considered as equivalent if they differ only by a rescaling with $\lambda \in \mathbb{R}$, a "gauge" can be fixed by demanding

$$\left(x^0\right)^2 + \left(x^{d+1}\right)^2 = 1 = \sum_{i=1}^{d} \left(x^i\right)^2 \ .$$

[4]This relies on the fact that $AdS(d+1)$ approaches the origin light cone at infinity. Computing the limit point which can be characterised by t and the angles of the $d-1$-sphere, the rays on the light cone can be identified with one radial lightlike geodesic in $AdS(d+1)$ and its equivalence class.

This shows further that $\partial AdS(d+1) \simeq \left(\mathbb{S}^1 \times \mathbb{S}^{d-1}\right)/\mathbb{Z}_2$ (cfr. [89]). The quotient by $\mathbb{Z}_2$ is necessary as $[x]_o = [-x]_o$.

Having a precise definition of the boundary, it is possible to study the symmetries of the boundary space. As the action of $SO(2,d)$ on $\mathcal{M}_{2,d}$ and on $AdS(d+1)$ is defined, the same action can be defined on the geodesics of the light cone. Indeed, the action of $SO(2,d)$ on $\partial AdS(d+1)$ is the induced action. A detailed analysis proves that the corresponding action on the boundary is the conformal group $C(1,d)$. This is motivated by the following statements

- $\partial AdS(d+1)$ is a projective space and as such, has only a conformal structure. The single rays are identified by their relative angles, which are preserved by conformal transformations.
- The algebra $\mathfrak{so}(2,d)$ is isomorphic to the algebra of conformal transformations, as shown in e.g. [89]. Due to this, it is possible to rearrange the group elements of $SO(2,d)$ on $\mathcal{M}_{2,d}$ and $AdS(d+1)$ in terms of conformal transformations on $\partial AdS(d+1)$.
- In the logic of [90] the isometries of $AdS(d+1)$ can be classified in terms of the number of fixed points (FP) in the bulk and the boundary. Transformations in $SO(2,d)$ can be mapped into $C(1,d)$ transformations by analysing these fixed points.

As a last step, metrics on the boundary are constructed. Starting with global coordinates of Eq. (2.1.5), the surface $r = const.$ cuts each ray on $AdS(d+1)$ exactly once. Recall that a ray can be labelled by a lightlike geodesic and these are straight lines in $\mathcal{M}_{2,d}$ determined by their angle in the $x^0 - x^{d+1}$-plane and the angle in $\mathbb{S}^{d-1}$. It follows that the induced metric for $r = r_o = const.$ is

$$\mathrm{d}s^2\Big|_{r=r_o} = -\left(1 + \frac{r_o^2}{L^2}\right)\mathrm{d}t^2 + r_o^2 \mathrm{d}\Omega_{d-1}^2 \,. \tag{2.3.4}$$

The t coordinate can be rescaled according to $r_o\bar{t} = \sqrt{1 + {}^{r_o^2}/_{L^2}} \cdot t$, to get to

$$\mathrm{d}s^2\Big|_{r=r_o} = r_o^2\left(-\mathrm{d}\bar{t}^2 + \mathrm{d}\Omega_{d-1}^2\right) \,. \tag{2.3.5}$$

Note that the coordinates $(\bar{t}, \theta_i)$ completely parametrise $\partial AdS(d+1)$, i.e. Eq. (2.3.5) can be considered as a metric on the boundary. Nevertheless, the same is true for using any other point r_o, which cuts all rays at a different radius. Compatible with the observation that the symmetries of the boundary are conformal transformations, the metric is only

determined up to a conformal factor. Hence, the metric

$$\mathrm{d}s^2_{\partial AdS} = -\mathrm{d}\bar{t}^2 + \mathrm{d}\Omega^2_{d-1} \tag{2.3.6}$$

could be used as representative of the equivalence class of conformally related metrics on $\partial AdS(d+1)$ in global coordinates. Observe that one arrives at the same conclusion by sending $r \to \infty$ in Eq. (2.1.6) and dropping the (divergent) conformal factor r^2. This is due to the fact that $AdS(d+1)$ approaches the origin light cone of $\mathcal{M}_{2,d}$ for large radii r. The metric makes the $\mathbb{S}^1 \times \mathbb{S}^{d-1}$ part of the boundary topology of the boundary explicit[5].

The same construction can also be done in the Poincaré-patch coordinates (2.1.10). Here a $z = const.$ surface corresponds to a cut through the hyperboloid, although it cuts only half of it (cfr. Fig. 2.3). Nevertheless, due to the identification of the rays, it cuts each point of the boundary exactly once. The induced metric (cfr. Eq. (2.1.11)) is then

$$\mathrm{d}s^2\Big|_{z=z_o} = \frac{L^2}{z_o^2}\left(-\mathrm{d}t^2 + \sum_{i=1}^{d-1}\left(\mathrm{d}y^i\right)^2\right) . \tag{2.3.7}$$

Again, any value z_o is equally well suited, which shows that the metric can only be determined up to a conformal factor. Thus, another representative of the equivalence class of conformally related metrics on the boundary is

$$\mathrm{d}s^2_{\partial AdS} = -\mathrm{d}t^2 + \sum_{i=1}^{d-1}\left(\mathrm{d}y^i\right)^2 . \tag{2.3.8}$$

Note that this parametrisation indeed covers the full boundary space, although the Poincaré-patch covers only half of $AdS(d+1)$. This can be seen from the Penrose diagram Fig. 2.4. There the Poincaré-patch covers the region inside the red dashed line, which is completely attached to the boundary. The boundary in the conformal sense is in this case located at $z = 0$, while in the ray construction this is the "endpoint" of all rays. A huge advantage of the boundary parametrised by Poincaré-patch coordinates is that the metric is flat. Because of this, these coordinates constitute an easy metric as background for dual field theory computations in the holographic context, which is discussed below. Note that the metrics Eq. (2.3.8) and (2.3.6) are related by a conformal transformation, as expected. Hence, both descriptions are equivalent but the one or the other might be more useful depending on the application.

[5]The quotient by $\mathbb{Z}_2$ is non-obvious here, as already one particular representative of each ray is chosen. Nevertheless, the quotient can not be neglected as the metric is only one representative of the equivalence class of conformally related metrics.

Both boundary line elements demonstrate that the boundary $\partial AdS(d+1)$ of AdS space is indeed timelike. This leads to the conclusion:

The boundary of AdS space $\partial AdS(d+1)$ is

- a d-dimensional conformal space of signature $(1, d-1)$,
- equipped with the equivalence class of metrics, which are related to Minkowski space by a conformal transformation, and
- has the full conformal group $C(1, d)$ as symmetry group.

The identification of the boundary at finite z or r, as demonstrated above, is possible since a corresponding slice cuts each ray exactly once. Further, this makes the derivation of a conformal boundary metric well-defined. Nevertheless, this identification is counter-intuitive as the selection of which geodesic belongs to which ray is much harder at finite z and r.In contrast, at $z \to 0$ or $r \to \infty$ this selection of representatives is much simpler and due to the rule defined in Def. 2.3.3, all geodesics belonging to one ray become localised in a small neighbourhood. Therefore, it is convenient and intuitive to say that the boundary is located at $z \to 0$ or $r \to \infty$ as each independent point there belongs to exactly one independent ray. Furthermore, this matches the picture of geodesic compactification with conformal compatification. In the conformal compatification picture, i.e. the Penrose diagram, it is natural to identify $r \to \infty$ or $z \to 0$ with the boundary as this is the topological boundary of $\Phi(AdS(d+1))$. Another argument is that, as already mentioned, $AdS(d+1)$ approaches the light cone in $\mathcal{M}_{2,d}$ for $r \to \infty$ or $z \to 0$. This leads again to the conclusion that the boundary can be identified with this limit in $AdS(d+1)$. Due to this, also in this thesis the boundary of AdS will be referred to be located at $z \to 0$ or $r \to \infty$[6].

[6]Note that in different coordinates this statement might have a different form. In fact there exist charts which do not cover the full boundary space as e.g. the cosmological slicing.

3

The Holographic principle and the AdS/CFT Correspondence

In this chapter a motivation is given why gravity should have holographic aspects and the meaning of holography is clarified below. These ideas were developed by studying black holes and semi-classical aspects thereof. Due to this, properties of classical black holes are discussed first, followed by a discussion of how the holographic principle can be motivated at the example of semi-classical black holes. A concrete realisation of these holographic ideas is the so-called AdS/CFT correspondence [44], which is presented in Sec. 3.3.

3.1 Classical Black Holes

In this section certain basic features of black holes in GR are recalled. The chapter is mainly based on the content of [95, 96] and the lecture notes [97, 98]. Of main relevance are properties of the simplest kind of black holes, namely static and spherically symmetric non-charged Schwarzschild black holes. These play a central role in the later elaboration (cfr. Chpt. 6). As indicated, Schwarzschild black holes are static and spherically symmetric solutions of the Einstein equations, coupled to an energy-momentum tensor $\propto \delta(r)$. The matter density is hence concentrated at one point of radius $r = 0$, which makes the

these solutions "effectively vacuum solutions"[1], i.e. $R_{\mu\nu} = 0$ and $R = 0$. This class of metrics is parametrised by the Arnowitt-Deser-Misner (ADM)-mass M [95, 99] ($G = c = 1$) and has the form (in $4d$)

$$\mathrm{d}s^2 = -\left(1 - \frac{2M}{r}\right)\mathrm{d}t^2 + \frac{\mathrm{d}r^2}{1 - \frac{2M}{r}} + r^2\mathrm{d}\Omega_2^2 \,. \tag{3.1.1}$$

This spacetime is asymptotically flat and approaches Minkowski space in the limit $r \to \infty$. Furthermore, it can be approximated by the gravitational Newton potential of a spherical mass distribution of mass M in the weak gravity regime and non-relativistic limit ($M/r \ll 1$ and $v/c \ll 1$).

A still puzzling and fascinating property of this spacetime is the Killing horizon (see Def. B.3 in App. B) at $r = 2M$. Here, the Killing vector field $\partial/\partial t$ becomes lightlike

$$g\left(\frac{\partial}{\partial t}, \frac{\partial}{\partial t}\right) = -\left(1 - \frac{2M}{r}\right) \xrightarrow{r\to 2M} 0 \,.$$

The radius $r_s = 2M$ is known as the Schwarzschild radius. Further, the metric component $g_{tt} = -\left(1 - \frac{2M}{r}\right)$ vanishes at the horizon, while g_{rr} diverges. This shows that the Schwarzschild coordinates (t, r) are only valid up to this point and the line element (3.1.1) describes only the exterior (i.e. outside the horizon) patch of the black hole.

In contrast, the in-/outgoing Eddington-Finkelstein coordinates also describe the interior region. They are defined by (convention according to [98])

$$v = t + r_*(r) \quad , \quad u = t - r_*(r) \quad , \quad r_*(r) = \int_{2M}^{r} \mathrm{d}r' \frac{1}{1 - \frac{2M}{r'}} = r + 2M \log\left|\frac{r - 2M}{2M}\right| \,, \tag{3.1.2}$$

where (v, r) are the ingoing Eddington-Finkelstein coordinates and (u, r) the outgoing ones, respectively. In these coordinates, the line element has the form

$$\mathrm{d}s^2 = -\left(1 - \frac{2M}{r}\right)\mathrm{d}v^2 + 2\mathrm{d}v\mathrm{d}r + r^2\mathrm{d}\Omega_2^2 \,, \tag{3.1.3}$$

$$\mathrm{d}s^2 = -\left(1 - \frac{2M}{r}\right)\mathrm{d}u^2 - 2\mathrm{d}u\mathrm{d}r + r^2\mathrm{d}\Omega_2^2 \,. \tag{3.1.4}$$

[1]Note that the Schwarzschild solution is no vacuum solution. It is the solution in the vacuum region of spacetime, but spacetime is not empty as the name "vacuum" would suggest. The energy-momentum tensor is simply bounded in an (infinitely) small region.

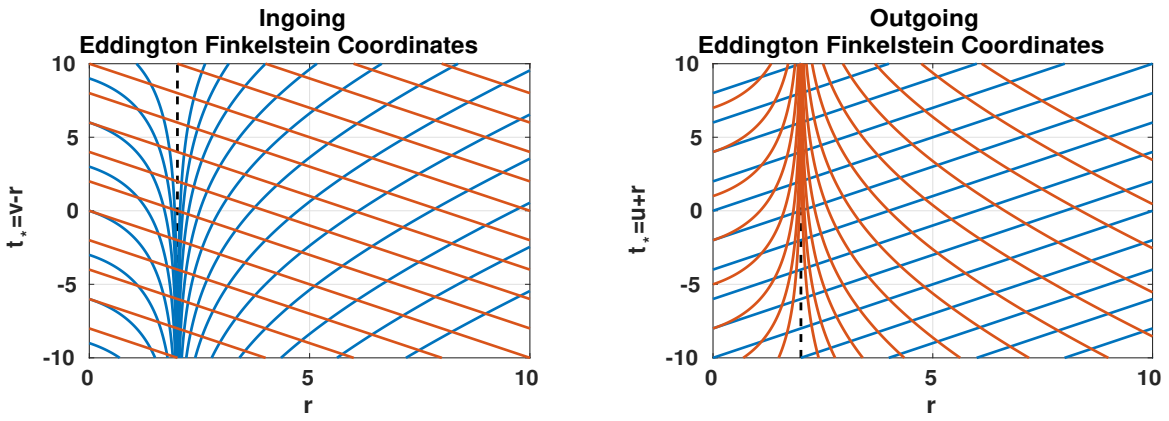

(a) (b)

FIGURE 3.1: *Plot of in- (red) and outgoing (blue) light rays in (a) in- and (b) outgoing Eddington-Finkelstein coordinates. In (a) ingoing light rays pass through the horizon in finite time $t_* = v - r$, while outgoing light rays originate at $t_* = -\infty$ at the horizon. The opposite is true for outgoing light rays in (b) and $t_* = u + v$. For the plot it was chosen $M = 1$. The plot is analogous to the presentation in [98]*

It is easy to verify that $v = const.$ surfaces describe radially ingoing lightlike geodesics and $u = const.$ outgoing ones, respectively. In these coordinates the line element is also valid for $r < 2M$, i.e. describes the interior region. Fig. 3.1 shows the in- and outgoing light rays in the different coordinates. In ingoing Eddington-Finkelstein coordinates, outgoing light rays originate at the horizon at $t_* = v - r = -\infty$, while ingoing ones cross the horizon (cfr. Fig. 3.1 (a)). The opposite is true in outgoing Eddington-Finkelstein coordinates, where ingoing light rays reach the horizon only asymptotically within infinite time $t_* = u + r = \infty$, while outgoing ones cross the horizon (cfr. Fig. 3.1 (b)). This indicates that the causal structure for $r < 2M$ is different in the two different sets of coordinates. Indeed, as it will become clear in the discussion below, there exist two physically different spacetime regions, both described by $r < 2M$, but one region is covered by (v, r) and the other by (u, r). Which part of the spacetime is covered by which coordinates is clearer in the Kruskal-Szekeres coordinates and the Penrose diagram, shown below. At this point some remarks are in order.

The e.g. ingoing Eddington-Finkelstein coordinates could be used to describe the black hole interior. Being in this spacetime region, the inverse transformation of Eq. (3.1.2) can be done and Schwarzschild-like coordinates (t, r) are recovered. The line element takes again the form of Eq. (3.1.1). Concluding, it is possible to also describe the interior region with (t, r) and Eq. (3.1.1). Nevertheless, it is not possible to describe any process going from interior to exterior and vice versa as the Schwarzschild time t would diverge in the moment the horizon is passed. This is where Eddington-Finkelstein coordinates are necessary.

Following the above construction, it is easy to see that the Killing vector $T = {}^{\partial}/_{\partial t}$ is spacelike in the interior region, $g(T,T) > 0$, $r < 2M$. In the interior the spacetime is thus not static any more, but homogeneous. This makes the spacetime a particular kind of cosmology, namely Kantowski-Sachs cosmology, which is anisotropic but homogeneous. This reflects that the condition of the exterior region being static becomes a homogeneity condition for the interior. It further has the consequence that reaching the point $r = 0$ is now a matter of time, not of space. Once the horizon is passed, r plays the role of a timelike coordinate and $r = 0$ has to be reached, unless causality is violated.

The point $r = 0$ is a very special point in this spacetime. Although the Ricci curvature vanishes everywhere $R = 0$, the Kretschmann curvature,

$$\mathcal{K} = R_{\alpha\beta\mu\nu}R^{\alpha\beta\mu\nu} = \frac{48M^2}{r^6} \,, \tag{3.1.5}$$

diverges, which shows the presence of a curvature singularity. The spacetime cannot be described by the metric (3.1.1) beyond this point and time (i.e. r) stops there. The situation is similar to the big bang in cosmology and denotes the breakdown of GR.

All the previously presented charts cover only certain patches of the whole spacetime. There exists a global chart given by the Kruskal-Szekeres coordinates (T, X) (cfr. [100, 101] and e.g. [102, 103]), which are defined as

$$T^2 - X^2 = \exp\left(a'(r_s)r_*(r)\right) = \left(1 - \frac{r}{2M}\right)e^{\frac{r}{2M}} \quad , \quad \frac{T}{X} = \begin{cases} \tanh\left(\frac{t}{2}a'(r_s)\right) & -1 < \frac{T}{X} < 1 \\ \coth\left(\frac{t}{2}a'(r_s)\right) & -1 < \frac{X}{T} < 1 \end{cases} , \tag{3.1.6}$$

with $a'(r_s) = \mathrm{d}a/\mathrm{d}r|_{r=r_s} = 1/2M$. These equations can be solved explicitly yielding

$$T = \pm\sqrt{\frac{r}{2M} - 1}\, e^{\frac{r}{4M}} \sinh\left(\frac{t}{4M}\right) \,, \tag{3.1.7}$$

$$X = \pm\sqrt{\frac{r}{2M} - 1}\, e^{\frac{r}{4M}} \cosh\left(\frac{t}{4M}\right) \,, \tag{3.1.8}$$

for the exterior region ($r > r_s$) and

$$T = \pm\sqrt{1-\frac{r}{2M}}\, e^{\frac{r}{4M}} \cosh\left(\frac{t}{4M}\right) , \tag{3.1.9}$$

$$X = \pm\sqrt{1-\frac{r}{2M}}\, e^{\frac{r}{4M}} \sinh\left(\frac{t}{4M}\right) , \tag{3.1.10}$$

for the interior region ($r < r_s$). Due to the different possibilities for signs, there are actually four different spacetime regions, which are interpreted below. Eq. (3.1.6) can be inverted, which gives t as a function of the ratio T/X through $\tanh^{-1}$ or $\coth^{-1}$. For r the inverse relation is

$$r = r(T,X) = 2M\left(1 + W_0\left(\frac{X^2-T^2}{e}\right)\right) ,$$

where $W_0(x)$ is the positive branch of the Lambert-W-function (see Def. B.5 in App. B). This expression is unique and thus, given values for (T,X) correspond to a unique set of (t,r) values, while the opposite is not true. The line element in (T,X) coordinates can be written as

$$\mathrm{d}s^2 = \frac{32M^3}{r^3}\exp\left(-\frac{r}{2M}\right)\left(-\mathrm{d}T^2 + \mathrm{d}X^2\right) + r^2\mathrm{d}\Omega_2^2 , \tag{3.1.11}$$

where $r = r(T,X)$. This line element is now well-defined for all values $r > 0$. Furthermore, the (T,X) part of the metric is conformally related to Minkowski spacetime. Due to this, in- and outgoing light rays have 45° angles in (T,X) charts, i.e. $T = \pm X + const.$ Using Eq. (3.1.6) it is possible to extract information about locations of singularity and horizon in the (T,X)-chart. The horizon is located at $r = r_s = 2M$, which gives

$$T^2 - X^2 = 0 \quad \Rightarrow T = \pm X . \tag{3.1.12}$$

These are 45° straight lines through the origin. The singularity is instead located at $r = 0$, which yields

$$T^2 - X^2 = 1 \quad \Rightarrow T = \pm\sqrt{1+X^2} , \tag{3.1.13}$$

and corresponds to two distinct hyperbolas. As the point $r = 0$ has two solutions in (T,X) chart, there are two singularities, one in the future and one in the past. As indicated already above, there are actually two interior regions, namely the black hole and the white hole interiors and each of them contain a singularity. Certainly, there is no restriction in the angular part of the metric, i.e. at each point (T,X) a full two-sphere is

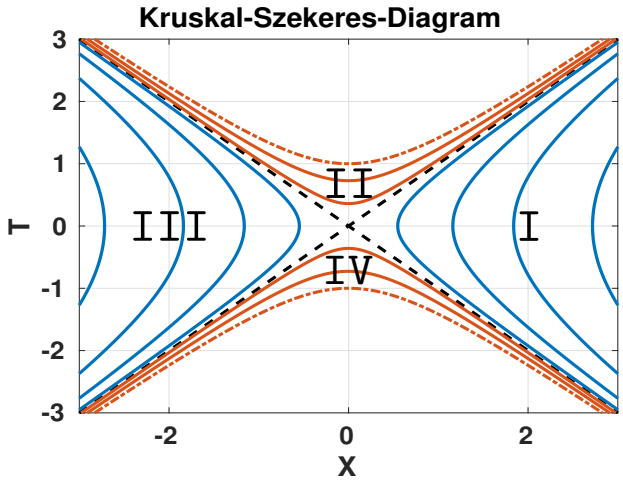

FIGURE 3.2: *Kruskal-Szekeres diagram for black hole with $M = 1$. Depicted are surfaces with $r = const$. Blue lines correspond to $r > r_s$ and red ones to $r < r_s$. The black dashed lines visualise the horizon, i.e. $r = r_s$ and the singularity $r = 0$ corresponds to the dotted-dashed red lines. As light rays are diagonal in this chart, blue lines are timelike, while red ones are spacelike. The spacetime consists of two exterior regions `I` and `III`, as well as a black hole interior region `II` and a white hole interior region `IV`.*

attached. Because of this, it is clear that the singularity and also the horizon are actually 3-dimensional surfaces of fixed areal radius r. The singularity is hence not a point in spacetime, it is rather a whole surface. Further, the condition Eq. (3.1.13) shows, that the singularity is spacelike and, as discussed above, it is only a matter of time (not space) to hit it. The situation is visualised in Fig. 3.2. The original Schwarzschild coordinates cover only one exterior region of this diagram, namely region `I`. As argued above it is also possible to use Schwarzschild coordinates to describe the other regions, but one set of these coordinates covers only one patch. Ingoing Eddington-Finkelstein coordinates instead describe region `I` and `II` simultaneously, as all ingoing light rays hit the singularity in the future (cfr. Fig. 3.1). For outgoing Eddington-Finkelstein coordinates the opposite is true and they cover the patches `I` and `IV`. Here region `IV` is the white hole interior as everything inside this region is forced by causality to exit this region. Not even light can stay inside the white hole region. Hence the white hole is the exact opposite of a black hole, where instead nothing, not even light, can exit. The other exterior region `III` is not covered by any of these charts. In fact, region `I` and `III` are causally disconnected.

A very useful tool are Penrose diagrams, which rely on conformal compactification as already used in Sec. 2. As global coordinates (T, X) were found, they can be conformally compactified by introducing the lightlike coordinates (U, V) and their compactifications $(\tilde{U}, \tilde{V})$

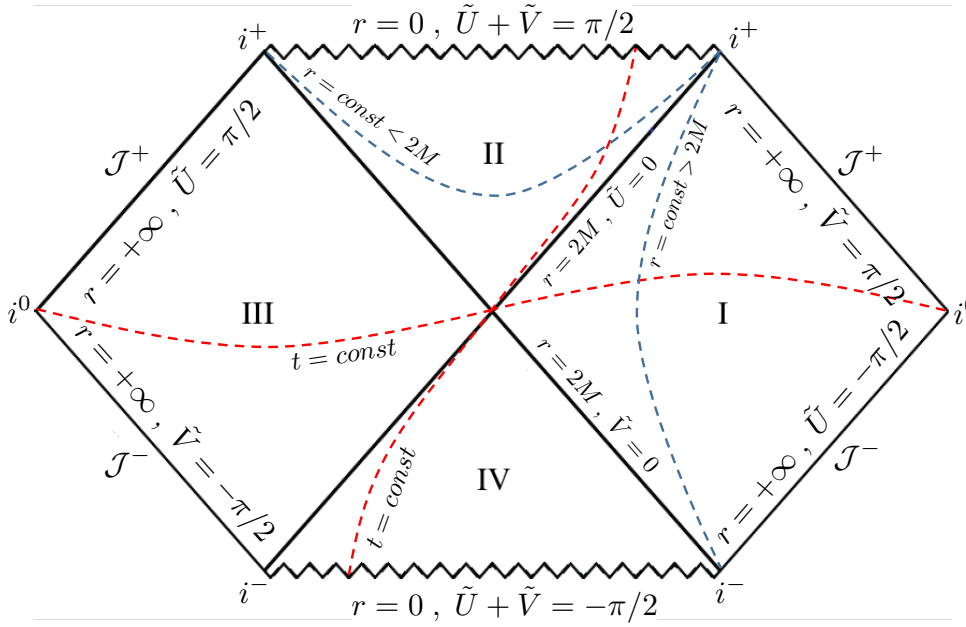

FIGURE 3.3: *Penrose diagram for the Kruskal extension of Schwarzschild spacetime. The angular coordinates θ, ϕ are suppressed so that each point of the diagram can be thought of as representing a 2-sphere of radius r.*

$$U = T - X \quad , \quad V = T + X \ , \tag{3.1.14}$$

$$\tilde{U} = \arctan(U) \quad , \quad \tilde{V} = \arctan(V) \ . \tag{3.1.15}$$

As (U, V) describe again in- and outgoing light rays, the compactifications preserve the causal structure of the spacetime. $(\tilde{U}, \tilde{V})$ have a finite range form $-\pi/2$ to $\pi/2$ which covers the full spacetime[2]. It is possible to construct compactified time- and spacelike coordinates

$$\tilde{T} = \frac{1}{2}\left(\tilde{V} + \tilde{U}\right) \quad , \quad \tilde{X} = \frac{1}{2}\left(\tilde{V} - \tilde{U}\right)$$

and plot horizon, singularity, etc. in these coordinates. This leads to the Penrose diagram Fig. 3.3, which contains all the causal information of the black hole spacetime in a finite size plot. In the Penrose diagram light rays have 45° and go either to the right (outgoing) of the left (ingoing). It is obvious that an outgoing light ray emitted at the horizon remains in the horizon. Ingoing light rays have to hit the singularity in the future. A future pointing timelike curve is always inside the light cone spanned at each point by in-

[2]It is easily possible to construct a conformal embedding (cfr. Def. 2.3.1) explicitly with this data given. however, this is of no practical interest.

and outgoing light rays. Thus, it always has an angle between 45° and 135° with respect to the $\tilde{X}$-axis. This makes apparent that no matter, once it reaches region `II`, could ever exit this black hole region. Moreover, since no light rays can escape from there, the horizon is also a causal horizon (see Def. 3.1.1 below).

The situation considered above is very non-physical. It describes a black hole, which is eternal and contains a white hole region `IV` and a parallel universe `III`. Both these regions contradict with what is expected to be realised in nature. Indeed, a black hole as it is observed in the sky [9, 10] is formed at a point in time by the collapse of matter. The Schwarzschild solution, as presented above, is therefore only valid in the vacuum region of this process[3]. Inside the collapsing matter, the metric has to be replaced by a (much more complicated) metric, solving the Einstein equations coupled to a non-trivial energy-momentum tensor. This has analytically been studied in simple cases (see e.g. [102]) and the Penrose diagram looks as depicted in Fig. 3.4. When the physical process of black hole formation is included in the model, the non-physical regions `III` and `IV` are not relevant any more.

There are some interesting classical properties pointing towards a holographic principle and they are needed as basic material for this thesis. The following presentation of the

[3]This is known as Birkhoff theorem [104, 105], which is discussed in e.g. [93, 102].

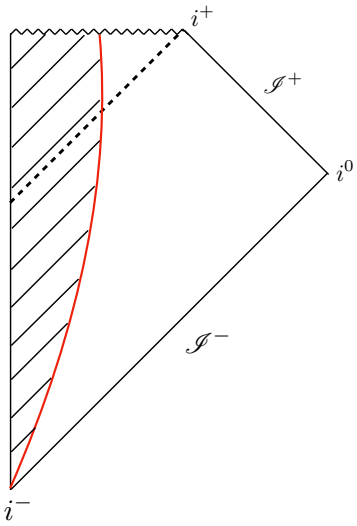

FIGURE 3.4: *Schematic Penrose diagram of a black hole collapse. In the region outside the matter the (locally) static Schwarzschild solution is valid (non-shaded region). The spacetime region inside the matter (shaded region) is described by some complex time dependent spacetime. The red line describes the surface of this matter. Its dynamics is model dependent and can be highly non-trivial. As the black hole formation process is taken into account, the non-physical regions `III` and `IV` are cut off. The dashed black line represents the black hole horizon.*

holographic principle and introductory material follows the review of Bousso [45].

The development of the holographic principle can be traced back to Hawking's discovery in 1971 [106], where he proved that the area of a causal horizon cannot decrease in time. Hawking formulated a theorem later known as the *Hawking area theorem*, which is stated below after providing some more preliminary material. First of all, it is necessary to precisely define a causal horizon by

Definition 3.1.1 (Causal horizon [95, 98])**:**
Given a spacetime (M, g) (smooth manifold M equipped with Lorenzian metric g). The *future causal horizon* H^+ is defined as the boundary of the past of future lightlike infinity, i.e.

$$H^+ := \partial J^- \left(\mathscr{I}^+\right) \ .$$

Similarly, the *past causal horizon* is defined as

$$H^- := \partial J^+ \left(\mathscr{I}^-\right) \ .$$

Here, $\mathscr{I}^\pm$ denotes future/past lightlike infinity and $J^\pm(A)$ the causal future/past of the spacetime region A (see Def. B.7 in App. B). This definition intuitively states that a horizon is the boundary of spacetime regions where light rays can or cannot reach infinity. Everything behind the horizon, the region where light rays cannot reach infinity, is causally disconnected to the outside. This definition is unavoidable in dynamic black hole spacetimes as there no (timelike) Killing vector field and thus no Killing horizon exists. In the case of stationary black holes Killing horizon and causal horizon coincide.

A further important ingredient are the energy conditions defined by

Definition 3.1.2 (Energy conditions [95, 96])**:**
It is possible to define the following *energy conditions* for the energy-momentum tensor $T_{\mu\nu}$:

Null energy condition
For all lightlike vector fields k^μ, $T_{\mu\nu}k^\mu k^\nu \geq 0$ holds.

Weak energy condition
For all timelike vector fields X^μ, $T_{\mu\nu}X^\mu X^\nu \geq 0$ holds, i.e. the energy density observed by any observer is positive.

Dominant energy condition
In addition to the weak energy condition for each future-pointing causal vector field

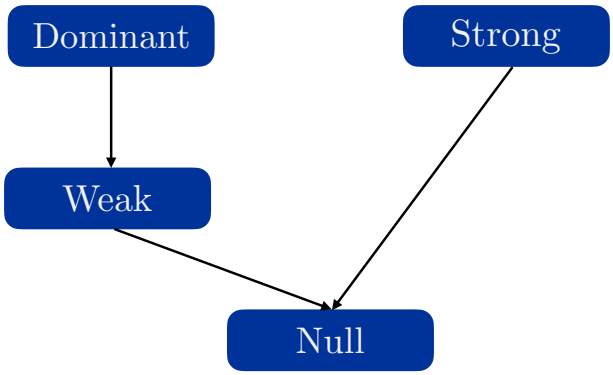

FIGURE 3.5: *Hierarchy of energy conditions.*

(timelike or null) Y^μ, the vector field $-T^\mu{}_\nu Y^\nu$ is also future-pointing and causal. This corresponds to the requirement that any flow of mass-energy is slower or equal to the speed of light.

Strong energy condition

For any timelike vector field X^μ it is

$$\left(T_{\mu\nu} - \frac{1}{2}T g_{\mu\nu}\right) X^\mu X^\nu \geq 0\,,$$

for $T = g^{\mu\nu}T_{\mu\nu}$.

The energy conditions follow the hierarchy shown in Fig. 3.5.

The important part about the energy conditions is the relation to geometry via the Einstein equations. Assuming that the Einstein equations hold, i.e. $R_{\mu\nu} - {}^1\!/_2 R\, g_{\mu\nu} = \kappa T_{\mu\nu}$ ($\kappa = 8\pi G$), the following geometric conditions are induced:

Null energy condition

For all lightlike vector fields k^μ,

$$\left(R_{\mu\nu} - \frac{1}{2}R\, g_{\mu\nu}\right) k^\mu k^\nu = G_{\mu\nu} k^\mu k^\nu \geq 0$$

holds, where $G_{\mu\nu}$ is the Einstein tensor.

Weak energy condition

For all timelike vector fields X^μ,

$$\left(R_{\mu\nu} - \frac{1}{2}R\, g_{\mu\nu}\right) X^\mu X^\nu = G_{\mu\nu} X^\mu X^\nu \geq 0$$

holds.

Dominant energy condition

In addition to the weak energy condition for each future-pointing causal vector field (timelike or null) Y^μ, the vector field $-G^\mu{}_\nu Y^\nu$ is also future-pointing and causal.

Strong energy condition

For any timelike vector field X^μ it is

$$R_{\mu\nu}X^\mu X^\nu \geq 0\,.$$

Hence, the Einstein equations translate the energy conditions, which are conditions on the energy-momentum tensor, into assumptions about the geometric properties of the spacetime, which are used to prove the area theorem.

The last component of the area theorem is the cosmic censorship conjecture[4], which states that there are no singularities on or outside a causal horizon.

The area theorem states:

Theorem 3.1.3 (Hawking [106] (cfr. [95, 98]))**:**
Given a spacetime (M, g) with a future causal horizon H^+ and global spatial slices Σ_1 and Σ_2, with $\Sigma_2 \subseteq J^+(\Sigma_1)$, i.e. Σ_2 is in the future of Σ_1. When the weak energy condition, the Einstein equations, as well as the cosmic censorship conjecture hold, it is

$$A_2 = Area(\Sigma_2 \cap H^+) \geq Area(\Sigma_1 \cap H^+) = A_1\,.$$

Hence, the area of the horizon can only increase in time $dA \geq 0$.

Note that the future causal horizon H^+ is a co-dimension 1 lightlike surface. The surface $\Sigma_i \cap H^+$ is the horizon at the instant of time defined on Σ_i and thus a co-dimension 2 spacelike surface.

This theorem is highly interesting due to two facts: Firstly, this is a fully dynamical result about full GR and holds for arbitrary complex systems. This means the theorem holds true for e.g. any configuration of several collapsing stars, black hole merging, or full galaxies. The topology of $\Sigma_i \cap H^+$ thus might be arbitrarily complex. For a single Schwarzschild black hole the topology is $\mathbb{S}^2$. Secondly, it seems that the horizon area behaves similar to thermodynamic entropy as it can only increase within any physical process.

[4]The cosmic censorship conjecture was introduced by Penrose [107] but there are different ways of formalising it, which are differently strong. Here the formulation of Dowker [98] is followed.

On top of this important theorem the analysis of classical black holes leads to the so-called no hair theorems [106, 108–111] (see [102] for an overview):

Theorem 3.1.4 (No-hair (cfr. [45] Bousso (2002), p. 6))**:**
A stationary black hole is only characterised by the three macroscopic quantities mass, angular momentum, and charge (M, L, Q)*, which enter the Kerr-Newmann metric [112, 113].*

This theorem implies that whichever matter collapses into a black hole, the final state will always be a Kerr-Newman black hole determined by the three macroscopic parameters (M, L, Q). The theorem states in other words that the initial state of the system may have arbitrary complexity and consequently entropy, but after the system has settled down to its final state will not know about these initial conditions and not even about the kind of matter, which has formed the black hole (see the discussion in [102]). Together with the area theorem this led to the development of the laws of black hole thermodynamics [114] with the first law [45, 97, 98]

$$\mathrm{d}M = \frac{\kappa}{8\pi}\mathrm{d}A + \Omega_H \mathrm{d}L + \Phi_H \mathrm{d}Q \ , \tag{3.1.16}$$

where κ is the surface gravity, Ω_H the angular velocity at the horizon and Φ_H the electric surface potential of the black hole at the horizon. These laws of black hole thermodynamics were first just thought to be a formal coincidence and were not meant to be thought of as physical thermodynamic properties.

3.2 Semi-classical Aspects of Black Holes and the Holographic Principle

The interpretation of Eq. (3.1.16) changed by means of a semi-classical analysis of Hawking [37, 38] and considerations of Bekenstein [39–41].

Bekenstein [39–41] argued that the entropy of a physical system dropped into a black hole would be lost for the external observer, leading to a decrease of the total entropy of the universe. The entropy lost in this process has to enlarge the entropy of the black hole, which would be visible as an increase of the horizon area. Bekenstein concluded that the entropy of the black hole has to be proportional to its area $S_{BH} \propto A$ and stated the *generalised second law* of thermodynamics

$$\mathrm{d}S_{\text{total}} = \mathrm{d}S_{BH} + \mathrm{d}S_{\text{matter}} \geq 0 \ . \tag{3.2.1}$$

It formalises that the entropy of the matter system and black hole together can only increase or stay the same. This furthermore permits an interpretation of area A and Eq. (3.1.16) as physical entropy.

Taking Bekenstein's result seriously and assigning thermodynamic entropy to a black hole, this would require the black hole also to have a temperature. This is impossible classically as the a black hole does not radiate and is a perfect absorber, and hence the temperature has to be zero $T = 0$ [115]. Hawking's semi-classical analysis [37, 38] of quantum fields on the curved but fixed black hole background changed this picture. Hawking observed that a scalar field in an initially pure state (the vacuum) at $\mathscr{I}^-$ turns out to be a thermal state of temperature T_H at $\mathscr{I}^+$, making the black hole a perfect black body radiator (see [98, 116]). The so-called Hawking temperature was determined to be

$$T_H = \frac{\kappa}{2\pi} = \frac{1}{8\pi M} \left(= \frac{\hbar c^3}{8\pi G k_B M} \right) . \tag{3.2.2}$$

This makes Eq. (3.1.16) a thermodynamic equation, i.e.

$$\mathrm{d}M = T_H \mathrm{d}S + \Omega_H \mathrm{d}L + \Phi_H \mathrm{d}Q \, , \tag{3.2.3}$$

and fixes the proportionality constant of Bekensteins analysis by means of[5]

$$S_{BH} = \frac{A}{4} \left(= \frac{k_B c^3 A}{4G\hbar} = \frac{k_B A}{4\ell_p^2} \right) . \tag{3.2.4}$$

According to this interpretation, Eq. (3.2.3) is a thermodynamic statement as T_H is the proper temperature of the black hole and $T_H \mathrm{d}S$ is the heat exchange, while the other terms describe ways of extracting work from the system (cfr. [97]).

The Bekenstein-Hawking entropy S_{BH} is given by the area of the black hole in units of Planck area ℓ_p^2 and can be interpreted as one bit of information sitting in a Planck size cell. Furthermore, this is a full quantum effect as in the limit $\hbar \to 0$ the temperature vanishes and the entropy diverges and thus infinitely much information can be stored at the horizon. This is exactly what classically happens, where in principle, an image of all in-falling matter is stored in an infinitely thin shell around the horizon (cfr. [117]).

The main puzzling consequence of this entropy formula is that the entropy grows with area instead of volume as it is known for any local field theory. This is in contradiction with all previously known physics and hints towards a holographic principle.

[5]The subscript BH here can have different interpretations as being short for "black hole" or for Bekenstein-Hawking as this entropy is known as Bekenstein-Hawking entropy.

The important question arising is: "Why is the generalised second law true?" In fact, one could think about a system, which is very light (mass of the system m compared to the black hole mass M is small, $m/M \ll 1$) and has low energy. Nevertheless, a priori there is no bound on the entropy, which this system can carry. Dropping it into the black hole would make this entropy inaccessible to the outside observer but the entropy of the black hole would still not increase significantly, since the mass was small ($A = 4\pi r_s^2 = 16\pi(M+m)^2 \approx 16\pi M^2$). This way the second law might be violated. This points towards a limit on how much entropy can be carried by matter of a certain energy E. Taking the generalised second law as a fundamental thermodynamic property of physics indeed shows such a bound on the entropy. This leads to the Bekenstein bound[6] [118]

$$S_{\text{matter}} \leq 2\pi ER \tag{3.2.5}$$

where E is the energy of the system and R is the radius of the smallest possible sphere enclosing the system. A detailed discussion can be found in [45].

A conceptually less subtle treatment compared to Bekenstein's arguments [118] on an entropy bound was given by Susskind [42]. The Susskind process describes how a system is converted into a black hole (cfr. [45]). Assume a system of isolated matter with entropy S_{matter} and mass E living in an asymptotically flat spacetime. A is the surface area of the smallest sphere completely enclosing the system. This notion is only meaningful if the metric is at least approximately spherically symmetric, i.e. in the weak gravity regime or in spherical symmetry. It is further assumed that the system is stable on a timescale larger than $\sqrt{A}$, and the time-dependence of A is negligible. The energy of the system has to be smaller than the mass M of a black hole of the same horizon area as the enclosing sphere $A = A_H = 8\pi M$. Otherwise, the system would have been collapsed to a black hole already.

The system can form a black hole by collapsing a shell of energy $M-E$ onto the system. For a well-separated shell the total entropy is given by

$$S_{\text{total}} = S_{\text{matter}} + S_{\text{shell}} \, .$$

In the final state of this process, a black hole has formed and the entropy is given by

$$S_{\text{total}} = S_{BH} = \frac{A}{4} \, .$$

[6]For the assumption of weakly gravitating matter in asymptotically flat spacetime.

By means of the generalised second law Eq. (3.2.1) the entropy has increased, which gives the spherical entropy bound for $S_{\text{shell}} > 0$ [42]

$$S_{\text{matter}} \leq \frac{A}{4} \,. \tag{3.2.6}$$

The spherical entropy bound is weaker than the Bekenstein bound as

$$S_{\text{matter}} \leq 2\pi MR \leq \pi R^2 = \frac{A}{4} \,.$$

Note that this argument is not regarding black holes but rather generic matter (with the assumptions stated above). Hence, given a matter system (satisfying the above assumptions), the entropy might scale with the volume V of the system as in local theories, but this entropy will always be smaller than the amount of entropy possibly being stored in the area of the enclosing sphere[7]. One could see this situation as follows [45]: A system, which collapses to a black hole has $N = e^S$, $S = A/4$, degrees of freedom in the final state. Assuming unitary evolution, the number of degrees of freedom is preserved, i.e. they heave to scale initially with area instead of volume. Keeping unitary and the generalised second law as a fundamental physical property led 't Hooft [43] and Susskind [42] to the development of the holographic principle:

Holographic principle

> "*A region with boundary of area A is fully described by no more than A/4 degrees of freedom, or about 1 bit of information per Planck area.*"

(cfr. [45] Bousso (2002), p. 14)

The considerations up to here do not take into account the discussion about the validity of the Bekenstein and spherical symmetric bound. Likewise, the holographic principle as stated above is only preliminary as it is just motivated by spherical symmetry and relies on spacelike volumes. Counterexamples to this can be found and the total discussion has many subtleties, which are addressed in [45]. As discussed in this reference, the above statement can be made covariant by introducing the covariant entropy bound [119], which relies on the entropy of lightlike surfaces.

[7] Note further that the area in Eq. (3.2.6) is given in Planck units, which makes this entropy extremely large for any macroscopic system. Still it scales with area, not volume.

3.3 Realisation of the holographic principle in AdS

The holographic principle as discussed above is a result of the semi-classical analysis of black holes. So far it is a principle and if it holds true, a fundamental theory of quantum gravity should respect it. Nevertheless, no theory of quantum gravity is known and hence no manifestation of the holographic principle is known either. A breakthrough was the discovery of the AdS/CFT correspondence by Maldacena [44]. It is a concrete realisation of the holographic principle in the context of string theory and AdS spaces. The full motivation comes from string theory, which is not further required in this thesis and hence not discussed here. Only the central statement and certain results of the AdS/CFT conjecture are shown here.

The AdS/CFT conjecture is a duality between two different theories and can be phrased as:

AdS/CFT correspondence

"$\mathcal{N} = 4$ Super Yang-Mills (SYM) theory with gauge group $SU(N)$ and Yang-Mills (YM) coupling constant g_{YM} [in $3+1$ dimensions]

is *dynamically equivalent* to

type II B superstring theory with string length $l_s = \sqrt{\alpha'}$ and coupling constant g_s on $AdS(5) \times \mathbb{S}^5$ with AdS-radius L (and N units of $F_{(5)}$ flux on $\mathbb{S}^5$).

The two parameters on the field theory side, i.e. g_{YM} and N, are mapped to the free parameters g_s and $L/\sqrt{\alpha'}$ on the string theory side by

$$g_{YM}^2 = 2\pi g_s \quad , \quad 2g_{YM}^2 N = L^4/\alpha'^2 \text{ ."} \tag{3.3.1}$$

(cfr. [89] Ammon and Erdmenger (2015), p. 180)

A few clarifications are needed at this point. First, SYM is the supersymmetric generalisation of YM theory[8]. While YM theory has conformal symmetry, $\mathcal{N} = 4$ SYM has superconformal-symmetry, which is the conformal group plus $\mathcal{N} = 4$ additional supersymmetric charges [89]. SYM is hence a theory of the gauge bosons A_μ and other scalar and fermionic non-gauge fields rendering the system supersymmetric. In $d = 3+1$, $\mathcal{N} = 4$ is the maximal amount of possible supersymmetry generators. The string theory lives on

[8] YM theory is given by the action $S_{YM} = \frac{1}{4g_{YM}} \int d^4x \, \mathrm{tr}\,(F_{\mu\nu}F^{\mu\nu})$, where $F = dA + \frac{1}{2}[A \wedge A]$ is the curvature 2-form of a $SU(N)$-connection A.

$AdS(5) \times \mathbb{S}^5$, which means that 5 of the 10 dimensions are compactified. The $\mathbb{S}^5$ part can be related to the internal (gauge) symmetries of the dual SYM theory. String theory admits, besides strings, further objects such as e.g. branes and (in the low energy limit) $F_{(5)}$-fluxes. Details of string theory, such as the meaning of branes and $F_{(5)}$-fluxes are not relevant in the rest of this thesis. Nevertheless, the number $F_{(5)}$-fluxes is related to the gauge degrees of freedom in the dual SYM theory. The spacetime is effectively $4+1$ dimensional, which is the number of non-compact dimensions. The above statement relates the quantum gravitational degrees of freedom, here given as string theory, to the local degrees of freedom in one dimension less, which is exactly what the holographic principle suggests.

This can be made more precise and is motivated as follows. AdS space plays a prominent role in this scenario. The reason is that it carries a "natural holographic screen", namely its boundary ∂AdS. As discussed above this is a conformal spacetime of one spatial dimension less (here $3+1$) and it is timelike. Hence, it could be thought of as a background on which some field theory is formulated. As ∂AdS is a projective space and has the conformal group as symmetry group, only CFTs can exist on this background[9]. The intuitive (but technically not correct) picture is that the CFT, here SYM theory, lives on the boundary of $AdS(5)$, which is the holographic screen. Further, it was discussed that $AdS(5)$ behaves as a box for massive particles and lightlike degrees of freedom are infinitely red shifted towards the boundary. This leads to strict fall-off conditions for all fields, including gravitational perturbations, which is central for imposing boundary conditions (see the discussion below).

On the CFT side 't Hooft [120] observed that in the limit of $N \to \infty$ and fixed 't Hooft coupling $\lambda = g_{YM}^2 N$, the so-called 't Hooft limit, SYM is effectively classical. By using Eq. (3.3.1), the 't Hooft limit implies on the gravitational side

$$\lambda = g_{YM}^2 N = \frac{L^4}{2\alpha'^2} = \text{fixed} \quad , \quad N = \frac{L^4}{4\pi\alpha'^2 g_s} = \frac{\lambda}{2\pi g_s} \to \infty \, , \tag{3.3.2}$$

i.e. $g_s \to 0$. As the string coupling g_s vanishes, the theory becomes effectively classical, which is classical string theory in this case. Further, requiring $\lambda \gg 1$, i.e. the large coupling limit in SYM, corresponds to vanishing string length $\alpha' = l_s^2 \to 0$. This limit of type II B string theory corresponds to type II B supergravity, i.e. a supersymmetric version of classical Einstein-Gravity (plus supersymmetric partners and additional fields) (see e.g. [89, 121]). These different regimes are depicted in Fig. 3.6. Note that this duality is a weak-strong duality, i.e. strong coupling in SYM corresponds to the weakly coupled supergravity regime.

[9] All other theories would break the conformal symmetry of the background ∂AdS.

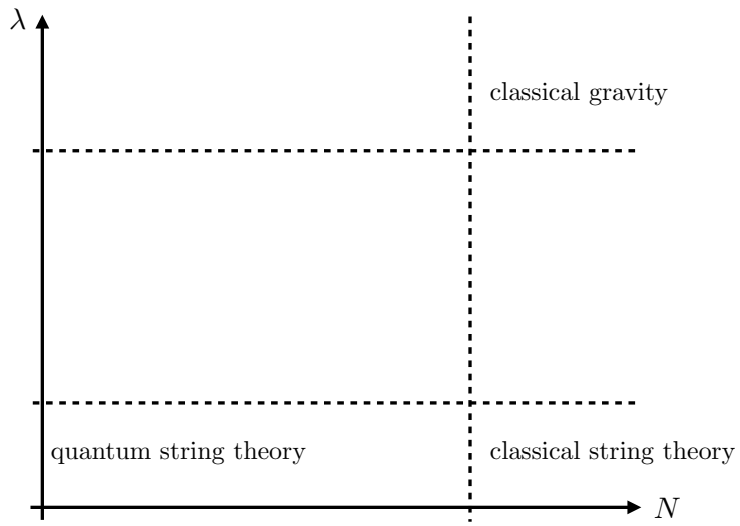

FIGURE 3.6: *Regimes of different approximations of quantum gravity depending on the parameter* (λ, N) *(see [122]).*

As a result of the above arguments, it is useful to realise this correspondences in AdS space and that it is natural that the dual theory is a CFT. The precise correspondence can be motivated by string theory, which explains the parameter matching Eq. (3.3.1) and all other details of the conjecture as $\mathcal{N} = 4$, the appearance of $\mathbb{S}^5$, etc. Although these are important components of the AdS/CFT correspondence, these details will not play any role in the following, and are therefore not further considered. A more important and insightful point is the precise mathematical formulation of the correspondence. The strong AdS/CFT conjecture can be phrased as follows [89]:

Strong AdS/CFT conjecture

The generating CFT partition function is equal to the string partition function with suitable boundary conditions, i.e.

$$\mathcal{Z}_{CFT}[\phi_o^i] = \int \mathcal{D}\Phi_I \, e^{-S_{CFT}[\Phi_I] + \int \mathrm{d}^D x \, \mathcal{O}^i(x)\phi_o^i(x)} \stackrel{!}{=} \mathcal{Z}_{\text{string}}|_{\lim_{z\to 0}(\phi^i(z,x)z^\alpha)=\phi_o^i(x)} \ , \tag{3.3.3}$$

where Φ_I is a representative for all dynamical fields of the CFT, $\mathcal{O}^i(x)$ are local (not further specified) operators, $D = d+1$ is the spacetime dimension of the CFT, $D+1$ the dimension of string theory, z the inverse radial coordinate of the Poincaré-patch (cfr. Eq. (2.1.11)) and α is a suitable exponent for imposing the boundary condition. The fields ϕ_o^i are the sources of th correlation function of $\mathcal{O}^i$ and are also the boundary values of all string theory fields (including the gravitational degrees of freedom).

The parameter α is related to the fall-off behaviour of the field ϕ. As AdS behaves like a box and one requires the fields to be normalisable in the boundary limit, i.e. $\lim_{z\to 0}\phi(z,x) = 0$, the field vanishes. The fall-off behaviour is determined by the kind of field under consideration, its mass and spacetime dimension. In the case of a scalar field of mass m, it is $\alpha = -\frac{d}{2} + \sqrt{\frac{d^2}{4} + m^2L^2}$ for which the limit $\lim_{z\to 0}\phi(z,x)z^\alpha$ is finite (see e.g. [47, 122]). In turn, the operator $\mathcal{O}$ is a conformal operator of a specific conformal weight Δ, i.e.

$$x \mapsto \lambda x \quad , \quad \mathcal{O}(x) \mapsto \lambda^{-\Delta}\mathcal{O}(x) = \mathcal{O}'(\lambda x) \ .$$

Since these operators couple to the fields ϕ_o in $\mathcal{Z}_{CFT}[\phi_o]$, their behaviour has to be compatible for leaving the coupling term conformally invariant. This relates the conformal weight Δ to the fall-off exponent α, i.e. the mass of the scalar field as (see [89, 122])

$$m^2L^2 = \Delta\,(\Delta - d) \ . \tag{3.3.4}$$

The equivalence Eq. (3.3.3) allows to compute correlations of operators $\mathcal{O}$ in the CFT by means of a string theory computation. On the other hand, knowing the CFT side, allows for string theory predictions. This strong form of the AdS/CFT conjecture can thus be thought of as a non-perturbative definition of the string theory partition function by means of non-redundant information encoded in a local field theory [44, 46, 47]. Nevertheless, there are some caveats with this. Firstly, one needs to know the AdS/CFT-dictionary, i.e.the information of which operator $\mathcal{O}$ couples to the boundary condition of which field

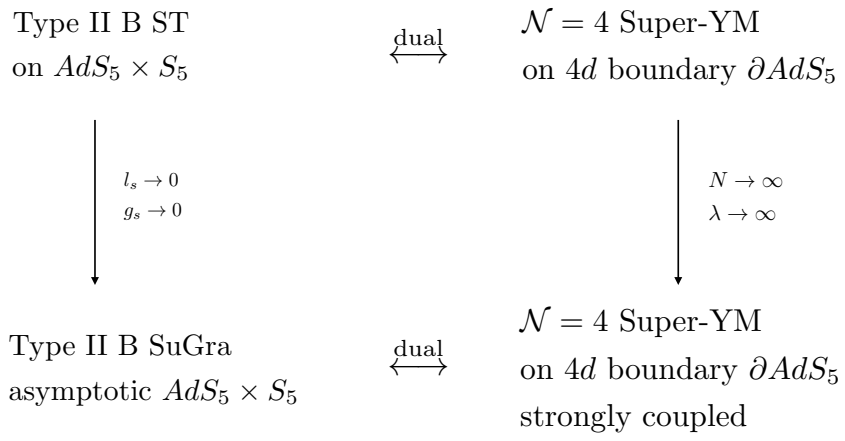

FIGURE 3.7: *Graphical representation of the strong and weak AdS/CFT conjecture.*

ϕ_o on the gravitational side. Eq. (3.3.3) is only meaningful and useful if this dictionary is known and complete, i.e. if all (physically) relevant operators of the CFT have a dual field. For example, perturbations of the metric in AdS correspond to the sources of the energy-momentum tensor of the CFT. Secondly, it is not clear how and if it is possible to extract all quantum string theory information from a known generating functional of the CFT. The research direction trying to answer this question is called bulk reconstruction (see e.g. [123, 124] for introductory lectures) and is essential for well-defining a theory of quantum gravity through this duality. The AdS/CFT conjecture might be summarised as follows:

The AdS/CFT-conjecture has three components,

1. the CFT in $D = d + 1$-dimensions,
2. non-perturbative string theory in $D + 1$ dimensions,
3. and the AdS/CFT dictionary containing all couplings $\int \mathrm{d}^D x \, \mathcal{O}(x)\phi_o(x)$.

If two of them are known, the third one might be extracted by means of Eq. (3.3.3).

The most studied regime of this conjecture is in the 't Hooft limit ($N \to \infty$) with $\lambda \gg 1$. This is the regime of the weak conjecture as the CFT becomes effectively classical. The weak conjecture states

$$\mathcal{W}_{CFT}[\phi_o] = \log\left(\mathcal{Z}_{CFT}[\phi_o]\right) \simeq S_{\text{Sugra}}[\phi]\Big|_{\lim_{z\to 0}(\phi(z,x)z^\alpha)=\phi_o(x)} . \tag{3.3.5}$$

Here, S_{Sugra} is the classical on-shell supergravity action with the given boundary conditions. Fig. 3.7 represents the strong and weak conjecture graphically.

Until now, the AdS/CFT conjecture is well-motivated, but still a conjecture. In the 't Hooft limit, i.e. the weak conjecture explicit computations are possible on both sides, and relations between quantities on the different sides can be derived. All tests so far were successful and give a strong evidence for the conjecture. Special entries of the dictionary were also derived, relating, e.g. the entanglement-entropy of the CFT to minimal surfaces in AdS (cfr. Ryu-Takayanagi formula [125, 126]) or geodesics to two-point correlators [127]. The latter will be of fundamental significance in Chpt. 5. The strong regime of the conjecture is not much studied as it is unknown how the dictionary translates from the weak to the strong regime and it is equally unknown how string theory can be defined non-perturbatively (besides using the strong conjecture). Due to this fact, it is impossible to perform computations on the quantum gravity side and compare these with CFT results.

3.4 Outlook: Gauge/Gravity Duality

The holographic principle as it was motivated at the beginning of this chapter only takes semi-classical gravity arguments into account. From this point of view, it should be considered in every quantum gravitational theory. Indeed, there are considerations of generalising the AdS/CFT correspondence to other asymptotic spacetimes as Minkowski/CFT [128] or de-Sitter/CFT [129]. A more general concept of AdS/CFT is the gauge/gravity duality, which simply states the duality of quantum gravity and a gauge theory. AdS/CFT is very interesting, as it is a concrete realisation of this idea. Nevertheless, to really prove this conjecture, it would be necessary to solve at least one side of the conjecture completely, which is out of reach. A further problem on the gravity side is that string theory is so far only well-defined in a perturbative sense, and hence the full string partition function $\mathcal{Z}_{\text{string}}$ is not known. An expansion of the framework to other approaches of quantum gravity might be useful. This allows to interchange techniques and gain knowledge on other approaches, string theory, and the holographic principle itself. LQG e.g. is a non-perturbative approach to quantum gravity and at least the partition function $\mathcal{Z}_{\text{LQG}}$ can be defined, although it cannot be computed explicitly. The idea of AdS/CFT can be used to test results in LQG by translating it to the field theory side and doing simulations there. This could in fact be viewed as an experiment or a test of the quantum gravity theory [69, 70]. If the gauge/gravity duality holds, the gravity result should be compatible with the CFT behaviour, where techniques are developed to perform computations. This gives some at least a hypothetical guideline for constructing and testing a theory of quantum gravity. Indeed, there is work in $3d$ gravity [130–132], which computes $\mathcal{Z}_{\text{LQG}}$ exactly in three Euclidean dimension, and the dual theory on a finite (not asymptotic) boundary. Approaches as LQG could be used to test the non-perturbative regime of AdS/CFT. The central problem is, that it is not known if LQG is applicable in this framework as

AdS/CFT is motivated by string theory, which up to current knowledge, is different from LQG. The long term strategy, which was started in this thesis and the projects presented in the following (cfr. Chpt. 5), is to test if LQG can be meaningfully embedded in the framework of AdS/CFT and holography in general, as well as which consequences this has for both approaches. In more general terms, the work of [130–132] might be extended and general holographic properties of LQG can be worked out. If this is true, LQG might be located at the up-left corner in Fig. 3.6 and the relation of LQG as a sub-sector of string theory could be studied further.

4

Loop Quantum Cosmology

As quantum theory of gravity LQG is a non-perturbative and background independent approach, which was developed over the last 30 years [48, 133, 134]. It is a non-perturbative approach and hence a candidate to describe the quantum behaviour around the singularity. The quantum corrected behaviour in the vicinity of the singularity could further be tested by going beyond the weak conjecture. In principle, it could be tried to solve the full quantum gravitational partition function $\mathcal{Z}_{QG}$. Progress has been made in the 3 dimensional Euclidean theory [130–132]. Nevertheless, for dimensions ≥ 4 and with a cosmological constant, this computation is without prospects, as the problem goes much further than fully solving classical GR, which is already technically impossible.

Further progress has been made in the context of symmetry reduced models and the loop quantisation of cosmology. Due to the high amount of symmetries, the strategy of full LQG can be explicitly worked out in these simplified settings. This will be the starting point of later investigations (see Chpt. 5). For this purpose, classical cosmology and its quantisation by means of loop techniques will be presented in the following chapter.

The chapter mainly follows the references [135, 136]. Further selected important reviews of the field are [16, 137–141]. The chapter first recalls classical cosmology and its Hamiltonian description. Then, classical polymerisation and the quantum theory are introduced. The chapter closes with discussing the connection to full LQC.

4.1 Classical Cosmology

Due to the cosmological principle, it is reasonably assumed that the universe on large scales is isotropic and homogeneous. This is reflected in the FLRW-metric

$$\mathrm{d}s^2 = -N(t)^2\mathrm{d}t^2 + \frac{a(t)^2}{1-kr^2}\mathrm{d}r^2 + a(t)^2 r^2 \mathrm{d}\Omega_2^2\,, \tag{4.1.1}$$

where $N(t)$ is the lapse function controlling the gauge freedom of choosing the time coordinate, $a(t)$ is the scale factor, which measures the size of the universe, r is a dimensionless coordinate, and $k \in \{-1, 0, 1\}$ is a constant controlling the spatial curvature of constant t-slices. Imposing maximal symmetry on these 3-dimensional surfaces allows three solutions, namely a 3-sphere ($k = 1$), flat space ($k = 0$) or hyperbolic space ($k = -1$) with constant positive, zero and negative curvature. For simplicity the following discussion is restricted to the simplest case of flat slices, i.e. $k = 0$. Nevertheless, LQC was also studied in the context of $k \neq 0$ (see [139]). The metric ansatz can be inserted into the Einstein-Hilbert action

$$S_{EH} = \frac{1}{16\pi G}\int_{\mathcal{M}} \mathrm{d}^4x\,\sqrt{-g}R\,, \tag{4.1.2}$$

which is further simplified by assuming vanishing cosmological constant $\Lambda = 0$. With $\sqrt{-g} = Na^3r^2\sin(\theta)$ this leads to

$$S_{EH}[N,a] = -\frac{V_o}{16\pi G}\int \mathrm{d}t\,\frac{6a(t)\left(a(t)N(t)\ddot{a}(t) - a(t)\dot{a}(t)\dot{N}(t) + N(t)\dot{a}(t)^2\right)}{N(t)^2}\,, \tag{4.1.3}$$

where the dot denotes derivatives with respect to t and

$$V_o = \int \mathrm{d}r\,\mathrm{d}\theta\mathrm{d}\phi\, r^2\sin(\theta)\,.$$

An important issue with symmetry reduced models is divergent integrals after the symmetry reduction. In the action appears V_o, the spatial coordinate volume. For non-compact topologies (e.g. $\mathbb{R}^4$) this integral diverges. Due to this, a fiducial cell of coordinate volume V_o is introduced to regularise these integrals [137]. The specific size is completely arbitrary and physical results cannot depend on it. For compact topologies as e.g. $\mathbb{R}\times\mathbb{T}^3$, the integral is finite, but the 3-coordinate volume is still completely ambiguous.

Due to partial integration, it is possible to remove the second derivatives from the action

$$\frac{6a\left(aN\ddot{a} - a\dot{a}\dot{N} + N\dot{a}^2\right)}{N^2} = \frac{6a\dot{a}^2}{N} - \frac{\mathrm{d}}{\mathrm{d}t}\left(\frac{6a^2\dot{a}}{N}\right) ,$$

and after neglecting the boundary term, leading to

$$S_{EH}[N,a] = -\frac{3V_o}{8\pi G}\int \mathrm{d}t\, \frac{a\dot{a}^2}{N} . \tag{4.1.4}$$

The dynamics of the gravitational sector is trivial, unless matter is coupled. A massless scalar field is used as matter source for simplicity. The matter action for a homogeneous scalar field $\phi = \phi(t)$ is

$$S_M = -\frac{1}{2}\int_M \mathrm{d}^4x\sqrt{-g}g^{\mu\nu}\left(\nabla_\mu\phi\right)\left(\nabla_\nu\phi\right) = V_o\int \mathrm{d}t\, \frac{a^3\dot{\phi}^2}{2N} . \tag{4.1.5}$$

In a last step,

$$\bar{a}^3 = V_o a^3 = \int \mathrm{d}r\mathrm{d}\theta\mathrm{d}\phi r^2\sin(\theta)a^3$$

is defined. This is the physical volume of the fiducial cell and will be used as canonical variable in the following.

The full action is

$$S[N,\bar{a},\phi] = \int \mathrm{d}t\, \underbrace{-\frac{3}{8\pi G}\frac{\bar{a}\dot{\bar{a}}^2}{N} + \frac{\bar{a}^3\dot{\phi}^2}{2N}}_{=:L} . \tag{4.1.6}$$

For the quantum theory a canonical analysis is necessary. Due to the large class of symmetries, the Einstein-Hilbert action is reduced to a mini-superspace model, i.e. it is effectively a one-dimensional system of a point particle, instead of a field theory. Clearly, there is no description of a point particle, as $\bar{a}$ is a component of the metric field $g_{\mu\nu}$. The canonical momenta are defined as usual by

$$p_a = \frac{\partial L}{\partial\dot{\bar{a}}} = -\frac{3}{4\pi G}\frac{\bar{a}\dot{\bar{a}}}{N} , \tag{4.1.7}$$

$$p_\phi = \frac{\partial L}{\partial\dot{\phi}} = \frac{\bar{a}^3\dot{\phi}}{N} , \tag{4.1.8}$$

$$p_N = \frac{\partial L}{\partial\dot{N}} \approx 0 . \tag{4.1.9}$$

Where $\approx$ denotes weak equality (see App. A for a detailed explanation) As $p_N \approx 0$, the system cannot be solved for the derivatives $\dot{\bar{a}}$, $\dot{\phi}$ and $\dot{N}$, which indicates constrains. This is expected from the ADM-formalism of full GR (see [95]), and consequently applies also to the cosmology sector. These constraints have to be analysed according to Dirac algorithm [142] (see also [143] for an introduction). First, the Legendre transform yields

$$\begin{aligned} H_T &= p_a \dot{\bar{a}} + p_\phi \dot{\phi} + \lambda p_N - L \\ &= \frac{N}{2}\left(-\frac{4\pi G}{3}\frac{p_a^2}{\bar{a}} + \frac{p_\phi^2}{\bar{a}^3}\right) + \lambda p_N \ , \end{aligned} \tag{4.1.10}$$

where λ is a Lagrange multiplier. Stability of the constraint $p_N \approx 0$ leads to the secondary constraint, here also called Hamiltonian constraint

$$\dot{p}_N = \{p_N, H_T\} = \frac{1}{2}\left(-\frac{4\pi G}{3}\frac{p_a^2}{\bar{a}} + \frac{p_\phi^2}{\bar{a}^3}\right) =: \mathcal{H} \overset{!}{\approx} 0 \ . \tag{4.1.11}$$

The Dirac algorithm terminates here as $\dot{\mathcal{H}} = \{\mathcal{H}, H_T\} = 0$ and thus the constraint $\mathcal{H}$ is stable during time evolution. N appears as a Lagrange multiplier whose dynamics ($\dot{N} = \lambda$, $\dot{p}_N = 0$) is completely encoded in the arbitrary function λ. Thus, it is possible to remove N and p_N from the phase space and treat N as arbitrary Lagrange multiplier. This is exactly what was expected from the beginning, as N simply encodes the choice of the t-coordinate, which is arbitrary and physics is independent thereof. The constraints in the Hamiltonian formalism are rendering this immediately visible. The Hamiltonian constraint generates gauge transformations, i.e. coordinate changes in t as well as the dynamics of the system. This is the exact same behaviour as full GR, however symmetry reduced (cfr. e.g. [95] or [48] for more details).

The canonical theory is described by the phase space spanned by $(\bar{a}, p_a)$, (ϕ, p_ϕ), the Hamiltonian, which is a constraint

$$H_T = N\mathcal{H} \quad , \quad \mathcal{H} = -\frac{2\pi G}{3}\frac{p_a^2}{\bar{a}} + \frac{p_\phi^2}{2\bar{a}^3} \approx 0 \ , \tag{4.1.12}$$

and the symplectic structure inducing the Poisson brackets

$$\{\bar{a}, p_a\} = \{\phi, p_\phi\} = 1 \ . \tag{4.1.13}$$

By means of a canonical transformation, the variables are changed to the physical quantities

$$v = \bar{a}^3 \ , \tag{4.1.14}$$

$$b = \frac{p_a}{3\bar{a}^2} = -\frac{1}{4\pi G}\frac{\dot{\bar{a}}}{N\bar{a}} \ . \tag{4.1.15}$$

Here v is the spatial volume of the fiducial cell and b is related to the Hubble rate $\dot{\bar{a}}/N\bar{a}$ (see e.g. [93, 95, 102]). Furthermore, on-shell, i.e. for solutions of the equations of motion, it is $R \propto b^2$. Hence b measures the curvature of the spacetime. Off-shell it is related to the extrinsic curvature of the spatial slice. This relation to R makes b a spacetime scalar, which will be important for the classical polymerisation (cfr. Sec. 4.2). In these variables, the Hamiltonian becomes

$$H_T = N\mathcal{H} \quad , \quad \mathcal{H} = -12\pi G\frac{vb^2}{2} + \frac{p_\phi^2}{2v} \approx 0 \ , \tag{4.1.16}$$

which makes it convenient to use units in which $12\pi G = 1$.

Having determined the Hamiltonian framework, it is instructive to study the solutions and solution strategies. The Hamiltonian equations of motion are

$$-\frac{vb^2}{2} + \frac{p_\phi^2}{2v} \approx 0 \ , \tag{4.1.17a}$$

$$\dot{v} = -Nvb \ , \tag{4.1.17b}$$

$$\dot{b} = \frac{Nb^2}{2} + \frac{Np\phi^2}{2v^2} \ , \tag{4.1.17c}$$

$$\dot{\phi} = N\frac{p_\phi}{v} \ , \tag{4.1.17d}$$

$$\dot{p}_\phi = 0 \ . \tag{4.1.17e}$$

A number of solution strategies are possible at this point. It is not possible to integrate these equations, as they are based on the arbitrary, not determined function N. One strategy would be to de-parametrise the equations by re-expressing them in terms of the scalar field ϕ, using this as a physical clock. This way, N would drop out and the equations are solvable. The other strategy is to set a convenient functional dependence of N. This is a gauge choice, as it determines the interpretation of the coordinate t. Physical results will not depend on this choice[1]. As this will also be used in Chpt. 6, the second strategy

[1]This fixing of N is possible even before computing the equations of motion. This might lead to additional terms which are proportional to the constraint as $\{\mathcal{O}, H_T\} = \mathcal{H}\{\mathcal{O}, N\} + N\{\mathcal{O}, \mathcal{H}\}$. The first term always vanishes after imposing $\mathcal{H} \approx 0$.

is adopted.

A useful choice is $N = 1$ which makes t the co-moving FLRW-time (cfr. Eq. (4.1.1)). From Eq. (4.1.17e) it is immediate that p_ϕ is an integration constant. Using the constraint (4.1.17a) gives

$$b = \pm\frac{p_\phi}{v} \,, \tag{4.1.18}$$

where the sign determines the contracting or expanding branch, and $v, p_\phi > 0$ is assumed without loss of generality. Inserting this into Eq. (4.1.17b) yields

$$\dot{v} = \mp p_\phi \quad \Longrightarrow \quad v = \mp p_\phi \,(t - t_i) + v_i \,, \tag{4.1.19}$$

with the initial condition $v(t_i) = v_i$. Note that for any N, inserting the Hamiltonian constraint (4.1.17a) into Eq. (4.1.17b), leads to

$$H_o^2 = \left(\frac{\dot{v}}{3Nv}\right)^2 = \frac{p_\phi^2}{9v^2} = \frac{2}{9}\rho \left(= \frac{8\pi G}{3}\rho\right) \,, \tag{4.1.20}$$

with the Hubble rate $H_o = {}^{\dot{\bar{a}}}/_{N\bar{a}}$ and $\rho = {}^{p_\phi^2}/_{2v^2}$ as the energy density of the scalar field. This is exactly the classical Friedmann equation (see e.g. [93, 102]) which will be modified in the next section.

Finally, with the solution (4.1.19), Eq. (4.1.17d) can be solved

$$\dot{\phi} = \frac{p_\phi}{\mp p_\phi \,(t - t_i) + v_i} \quad \Longrightarrow \quad \phi = \mp \ln\left(\frac{\mp p_\phi \,(t - t_i) + v_i}{v_i}\right) + \phi_i \,, \tag{4.1.21}$$

with the initial condition $\phi(t_i) = \phi_i$.

Several remarks are necessary at this point. The system is now solved completely in the gauge $N = 1$. Hence, the line element is given by

$$\mathrm{d}s^2 = -\mathrm{d}t^2 + a(t)^2 \left(\mathrm{d}r^2 + r^2 \mathrm{d}\Omega_2^2\right) \,, \tag{4.1.22}$$

with $a(t) = ({}^{v(t)}/_{V_o})^{\frac{1}{3}}$ and $v(t)$ given by Eq. (4.1.19). Changing the time coordinate changes N and the general functional form of the solutions. Nevertheless, it is possible to write down the solutions in a gauge independent way by de-parametrising the system and using

the matter ϕ as natural clock. This leads to

$$v(\phi) = v_i e^{\mp(\phi-\phi_i)} \,. \tag{4.1.23}$$

The quantity $v(\phi)$ can be used to compare different cosmological theories in possibly different charts, without the possible obstructions in choosing different gauges[2]. Still, v is not a physical observable as it depends on the fiducial volume V_o. Instead, b is physically observable. This is the Hubble rate and related to the spacetime curvature and $\rho = p_\phi^2/v^2$, which is the energy density of the scalar field.

The physically most important observation is that for $\phi \to \pm\infty$, the volume v vanishes. In co-moving eigentime t this happens at the finite value $t_s = \pm v_i/p_\phi + t_o$. At this instance of time, the curvature and the Hubble rate diverge, as $b = p_\phi/v \to \infty$. This is a curvature singularity of the spacetime, which is called big bang for the positive sign in Eq. (4.1.19) and big crunch for the negative sign. The predictions of GR are mostly valid up to this point, but fail at the singularity. It is expected that a quantum theory of gravity will play an essential part in understanding the physics at this singularity. A possible quantisation of cosmology is discussed in the following section.

4.2 Classical Polymerisation

The next sections will discussed how cosmology can be quantised according to LQG. A necessary step for this is a regularisation of the Hamiltonian, which is known as *classical polymerisation*. This method modifies the classical Hamiltonian such that it can be represented on a LQG-like Hilbert space. It has the advantage that high-curvatures and singularities are already resolved on this effective level and it results in quantised volumes in the quantum theory (see Sec. 4.3 for more details). The fact that volumes are quantised makes this approach independent from LQG to a certain extend and could be considered as a method of quantising symmetry reduced spacetimes, taking the idea that geometry is quantised in a quantum theory of gravity as physical guideline[3]. Nevertheless, the approach presented here is effective, but emerges from the full quantum theory framework (see Sec. 4.3). Polymerisation is a necessary first step for this construction, but could also be viewed as the approximation, where quantum states always peaked on classical geometries and remain peaked. In that case the quantum theory can be approximated

[2]The line element can be written as $\mathrm{d}s^2 = -N^2/\dot{\phi}^2\,\mathrm{d}\phi^2 + a(\phi)^2\left(\mathrm{d}r^2 + r^2\mathrm{d}\Omega_2^2\right)$ which is completely independent of the choice of t-coordinate. In fact, using the equations of motion, this line element can be written as $\mathrm{d}s^2 = -2/\rho(\phi)\mathrm{d}\phi^2 + (v(\phi)/V_o)^{\frac{2}{3}}\left(\mathrm{d}r^2 + r^2\mathrm{d}\Omega_2^2\right)$, which only depends on physical quantities.

[3]This is an insight coming from several different approaches, such as LQG, spin foams, Causal Dynamical Triangulation (CDT), NCG.

with the effective spacetime. This is discussed in detail below.

The idea of classical polymerisation is the replacement of certain phase space variables by means of *point holonomies*. In the case of cosmology, b is a suitable variable and the replacement

$$b \mapsto e^{ib}$$

allows a quantisation along the lines of LQG. This will become clearer when the quantum theory and operator representations are discussed in the next section, Sec. 4.3. On this basis, the Hamiltonian is regularised by simply replacing

$$b \longmapsto f(e^{i\lambda b}) \ . \tag{4.2.1}$$

The scale λ is the so-called polymerisation scale and should be presumed as proportional to the Planck length ℓ_p. The critical and model building ingredient is the choice of f on the one hand and the choice of λ on the other hand. One requirement is that f should be chosen so that it reduces to b in the "classical regime" i.e.

$$f(e^{i\lambda b}) \xrightarrow{\lambda b \ll 1} b \ . \tag{4.2.2}$$

This guarantees that classically reliable physics is not changed. The choice of λb defines the "classical regime". In principle, one should think of λ as an arbitrary phase space function, as it has been used in the original LQC paper (see [144]). Such a choice would be called $\bar{\mu}$-scheme (historically λ was represented by μ). Allowing λ to be phase space dependent is equivalent to changing variables and using constant λ there. This is exactly the reason why (v, b)-variables were chosen in the previous section. As argued there, b is related to the Ricci scalar. Hence, b becomes large only in the high curvature regime. Considering $\lambda = const. = \mathcal{O}(\ell_p)$ corresponds to $\lambda b = \mathcal{O}(1)$ in the regime of Planck curvature, which is where classical GR is expected to break down. Choosing this kind of λ implies together with Eq. (4.2.2) that the classical theory still holds true in the low (with respect to the Planck scale) curvature regime. Note that other choices are possible. One example is the μ_o-scheme, which was originally introduced in [145, 146]. For LQC there is no more promising scheme known, although alternatives are discussed. As function f, the sin-function can be chosen as it is the simplest possibility for which Eq. (4.2.2) holds true.

Also for this choice alternatives are discussed [59, 147, 148][4]. The classical Hamiltonian is thus modified by replacing

$$b \longmapsto \frac{\sin(\lambda b)}{\lambda} \,. \tag{4.2.3}$$

Note that this function is bounded and the maximal value for the curvature is $\propto 1/\lambda^2$. The effective Hamiltonian (classical Hamiltonian which takes quantum corrections into account) is

$$H_{eff} = N\mathcal{H}_{eff} \quad . \quad \mathcal{H}_{eff} = -\frac{v\sin(\lambda b)^2}{2\lambda^2} + \frac{p_\phi^2}{2v} \approx 0 \,. \tag{4.2.4}$$

It is already visible at this point that the energy density of the scalar field $\rho = p_\phi^2/2v^2$ remains bounded on the constraint surface, since $\sin(\lambda b)/\lambda$ is bounded also.

The new physics of this model can be analysed in more detail. For doing so the model is solved "classically". This means that the system is treated as a classical Hamiltonian system and also the spacetime in the end will be classical. Nevertheless, the dynamics is modified according to additional (non-perturbative) terms which are expected from the quantum theory and can be viewed as effective treatment of quantum cosmology. The approximation is taking quantum states that are always peaked on classical geometries and remain peaked. Only this allows the approximation of the quantum region by the effective spacetime. It remains to be discussed in the full quantum theory if this approximation is valid. The effective equations of motion are

$$\dot{v} = -Nv\frac{\sin(\lambda b)}{\lambda}\cos(\lambda b) \quad , \quad \dot{b} = \frac{N}{2}\frac{\sin(\lambda b)^2}{\lambda^2} + N\frac{p_\phi^2}{2v^2} \,, \tag{4.2.5a}$$

$$\dot{\phi} = N\frac{p_\phi}{v} \quad , \quad \dot{p}_\phi = 0 \,, \tag{4.2.5b}$$

$$-\frac{v}{2}\frac{\sin(\lambda b)^2}{\lambda^2} + \frac{p_\phi^2}{2v} = 0 \,. \tag{4.2.5c}$$

Again, using $p_\phi = const.$ as well as the Hamiltonian constraint yields

$$\frac{\sin(\lambda b)}{\lambda} = \pm\frac{p_\phi}{v} \,. \tag{4.2.6}$$

[4]Further ambiguities come from allowing also other regularisations. E.g. one could consider to polymerise also p_ϕ or modify v in order to preserve different classical structures [149–153]. All in all there is a lot of freedom in the model building, nevertheless it is hoped and already true that important lessons about quantum gravity can be learned from these simple models.

Inserting this result in the equation for v, Eq. (4.2.5a), this can be rewritten as

$$\begin{aligned} H_o^2 &= \left(\frac{\dot{v}}{3Nv}\right)^2 = \frac{1}{9}\frac{\sin(\lambda b)^2}{\lambda^2}\cos(\lambda b)^2 = \frac{p_\phi^2}{9v^2}\left(1-\sin(\lambda b)^2\right) \\ &= \frac{p_\phi^2}{9v^2}\left(1-\lambda^2\frac{p_\phi^2}{v^2}\right) = \frac{1}{9}\rho\left(1-\frac{\rho}{\rho_{crit}}\right) , \end{aligned} \tag{4.2.7}$$

with the Hubble rate $H_o = \dot{a}/Na$, the energy density of the scalar field $\rho = p_\phi^2/2v^2$, and $\rho_{crit} = 1/2\lambda^2$ the critical density. This equation is also known as modified Friedmann equation [16]. It manifests that the energy density is bounded by a universal (phase space independent) critical density ρ_{crit}. When this critical density is reached, $H_o = 0$ and the spacetime collapse stops. The curvature singularity is avoided. Furthermore, for low energy densities this equation reduces to the classical Friedmann equation Eq. (4.1.20).

Fixing the lapse $N = 1$ allows to solve Eq. (4.2.7) with the result

$$\frac{v\dot{v}}{\sqrt{v^2-\lambda^2p_\phi^2}} = \pm p_\phi \quad \Longrightarrow \quad v(t) = \sqrt{\left(\pm p_\phi\,(t-t_i) + \sqrt{v_i^2-\lambda^2p_\phi^2}\right)^2 + \lambda^2p_\phi^2}\,, \tag{4.2.8}$$

again with the initial condition $v(t_i) = v_i$. Inserting this into the first equation of (4.2.5b) leads to

$$\phi(v) = \pm\left(\sinh^{-1}\left(\frac{v}{\lambda p_\phi}-1\right) - \sinh^{-1}\left(\frac{v_i}{\lambda p_\phi}-1\right)\right) + \phi_i \tag{4.2.9}$$

with $\phi(t_i) = \phi_i$ which solves the system completely.

From Eq. (4.2.8) it becomes evident that v never reaches zero and in fact has the minimal value $v_{min} = \lambda p_\phi$. The singularity is thus resolved as the curvature is $|R| \leq 2/\lambda^2$ and remains bounded. Also, the energy density is bounded by $\rho \leq \rho_{crit} = 1/2\lambda^2$. Both bounds are independent of initial conditions and hence unique. The Hubble rate $\dot{v}/v$ vanishes at this minimal value, i.e. the contraction is converted into an expansion. This resolves the big bang by means of a *big bounce*. Finally, the expression Eq. (4.2.9) can be inverted, leading to

$$v(\phi) = \lambda p_\phi \cosh\left(\pm(\phi-\phi_i) + \cosh^{-1}\left(\frac{v_i}{\lambda p_\phi}\right)\right) . \tag{4.2.10}$$

Due to $\cosh(x) \geq 1$ this makes obvious that $v \geq \lambda p_\phi$. As argued above, this expression

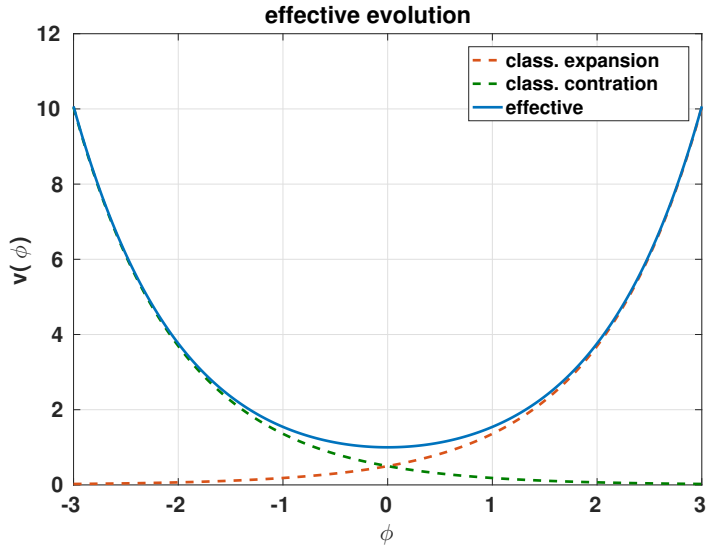

FIGURE 4.1: *Classical and effective evolution of the volume $v(\phi)$. It is visible that the effective dynamics quickly approach the classical solutions for expansion and contraction. Here, $\lambda = 1$ and $\phi_i, v_i = 0$ was chosen. As the volume is not a physical observable, the prefactor (here λp_ϕ) can be absorbed in the coordinate choice.*

is independent of any coordinate choice and can be compared with the classical result Eq. (4.1.23). This is shown in Fig. 4.1. Indeed, for large $|\phi|$ it is

$$v(\phi \to \pm\infty) \propto e^{\pm|\phi|} \,, \tag{4.2.11}$$

which coincides with the classical solution far away from the bounce[5]. Note that v is no physical observable as it depends on the fiducial cell size V_o. Also v/V_o, which is a^3 and fiducial cell independent, is not a scalar as the pre-factor can be absorbed by means of rescaling the r-coordinate. This discussion plays a crucial role in the analysis of effective polymer black holes, see Sec. 6.

[5]The prefactor of the effective model and the classical model does not match completely. Nevertheless this factor can simply be absorbed by rescaling the coordinate r.

Effective polymer cosmology is a regularised version of cosmology,

- which can be quantised with LQG techniques,
- whose effective equations replace the classical singularity by a bounce at a universal energy density $\rho_{crit} = {}^1/_{2\lambda^2}$,
- which predicts a unique upper curvature bound, and
- which is well-approximated by the classical Friedmann dynamics in the low curvature regime.

It is important that these effective dynamics should be considered as the evolution of expectation values with respect to coherent states. It is assumed that these states are peaked on classical geometries and remain peaked there during quantum evolution. It is necessary to check the full quantum evolution (see next section) to see to which extend this approximation is valid. Especially for small v, i.e. close to the big bounce, this effective approximation might break down.

4.3 Loop Quantum Cosmology

The treatment discussed in the previous section was so far semi-classical and effective in the sense that spacetime is still treated classical although the dynamics is modified by means of (non-perturbative) corrections in $\lambda = \mathcal{O}(\ell_p)$, which vanish for $\lambda, \ell_p \to 0$. There is no guarantee that this effective spacetime is really the outcome of a quantum theory, and that the approximation that spacetime is classical, even in the Planck regime, holds. This section discusses the construction of LQC, which is a proper quantum theory in the sense of operator representations on a Hilbert space. As always in the context of quantum gravity, there are different approaches, such as Wheeler-de Witt (WdW) cosmology [154–156], and there are quantisation ambiguities. This presentation follows [135, 136]. A reference with many mathematical details is [48], see also [138].

Quantisation in the common (Schrödinger) sense would imply to take the phase space variables and represent them on a Hilbert space according to the rule

$$\widehat{\{v,b\}} \mapsto -i\left[\hat{v},\hat{b}\right] \quad , \quad \widehat{\{\phi,p_\phi\}} \mapsto -i\left[\hat{\phi},\hat{p_\phi}\right] \ , \tag{4.3.1}$$

where $\hat{\cdot}$ denotes the corresponding operator on the Hilbert space. In the same spirit, it is

also possible to define the unitary exponential operators

$$\hat{U}(\mu) = \widehat{e^{i\mu v}} \quad , \quad \hat{W}(\nu) = \widehat{e^{i\nu b}} \quad , \quad \dots \, , \tag{4.3.2}$$

and demand the Weyl form of the Canonical Commutation Relations (CCR)

$$\hat{U}(\mu)\hat{W}(\nu) = \hat{W}(\nu)\hat{U}(\mu)e^{-i\mu\nu\{v,b\}} \, , \tag{4.3.3}$$

which are motivated by the Baker-Campbell-Hausdorff formulas for operator exponentials. Note that these operators are by definition unitary, as $\hat{U}(-\mu) = \hat{U}(\mu)^{-1} = \hat{U}(\mu)^\dagger$. Furthermore, this way only the exponentials of v and b are quantised. The operators $\hat{v}$ and $\hat{b}$ do not exist a priori. Nevertheless, both points of view are equivalent as long as the representation is *weakly continuous*, i.e.

$$\lim_{\mu\to 0} \left\langle \psi \middle| \hat{U}(\mu)\Phi \right\rangle = \left\langle \psi \middle| \lim_{\mu\to 0} \hat{U}(\mu)\Phi \right\rangle = \langle \psi|\Phi\rangle \ . \tag{4.3.4}$$

In that case the operator

$$\hat{v} := -i \lim_{\mu\to 0} \frac{\hat{U}(\mu) - 1}{\mu} \, , \tag{4.3.5}$$

and the other operators ($\hat{b}$, $\hat{\phi}$, $\widehat{p_\phi}$) are well-defined and satisfy the standard CCR Eq. (4.3.2).

The *Stone-von Neumann theorem* states that all joint (irreducible) and weakly continuous representations of $\hat{U}$ and $\hat{W}$ on separable Hilbert spaces are equivalent up to unitary transformations. Hence, this leads uniquely to WdW quantum cosmology which does not avoid the singularity generically [136, 157–160]. To generate new physics and a possible singularity avoidance, it is necessary to circumvent the Stone-von Neumann theorem. In LQG and also in LQC this is done by dropping the requirement of weak continuity. In particular LQC is a special case of polymer quantum mechanics [161, 162].

The construction is as follows: Starting point is the Hilbert space $\mathscr{H}_{kin}$, which is spanned by states $|\rho, \phi\rangle$ with $\rho, \phi \in \mathbb{R}$. The scalar product is defined by[6]

$$\langle \rho', \phi' | \rho, \phi \rangle = \delta_{\rho'\rho} \delta\left(\phi' - \phi\right) \ . \tag{4.3.6}$$

The main interest is about the gravitational part of the quantisation and hence the second

[6]Note that the scalar product gives a Kronecker delta in ρ instead of the usual Dirac delta. The latter would lead to the usual Hilbert space of square-integrable functions $L^2(\mathbb{R}^2, \mathrm{d}\rho\mathrm{d}\phi)$.

label ϕ is dropped in the following. The Weyl operators are defined as

$$\widehat{e^{\frac{i}{\lambda^3}\mu v}}\,|\rho\rangle := e^{i\mu\rho}\,|\rho\rangle \ , \tag{4.3.7}$$

$$\widehat{e^{-i\lambda\nu b}}\,|\rho\rangle := |\rho+\nu\rangle \ , \tag{4.3.8}$$

where λ is the polymerisation scale, which makes μ, ν dimension free. This representation is weakly continuous only in v as

$$\lim_{\mu\to 0}\left\langle\rho\middle|\widehat{e^{i\mu v}}\middle|\rho'\right\rangle = \lim_{\mu\to 0} e^{\frac{i}{\lambda^3}\mu\rho'}\,\langle\rho|\rho'\rangle = \delta_{\rho\,\rho'} = \langle\rho|\rho'\rangle \ , \tag{4.3.9}$$

but also

$$\lim_{\nu\to 0}\left\langle\rho\middle|\widehat{e^{-i\lambda\nu b}}\middle|\rho\right\rangle = \lim_{\nu\to 0}\langle\rho|\rho+\nu\rangle = 0 \neq 1 = \langle\rho|\rho\rangle \ . \tag{4.3.10}$$

Thus, the operator $\hat{v}$ is well-defined as $\hat{v}\,|\rho\rangle = \lambda^3\rho\,|\rho\rangle$, while there is no operator $\hat{b}$. On that Hilbert space, arbitrary but finite shifts in v are possible. This makes the volume "grainy" and points towards a quantisation. This will become be clearer in the discussion below. It is easy to check that the operators $\widehat{e^{\frac{i}{\lambda^3}\mu v}}$ and $\widehat{e^{-i\lambda\nu b}}$ satisfy the Weyl-CCR. The quantisation of ϕ and p_ϕ is done in the usual weakly continuous way, leading to multiplication and derivative operators. The Hilbert space is hence given by

$$\mathscr{H}_{kin} = \left\{ |\chi\rangle = \sum_{\rho\in\mathbb{R}}\int \mathrm{d}\phi\,\chi(\rho,\phi)\,|\rho,\phi\rangle \;\middle|\; \sum_{\rho\in\mathbb{R}}\int \mathrm{d}\phi\,\overline{\chi(\rho,\phi)}\chi(\rho,\phi) < \infty \right\} \ , \tag{4.3.11}$$

$$\langle\chi|\psi\rangle = \sum_{\rho\in\mathbb{R}}\int \mathrm{d}\phi\,\overline{\chi(\rho,\phi)}\psi(\rho,\phi) \ ,$$

where the sum over ρ is countable[7]. It is possible to consider the states $\langle b,\phi|\rho,\phi'\rangle = \delta(\phi-\phi')e^{-i\lambda\rho b}$ as basis states, where $\rho\in\mathbb{R}$. A generic wave function can be written as $\chi(b,\phi) = \sum_{\rho\in\mathbb{R}}\chi(\rho,\phi)e^{-i\lambda\rho b}$. This is almost like a Fourier series, but the label ρ is not restricted to integers. The elements $e^{-i\lambda\rho b}$ are more general than $U(1)$ representations.

The kinematics of the system is now determined. The next steps are the dynamics and especially the representation of the Hamiltonian on that Hilbert space. As there is

[7]The gravitational part of this Hilbert space are the square integrable function on the Bohr compactification of the real line $\mathbb{R}_{\mathrm{Bohr}}$ (see [48, 138] for more details).

no operator $\hat{b}$, it is obvious that the Hamiltonian in the form of Eq. (4.1.16) cannot be represented. This makes polymerisation as described in the previous section unavoidable. Indeed, the polymerised Hamiltonian Eq. (4.2.4) depends only on exponentials of b and thus has possible representations on $\mathscr{H}_{kin}$. In quantising the Hamiltonian there are two main obstructions:

1. The polymerisation, i.e. the replacement of $b \mapsto f(e^{i\lambda b})$ and
2. factor ordering, as in any quantum theory.

The first issue was addressed in Sec. 4.2 and the polymerisation

$$b \longmapsto \frac{\sin(\lambda b)}{\lambda} \,, \tag{4.3.12}$$

was applied. Indeed, the operator

$$\widehat{\sin(\lambda b)} := \frac{1}{2i}\left(\widehat{e^{i\lambda b}} - \widehat{e^{-i\lambda b}}\right) \,, \tag{4.3.13}$$

can be assigned and is well-defined on $\mathscr{H}_{kin}$.

The second point is a problem of any quantum theory, and it increases the ambiguities in the theory. The ordering should be chosen at least so that the Hamiltonian operator is self-adjoint. One possibility the symmetric ordering[8]. For this the lapse is fixed to $N = v$, which leads to the Hamiltonian operator

$$\hat{H} = \frac{1}{2}\widehat{p_\phi}^2 - \frac{1}{2\lambda^2}\sqrt{|\hat{v}|}\widehat{\sin(\lambda b)}|\hat{v}|\widehat{\sin(\lambda b)}\sqrt{|\hat{v}|} \,. \tag{4.3.14}$$

This Hamiltonian is indeed symmetric with respect to the scalar product. The physical and dynamical Hilbert space is defined according to Dirac quantisation [142] by

$$\mathscr{H}_{phys} := \left\{ |\chi\rangle \in \mathscr{H}_{kin} \;\middle|\; \hat{H}\,|\chi\rangle = 0 \right\} \,. \tag{4.3.15}$$

Acting with $\hat{H}$ on a basis state $|\rho, \phi\rangle$ leads to

[8] This symmetric ordering was also used in [136]. Further improvements of this ordering were discussed in [163].

$$\begin{aligned}\hat{H}\,|\rho,\phi\rangle = &-\frac{1}{2}\frac{\partial^2}{\partial\phi^2}\,|\rho,\phi\rangle \\ &+\frac{\lambda^4}{8}|\rho+1|\sqrt{|\rho||\rho+2|}\,|\rho+2,\phi\rangle \\ &-\frac{\lambda^4}{8}|\rho|\,(|\rho+1|+|\rho-1|)\,|\rho,\phi\rangle \\ &+\frac{\lambda^4}{8}|\rho-1|\sqrt{|\rho||\rho-2|}\,|\rho-2,\phi\rangle\ . \end{aligned} \tag{4.3.16}$$

This shows first of all that the ϕ and ρ sectors factorise and they can be treated separately. Secondly, the Hamiltonian preserves a grid in ρ of step size $2\mathbb{Z}$. Thus, the physical Hilbert space is restricted to the lattice $\rho \in 2\mathbb{Z}+c$ where $c \in \mathbb{R}$ is an arbitrary offset. Without loss of generality, it is possible to chose $c = 0$. This induces that physical volumes (eigenvalues of $\hat{v}$ in $\mathscr{H}_{phys}$) can only have discrete values of integer steps $v \in 2\lambda^3\mathbb{Z}$:

> The polymer quantisation of cosmology, together with the chosen polymerisation and factor ordering of the Hamiltonian constraint, leads to quantised volumes with spectrum
>
> $$v \in 2\,\lambda^3\,\mathbb{Z}\ .$$

As $\rho \in 2\mathbb{Z}$ the states $\langle b,\phi'|\rho,\phi\rangle = \delta(\phi'-\phi)e^{-i\lambda\rho b}$ are simply different representations of $U(1)$. After a careful analysis of the physical scalar product on $\mathscr{H}_{phys}$ [48, 138], $\mathscr{H}_{phys}$ can be viewed as square integrable functions over $U(1)$ with respect to the Haar-measure, i.e. $L^2\Big(U(1), \mathrm{d}\mu_{Haar}(U(1))\Big)$.

Another important conclusion from Eq. (4.3.16) is that positive and negative volume states are separated and $|\rho = 0\rangle$ is isolated. It is easy to check that no state $|\rho\rangle$ can be mapped to zero or to the opposite sign.

The system can be analysed in more details (see e.g. [136, 139, 144, 164]). This analysis will not be pursued here, and only central results without their technical difficulties will be stated.The Hamiltonian constraint can be solved analytically and the physical Hilbert space as well as the scalar product can be constructed explicitly. It can be shown that for generic states $|\chi\rangle \in \mathscr{H}_{phys}$

$$\langle\chi|\hat{v}|\chi\rangle > v_{min}$$

is bounded and hence the singularity is avoided. A further important result is the existence of coherent states $|\chi_{coh}\rangle$, which are peaked on classical geometries for large quantum numbers and remain peaked on this classical geometry during their evolution. The dy-

namics of $\langle\chi_{coh}|\hat{v}|\chi_{coh}\rangle$ is given by $H_{eff} = \left\langle\chi_{coh}\middle|\hat{H}\middle|\chi_{coh}\right\rangle$ where H_{eff} is the effective Hamiltonian of Eq. (4.2.4). Based on this, the approximation of the previous chapter, where the spacetime was treated classical, but the evolution was modified by quantum corrections in H_{eff}, can be considered valid for large quantum numbers. Conversely, the effective quantum dynamics should not be trusted for small quantum numbers. This was thoroughly analysed in several works [165–168].

In LQC the singularity is generically avoided. Coherent states peaked on large quantum numbers, resembling to classical geometry and remaining peaked on this during ϕ evolution, exist. The dynamics of $\langle\chi_{coh}|\hat{v}|\chi_{coh}\rangle$ is given by

$$\left\langle\chi_{coh}\middle|\hat{H}\middle|\chi_{coh}\right\rangle = H_{eff}$$

where H_{eff} is the effective Hamiltonian of Eq. (4.2.4).

In conclusion, it should be stressed that LQC is well-developed, but there are many technical details, which require specific choices (factor ordering, polymerisation, physical scalar product,...). These are still part of recent discussions (see e.g. [68, 169]). Another open question is about the relation of LQC and LQG. Although both share the same quantisation strategy, it is not clear if the cosmological sector of LQG reduces to the model presented here (see e.g. [59, 62, 147, 148]).

4.4 Relation to full LQG

In this section the construction of LQG is sketched without technical details. The aim is to show how the above techniques are motivated from full LQG and how connections can be made. More detailed overviews and introductions into the field are e.g. [49, 136] or for even more details [48, 134, 170, 171]

LQG is formulated in the Hamiltonian framework. Hence, the first step in the theory construction is the Hamiltonian analysis of GR. Spacetime is split into time and space also known as $3+1$-split. The central object of the Hamiltonian analysis is q_{ab}, which is the metric of the 3-dimensional slice. It turns out that the other four components of the spacetime metric, lapse and shift, are Lagrange multipliers and thus can be arbitrarily chosen, which corresponds to fixing the gauge and coordinates. The Hamiltonian formulation of GR deals with the spatial metric q_{ab} and its momentum P^{ab}, which is closely related to the extrinsic curvature of this spatial slice, i.e. how this slice is embedded into the 4-dimensional spacetime. The Hamiltonian equations predict how this spatial slice is evolving in "time". Nevertheless, the notion of time is subtle in GR as the Hamiltonian is

a constraint composed by the generators of space- and timelike diffeomorphism. As the system is fully constrained $H_{grav} \approx 0$, there is no dynamics in the standard Hamiltonian sense. This is at the heart of GR. In fact, there is no gauge independent "time" direction along which the spatial slice can evolve. Dynamics can thus only be specified relative to a given observer (see e.g. the discussion in [134]).

A phase space extension and canonical transformation is performed, mapping the degrees of freedom (q_{ab}, P^{ab}) to the so-called Ashtekar variables (A_a^i, E_i^a), which are used in the loop quantisation. Here E_i^a is the densitised triad and is related to the spatial metric, due to $\eta^{ij} E_i^a E_j^b = \sqrt{q} q^{ab}$. The Ashtekar connection A_a^i is a sum of the spin-connection of the spatial slice Γ and its extrinsic curvature K

$$A_a^i = \Gamma_a^i + \gamma K_a^i \,, \tag{4.4.1}$$

where γ is the Babero-Immirzri parameter, which is undetermined at this point. This way, A_a^i has knowledge about the full 4-dimensional curvature. The central point of this construction is that A_a^i is a $SU(2)$-connection (i runs in $\mathfrak{su}(2)$) which rephrases the gravitational degrees of freedom in terms of those of a $SU(2)$-gauge theory.

Out of this $SU(2)$-connection one can construct a parallel transport or in physicist language a holonomy[9] $h_\gamma(A) : T_{\gamma(t_i)}M \longrightarrow T_{\gamma(t_f)}M$, which parallel transports a vector along the curve γ[10]. Along the same lines, it is possible to canonically integrate the densitised triads E_i^a over a 2-dimensional surface S, leading to the so-called fluxes $E(S)$. holonomies and fluxes are both non-local objects, which form the holonomy-flux-algebra. The idea of LQG is to represent this algebra on a Hilbertspace. Due to the non-local character of $h_\gamma(A)$ and $E(S)$ natural divergences due to Dirac deltas are avoided.

This quantisation, i.e. representation of the holonomy-flux-algebra as operators on a Hilbert space is done in a weakly-discontinuous way, following the explanations of the previous section. This makes the quantisation scheme generically different form WdW-quantum gravity and allows to define a well-defined scalar product. Elements of the Hilbert space are cylindric functions depending on the connection A only through holonomies, i.e.

$$\psi \in \mathscr{H}_{kin}^{LQG} \quad \Rightarrow \quad \psi(A) = \psi(h_{\gamma_1}(A), \ldots, h_{\gamma_n}(A)) \,,$$

where n is a finite but arbitrary natural number. The set of n curves γ_i represent an ori-

[9] In contrast to the mathematics notation, here holonomies are not necessarily parallel transports along closed curves.

[10] γ is a curve in the spatial slice starting at curve parameter t_i and ending at t_f.

ented graph. The Hilbert space thus contains square-integrable functions over arbitrary finite copies of $SU(2)$. The scalar product is given by the Haar-measure over $SU(2)$. In LQC discussed in the previous section, the physical Hilbert space was based on functions over $U(1)$. This is furthermore exactly along the lines of lattice Quantum Chromo Dynamics (QCD) techniques, where holonomies are also quantised. The central difference is that in LQG the underlying lattice is completely arbitrary and dynamical as it can be modified by the action of the quantum operators. Moreover, there are additional (highly non-trivial) constraints.

This Hilbert space was heavily studied and the up to today most efficient realisation of it is in terms of so-called spin networks, mentioned here just for completeness. An important step is to also implement the Hamiltonian (the constraints) on that Hilbert space. As in LQC, there is only an operator for $\widehat{h_\gamma(A)}$ but not for $\hat{A}$. In order to find a well-defined operator for the constraints, it is necessary to re-express all direct A dependencies in the Hamiltonian by means of holonomies $h_\gamma(A)$. This step was called polymerisation in the above construction. The main dependence of A in the Hamiltonian comes through the curvature $F_{ab}(A)$. This is, without going into detail, replaced by a holonomy along a closed loop, as (see [172])

$$h_\square(A) \simeq \mathbb{I} + \frac{1}{2} F_{ab} \int_\square \mathrm{d}\sigma^{ab} + \mathcal{O}\left(\mathrm{Area}(\square)^2\right) \ , \tag{4.4.2}$$

where $\square$ denotes a closed curve and $\mathrm{d}\sigma^{ab}$ is the area-two form of the enclosed surface. Consequently, $\int_\square \mathrm{d}\sigma^{ab}$ is related to the enclosed area $\mathrm{Area}(\square)$.

A central result of this theory is the construction of area and volume operators and that their spectrum is quantised. This was part of the motivation for doing a polymerisation in the cosmological context. Indeed, the area is quantised and the smallest possible area value, the area gap [144], is

$$\Delta = (2\sqrt{3}\pi\gamma)\ell_p^2 \tag{4.4.3}$$

Nevertheless, it is hard to implement the Hamiltonian completely on this (kinematical) Hilbert space and it is even harder to solve the constraint equations. Hence, neither the physical Hilbert space, nor the physical scalar product and consequently the spectrum of the geometric operators on physical states are known.

Let us relate these ideas and constructions to what was discussed in the previous sections. The strategy applied there precisely followed this LQG logic. The variables were polymerised, i.e. expressed by means of point holonomies $h^n(b) = e^{-i\lambda n b}$, which were $U(1)$ instead of $SU(2)$-valued and centred at a single point instead of a full curve. Both is a

result of the large symmetry class of cosmology. Wave functions are cylindrical functions of these point holonomies. The representation was also chosen weakly discontinuous so that only the point holonomy operator $\widehat{h^n(b)} = \widehat{e^{-i\lambda nb}}$ but not the operator $\hat{b}$ itself exist. As argued above, geometric quantities, in cosmology volumes, became quantised on the physical Hilbert space due to this construction. The main point, which was missed in the cosmological construction was the use of Ashtekar variables and the polymerisation scheme, which a priori has no relation to Eq. (4.4.2). In the original work on LQC [144–146], coming from LQG, Ashtekar variables were used. Starting with the classical formulation of GR in Ashtekar variables, one can impose the cosmological symmetries leading to [144]

$$A_a^i = cV_o^{-\frac{1}{3}} {}^o\omega_a^i \quad , \quad E_i^a = p\sqrt{{}^oq}V_o^{-\frac{2}{3}} {}^oe_i^a \ , \tag{4.4.4}$$

where (c,p) are the only degrees of freedom and $({}^oe_i^a, {}^o\omega_a^i)$ are the orthonormal triads and co-triads compatible with the metric ${}^og_{ab}$ adapted to the edges of the fiducial cell of volume V_o. The phase space is spanned by (c,p) with the Poisson brackets

$$\{c,p\} = \frac{8\pi G\gamma}{3} \ .$$

The variables (c,p) are related to (v,b), used in Sec. 4.1-4.3, by the canonical transformation [149]

$$c = \gamma(4\pi Gv)^{\frac{1}{3}}b \quad , \quad p = (4\pi Gv)^{\frac{2}{3}} \tag{4.4.5}$$

In this simplified setting, a holonomy along $\mu\, {}^oe_k^a$ is given by

$$h_k^\mu(A) = \mathcal{P}\exp\left(\int_0^\mu A_a^i\tau_i e_k^a \mathrm{d}x\right) = \cos\left(\frac{\mu c}{2}\right)\mathbb{I} + 2\sin\left(\frac{\mu c}{2}\right)\tau_k \ , \tag{4.4.6}$$

where $\mathcal{P}\exp$ is the path-ordered exponential and it is $2i\tau_k = \sigma_k$, $k = 1,\ldots,3$ with the Pauli matrices σ_k. Hence, τ_k is a basis of $\mathfrak{su}(2)$ in the fundamental representation $j = 1/2$ [11]. The aim is to re-express all A_a^i in the Hamiltonian by means of these holonomies. Among others, this means that the curvature has to be replaced by means of holonomies according

[11] Choosing the fundamental representation is here definitely a restriction for simplicity. Coming from full LQG one should take *all* representation into account.

to

$$F^k_{ab} = -2 \lim_{\text{Area}(\square)\to 0} \text{Tr}\left(\frac{h^\mu_{\square_{ij}} - \mathbb{I}}{\mu^2 V_o^{\frac{2}{3}}}\right) \tau^k \, {}^o\omega^i_a \, {}^o\omega^j_b \,, \tag{4.4.7}$$

where $h^\mu_{\square_{ij}}$ denotes the holonomy along a square with edges ${}^oe^a_i$, ${}^oe^a_j$ with edge-length μ. This replacement changes the classical Hamiltonian after carefully replacing all connections c by holonomies from [149]

$$H_{class} = N\left[\frac{p_\phi^2}{2p^{\frac{3}{2}}} - \frac{3}{8\pi G\gamma^2}\sqrt{p}c^2\right] \tag{4.4.8}$$

to

$$H_{eff} = \lim_{\mu\to 0} N\left[\frac{p_\phi^2}{2p^{\frac{3}{2}}} - \frac{3}{8\pi G\gamma^2}\sqrt{p}\frac{\sin(\mu c)^2}{\mu^2}\right] \tag{4.4.9}$$

In the limit $\mu \to 0$, i.e. $\text{Area}(\square) \to 0$, this replacement is exact. LQG gives the insight that areas cannot be arbitrarily small and should be larger or equal to the area gap Δ. The best approximation is thus done for the smallest possible area, i.e. $\text{Area}(\square) = \Delta$. Imposing that the *physical area* enclosed by the plaquette $\square_{ij}$ is Δ, gives

$$|p|\mu^2 = \Delta = (2\sqrt{3}\pi\gamma)\ell_p^2 \,, \tag{4.4.10}$$

thus it is specified

$$\mu = \bar{\mu} = \sqrt{\frac{\Delta}{|p|}} \,,$$

which is known as the $\bar{\mu}$-scheme [144]. A crucial point is that this *polymerisation scale* is phase space dependent. The polymerised Hamiltonian becomes

$$H_{eff} = N\left[\frac{p_\phi^2}{2p^{\frac{3}{2}}} - \frac{3}{8\pi G\gamma^2}\sqrt{p^3}\frac{\sin\left(\sqrt{\frac{\Delta}{|p|}}c\right)^2}{\Delta}\right] \tag{4.4.11}$$

As $\bar{\mu}$ is phase space dependent, one could equally well ask for other variables in which the polymerisation scale is constant, i.e. c absorbs the phase space dependence of $\bar{\mu}$. Indeed,

in the case of cosmology, these variables are (v, b) (cfr. Eq. (4.4.5)), which leads to

$$H_{eff} = N\left[\frac{p_\phi^2}{8\pi G v} - \frac{3}{2} v \frac{\sin(\gamma\sqrt{\Delta}b)^2}{\gamma^2\Delta}\right] \tag{4.4.12}$$

which is exactly the effective Hamiltonian of Eq. (4.2.4). So polymerisation in (c, p) with the phase space dependent $\bar{\mu}$-scheme is equivalent to the polymerisation in geometrical variables (v, b) with a constant polymerisation scale

$$\lambda = \gamma\sqrt{\Delta} = \sqrt{2\sqrt{3}\pi\gamma^3}\ell_p \,. \tag{4.4.13}$$

In this sense, the polymerised theory and its quantisation is inspired by LQG. There were numerous choices and simplification, and especially allowing phase space dependent polymerisation schemes allows to use any kind of variables, as long as they offer a sensible interpretation in some sense. Further note that this construction is a symmetry reduction in Ashtekar variables on the classical level. As mentioned above, it is not clear how this model emerges as the cosmological sector of the full theory. Some preliminary insight has been gained in the work of [59, 147, 148], but the question is still far from understood, as most likely also renormalisation has to be taken into account [152, 153, 173–176]. The opposite approach is taken in [62] where LQC in (v, b) variables is embedded in the full theory context.

Part II

Holographic Signatures and Resolved Singularities

5

Holographic Signatures of Resolved Cosmological Singularities

All introductory material for the following work has now been established. As discussed in Sec. 3.4, the holographic principle and the AdS/CFT correspondence might be a more general property of gravity going beyond string theory. The classical description of gravity with GR breaks down close to singularities, and a need for a quantum theory of gravity is exposed. Given the AdS/CFT correspondence as a non-perturbative definition of string theory [44, 46, 47], the problem could be treated within the dual field theory. The question about a singularity in gravity could be translated into the boundary field theory. An answer could be found in the latter, since physical intuition and established techniques have been for QFT. Indeed, the question of singularities in string theory has been studied extensively [23, 177–185], but no clear picture has emerged yet.

In a similar sense, the problem could be turned around. In the framework of symmetry reduced LQG (see Chpt. 4) singularities are resolved and the quantum theory can be formulated. Using the AdS/CFT correspondence this behaviour could be translated into the dual field theory and tested against consistency and numerical simulations. Nevertheless, the AdS/CFT correspondence is only well-motivated in the context of string theory and

it is not clear how LQG fits in this picture, as it is a priori non-holographic. Moreover, it is not clear if singularity resolution is meaningful in the context of holography [27, 28].

In the following chapter, building on the preceding work [71, 72], cosmological singularities are resolved by means of LQC. The meaningfulness of this singularity resolution in the context of holography is tested within this simple setting. Herein the simplifications of the preceding work [73] are dropped. This simplified framework is used for first conceptional checks of these ideas.

This chapter is based on the author's published work [1] and starts by referring back to previous results of [71–73] and presenting the framework. In Sec. 5.3 the improved spacetime is introduced and discussed. The main strategy of the problem is outlined in Sec. 5.4 and the results are presented in Sec. 5.5. The chapter closes with the conclusions and further directions in Sec. 5.6.

5.1 Setup and Previous work

In preceding work, the authors studied holographic signatures of cosmological singularities in the context of AdS/CFT [71, 72]. Their setup is especially interesting in the context here studied and is given by the following.

In the bulk sapcetime is assumed to be Kasner-AdS cosmology, which is an anisotropic version of AdS space and described by the metric (in units of the AdS radius, i.e. $L = 1$)

$$\mathrm{d}s_5^2 = \frac{1}{z^2}\left(\mathrm{d}z^2 + \mathrm{d}s_4^2(t)\right) \quad , \quad \mathrm{d}s_4^2(t) = -\mathrm{d}t^2 + \sum_{i=1}^{3} t^{2p_i}\mathrm{d}(x^i)^2 \, . \tag{5.1.1}$$

This metric is equal to Eq. (2.1.11), however the 4-dimensional Minkowski metric is replaced by the so-called Kasner spacetime. Indeed, $\mathrm{d}s_4^2$ is a solution of the 4d vacuum Einstein equations if the Kasner exponents p_i satisfy the Kasner conditions

$$\sum_{i=1}^{3} p_i = 1 \quad , \quad \sum_{i=1}^{3} p_i^2 = 1 \, . \tag{5.1.2}$$

Moreover, in this case $\mathrm{d}s_5^2$ is a solution of the 5d Einstein equations with negative cosmological constant. This makes $\mathrm{d}s_5^2$ relatable to AdS, nevertheless $\mathrm{d}s_5^2$ is not maximally symmetric as it is anisotropic. There is a curvature singularity in both, the 4- and 5-dimensional case, as their curvatures diverge at $t = 0$. In addition to the translational symmetry in x^1, x^2 and x^3, the anisotropic-AdS spacetime (5.1.1) is scaling symmetric

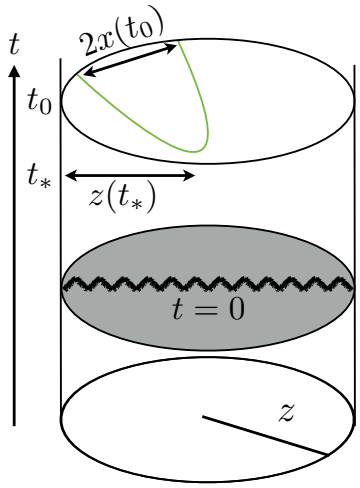

FIGURE 5.1: *Basic setup to probe bulk singularities by studying the equal-time correlator in the dual field theory: in the geodesics approximation the two-point function of a heavy ($m \gg 1$) scalar operator $\mathcal{O}$ is specified by the length of spacelike bulk geodesics anchored at two points on a boundary time slice $t = t_o$.*

with respect to

$$z \longmapsto \Lambda z \quad , \quad t \longmapsto \Lambda t \quad , \quad x^i \longmapsto \Lambda^{1-p_i} x^i \ . \tag{5.1.3}$$

According to the reasoning in [71, 72] and the AdS/CFT conjecture, the bulk theory is dual to SYM on a Kasner background (cfr. right equation in Eq. (5.1.1)).

Consider a scalar bulk operator $\mathcal{O}$ of this SYM theory on Kasner background in the large N-limit with large conformal weight $\Delta \gg 1$. According to the AdS/CFT-dictionary, this operator is dual to a scalar field on AdS spacetime with large mass $m \gg 1$ (cfr. Eq. (3.3.4)). This is the regime where the geodesic approximation [127] is valid and the equal-time two-point correlator is given by

$$\left\langle \mathcal{O}(t, x^i)\mathcal{O}(t, -x^i) \right\rangle \sim \exp(-\Delta L_{ren}) \ , \tag{5.1.4}$$

where $L_{ren} = \lim_{z\to 0} (L(t, x^i, z) + 2\log(z))$ is the renormalised geodesic length[1] and $L(t, x^i, z)$ is a spacelike geodesic connecting the points (t, x^i, z) and $(t, -x^i, z)$. The situation is depicted in Fig. 5.1. Here, two-point correlators of operators are considered at a given time slice t_o, and they are only separated in one spatial direction, for example x^1. In the following, this direction is simply denoted by x and the corresponding Kasner exponent p. This reduces the 5d problem of finding this spacelike geodesic to effectively

[1]The origin of this renormalisation is the boundary condition of the bulk fields, which becomes zero towards the boundary $\phi(z, x) \xrightarrow{z\to 0} 0$. The boundary conditions are imposed for $z^\Delta \phi(z, x)$ ($\Delta \gg 1$) which remains finite at the boundary (see Sec 3.3).

$2+1$ dimensions.

Note that it is possible that several geodesics exist, satisfying the given boundary conditions. For evaluating the two-point correlator all contributions have to be added in Eq. (5.1.4). Also complex geodesics have to be taken into account as they contribute to the long-distance behaviour [72].

The authors of [71, 72] and also [1, 73] where especially interested in probing the singularity. Studying the geodesics shows that timelike geodesics are bent away from the singularity for spatial directions with $p > 0$, but they are bent towards the singularity for $p < 0$. A geodesic satisfying the given boundary condition has a turning point in the bulk at time t_* and Poincaré coordinate $z(t_*) = z_*$. This turning point data classifies the geodesic. In the case of $p < 0$, t_* can reach the singularity at $t = 0$, i.e. comes arbitrarily close to the high-curvature regime. This should be reflected in the two-point correlator, which are exactly the signatures of interest. In the case of isotropic cosmology, these exponents are always positive (cfr. Eq. (4.1.19)) and thus the high-curvature regime cannot be tested in this framework. Allowing anisotropies changes this situation and gives the possibility of $p < 0$ to test the interesting high-curvature regime.

In the work [71, 72] this was studied in detail and the authors found a finite distance pole in the two-point correlator for a boundary separation where the geodesic hits the singularity. The presence of such a pole indicates non-renormalisability of the state in the dual field theory description [72].

5.2 Improved Correlator by Effective Bulk Quantum Geometry

Quantum gravity effects could resolve this classical singularity and possibly improve the behaviour of the finite distance pole of the two-point correlator. This possibility was already discussed in [71], although no concrete mechanism was given. As demonstrated in Sec. 4.2, a symmetry reduced quantisation inspired by LQG does resolve cosmological singularities. In the preceding work [73] an effective quantum corrected spacetime and the influence of the singularity resolution was studied. The result was a proof of principle, although strong simplifications were needed. This is due to the fact that a loop-quantisation, or polymerisation, of Kasner-AdS spacetimes is complicated and still not known today. This constitutes the starting point of the here presented work.

The quantum corrections in [73] are introduced along the lines of LQC. Here the authors made the simplification that each of the constant z-slices is polymerised by its own. This reduces the complexity from 5 to 4-dimensions and ignores the z-dependence.

This is motivated by the fact that the metric (5.1.1) is only singular in the 4d-part. The effective spacetime is given by

$$\mathrm{d}s_5^2 = \frac{1}{z^2}\left(\mathrm{d}z^2 + \mathrm{d}s_4^2(t)\right) \quad , \quad \mathrm{d}s_4^2(t) = -\mathrm{d}t^2 + \frac{a_{ext}^2}{\lambda^{2p}}\left(t^2+\lambda^2\right)^p \mathrm{d}x^2 + \dots \ , \tag{5.2.1}$$

where the dots denote the other similarly corrected spatial directions, λ is the polymerisation scale and a_{ext} the extremal value of the scale factor. For $p = 1/3$ this corresponds exactly to the effective dynamics of Eq. (4.2.8)[2]. The classical singularity is resolved by a bounce and for large t the classical solution is approached. In the limit $\lambda \to 0$ and ${}^{a_{ext}}/_{\lambda^p} \to 1$ this also reduces to the classical metric (5.1.1). The second assumption is that the different spatial directions were treated as decoupled and the exponent ${}^1/_3$ was generalised to p. If these exponents satisfy the Kasner conditions (5.1.2), $\mathrm{d}s_4^2$ is a solution to the classical Einstein equations up to orders of λ. Nevertheless, anisotropic LQC has been studied and qualitatively more complex solutions (see Sec. 5.5.2) were found. It was found out that the quantum effects replace the singularity with a smooth transition between two Kasner spacetimes. Further, it was shown that the Kanser exponents are changing during the quantum transition. This transition between one set of exponents to another one, both satisfying Eq. (5.1.2), is called *Kasner transition*, which was neglected in [73].

These simplifications seem drastic, but they allow analytic computations. If this simplified setting shows that singularity resolution is useful in the context of holography, it is appropriate to go beyond these simplifications and make the model more realistic. Within this setting it is possible to analytically solve the geodesic equations in the spacetime given by Eq. (5.2.1). The solution can be parametrised in terms of the geodesic length s, which gives for the z-component of the geodesic

$$z(s) = \frac{z(t_*)}{\cosh(s)} \ , \tag{5.2.2}$$

where the geodesic length s is measured starting at the turning point t_* of the geodesic (cfr. [73]). The value $z_* = z(t_*)$ is directly related to the spatial coordinate separation $l = 2x(t_o)$. The length of the geodesic is given by $2s(z \to 0)$, which is divergent. Nevertheless, within the geodesic approximation, it is important to compute the renormalised geodesic length given by

$$L_{ren} = \lim_{z\to 0}(2s(z) - 2\log(z)) = \lim_{z\to 0}(2\log(2z_*) - 2\log(z) + 2\log(z)) = 2\log(2z_*) \ . \tag{5.2.3}$$

[2]To show this, one has to choose $t_i = 0$, $v_i = \lambda p_\phi$ and $a_{ext} = (\lambda p_\phi)^{\frac{1}{3}}$.

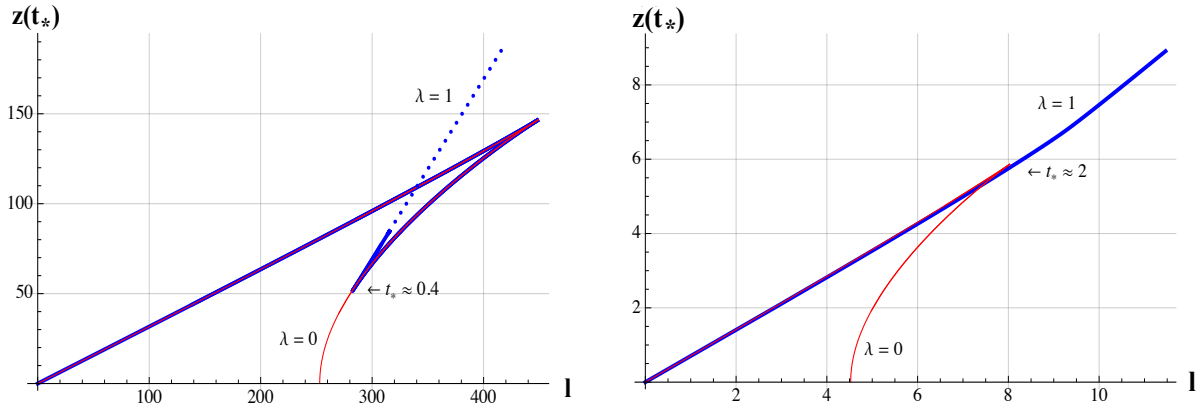

(a) (b)

FIGURE 5.2: *Plots of $z(t_*)$ vs. $l = x(t_0)$ for $p = -1/4$ and $a_{ext} = 1$ taken from [73]. The red line represents the classical case with $\lambda = 0$, while the blue line represents the quantum corrected case with $\lambda = 1$ respectively for $t_* = t_0 = 100$ at (0,0) (a), and $t_* = t_0 = 4$ at (0,0) (b). The solid blue line was obtained from numerically evaluating the analytic solutions, while the dashed blue line is an asymptotic expansion for $t_* \to 0$ [73].*

The two-point correlator is thus given by

$$\langle \mathcal{O}(t_o, x(t_o))\mathcal{O}(t_o, -x(t_o))\rangle \sim (2z_*(x))^{-2\Delta} \ , \tag{5.2.4}$$

which diverges only for $z_* = 0$. The relation of z_* with the boundary separation $l = 2x(t_o)$ can be seen in Fig. 5.2. As visible from the plot, z_* does not vanish for $\lambda \neq 0$ (blue curve) unlike the classical case (red curve). In both cases z_* vanishes at the point $(0, 0)$, which is the usual coincidence limit. This shows that indeed the finite distance pole is resolved for $\lambda \neq 0$. Interesting to observe is furthermore the fact that for given boundary data $l = 2x(t_o)$, multiple values for z_* exist. This corresponds to several geodesics, which all have to be taken into account for the two-point correlator, while the dominant contribution comes from the minimal value of z_*. When t_o becomes closer to the scale of λ, the qualitative behaviour changes to Fig. 5.2 (b). Nevertheless, the conclusion remains the same and the finite distance pole is resolved.

5.3 QUANTUM CORRECTED METRIC

The full problem of quantising the bulk would demand to apply 5d LQG based on [186–188] with the given boundary conditions to this framework and to extract an effective metric. Unfortunately this is remaining unobtainable until today. The problem is thus simplified in the following way.

As already noticed, the singularity of the metric (5.1.1) comes from the 4d part of

the metric. Resolving the singularity there, resolves the full 5d singularity. As discussed above (cfr. Sec. 4), there was lot of effort going towards symmetry reduced models of LQG. Beside homogeneous cosmology, effective Kasner spacetimes were also discussed [189]. They are in accordance with the numerical treatment of the quantum theory [165]. Further work showed possibilities of embedding these mini-superspace models into the full LQG framework [52, 60]. The resulting picture of quantised Kasner spacetimes is again a resolved singularity, which mediates between two classical Kasner spacetimes, which in turn change their set of Kasner exponents during the bounce. This process is called Kasner transition. The key assumption for this strategy to work in the 5d context is that the z from each $z = const.$ slice to another one is small. This will be discussed below.

Further there needs to be a meaningful generalisation of the 4d quantisation to the 5d context. Quantum effects in the 4d picture are controlled by the polymerisation scale λ which is related to $\hbar$ through the Planck length ℓ_p (cfr. Eq. (4.4.13) and [144]). A reasonable model induces quantum effects when the 4d curvature becomes of order Planck curvature, i.e. $\sim 1/\lambda^2$. As the 5d context is considered here, the full effective metric should have quantum effects when the 5d curvature reaches Planck scale. This is not ensured by following the above strategy. Nevertheless, there is a relation between the Kretschmann scalars

$$\mathcal{K}^{(5)} = R^{(5)}_{\alpha\beta\mu\nu} R^{(5)\alpha\beta\mu\nu} = z^4 \mathcal{K}^{(4)} + \dots \,. \tag{5.3.1}$$

As $\mathcal{K}^{(4)}$ is bonded by $const./\lambda^4$, this motivates to replace $\lambda \mapsto z\lambda$ to obtain an onset of quantum effects at the 5d Planck scale.

Besides the onset of quantum effects, Kasner transitions are expected, i.e. the change of Kasner exponents during the quantum bounce. Both features, the z-dependence of λ and Kasner transitions were neglected in Eq. (5.2.1) to allow for analytic computations and first insights on the effect of singularity resolution in [73]. In principle, both could have important qualitative effects for the two-point correlator:

Firstly, in [72] it was shown that the pole of the two-point correlator comes from the geodesic with $z_* \to 0$. On the boundary $z = const. = 0$ a null geodesic exists, which is continuously approached by the spacelike bulk geodesics, resulting in the singular geodesic causing the finite-distance pole. In the scenario of $z\lambda$ as polymerisation scale, the boundary remains unchanged and is still singular. Thus the null geodesic still exists and it has to be determined if a family of bulk geodesics is also continuously approaching it.

Secondly, the long distance behaviour of the two-point correlator in [73] is given by geodesics approaching $t = 0$ arbitrarily close, which is a maximum for $(t^2 + \lambda^2)^p$ $(p < 0)$.

A Kasner transition as in [189], where a positive exponent changes to a negative one, alters the behaviour of the metric around $t = 0$ as it has no extremal value any more.

Both simplifications are lifted successively in the following and their effect is studied numerically.

5.4 Solution Strategy

Due to the geodesic approximation Eq. (5.1.4), the problem of computing the two-point correlator reduces to solving the geodesic equation on a given background with specific boundary conditions. As motivated above, the bulk metric takes the general form

$$ds^2 = \frac{1}{z^2}\left(-dt^2 + a(t,z)^2 dx^2 + dz^2\right) . \tag{5.4.1}$$

The two-point correlator is given by spacelike geodesics starting and terminating at a constant time slice t_o, with a given boundary length separation $L_{bdy} = 2a(t_o, z = 0)x(t_o)$. Due to the translation symmetry in x, it is always possible to shift the coordinate system so that initial and final points are distributed symmetrically around the coordinate origin. The problem here is to find all spacelike geodesics on the background Eq. (5.4.1) which start $(t = t_o, x = x(t_o), z = 0)$ and end at $(t = t_o, x = -x(t_o), z = 0)$, where t_o and $x(t_o)$ is the input data[3].

5.4.1 Affine Parametrisation and Compactification

The geodesic equation can be derived form the following action

$$S = \int \mathrm{d}\tau \sqrt{g_{\mu\nu}\frac{dx^\mu}{ds}\frac{dx^\nu}{ds}} = \int \mathrm{d}\tau \sqrt{-\frac{\dot{t}^2}{z^2} + \frac{a(t,z)^2}{z^2}\dot{x}^2 + \frac{\dot{z}^2}{z^2}} , \tag{5.4.2}$$

where the dot denotes derivatives with respect to τ, which is an arbitrary curve parameter. As the geodesics start and terminate at the same time- and z-slice, there is a turning point in t and z. Due to the translation symmetry, the solution is symmetric around this turning point. A parametrisation of the curve in terms of t or z is consequently not suited, since only one of the two branches could be covered (cfr. [72, 73]). A suitable parameter, which allows a treatment of both branches at the same time, is the affine parameter s, for which $-\frac{\dot{t}^2}{z^2} + \frac{a(t,z)^2}{z^2}\dot{x}^2 + \frac{\dot{z}^2}{z^2} = 1$ with $\tau = s$. In this case the geodesic equations read

[3] In principle also complex geodesics have to be taken into account. As discussed in [73], these lie outside the quantum region and do not give new insight. The computation here restricts to real geodesics only.

$$\ddot{t} - \frac{2\dot{t}\dot{z}}{z} + \frac{\dot{x}^2}{2}\frac{\partial(a^2)}{\partial t} = 0 \,, \tag{5.4.3a}$$

$$\frac{d}{ds}\left(\frac{a(t,z)^2}{z^2}\dot{x}\right) = 0 \,, \tag{5.4.3b}$$

$$\ddot{z} - \frac{2\dot{z}^2}{z} + z - \frac{\dot{x}^2}{2}\frac{\partial(a^2)}{\partial z} = 0 \,. \tag{5.4.3c}$$

Eq. (5.4.3b) reflects the constant of motion related to the translation symmetry in x. As the scale factor $a(t,z)$ is z-dependent, Eq. (5.4.3c) has an additional term (with respect to [72, 73]) which does not allow to decouple the equations, and it is not possible to analytically solve the equations.

The geodesic length diverges towards the boundary, i.e. $z = 0$ lies at $s \to \infty$. To make the problem tractable for numerical integration, the compactified parameter σ is introduced

$$\sigma = \tanh(s), \quad \sigma \in (-1, 1) \,. \tag{5.4.4}$$

In this parametrisation the full boundary value problem reads

$$\begin{cases} t' = p_t \\ x' = p_x \\ z' = p_z \\ p_t' = \frac{2\sigma}{1-\sigma^2}p_t + \frac{2p_t p_z}{z} - \frac{p_x^2}{2}\frac{\partial(a^2)}{\partial t} \\ p_x' = \frac{2\sigma}{1-\sigma^2}p_x + \frac{2p_x p_z}{z} - \frac{p_x}{a(t,z)^2}\left(\frac{\partial(a^2)}{\partial t}p_t + \frac{\partial(a^2)}{\partial z}p_z\right) \\ p_z' = \frac{2\sigma}{1-\sigma^2}p_z + \frac{2p_z^2}{z} - \frac{z}{(1-\sigma^2)^2} + \frac{p_x^2}{2}\frac{\partial(a^2)}{\partial z} \\ \\ t(-1) = t(1) = t_0 \\ x(-1) = -x(1) = -l \\ z(-1) = z(1) = 0 \end{cases} , \tag{5.4.5}$$

where prime denotes derivatives with respect to σ, $l = x(t_0)$, and we introduced p_t, p_x, p_z to rewrite the equations as first order Ordinary Differential Equations (ODEs). The additional σ terms originate in the reparametrisation properties of derivatives,

$$\frac{\frac{d^2\sigma}{ds}}{\left(\frac{ds}{d\sigma}\right)^2} = -\frac{2\sigma}{1-\sigma^2} \quad , \quad \frac{d\sigma}{ds} = 1-\sigma^2 \, .$$

5.4.2 Mapping Boundary Value Problem into Initial Value Problem

There are well-established numerical methods to solve boundary value problems, such as the relaxation method (see e.g. [190, 191]) or the shooting method [192]. For the presented situation it is more appropriate to reformulate the problem as initial value problem, which simplifies the numerical strategy and has further advantages as will be discussed later. The idea is the following:

Due to the boundary conditions, only geodesics with a turning point are of interest. Denoting t_* and z_* the coordinate values at this turning point, t_*, z_* characterise a unique solution to the boundary value problem Eq. 5.4.5. The turning point is given by $(t_*, 0, z_*)$, where the translation invariance is used to shift the turning point to $x = 0$. Furthermore, the curve parameter can be shifted such that $s = 0 \Leftrightarrow \sigma = \tanh(0) = 0$ corresponds to the turning point. Finally, also the velocities in t and z have to vanish there, i.e.

$$\begin{aligned} 0 = \dot{t}(s=0) = t'(\sigma=0) \cdot \frac{d\sigma}{ds}(\sigma=0) = t'(\sigma=0) \, , \\ 0 = \dot{z}(s=0) = z'(\sigma=0) \cdot \frac{d\sigma}{ds}(\sigma=0) = z'(\sigma=0) \, . \end{aligned}$$

With $-\frac{\dot{t}^2}{z^2} + \frac{a(t,z)^2}{z^2}\dot{x}^2 + \frac{\dot{z}^2}{z^2} = 1$, the velocity in x at the turning point is fixed

$$\dot{x}(s=0) = \frac{z_*}{a(t_*, z_*)} = \frac{z_* \lambda^p}{a_{ext}\left(t_*^2 + \lambda^2 z_*^2\right)^{\frac{p}{2}}} = x'(\sigma=0) \cdot \frac{d\sigma}{ds}(\sigma=0) = x'(\sigma=0) \, . \quad (5.4.6)$$

The boundary value problem (5.4.5) can be accordingly rephrased as the following initial

value problem

$$\begin{cases} t' = p_t \\ x' = p_x \\ z' = p_z \\ p_t' = \frac{2\sigma}{1-\sigma^2} p_t + \frac{2p_t p_z}{z} - \frac{p_x^2}{2} \frac{\partial(a^2)}{\partial t} \\ p_x' = \frac{2\sigma}{1-\sigma^2} p_x + \frac{2p_x p_z}{z} - \frac{p_x}{a(t,z)^2} \left(\frac{\partial(a^2)}{\partial t} p_t + \frac{\partial(a^2)}{\partial z} p_z \right) \\ p_z' = \frac{2\sigma}{1-\sigma^2} p_z + \frac{2p_z^2}{z} - \frac{z}{(1-\sigma^2)^2} + \frac{p_x^2}{2} \frac{\partial(a^2)}{\partial z} \\ \\ t(0) = t_*, \ x(0) = 0, \ z(0) = z_* \\ p_t(0) = 0, \ p_x(0) = z_*/a(t_*, z_*), \ p_z(0) = 0 \end{cases} , \tag{5.4.7}$$

where the initial data $(t_*, 0, z_*)$ and the velocities $(0, z_*/a(t_*, z_*), 0)$ are expressed only in terms of the turning point values t_*, z_*, which are given as input. The parameter σ runs from 0 to 1 and thus covers only one of the two branches. Due to the symmetry in t and z, and the anti-symmetry in x, the other branch is easily constructed.

The input values t_* and z_* solely label a geodesic of interest. To finally solve the boundary value problem, it is necessary to relate these values to the given boundary data t_o and l. There exists a well-defined map

$$\begin{aligned} f &: \mathbb{R}^2 \longrightarrow \mathbb{R}^2 \\ &(t_*, z_*) \longmapsto f(t_*, z_*) = \Big(f^1(t_*, z_*), f^2(t_*, z_*) \Big) \end{aligned} \tag{5.4.8}$$

with

$$\begin{aligned} f^1(t_*, z_*) &= t(\sigma = 1) = t_o(t_*, z_*) \\ f^2(t_*, z_*) &= x(\sigma = 1) = l(t_*, z_*) \end{aligned} \tag{5.4.9}$$

where $t(\sigma)$, $x(\sigma)$ are solutions of Eq. (5.4.7). The preimage of this map of a point (t_o, l) is a set of initial conditions for all geodesics, solving the boundary value problem. All solutions with a fixed value t_o correspond to level lines of $t_o(t_*, z_*)$, which relate t_* to z_* (see Eq. (5.2) in [72] for such a relation in the classical case) and can be thought of as a curve $(t_*(\mu), z_*(\mu))$ in the $t_* - z_*$-plane parametrised by μ. In the same way, geodesics with a fixed l correspond to a level line of $l(t_*, z_*)$, which yields another (t_*, z_*)-curve. Intersections of these curves for given t_o and l, (t_*^i, z_*^i), $i = 1, 2, \ldots$, correspond to all

solutions of the boundary value problem Eq. (5.4.5).

The reformulation of the boundary value problem is completed. It is rephrased in terms of first solving initial value problems and afterwards computing level lines and finding intersections of these. This requires to solve the initial value problem multiple times, which makes the solution strategy effectively a shooting method. Nevertheless, the two-point correlator is a function of different values of l and in principle also of several values of t_o. The numerical effort is reduced by not discarding the "miss shots" but rather rearranging them as solutions for a fixed t_o and several values of l.

This method is implemented numerically in Matlab using its built-in library. The ODEs are solved with the routine `ode45`, which is based on a fifth-order Runge-Kutta algorithm with adaptive step size. Level lines can be computed with `contourc`. Since the Eqs. (5.4.7) diverge at $\sigma = \pm 1$, the numerical integration is cut at $1 - \epsilon$ with $\epsilon = 0.00001$. Extensive cross-checks on the numerics, including the reproduction of the analytic results of [73], were performed.

5.4.3 Renormalised Geodesic Length and Two-Point Correlator

The above strategy allows to extract the geodesic length $L = 2s$ in affine parametrisation with $s = 0$ at the turning point. As already discussed, this is divergent for $z \to 0$. For the two-point correlator it is relevant to renormalise the geodesic length. The length renormalsation works according to the formula below Eq. (5.1.4), which yields

$$L_{ren} = \lim_{z\to 0} \left(2s(z) + 2\log(z)\right) \simeq \lim_{z\to 0} \left(2s(z) + 2\log\left(\frac{z}{t}\right)\right) \ , \tag{5.4.10}$$

Here $s(z)$ is the geodesic length evaluated up to z and the missing term $2\log(t)$ is neglected as it only appears as a global factor in the two-point correlator. This additional term was introduced as the fraction z/t is invariant under the scaling symmetry Eq. (5.1.3) and corresponds to a constant UV cutoff in pure AdS (cfr. [72]). In the case where analytic results for $s(z)$ are available, this limit can be treated easily, because divergent terms can be isolated (see Sec. 5.2 and [73]). Numerically this is not possible and a cut-off value z_{UV}, which is finite but small, is defined. The limit is evaluated up to this value. For small enough values of z_{UV} the result should be nearly independent and coincide with $z/t \to 0$ (see also [190, 191]).

The numerical solutions are in terms of σ, which is in the range $[0, 1]$[4] and related to s by $s = \operatorname{arctanh}(\sigma)$. The solutions are evaluated up to a specific value z_{UV}, which

[4]To be presice the range is up to $1 - \epsilon$ (see Sec. 5.4.2), but ϵ is small enough to not conflict the following.

corresponds to the parameter value $\bar{\sigma}$, defined by $z(\bar{\sigma}) = z_{UV}$. With this cut-off, it is

$$\sigma \in [0, 1-\delta] \quad , \quad \delta = 1 - \bar{\sigma} \ll 1 \, , \tag{5.4.11}$$

where the condition $\delta \ll 1$ is satisfied as long as ${}^{z_{UV}}/_{t} \ll {}^{z_*}/_{t_*}$. The renormalised length can be written as

$$L_{\text{ren}} = 2\text{arctanh}\,(1-\delta) + 2\log\left(\left|\frac{z_{UV}}{t(\bar{\sigma})}\right|\right) . \tag{5.4.12}$$

In the limit ${}^{z_{UV}}/_{t} \to 0$ (i.e. $\bar{\sigma} \to 1$, $\delta \to 0$) this expression is finite as

$$\text{arctanh}\,(1-\delta) + \log\left(\left|\frac{z_{UV}}{t(\bar{\sigma})}\right|\right) = -\frac{1}{2}\log\left(\frac{\delta \cdot t(\bar{\sigma})^2}{z_{UV}^2}\right) + \frac{1}{2}\log(2) + \mathcal{O}(\delta) \, , \tag{5.4.13}$$

and, as can be checked numerically, for small values of z_{UV}, the quantity (5.4.12) approaches a non-zero constant.

In order to conclude that the two-point correlator is non-singular, it has to be verified that L_{ren} remains finite. In the classical case [71, 72] as well as in the quantum corrected case [73] this relation was (cfr. Eq. (5.2.3))

$$\frac{L_{\text{ren}}}{2} = \log\left(\frac{2z_*}{t_0}\right) . \tag{5.4.14}$$

A similar logarithmic behaviour is also expected for the cases under consideration. The main changes come from the relation of z_* with l, which is computed in the first step. The numerical results are presented in the next section.

5.5 Results

The above discussed strategy is in the following applied for metrics which go beyond the previous simplifications. In a first instance, it is taken into account that the quantum effects become relevant at the 5d Planck scale (i.e. $\lambda \mapsto z\lambda$) and the inclusion of Kasner transitions is discussed.

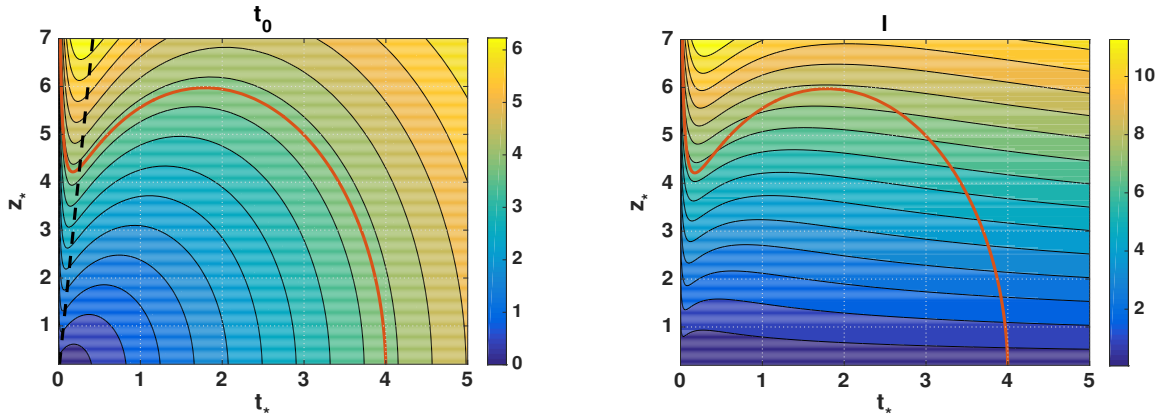

(a) (b)

FIGURE 5.3: *Colour plot of (a) $t_0(t_*, z_*)$ and (b) $l(t_*, z_*)$ for $p = -1/4$, $\lambda = 0.06$, $a_{ext} = \lambda^p$. The red curve corresponds to the $t_0 = 4$ level line. This contour is also plotted in (b). The black dashed line corresponds to $t^2 = \lambda^2 z^2$ and separates quantum and classical regime.*

5.5.1 5D PLANCK SCALE

As discussed, the onset of quantum effects can be set at the 5d Planck by replacing $\lambda \mapsto z\lambda$ in Eq. (5.2.1) leading to

$$ds_5^2 = \frac{1}{z^2}\left(dz^2 - dt^2 + \frac{a_{ext}^2}{\lambda^{2p}}\left(t^2 + \lambda^2 z^2\right)^p dx^2 + \dots\right) . \tag{5.5.1}$$

This goes beyond the first simplification but still neglects Kasner transitions. In the regime $t \gg z\lambda$ quantum effects are negligible and Eq. (5.5.1) is well-approximated by the classical Kasner-AdS metric. The z-derivative $\frac{\partial a(z,t)}{\partial z} = \mathcal{O}(\lambda^2)$ remains small and therefore, the z-dependence is caused by small quantum corrections, which are systematically neglected here. In the boundary limit $z \to 0$ the classical (singular) Kasner spacetime is recovered.

The missing derivatives of Eq. (5.4.7) are

$$\frac{\partial(a^2)}{\partial t} = 2p\frac{a_{ext}^2}{\lambda^{2p}} t\left(t^2 + \lambda^2 z^2\right)^{p-1} = 2a(t,z)^2 \frac{pt}{t^2 + \lambda^2 z^2} , \tag{5.5.2}$$

$$\frac{\partial(a^2)}{\partial z} = 2p\frac{a_{ext}^2}{\lambda^{2p}} \lambda^2 z\left(t^2 + \lambda^2 z^2\right)^{p-1} = 2a(t,z)^2 \frac{p\lambda^2 z}{t^2 + \lambda^2 z^2} , \tag{5.5.3}$$

which determine the system of equations. The initial value problem (5.4.7) is solved numerically for $t_*, z_* \in [0, 10]$ and parameters $p = -1/4$, $\lambda = 0.06$. The solutions $t_o(t_*, z_*)$ and $l(t_*, z_*)$ are depicted as colour plots in Fig. 5.3 where the t_o- and l-axis are represented by a colour scale. The corresponding classical result is shown in Fig. 5.4. For the two-

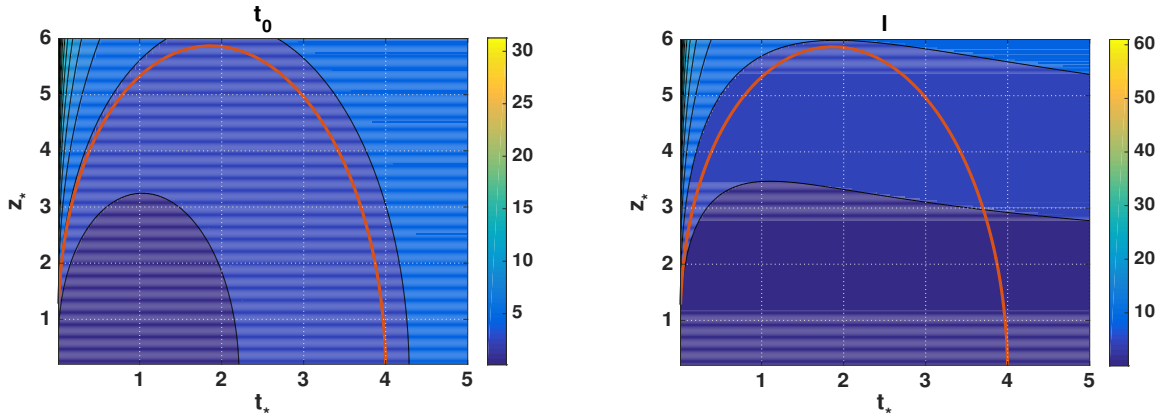

(a) (b)

FIGURE 5.4: *Colour plot of (a) $t_o(t_*, z_*)$ and (b) $l(t_*, z_*)$ for the classical Kasner-AdS metric ($\lambda = 0$ in (5.5.1)) with $p = -1/4$. The red curves correspond to the $t_o = 4$ level line.*

point correlator, all geodesics with a fixed time value, for example $t_o = 4$ are of interest. In Fig. 5.3 (a) these correspond to the red curve in the (t_*, z_*)-plane. Quantum effects become relevant when $t^2 \sim z^2\lambda^2$, which is represented by the black dashed line in Fig. 5.3. Due to the small value of $\lambda = 0.06$, this line is close to the z-axis. Indeed, comparing Fig. 5.3 (a) and Fig. 5.4 (a) both results coincide in the classical regime.

A geodesic hits the bulk singularity when it reaches the value $t_* = 0$. In the classical case a family of geodesics exists for which $z_* \to 0$ for $t_* \to 0$, and therefore, hitting the bulk singularity ($t_* = 0$) corresponds to $z_* = 0$, which causes the finite distance pole. This is avoided ($z_* > 0$) in the quantum corrected case, where the red curve in Fig. 5.3 turns around and z_* becomes large for $t_* \to 0$ (within the numerical accuracy $t_* \gtrsim 10^{-8}$). This shows that the singular boundary null geodesic is not reached in a limit of bulk geodesics.

It is possible to extract the dependence between l and z_* out of the numerical results of Fig. 5.3. Evaluating the corresponding l value along the $t_o = 4$ curve (cfr. Fig. 5.3 (b)) leads to Fig. 5.5. The dashed red line shows the classical behaviour and a continuous line of geodesics approaching $z_* = 0$ at finite l. As discussed in Sec. 5.1 this causes the finite distance pole in the two-point correlator. Due to the numerical cut-off in z_* this in never reached, neither in the coincidence point $z_* = l = 0$. The quantum solution (blue line) behaves differently, as it starts to approach $z_* = 0$ but has a second turning point in the quantum regime. As in the case discussed in Sec. 5.2 and Fig. 5.2, there are multiple solutions for z_* at a given l-value which all have to be taken into account for the two-point correlator.

Up to now it is not possible to conclude any resolution of the finite distance pole as the relation $L_{ren}(z_*)$ is not known. The renormalised geodesic length L_{ren} is computed

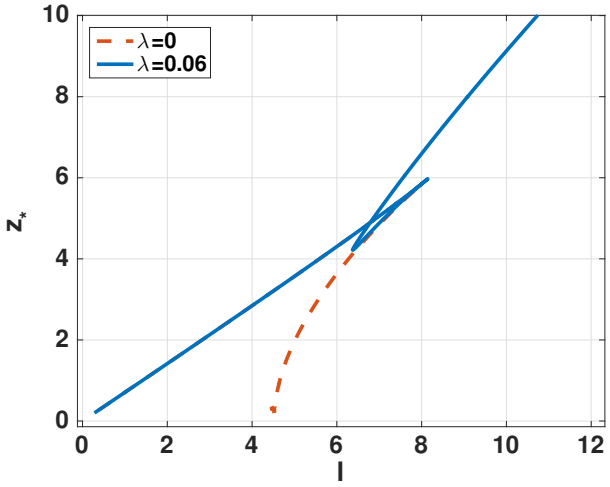

FIGURE 5.5: *Plot of z_* vs. l for $t_o = 4$ and $p = -1/4$, $\lambda = 0.06$, $a_{ext} = \lambda^p$. The blue curve corresponds to the quantum corrected metric (5.5.1), the red curve to the classical metric ($\lambda = 0$ in (5.5.1)).*

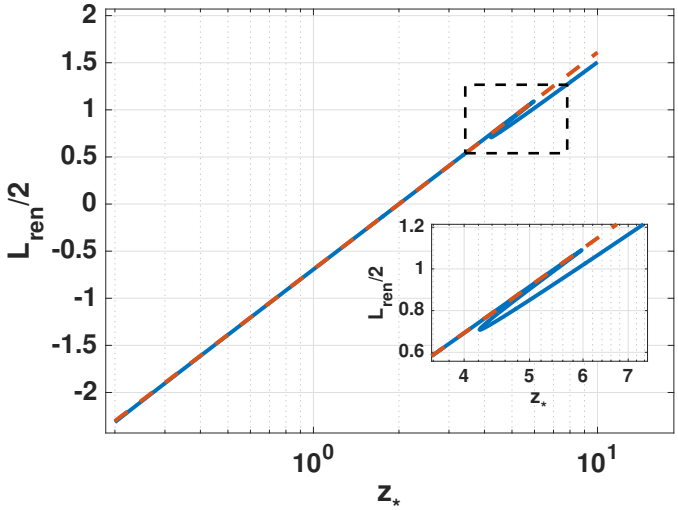

FIGURE 5.6: *Plot of L_{ren} on y-axis vs. z_* on a logarithmic x-axis for the metric (5.5.1) (blue) with $t_o = 4$, $\lambda = 0.06$, $p = -1/4$, $a_{ext} = \lambda^p$. The almost linear behaviour indicates a* log*-dependence of L_{ren} from z_* like Eq. (5.4.14) (red dashed).*

according to the method described in Sec. 5.4.3 and visualised in a log-plot in Fig. 5.6. In the classical regime (lower left part of the plot), the log behaviour Eq. (5.4.14) is recovered. Also in the deep-quantum regime (upper right part), a logarithmic behaviour is found, however, the slope is smaller. This part contributes to the long distance behaviour of the two-point correlator. In agreement with the results of [73], due to the smaller slope (causes a smaller negative exponents in the correlator) this contribution is subdominant in the short distance behaviour. In the intermediate regime there are three branches which are caused by the multiple solutions already visible in Fig. 5.5. In the classical regime (lower left part), possible deviations from the classical behaviour can occur. These are

numerical artefacts as there the approximation $z_{UV}/t_o \ll z_*/t_*$ fails and the numerical error increases.

The main conclusion from Fig. 5.6 is that L_{ren} is non-divergent for any value of z_*. Together with Fig. 5.5 the two-point correlator can be extracted and it is finite for all boundary separations l. Although the boundary coincides with the classical one, i.e. the singular null geodesic exists, bulk geodesics do not approach this solution continuously and thus the finite distance pole is resolved by resolving the bulk singularity.

5.5.2 Kasner Transitions

The next step is to go also beyond the second simplification and include Kasner transitions. As it turns out this is highly non-trivial. Kasner transitions were found numerical investigations of 4d anisotropic LQC [17, 189], which would provide the proper 4d effective metric. It is impractical to proceed with these numerical results, as they would complicate the numerics and further compromise a generalisation to the 5d setting above. A simpler model was introduced by Chamseddine and Mukhanov [193], which was applied to anisotropic cosmology [33]. The main advantage of this model is that the effective metric is available in an easy analytical form and respects the key features, such as the onset of quantum effects and Kasner transitions. The Chamseddine-Mukhanov model was proposed as a toy model for an effective theory of quantum gravity[5] [194, 195] and it coincides with effective LQC in the isotropic sector even though deviations are known in the anisotropic case [2, 194]. Nevertheless, it carries the main qualitative features of interest and is an appropriate starting point for the following discussion.

5.5.2.1 Models of Kanser Transitions

The Chamseddine-Mukhanov model [33] yields for anisotropic cosmology

$$\mathrm{d}s^2 = -\mathrm{d}t^2 + a(t)^2\mathrm{d}x^2 + \dots \quad , \quad a(t) = \frac{a_{ext}}{\lambda^p}\left(t^2+\lambda^2\right)^{\frac{p}{2}} \exp\left[\Delta p \sinh^{-1}\left(\frac{t}{\lambda}\right)\right] , \quad (5.5.4)$$

where the dots denote the other spatial directions with similar scale factors[6]. For $p = -1/3$, $\lambda = 1/\sqrt{3\epsilon_m}$, and special values for a_{ext}, Δp this reduces exactly to [33] with limiting

[5] In the original work [33] it was explicitly assumed that the curvature is limited by a value orders of magnitude above the Planck scale, thus avoiding the quantum regime.

[6] Note that the parameters a_{ext} and λ are the same for the other spatial directions. In contrast, the Kasner exponents $p^i_\pm = p^i \pm \Delta p^i$, are different for each direction i, but constrained due to the Kasner conditions Eq. (5.1.2). This is discussed in [33] in detail.

curvature ϵ_m, where the values p, Δp, a_{ext} are fixed. For the purpose of this work these parameters not further specified.

As discussed above, replacing the 4d part of Eq. (5.1.1) by Eq. (5.5.4) would resolve the singularity, but quantum effects are driven by the 4d curvature scale instead of the 5d scale. Note that an extension such as in the previous section is non-trivial, and no conclusive metric was found.

According to the argument given in Sec. 5.3 a simple solution indeed shifts the onset of quantum effects to the 5d Planck scale by replacing $\lambda \mapsto z\lambda$. This leads to the line element

$$ds_5^2 = \frac{1}{z^2}\left(dz^2 - dt^2 + a(t,z)^2 dx^2 + \dots\right) , \tag{5.5.5}$$

with

$$a(t,z)^2 = \frac{a_{ext}^2}{\lambda^{2p}}\left(t^2 + \lambda^2 z^2\right)^p \exp\left[2\Delta p \sinh^{-1}\left(\frac{t}{z\lambda}\right)\right], \qquad \Delta p \in \mathbb{R} . \tag{5.5.6}$$

As claimed above also Kasner transitions are modelled as in the limit $|t/z\lambda| \gg 1$ and with the approximation

$$\sinh^{-1}\left(\frac{t}{z\lambda}\right) \simeq \mathrm{sign}(t) \log\left|2\frac{t}{z\lambda}\right| , \tag{5.5.7}$$

the scale factor (5.5.6) reduces to

$$a(t,z)^2 \simeq \frac{a_{ext}^2}{\lambda^{2p}}\left(\frac{2}{\lambda z}\right)^{\pm 2\Delta p} t^{2p_\pm} , \tag{5.5.8}$$

with Kasner exponents

$$p_\pm = p \pm \Delta p . \tag{5.5.9}$$

The scale factor for different constant values of z is shown in Fig. 5.7. For a fixed value of z, the classical behaviour of Kasner spacetime is approached for late and early times $\pm t \gg 1$. In between $|t/z\lambda| \ll 1$ quantum effects become dominant and replace the classical singularity with a smooth transition between the two Kasner spacetimes of exponents p_- to $p_+ = p_- + 2\Delta p$. This is in qualitative agreement with the behaviour of [189][7]. In the

[7]It is shown that this is the only possible transition behaviour in accordance with the correct classical limit for both early and late times [17].

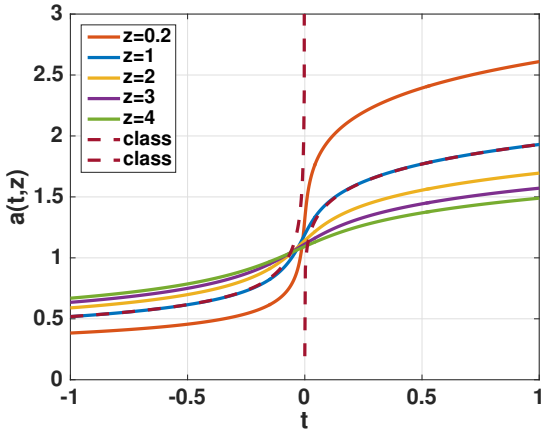

FIGURE 5.7: *Plot of the scale factor (5.5.6) vs. t for $\lambda = 0.06$, $p = -1/16$, $\Delta p = 3/16$. Away from the immediate vicinity of the bounce point ($t = 0$) the different lines corresponding to different values of z, agree with the classical behaviour (explicitly reported for $z = 1$ in dashed lines), and show a smooth transition during the bounce.*

quantum regime $|t/z\lambda| \ll 1$ the metric is approximately given by

$$a(t,z)^2 \simeq a_{ext}^2 z^{2p} \left(1 + 2\Delta p \frac{t}{z\lambda}\right) , \tag{5.5.10}$$

which is, as discussed, regular around $t = 0$. For $\Delta p = 0$ no Kasner transition occurs and Eqs. (5.5.5), (5.5.6) reduce to Eq. (5.5.1).

Although seemingly being a promising 5d quantum corrected metric, the following complications have been observed:

First, it does not solve the 5d Einstein equations up to orders of λ. This can be explained by a closer look at Fig. 5.7. The scale factor connects two classical Kasner branches by a monotonically increasing (or decreasing) transition. This can only be achieved when the prefactors in front of t^{2p_+} and t^{2p_-} are scaled relative to each other. Indeed this prefactor is different for the two sides as shown in Eq. (5.5.8), leading to a divergence for $\lambda \to 0$ or $z \to 0$ for positive Kasner exponents, and it vanishes for negative ones. This behaviour is also depicted in Fig. 5.7. As this z dependence is still present even at large t, this causes Eq. (5.5.5) not solving the 5d Einstein equations approximately up to orders of λ. A shown below, the z-derivative of $a(t,z)$ (see below Eq. (5.5.14)) can be arbitrarily large even in the classical regime ($\lambda \ll 1$ or $\pm t \gg 1$).

This already points towards the second problem. In the limit $z \to 0$ or for $\lambda \to 0$ Eq. (5.5.8) diverges (vanishes) and it is not possible to recover the classical Kasner spacetime globally. This is true for the classical limit $\lambda \to 0$, as well as for the boundary limit $z \to 0$, where the latter is the main issue.

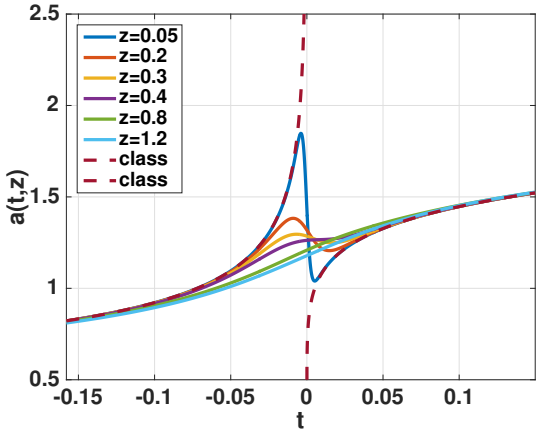

FIGURE 5.8: *Plot of the scale factor (5.5.11) vs. t for $\lambda = 0.06$, $p = -1/16$, $\Delta p = 3/16$. Away from the immediate vicinity of the bounce point ($t = 0$) the different lines, which correspond to different values of z, agree with the classical behaviour (dashed lines) for all values of z, and show a smooth transition during the bounce. Nevertheless, this deviates qualitatively from the LQC behaviour.*

The problem could be solved by modifying the metric (5.5.6) so that the divergent prefactor in Eq. (5.5.8) is cancelled. One possibility is the following scale factor

$$a(t,z)^2 = \frac{a_{ext}^2}{\lambda^{2p}} \left(t^2 + \lambda^2 z^2\right)^p \exp\left[2\Delta p \sinh^{-1}\left(\frac{t}{z\lambda}\right)\right] (\lambda z)^{2\Delta p \tanh\left(\frac{t}{z\lambda}\right)} , \tag{5.5.11}$$

where the additional factor $(\lambda z)^{2\Delta p \tanh\left(\frac{t}{z\lambda}\right)}$ allows to recover the proper boundary and classical limit. For $|t/z\lambda| \gg 1$, it is $\tanh\left(\frac{t}{z\lambda}\right) \simeq \text{sign}(t)$ $(z, \lambda > 0)$ and Eq. (5.5.11) becomes

$$a(t,z)^2 \simeq a(t)^2 = \frac{a_{ext}^2}{\lambda^{2p}} t^{2p_\pm} . \tag{5.5.12}$$

Indeed, the divergent prefactor (cfr. Eq. (5.5.8)) is cancelled and the result is z independent and reduces to the classical Kasner spacetime in the double scaling limit $\lambda \to 0$ and $a_{ext}/\lambda^p \to 1$. The dependence of z is depicted in Fig. 5.8. In contrast to Eq. (5.5.6), this modified scale factor has the same asymptotic behaviour for all z and no rescaling is needed. This enforces the non-monotonic behaviour around $t = 0$ which qualitatively differs from the LQC results [189].

The modified scale factor Eq. (5.5.11) has the further advantage that it solves the Einstein equations in first orders of λ. The initially discussed conditions (cfr. Sec. 5.3), namely a well-defined boundary metric solving 4d Einstein equations (up to orders of λ) and a small z derivative, i.e. suppressed by λ are both satisfied for Eq. (5.5.11). Nevertheless, the Kretschmann scalar of Eq. (5.5.11) is not constant in z and can become arbitrarily large for $z \to 0$. This can be analytically verified by using computer algebra

	qualitative LQC behaviour	Correct onset of qu. effects	Boundary limit	Solution of EE + $\mathcal{O}(\lambda)$
Eq. (5.5.6)	✔	✔	✘	✘
Eq. (5.5.11)	✘	✘	✔	✔

TABLE 5.1: *Comparison of the two discussed 5d Kasner transition models Eqs. (5.5.6) and (5.5.11). The evaluated criteria are qualitative LQC behaviour, correct onset of quantum effects, existence of the boundary limit, and if the Einstein Equations (EE) are solved up to quantum corrections.*

software. Due to this, the interpretation of Eq. (5.5.11) as an effective metric extracted from a quantum gravity theory with limiting curvature as LQC or the Chamseddine-Mukhanov model [33] fails.

To conclude, it is shown that it is highly non-trivial to "guess" a suitable 5d metric including Kasner transitions and the above discussed requirements. The full problem, having to be solved here, is to set up 5d Einstein equations with negative cosmological constant, symmetry reduce the system and perform a polymerisation and quantisation as sketched in Chpt. 4. This would lead to a quantum theory of $a(t, z)$ which is a so-called midi-superspace model, i.e. it depends on two coordinates. This is technically out of scope and is left for future research. Due to this, here the two-point correlator for the metrics (5.5.6) and (5.5.11) is studied. Their properties are summarised in Tab. 5.1. In the following the analysis focusses on the first metric (5.5.6) as it behaves qualitatively as LQC and has the correct onset of quantum effects. Furthermore, it has no maximum around $t = 0$, which as discussed in Sec. 5.3 might change the qualitative behaviour of the two-point correlator. The analysis has also been done for the second metric (5.5.11) and the results qualitatively behave the same. Nevertheless, the following should be considered as an analysis of a special case and probe the generality of the absence of the finite distance pole. Neither Eq. (5.5.6) nor (5.5.11) are considered as the correct effective metric.

5.5.2.2 Two-point Correlator

To evaluate the two-point correlator the strategy described in Secs. 5.4.2 and 5.4.3 is applied to Eq. (5.5.11). The missing derivatives entering Eq. (5.4.7) are

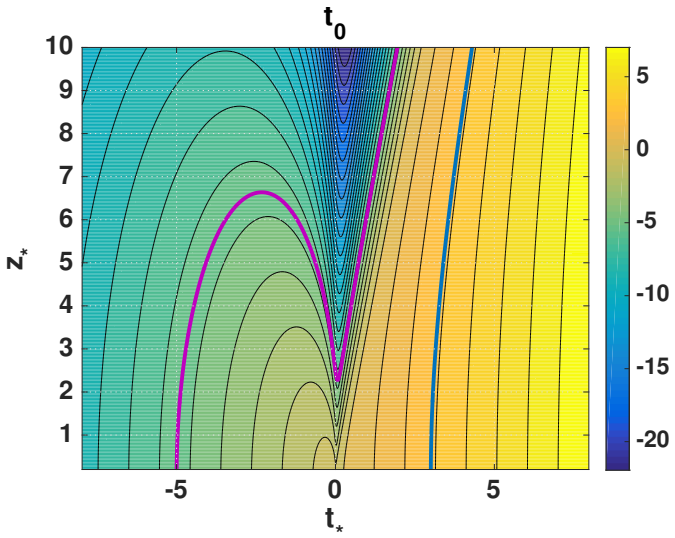

FIGURE 5.9: *Colour plot of $t_o(t_*, z_*)$ for the metric (5.5.5) with $t_o = -5$ (purple) and $t_o = 3$ (blue), $\lambda = 0.06$, $p = {}^{-1}/_{16}$, $\Delta p = {}^{3}/_{16}$, $a_{ext} = \lambda^p$. Passing from negative to positive t, there is a transition from $p_- = {}^{-1}/_{4}$ to $p_+ = {}^{1}/_{8}$. Two kinds of solutions are visible: The ones starting at negative t_o, which are bent towards the (resolved) singularity and eventually passing it (purple) and the ones starting at positive t_o, which are bent away from the (resolved) singularity (blue).*

$$\frac{\partial(a^2)}{\partial t} = 2a(t,z)^2 \left[\frac{pt}{t^2+\lambda^2 z^2} + \Delta p \frac{1}{\sqrt{t^2+\lambda^2 z^2}} \right] , \tag{5.5.13}$$

$$\frac{\partial(a^2)}{\partial z} = 2a(t,z)^2 \left[\frac{p\lambda^2 z}{t^2+\lambda^2 z^2} - \frac{\Delta p}{z} \frac{t}{\sqrt{t^2+\lambda^2 z^2}} \right] . \tag{5.5.14}$$

The corresponding t_o colour plot is shown in Fig. 5.9. Unlike the previous case $t_* < 0$ behaves different than $t_* > 0$ as the Kasner exponents change from negative to positive. It is possible to study initial times before and after the resolved singularity $t = 0$ and in Fig. 5.9 a line with $t_o = -5$ (purple) and $t_o = 3$ (blue) is highlighted. Again, there is a turning point for z_* around $t_* = 0$. In contrast to the previous case without Kasner transitions, geodesics can pass through the resolved singularity. Fig. 5.9 shows that geodesics with $t_o = -5$ exists, but turning point is at $t_* > 0$ In coherence with the analysis in [72], geodesics in the regime of $p < 0$ are bent towards the resolved singularity while in the regime with $p > 0$ they are bent away. Consequently for $t_* < 0$ the plot resembles the mirrored result of Fig. 5.3 (a) just mirrored, while for $t_* > 0$ the behaviour equals the classical case for $p > 0$. Fig. 5.10 shows the relation of z_* and l for the two cases $t_o = -5$ and $t_o = 3$. As the geodesics with $t_o = 3$ do not reach the singularity, they are not relevant in studying the finite distance pole of the two-point correlator. Nevertheless, in both cases z_* does not vanish for any finite boundary separation l.

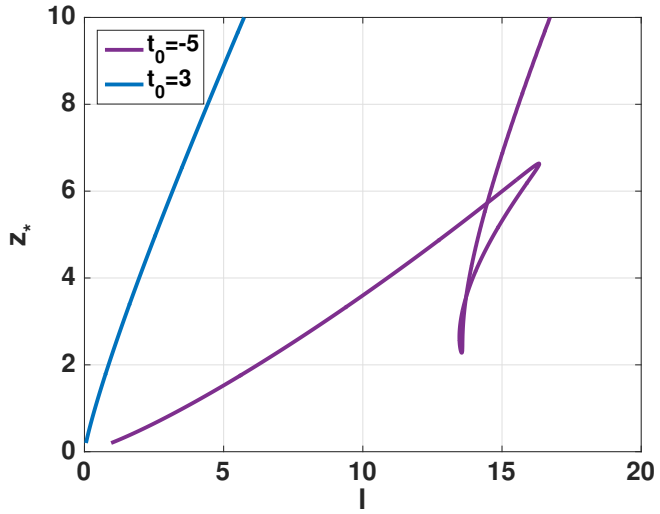

FIGURE 5.10: *z_* vs. l for $t_0 = -5$ (purple) and $t_0 = 3$ (blue) and $\lambda = 0.06$, $p = -1/16$, $\Delta p = 3/16$, $a_{ext} = \lambda^p$.*

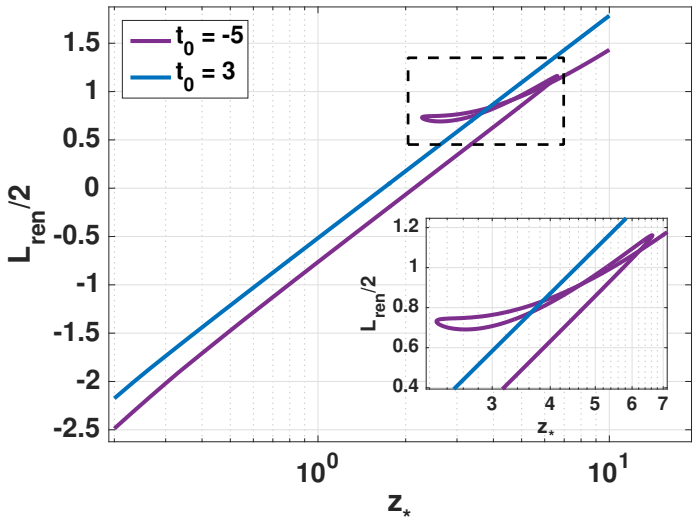

FIGURE 5.11: *Log-scale plot of L_{ren} vs. z_* for the metric (5.5.5) for $t_o = -5$ (purple) and $t_o = 3$ (blue), $\lambda = 0.06$, $p = -1/16$, $\Delta p = 3/16$, $a_{ext} = \lambda^p$. Again an asymptotic* log*-behaviour is visible.*

Before concluding a resolution of the finite distance pole, the relation of L_{ren} and z_* needs to be determined. This is computed again as described above and shown in Fig. 5.11. Again a log-dependence is visible in the classical regimes and deviations occur in the quantum regime. Numerical errors occur in the same manner as already discussed in Sec. 5.5.1. For completeness the blue line for $t_o = 3$ is also included in Fig. 5.11. The conclusion is the same: L_{ren} remains finite for all finite values of z_* and thus all boundary separations l. The finite distance pole is resolved, despite the different qualitative behaviour of the metric around $t = 0$. The effect of not having a maximum in $a(t, z)$ at $t = 0$ is that, as discussed above, geodesics can pass through the singularity and turn

around on the other side. This is a qualitative difference to both previous cases, [73] and for the metric (5.5.1).

5.6 Conclusion and Outlook from Resolved Cosmological Singularities

In the work presented in this chapter, the results of [73] were extended and previously made simplifications were overcome by using numerical methods. Although the qualitative features of the different metric under consideration changed, the conclusion remains the same: The resolved cosmological singularity is dual to the resolved finite distance pole in the dual CFT. This contributes to the discussion of a NTP [27, 28], as it was shown that singularity resolution in principle improves the behaviour of the two-point correlator.

An independent dual computation is still missing. Only if this is present, deeper conclusions about the singularity resolution can be made. Until now, it is uncertain what the inclusion of non-perturbative quantum effects is dual to on the CFT-side, i.e. finite N- or 't Hooft coupling-effects or a different state, in which the correlator is evaluated. Issues about definiteness of the dual CFT on a boundary, which is separated by a singularity as discussed in [27, 28], are not addressed either. In principle, independent CFT computations are possible, but technically out of reach. This is due to the fact that the CFT background is a time-dependent cosmological Kasner spacetime. Due to the large coupling λ, only non-perturbative approaches, such as lattice QCD techniques, are applicable. As the background is time-dependent, lattice techniques are not realisable and independent boundary computations are not in sight in the near future.

Another open problem is the fact that there is no final answer to the question of the correct 5d quantum metric. As argued in the previous chapter, a loop quantisation of the full 5d system is even in the symmetry reduced setup (midi-superspace model) out of reach. One possible strategy would be applying the mimetic gravity model [33, 193] to the 5d setting. This is possible as mimetic gravity is not restricted to any symmetry assumption and has the advantage of sharing the idea of a limiting curvature with LQG and LQC. In further work related to this thesis, the deeper connection between anisotropic LQC and mimetic gravity was analysed [2]. It was argued already in [194] that LQC and mimetic gravity differ in the anisotropic sector. The work [2] reformulates anisotropic mimetic gravity and demonstrates that it cannot be viewed as a polymer model. Consequently, a loop-quantisation cannot be performed. This supplements work in the spherically symmetric sector [36]. Note that for quantitative comparisons on both sides (gravity and dual CFT), it is crucial to have the correct quantum corrected metric.

The presented framework suffers from two main issues. Firstly, due to the time-

dependence of the background spacetime, independent CFT computations are not possible. Secondly, the quantum gravitational side is not accessible and it is very complex to go beyond the assumptions of the previous chapter. A possible way to improve the situation, still following the same idea, would be to change the framework to black holes. Considerable effort in the field of LQG inspired black holes has been done in the past years (see [18, 78, 87, 88, 196, 197]).

This framework promises better applicability, since for large distances from the singularity, the classical AdS-black hole reduces to AdS in global coordinates (cfr. Eq. (2.1.5)). In this case, the boundary is proper ∂AdS, i.e. fully symmetric and most importantly static. Hence, the boundary CFT would live on a Einstein-static universe (cfr. Eq. (2.2.7)) or if rephrased in Poincaré coordinates (2.1.11) simply flat Minkowski space. As a consequence, the background is static and even flat, and there is reason to assume that standard lattice techniques can be applied and independent computations become accessible. Also, the gravitational side is under better control. There is work in the framework of LQG, which already made progress in quantising spherically symmetric black hole interiors [78, 80, 88, 198, 199]. Nevertheless, in LQG there is still no consensus about black holes, which is addressed in the next chapter. This strategy will be pursued throughout the remainder of this thesis and the focus will shift towards quantum black holes.

Part III

Effective Polymer Black Holes

6

Effective Polymer Black Holes

As argued in the last chapter, black holes are suitable candidates for generalising the cosmological framework for studying holographic signatures of resolved singularities. Beside of this particular application, black holes are interesting objects in their own right. Originally discovered by Schwarzschild [200] and perceived as purely theoretical objects, it was later shown that they exist in nature and are part of modern astronomy [9, 10]. In different approaches of understanding their nature, especially the horizon and the singularity, important insights about quantum gravity were gained in the past. For example, black hole thermodynamics and the holographic principle are based on semi-classical considerations of black holes (cfr. Chpt. 3). Apart from cosmology, they are also explicit examples of singular spacetimes predicted by GR.

As such, black holes are a perfect test bed to study physics beyond classical GR. A further advantage is the high amount of symmetries, which allows analytic computations in the classical and semi-classical regime. Due to this, black holes are of special interest in all main approaches to quantum gravity as LQG [14–18], string theory [13, 19–22], AdS/CFT [23–28], as well as NCG [29–32] and related contexts [33–36]. In the following the approach of LQG is applied.

Black holes were studied extensively within the field of LQG [18, 74–86], but there is still a lack of agreement on a LQG-black hole model. This becomes obvious in recent activities of the field [18, 78, 87, 88, 196, 197, 201], where also the work [3, 5, 6] belongs

to, on which the following chapter is based.

For an application in the holographic setting, effective black hole models should be discussed in D-dimensions and negative cosmological constant. As the problem is not solved for $D = 4$ and $\Lambda = 0$, this simpler case is examined first. Furthermore the focus lies on effective (quantum corrected but classical) models, which is the first step in constructing a physically sensible model. Following the lines of LQG and polymerisation as shown in Chpt. 4, quantum effects are included by modifying the classical Hamiltonian before quantising the system. The effective solutions are an intermediate step and an approximation, assuming that quantum spacetime can always be approximated by a metric over a manifold. The validity of this approximation has to be studied as a next step. For the application to holography in the sense of Chpt. 5, this effective level would already be sufficient.

The Chapter is organised as follows: In a first instance, previous models of polymer black holes are reviewed and criteria for the validity of black hole models are worked out. In the next step, the classical canonical theory is reviewed in Sec. 6.2 and new variables are introduced. This is the basis for the following investigation. A first new model based on the polymerisation of these variables is introduced in Sec. 6.3. The effective solution, the causal structure of the spacetime and the onset of quantum effects are worked out in the Secs. 6.3.1-6.3.3. The obstruction of this first model are discussed and again new variables are introduced to overcome these limitations in Sec. 6.4. In the following subsections 6.4.1 and 6.4.2, the effective spacetime and the onset of quantum effects within this second model are discussed. The chapter concludes with Sec. 6.5, where achievements and limitations of the model are reviewed and an outlook on general future directions is given.

6.1 Previous Polymer Black Hole Models

Although there was much effort in constructing models of black holes based on LQG techniques, there is no final consensus about them. To understand this better, previous models are summarised here. On the basis of LQG, traditional formulations follow symmetry reduced Ashtekar-variables. As discussed in Sec. 3.1, the interior of a Schwarzschild black hole is spherically symmetric and homogeneous, thus describing Kantowski-Sachs cosmology. The standard formulation is in terms of the canonical pairs (b, p_b) and (c, p_c). Herein b and c are related to the components of the symmetry reduced Ashtekar connection, and p_b and p_c are related to the symmetry reduced densitised triads (see e.g. [87]

and Sec. 4.4)[1]. The line element takes the form

$$\mathrm{d}s^2 = -N_T^2(T)\mathrm{d}T^2 + \frac{p_b^2(T)}{L_o^2|p_c(T)|}\mathrm{d}x^2 + |p_c(T)|\mathrm{d}\Omega_2^2 \,, \tag{6.1.1}$$

where L_o is the length of the fiducial cell (cfr. Chpt. 4) and N_T is the Lapse function, which is a Lagrange multiplier. Note that by identifying $T = r$ and $x = t$, for $r < r_s$ the Schwarzschild metric (3.1.1) takes exactly this form. The above line element is restricted to the interior of the black hole. Outside, the spacetime is static and cannot be treated by symmetry reducing the ADM-Hamiltonian of GR (see [95]). For the interior, a proper Hamiltonian formulation exists, where the canonical variables satisfy the non-trivial Poisson brackets

$$\{b, p_b\} = \gamma \quad , \quad \{c, p_c\} = 2\gamma \,, \tag{6.1.2}$$

with $G = 1$ and γ the Barbero-Immirzi parameter (cfr. Sec. 4.4). The Hamiltonian describing the system is given by

$$H = N_T\mathcal{H} \quad , \quad \mathcal{H} = -\frac{b}{2\gamma^2 \mathrm{sign}(p_c)\sqrt{|p_c|}}\left(2cp_c + \left(b + \frac{\gamma^2}{b}\right)p_b\right) \approx 0 \,. \tag{6.1.3}$$

Solutions of the equations of motion lead to Schwarzschild spacetime. The next step is the polymerisation according to the replacement (see e.g. [78, 79, 88])

$$c \longmapsto \frac{\sin(\delta_c c)}{\delta_c} \quad , \quad b \longrightarrow \frac{\sin(\delta_b b)}{\delta_b} \,, \tag{6.1.4}$$

where δ_c and δ_b are the polymerisation scales controlling the onset of quantum effects[2]. These polymerisation scales should be considered as phase space functions and should be related to the Planck scale. In the regime where $\delta_c c$, $\delta_b b$ are small, the classical behaviour is recovered. In literature several different schemes were studied and classified as follows:

1. In the *μ_o-scheme*, polymerisation scales are chosen to be constant, so they are independent of the phase space. A selection of μ_o-models is [74, 75, 79, 203, 204].

2. More generic, one can allow δ_c, δ_b to be any phase space function of p_b and p_c,

[1] Do not confuse b with the areal radius introduced in Sec. 6.2, they are entirely different objects. Nevertheless, conventionally b is used for both without conflict, since it is used in different contexts. For keeping these conventions, this double notation is used here.

[2] As in cosmology, different polymerisation functions are possible in addition to the sin-function (see e.g. [59, 79, 83, 201, 202]).

which is then called *$\bar{\mu}$-scheme*, as in [80, 81] (see also [198, 199] for the cosmological Kantowski-Sachs setting).

3. A more recent development is provided by the so-called *generalised μ_o-schemes* where δ_c, δ_b are phase space dependent only through Dirac observables [18, 78, 87, 88].

The specification of polymerisation scales is a delicate procedure, which was executed in the different work above, due to different arguments. Usually these arguments come from full LQG and regard areas enclosed by a loop, similar as discussed in the case of cosmology in Sec. 4.4. However, none of the above models were fully consistent.

Approaching the problem from a different angle, it is possible to raise the question of when such a black hole model is acceptable. A first obvious requirement is the independence of physical results of the fiducial cell L_o. This was first achieved in [78]. Secondly, quantum effects should be constrained to the "quantum regime" only. That means in turn that the model should be in accordance with GR in a trustable regime. In the case of black holes, the horizon of large black holes is considered as a strong gravity regime, which has a valid description by GR. This classical regime can be classified by small (with respect to Planck) curvatures and large distance scales (see [205]). The models [80, 81] suffer from this feature, as quantum effects become large at the horizon, where the curvature is small. As a last point, the curvature should become bounded by quantum effects at a unique scale. It should not be possible to make the curvature (and matter densities) arbitrarily large by changing the system parameters, e.g. the masses. This would contradict the universality of the relevance of quantum effects, which is expected from a full theory of quantum gravity. Note that this universal bound was achieved in LQC (see Sec. 4.2). The first model achieving this was presented in [87, 88]. Nevertheless, technical difficulties were seen in regards to the applied generalised μ_o-scheme [4]. Further, it requires a careful analysis to argue that the asymptotic behaviour is in accordance with the second condition. The spacetime is asymptotically flat, however, not in the standard sense [206, 207].

In the following, different models are introduced, trying to meet the provided requirements. The main obstructions are quantum effects in the high curvature regime only and the unique upper curvature bound. As in LQC, the search of a proper polymerisation scheme is shifted towards finding suitable variables for describing the problem. As was shown in Sec. 4.4, it is equivalent to find a phase space dependent polymerisation scheme or to find variables where the same scheme has constant polymerisation scales.

6.2 Canonical Theory

The classical description of a Schwarzschild black hole was reviewed in Sec. 3.1. For a quantisation or better polymerisation as presented in Sec. 4.2, it is required to formulate a Hamiltonian framework for black holes. First of all, the assumption of a static and spherically symmetric spacetime is made. A generic line element satisfying both of these requirements is [208, 209]

$$\mathrm{d}s^2 = -\bar{a}(r)\mathrm{d}t^2 + N(r)\mathrm{d}r^2 + 2\bar{B}(r)\mathrm{d}t\mathrm{d}r + \bar{b}^2(r)\mathrm{d}\Omega_2^2 \,, \tag{6.2.1}$$

where $\bar{a}(r)$, $N(r)$, $\bar{B}(r)$ and $\bar{b}(r)$ are some functions depending only on r[3]. This line element can be substituted into the Einstein-Hilbert action ($G = c = 1$)

$$S_{EH} = \frac{1}{16\pi}\int \mathrm{d}^4x\,\sqrt{-g}R \,, \tag{6.2.2}$$

which leads after a straightforward computation, up to boundary terms, to

$$S_{EH} = \frac{1}{4}\int \mathrm{d}r\, L(\bar{a},\bar{b},\bar{n}) \,, \tag{6.2.3}$$

where the effective Lagrangian is given by

$$L(\bar{a},\bar{b},\bar{n}) = 2L_o\sqrt{\bar{n}}\left(\frac{\bar{a}'\bar{b}'\bar{b}}{\bar{n}} + \frac{\bar{a}\bar{b}'^2}{\bar{n}} + 1\right) \,, \tag{6.2.4}$$

and primes denote derivatives with respect to r. The new quantity $\bar{n}$ is defined as

$$\bar{n}(r) = \bar{a}(r)N(r) + \bar{B}^2(r) \,, \tag{6.2.5}$$

which is a Lagrange multiplier and reflects the gauge freedom of choosing different coordinates r and t. The metric quantities N and $\bar{B}$ can be related to the lapse and shift of the metric and thus are purely gauge. This is in accordance with $\bar{n}$ playing no physical role. Further, a fiducial cell in the divergent t-direction was introduced. As discussed in Sec. 4.1, due to the staticity of the system, the t-integral of the Einstein-Hilbert action diverges, unless it is regularised by a fiducial cell, here of coordinate size L_o. This fiducial length L_o in the Lagrangian (6.2.4) can be absorbed into the dynamical variables, leading

[3]Note that this ansatz is completely equivalent to Eq. (6.1.1), identifying the coordinates $r = T$ and $t = x$ as well as the metric components properly. Do not confuse b = component of Ashtekar connetion with b = areal radius.

to the smeared quantities

$$\sqrt{n} = \int_0^{L_o} \mathrm{d}t\sqrt{\bar{n}} = L_o\sqrt{\bar{n}} \quad , \quad \sqrt{a} = \int_0^{L_o} \mathrm{d}t\sqrt{\bar{a}} = L_o\sqrt{\bar{a}} \, ,$$
$$b = \bar{b} \quad , \quad B = \int_0^{L_o} \mathrm{d}t\bar{B} = L_o \, \bar{B} \, .$$

The Lagrangian takes the new form

$$L(a,b,n) = 2\sqrt{n}\left(\frac{a'b'b}{n} + \frac{ab'^2}{n} + 1\right) \, . \tag{6.2.6}$$

The dynamical variable $\sqrt{a}$ measures the physical size of the fiducial cell and is coordinate independent, as will be relevant below. This shows that L_o is only the coordinate size of the fiducial cell in t-coordinates and has to change when the coordinates change. A useful quantity is thus the size of the fiducial cell at a given reference point r_{ref}

$$\mathscr{L}_o := \sqrt{a}\Big|_{r=r_{\mathrm{ref}}} = L_o \, \sqrt{\bar{a}}\Big|_{r=r_{\mathrm{ref}}} \, , \tag{6.2.7}$$

which by construction is coordinate independent. Nevertheless, rescaling the fiducial cell by a constant factor α leads to the rescaling $\mathscr{L}_o \mapsto \alpha\mathscr{L}_o$ and $L_o \mapsto \alpha L_o$. Note that $\mathscr{L}_o$ is coordinate independent, but completely fiducial, because it depends on the reference point r_{ref} and the fiducial length L_o. In all physical quantities, both $\mathscr{L}_o$ and L_o have to drop out.

Having the Lagrangian settled, the Hamiltonian is achieved by a Legendre transformation[4]. The canonical momenta are given by

$$p_a = \frac{\partial L}{\partial a'} = \frac{2bb'}{\sqrt{n}} \quad , \quad p_b = \frac{\partial L}{\partial b'} = \frac{4ab' + 2a'b}{\sqrt{n}} \quad , \quad p_n = \frac{\partial L}{\partial n'} = 0 \, , \tag{6.2.8}$$

and the vanishing of p_n shows the existence of constraints, as expected. The Hamiltonian

[4]Note that this Hamiltonian is not the same as gained by symmetry reducing the usual ADM-Hamiltonian of GR. The difference is the $3+1$ split, which foliates spacetime in spatial slices. While in the ADM-formulation this foliation is always timelike, this is not true in the present case. Here, the normal to the foliation is $\propto {}^{\partial}/_{\partial r}$, which is spacelike for the exterior region and thus can not be covered by the ADM-Hamiltonian. In the interior, where ${}^{\partial}/_{\partial r}$ is timelike, the foliation is again timelike and both descriptions coincide.

is given by

$$H_{cl} = \sqrt{n}\mathcal{H}_{cl} + \Lambda p_n \quad , \quad \mathcal{H}_{cl} = \frac{p_a p_b}{2b} - \frac{a p_a^2}{2b^2} - 2 \, , \tag{6.2.9}$$

where the primary constraint $p_n \approx 0$ is implemented via the Lagrange multiplier $\Lambda(r)$. The Dirac stability algorithm leads to the secondary constraint $\mathcal{H}_{cl} \approx 0$, where it terminates. As the equations of motion lead to $n' = \{n, H\} = \Lambda$, the canonical pair (n, p_n) is completely arbitrary and can be removed from the phase space by treating n as arbitrary Lagrange multiplier. The Hamiltonian equations of motion are

$$\begin{aligned} a' &= \sqrt{n}\left(\frac{p_b}{2b} - \frac{a p_a}{b^2}\right) \\ p_a' &= \sqrt{n}\frac{p_a^2}{2b^2} \\ b' &= \sqrt{n}\frac{p_a}{2b} \\ p_b' &= \sqrt{n}\left(\frac{p_a p_b}{2b^2} - \frac{a p_a^2}{b^3}\right) \\ \mathcal{H}_{cl} &= \frac{p_a p_b}{2b} - \frac{a p_a^2}{2b^2} - 2 \approx 0 \end{aligned} \tag{6.2.10}$$

where n is an arbitrary function which needs to be specified before solving the system. It is possible to perform a canonical transformation, mapping the Hamiltonian Eq. (6.2.9) to Eq. (6.1.3) in terms of connection variables, showing equivalence of the two descriptions (cfr. [3]).

An important observation is the scaling behaviour of the canonical variables. When the fiducial cell is rescaled by a constant factor $L_o \mapsto \alpha L_o$, the canonical variables transform as

$$\sqrt{n} \mapsto \alpha\sqrt{n} \quad , \quad a \mapsto \alpha^2 a \quad , \quad b \mapsto b \quad , \quad p_a \mapsto \alpha^{-1} p_a \quad , \quad p_b \mapsto \alpha \, p_b \, , \tag{6.2.11}$$

due to their definitions in Eqs. (6.2.6) and (6.2.8). Obviously, physical quantities cannot depend on fiducial structures, i.e. can only be dependent on b, $a/\mathscr{L}_o^2$, $\mathscr{L}_o p_a$ and $p_b/\mathscr{L}_o$. It can be shown that the equations of motion (6.2.10) are invariant under fiducial cell rescaling.

As discussed in e.g. [209], these equations of motion lead to the Schwarzschild solution of mass M in Schwarzschild coordinates for $N(r) = \left(1 - \frac{2M}{r}\right)^{-1}$ (cfr. Eq. (3.1.1)). It is nevertheless instructive to study their solutions and the solution strategy in more detail.

For doing so, a canonical transformation is performed to the variables polymerised in

the following. The new variables are defined as

$$\begin{aligned} v_1 &= \frac{2}{3}b^3 \quad , \quad P_1 = \frac{a'}{\sqrt{n}\,b} = \left(\frac{p_b}{2b^2} - \frac{a p_a}{b^3}\right) , \\ v_2 &= 2ab^2 \quad , \quad P_2 = \frac{b'}{\sqrt{n}\,b} = \frac{p_a}{2b^2} , \end{aligned} \tag{6.2.12}$$

which satisfy the Possion brackets

$$\{v_1, P_1\} = 1 \quad , \quad \{v_2, P_2\} = 1 ,$$

while all other brackets vanish. Under fiducial cell rescaling these variables transform as

$$v_1 \mapsto v_1 \quad , \quad v_2 \mapsto \alpha^2\, v_2 \quad , \quad P_1 \mapsto \alpha\, P_1 \quad , \quad P_2 \mapsto \alpha^{-1}\, P_2 . \tag{6.2.13}$$

With these variables the Hamiltonian takes the particularly simple form

$$H_{cl} = \sqrt{n}\mathcal{H}_{cl} \quad , \quad \mathcal{H}_{cl} = 3v_1P_1P_2 + v_2P_2^2 - 2 \approx 0 . \tag{6.2.14}$$

The corresponding equations of motion are thus given by

$$v_1' = 3\sqrt{n}v_1P_2 \tag{6.2.15a}$$
$$v_2' = 3\sqrt{n}v_1P_1 + 2\sqrt{n}v_2P_2 \tag{6.2.15b}$$
$$P_1' = -3\sqrt{n}P_1P_2 \tag{6.2.15c}$$
$$P_2' = -\sqrt{n}P_2^2 \tag{6.2.15d}$$
$$\mathcal{H}_{cl} = 3v_1P_1P_2 + v_2P_2^2 - 2 \approx 0 , \tag{6.2.15e}$$

which can be easily solved by choosing the gauge $\sqrt{n} = const. = \mathscr{L}_o$. Integrating the Eq. (6.2.15d) yields

$$P_2(r) = \frac{1}{\sqrt{n}(r + A)} , \tag{6.2.16}$$

which can be inserted into Eqs. (6.2.15c) and (6.2.15a), and yields after another integration

$$P_1 = -\frac{C}{(r + A)^3} \quad , \quad v_1 = D(r + A)^3 , \tag{6.2.17}$$

with the integration constants A, C and D. The solution for v_2 can be derived from the Hamiltonian constraint (Eq. (6.2.15e)) as

$$v_2(r) = \frac{2}{P_2^2(r)} - 3v_1(r)\frac{P_1(r)}{P_2(r)} = \sqrt{n}(r+A)^2\left(2\sqrt{n} - \frac{3CD}{r+A}\right) . \tag{6.2.18}$$

Note that the integration constant A is only a shift in r and can be removed by a coordinate redefinition. Without loss of generality, $A = 0$ can be chosen, and the system is left with two integration constants C, D, needing to be fixed by means of initial conditions. This is perfectly consistent with the Dirac analysis of the system. The phase space is four dimensional and there is one first class constraint $\mathcal{H} \approx 0$, removing two physical degrees of freedom. The constraint surface is two dimensional, corresponding to the need for two initial conditions or Dirac observables to determine the system. Fixing the value of these Dirac observables, which are by definition gauge independent, should determine the integration constants C, D. Under a rescaling of the fiducial cell C, D transform as

$$C \mapsto \alpha C \qquad , \qquad D \mapsto D \, , \tag{6.2.19}$$

indicating that the above procedure might not work, as C is dependent on the fiducial structures.

A straightforward way of interpreting the integration constants is to reconstruct the line element (6.2.1). Further all dependencies by r are re-expressed in terms of b, which is the areal radius[5] and a scalar in the spherically symmetric setting. This way all ambiguities coming from coordinate transformations are removed. Reversing the expressions (6.2.12) gives

$$a(b) = \frac{\mathscr{L}_o^2}{\left(\frac{3D}{2}\right)^{\frac{2}{3}}}\left(1 - \left(\frac{3}{2}D\right)^{\frac{4}{3}}\frac{C}{\sqrt{n}}\frac{1}{b}\right) , \tag{6.2.20}$$

where $\sqrt{n} = \mathscr{L}_o$ was used. It follows immediately $\bar{a}(r) = a/L_o^2$ and the line element

$$\mathrm{d}s^2 = -\frac{\mathscr{L}_o^2}{L_o^2\left(\frac{3D}{2}\right)^{\frac{2}{3}}}\left(1 - \left(\frac{3}{2}D\right)^{\frac{4}{3}}\frac{C}{\sqrt{n}}\frac{1}{b}\right)\mathrm{d}t^2 + N(b)\mathrm{d}r^2 + 2\bar{B}\mathrm{d}t\mathrm{d}r + b^2\mathrm{d}\Omega_2^2 . \tag{6.2.21}$$

[5]The area of a spherical region is given by $\mathcal{A} = 4\pi b^2$ and a scalar with respect to spherically symmetry preserving diffeomorphisms. Consequently $b = \sqrt{\mathcal{A}/4\pi}$ is a scalar determined by the area. Therefore, the name is justified, as it is the radius of a sphere with surface area $\mathcal{A}$.

$\bar{B} = 0$ is a convenient gauge[6], with Eq. (6.2.5) leading to $N = {}^{n}/_{a} = {}^{\mathscr{L}_o^2}/_{a}$. Further changing the coordinates $t \mapsto \tau = \mathscr{L}_o(3D/2)^{-\frac{1}{3}}t/L_o$ and $r \mapsto b = (3D/2)^{\frac{1}{3}}r$ yields the final metric

$$\mathrm{d}s^2 = -\left(1 - \frac{2M}{b}\right)\mathrm{d}\tau^2 + \frac{1}{1-\frac{2M}{b}}\mathrm{d}b^2 + b^2\mathrm{d}\Omega_2^2 \,, \tag{6.2.22}$$

where

$$2M = \left(\frac{3}{2}D\right)^{\frac{4}{3}}\frac{C}{\sqrt{n}} \,, \tag{6.2.23}$$

was identified as the black hole mass. There are two main observations to be made. Firstly, the line element is the classical Schwarzschild metric (3.1.1) and does not contain any dependencies on fiducial structures. This can be viewed as a cross check of the Hamiltonian analysis and the chosen variables. Secondly, the metric only depends on $2M$, which is a function on the combination of C and D, but not the integration constants individually. The physical situation is determined by giving the physical input of the black hole mass M. This does not fix the values of C and D, but only their combined value.

This can be understood in terms of Dirac observables. As argued, there should be two Dirac observables, i.e. commuting with the Hamiltonian constraint $\mathcal{H}_{cl}$. Indeed, there are two independent ones, namely

$$\mathcal{M} = \left(\frac{3}{2}v_1\right)^{\frac{4}{3}}\frac{P_1P_2}{2} = \frac{b^2a'b'}{2n} \,, \tag{6.2.24}$$

$$\mathcal{O} = v_1P_1 \,. \tag{6.2.25}$$

The first one is the black hole mass as

$$\mathcal{M} \overset{\text{on-shell}}{=} M = \left(\frac{3}{2}D\right)^{\frac{4}{3}}\frac{C}{2\sqrt{n}} \,,$$

where on-shell means evaluated on the solutions of the equations of motion and the constraint surface. The second observable $\mathcal{O}$ reduces on-shell to the product CD. Fixing a specific value for $\mathcal{M}$ and $\mathcal{O}$ uniquely determines the values for the integration constants

[6]This leads to the classical black hole metric in Schwarzschild coordinates. It is of course possible to choose $\bar{B} \neq 0$ which allows to bring the metric in e.g. in-/outgoing Eddington-Finkelstein coordinates.

C and D. The observation above was that the value of $\mathcal{O}$ is insignificant for determining the physical situation. As already indicated above, there is no other possibility, as the observables transform under fiducial cell rescaling as

$$\mathcal{M} \longmapsto \mathcal{M} \quad , \quad \mathcal{O} \longmapsto \alpha\mathcal{O} \, , \tag{6.2.26}$$

which proves on the one hand that the line element (6.2.22) is fiducial cell independent and on the other hand that $\mathcal{O}$ can not appear in any physical observable due to this fiducial cell dependence. It has to be physically irrelevant, which is consistent with the above observation.

This appears to be a contradiction to the canonical analysis and the constraints. As the observable $\mathcal{O}$ is not of physical relevance, it has to be a gauge degree of freedom. Hence, there has to be a corresponding gauge transformation and a constraint generating it. The paradox can be solved as follows: The transformation done to remove $\mathcal{O}$ from the metric[7] was rescaling $t \mapsto \tau = const. \cdot t$. This is exactly the gauge transformation which was missing in the analysis above. The crucial point is that this transformation is not present on the phase space. The factor $D^{1/3}$ was removed in front of $\bar{a}$ but not in front of a, as the latter is a spacetime scalar. Indeed, changing the time coordinate $t \mapsto const. \cdot t$ leads to the transformation behaviour

$$\sqrt{a} = L_o\sqrt{\bar{a}} = \int_0^{L_o} dt\sqrt{\bar{a}} = \int_{\tau(0)}^{\tau(L_o)} d\tau\sqrt{\tilde{\bar{a}}} = \tau(L_o)\sqrt{\tilde{\bar{a}}} = \sqrt{a} \, , \tag{6.2.27}$$

which is the identity map on the phase space. As such, it is not present on the phase space and there is no constraint generating this transformation. Thus, the counting of canonical degrees of freedom was correct. The remaining freedom becomes obvious only after going back to metric quantities $\bar{a}$, where this transformation is non-trivial.

The reason why this time rescaling is not present on the phase space is due to the integration over the fiducial cell. This integration makes the quantity a effectively a scalar but dependent on the fiducial cell. Turning the logic around, the fiducial cell dependence indicated that the canonical quantity is no scalar, once rephrased in terms of metric components. This reasoning can be summarised as follows:

There are residual diffeomorphisms redefining the time coordinate. In order to regularise the phase space and to make the canonical quantities scalars, with respect to these residual diffeomorphism, they were integrated over a fiducial cell. The integrated quantities are effectively scalars and thus do not transform under these residual diffeomor-

[7]The factor $D^{\frac{1}{3}}$ was removed which corresponds to the fraction $\mathcal{M}/\mathcal{O}$

phisms. As demonstrated above, this transformation is not present on the phase space. The dependence on these diffeomorphisms is still visible, because it was integrated over the fiducial structure, and thus the corresponding canonical variables scale as the fiducial cell is rescaled. Going back to the metric components, the fiducial cell dependence is removed, but the metric transforms non-trivially under residual diffeomorphism. This freedom can be used to remove the value of $\mathcal{O}$ evaluated on-shell from the physical metric.

This issue was first observed in [3] and discussed in detail in [6] and will play a crucial role in constructing observables in the effective quantum model.

Finally, it is possible to interpret the chosen variables, especially the momenta on-shell, which can be written as

$$\frac{P_1(b)}{\mathscr{L}_o} = \frac{2M}{b^3}\left(\frac{2}{3D}\right)^{\frac{1}{3}} \quad , \quad P_2(b)\mathscr{L}_o = \frac{1}{b}\left(\frac{3D}{2}\right)^{\frac{1}{3}} \, , \tag{6.2.28}$$

from which follows that for mass independent D, $P_1/\mathscr{L}_o$ is related to the square root of the Kretschmann scalar (cfr. Eq. (3.1.5)). Thus, this variable will be useful to identify the high and low curvature regime and to relate the onset of quantum effects to a curvature scale. Details and subtleties will be discussed below. Further, for mass independent D, the second momentum $P_2\mathscr{L}_o$ is related to inverse length. This variable is useful, as it relates the onset of quantum effects to small length scales, which is physically plausible. In the following section effective quantisation schemes based on Chpt. 4 are discussed. An important part of the discussion will be the problem of how to fix the onset of quantum effects to a certain curvature and length scale. The above defined variables represent a good starting point for this.

6.3 Polymerisation 1: (v_i, P_i)-variables

In the next step, quantum effects are included by means of polymerisation as introduced already in Sec. 4.2. As for the interior of the black hole $(a, N < 0)$, the spacetime becomes homogeneous Kantowski-Sachs cosmology and thus constant r-slices are spatial, the notion of polymerisation is well-defined and can be motivated along the same lines as in Sec. 4.2. Indeed, as discussed, this method was used by a series of earlier approaches [74, 75, 78–81, 87, 88]. The following procedure could be viewed as only describing the interior of the black hole and the exterior solution is achieved by analytical continuation. As will be shown below, the equations of motion do not make a distinction between interior and exterior and thus the solutions are directly valid for both regions.

In practice, polymerisation means a replacement of the canonical momenta in terms of

their point holonomies with a given polymerisation scale λ, related to $\hbar$. As discussed in Sec. 4.4 and the beginning of this chapter, there are several possibilities of choosing the scheme, i.e. a μ_o-scheme in which the polymerisation scale is constant on the phase space, or a $\bar{\mu}$-scheme, where the scale is phase space dependent. In recent works [87, 88] the intermediate generalised μ_o-scheme was introduced. In this scheme the polymerisation scale depends on the phase space through Dirac observables. Due to this ambiguity in choosing the scheme, it is equivalent to keep a μ_o-scheme with constant polymerisation scales and analyse different variables. This is exactly what happens in (v, b) variables for cosmology, where in these variables the polymerisation scale is constant, while it is phase space dependent in connection variables (cfr. Sec. 4.4). These kind of models can be viewed as phenomenological models whose physical consequences of a particular scheme have to be analysed. A necessary step is a relation of the model to the symmetry reduced sector of a fundamental quantum theory[8].

As discussed above, the physical requirement on an effective quantum model of black holes is that quantum effects occur in the high curvature regime and are negligible in the low curvature regime. The variables P_1 and P_2 are suitable variables to achieve this with constant polymerisation scales λ_1 and λ_2. Polymerisation refers to the replacement of these momenta by means of a function of their exponentials, i.e. point holonomies. As motivated above (see Sec. 4.2), a common choice in the LQC literature (see e.g. [16, 138]) is the sin-function, i.e.

$$P_1 \longmapsto \frac{\sin(\lambda_1 P_1)}{\lambda_1} , \tag{6.3.1}$$

$$P_2 \longmapsto \frac{\sin(\lambda_2 P_2)}{\lambda_2} . \tag{6.3.2}$$

Different choices are possible, however, this simple choice is most likely not the "correct" one. More sophisticated approaches require input from the anomaly-freedom condition of the constraint algebra (see e.g. [212, 213]), preserving algebraic structures on the phase space [149], or renormalisation, e.g. [152, 153]. Although different choices lead to different phenomenology [59, 214], this simple choice is analysed here.

A quick preliminary analysis is instructive to lay out the expectations for this scheme. In the classical regime it holds $\lambda_1 P_1 \ll 1$ and $\lambda_2 P_2 \ll 1$, as

[8]There is much work in the literature which construct examples for this, see e.g. [54, 56, 57, 62, 63, 210]. Conceptually, one has to bridge a description of many small quantum numbers to a description of only few large quantum numbers, see e.g. [152, 153]. Going beyond the homogeneous sector might also result in non-trivial physics as a signature change [83, 211].

$$\frac{\sin(\lambda_1 P_1)}{\lambda_1} \simeq P_1 + \mathcal{O}\left(\lambda_1^2\right), \quad \lambda_1 P_1 \ll 1 ,$$
$$\frac{\sin(\lambda_2 P_2)}{\lambda_2} \simeq P_2 + \mathcal{O}\left(\lambda_2^2\right), \quad \lambda_2 P_2 \ll 1 .$$

As both scales λ_1 and λ_2 are related to the Plank scale ℓ_p, and P_1 is related to the Kretschmann scalar as well as P_2 to inverse distances, the classical regime is expected to be at low curvatures and long distances. This can be made more precise by analysing the dimensions. Since $\bar{a}$ is dimensionless, it is $[a] = L^2$, $[n] = L^2$ and $[b] = L$, where L denotes the dimension of length. Recalling the definition of the variables (6.2.12), yields the dimensions

$$[P_1] = \left[\frac{a'}{\sqrt{n}b}\right] = \frac{1}{L} ,$$
$$[P_2] = \left[\frac{b'}{\sqrt{n}b}\right] = \frac{1}{L^2} .$$

Note that P_1 and P_2 transform under fiducial cell rescaling according to Eq. (6.2.13), and also the polymerisation scales have to scale as

$$\lambda_1 \longmapsto \frac{1}{\alpha}\lambda_1 \quad , \quad \lambda_2 \longmapsto \alpha\lambda_2 , \tag{6.3.3}$$

in order to keep the product $\lambda_i P_i$ invariant. The scale invariant and hence physical scales are thus the combinations $\mathscr{L}_o\lambda_1$ and $\lambda_2/\mathscr{L}_o$. Out of all hypothetical experiments, only these combinations can be determined and have physical relevance. As further the product $\lambda_i P_i$ has to be dimension-free, this implies

$$[\lambda_1] = \left[\frac{1}{P_1}\right] = L \quad , \quad [\mathscr{L}_o\lambda_1] = L^2 ,$$
$$[\lambda_2] = \left[\frac{1}{P_2}\right] = L^2 \quad , \quad \left[\frac{\lambda_2}{\mathscr{L}_o}\right] = L .$$

The physical scale $\mathscr{L}_o\lambda_1$ has the dimension of an inverse curvature scale and should be related to inverse Planck curvature. On the other hand, $\lambda_2/\mathscr{L}_o$ has dimension length and should be directly related to the Planck length. The expectation is that $\mathcal{L}_o\lambda_1$ controls the

onset of curvature quantum effects, while $\lambda_2/\mathscr{L}_o$ controls the small length effects.

As stated above, it is possible to map the variables (v_i, P_i) to connection variables[9] $(b^{(\mathrm{conn})}, p_b^{(\mathrm{conn})})$, $(c^{(\mathrm{conn})}, p_c^{(\mathrm{conn})})$ by means of a canonical transformation [3]. This allows to classify the scheme where P_i is polymerised with constant λ_i. If the polymerisation scheme is adopted by means of the conditions

$$\lambda_1 P_1 \stackrel{!}{=} \delta_c c^{(\mathrm{conn})} \quad , \quad \lambda_2 P_2 \stackrel{!}{=} \delta_b b^{(\mathrm{conn})} \, ,$$

the corresponding effective Hamiltonian leads to the same dynamics. It turns out that this implies

$$\begin{aligned} \delta_c &= \pm \frac{8\lambda_1}{\beta\sqrt{|p_c^{(\mathrm{conn})}|}} \, , \\ \delta_b &= \pm \frac{4\lambda_2}{\beta|p_b^{(\mathrm{conn})}|} \, , \end{aligned}$$

which allows to classify the applied polymerisation (λ_i being constant) as a $\bar{\mu}$-scheme.

6.3.1 Solutions

After polymerising the effective Hamiltonian takes the form[10]

$$H_{\mathrm{eff}} = \sqrt{n}\mathcal{H}_{\mathrm{eff}} \quad , \quad \mathcal{H}_{\mathrm{eff}} = 3v_1 \frac{\sin(\lambda_1 P_1)}{\lambda_1}\frac{\sin(\lambda_2 P_2)}{\lambda_2} + v_2 \frac{\sin(\lambda_2 P_2)^2}{\lambda_2^2} - 2 \approx 0 \, . \tag{6.3.4}$$

For what follows, the gauge is fixed by $\sqrt{n} = \mathscr{L}_o = const.$ The effective equations of motion read

[9] The superscript makes explicit that here instead of the areal radius b and its conjugate momentum p_b from Sec. 6.2, connection variables $(b^{(\mathrm{conn})}, p_b^{(\mathrm{conn})})$ are intended.

[10] It is significant that this Hamiltonian has a relatively simple structure thinking about a possible quantum theory. Assigning operators to the canonical variables is (up to the usual ordering ambiguities) straightforward, since all variables occur only with positive and at most quadratic powers (see [3]).

$$v_1' = 3\sqrt{n}v_1 \cos(\lambda_1 P_1) \frac{\sin(\lambda_2 P_2)}{\lambda_2} , \tag{6.3.5a}$$

$$v_2' = 3\sqrt{n}v_1 \frac{\sin(\lambda_1 P_1)}{\lambda_1} \cos(\lambda_2 P_2) + 2\sqrt{n}v_2 \frac{\sin(\lambda_2 P_2)}{\lambda_2} \cos(\lambda_2 P_2) , \tag{6.3.5b}$$

$$P_1' = -3\sqrt{n} \frac{\sin(\lambda_1 P_1)}{\lambda_1} \frac{\sin(\lambda_2 P_2)}{\lambda_2} , \tag{6.3.5c}$$

$$P_2' = -\sqrt{n} \frac{\sin(\lambda_2 P_2)^2}{\lambda_2^2} , \tag{6.3.5d}$$

$$\mathcal{H}_{\text{eff}} = 3v_1 \frac{\sin(\lambda_1 P_1)}{\lambda_1} \frac{\sin(\lambda_2 P_2)}{\lambda_2} + v_2 \frac{\sin(\lambda_2 P_2)^2}{\lambda_2^2} - 2 \approx 0 . \tag{6.3.5e}$$

The coupling structure of the equations is the same as for the classical equations (6.2.15). Consequently, it is possible to apply the same solution strategy as classically, namely first solving the equation for P_2 and inserting the result in the equation for P_1 and v_1, which are then decoupled. Once these equations are solved, v_2 can be extracted by using the Hamiltonian constraint.

Integrating Eq. (6.3.5d) yields

$$\cot(\lambda_2 P_2) = \frac{\sqrt{n}}{\lambda_2} (r + A) , \tag{6.3.6}$$

where A is an integration constant. As in the classical analysis, A corresponds to a shift in the r coordinate that can be chosen to be zero without loss of generality. Inverting this equation to get $P_2(r)$ is subtle due to the different branches of cot. By inverting it, the branches are selected so that P_2 remains smooth in $r = 0$, i.e.

$$P_2(r) = \frac{1}{\lambda_2} \cot^{-1}\left(\frac{\sqrt{n}\, r}{\lambda_2}\right) + \frac{\pi}{\lambda_2} \theta\left(-\frac{\sqrt{n}\, r}{\lambda_2}\right) , \tag{6.3.7}$$

where $\theta(x)$ is the Heavyside-step-function. Note that this solution is valid for all $r \in (-\infty, \infty)$. This is counter-intuitive as r is classically directly related to the areal radius. It is nevertheless well-posed as r is only a coordinate and the physical quantity is the areal radius $b(r)$, which is always positive. For $\sqrt{n}r/\lambda_2 \gg 1$, this reduces to

$$P_2(r) = \frac{1}{\lambda_2} \cot^{-1}\left(\frac{\sqrt{n}\, r}{\lambda_2}\right) + \frac{\pi}{\lambda_2} \theta\left(-\frac{\sqrt{n}\, r}{\lambda_2}\right) \xrightarrow{\frac{\sqrt{n}r}{\lambda_2} \to \infty} \frac{1}{\sqrt{n}\, r} , \tag{6.3.8}$$

which corresponds to the classical result Eq. (6.2.16). Only the expressions

$$\frac{\sin\left(\lambda_2 P_2\right)}{\lambda_2} = \frac{1}{\lambda_2}\frac{1}{\sqrt{1+\left(\frac{\sqrt{n}\,r}{\lambda_2}\right)^2}}\,, \tag{6.3.9}$$

$$\cos\left(\lambda_2 P_2\right) = \frac{1}{\lambda_2}\frac{\sqrt{n}\,r}{\sqrt{1+\left(\frac{\sqrt{n}\,r}{\lambda_2}\right)^2}}\,, \tag{6.3.10}$$

are of physical importance. Inserting Eq. (6.3.9) into Eq. (6.3.5c) yields

$$P_1' = -3\sqrt{n}\,\frac{\sin\left(\lambda_1 P_1\right)}{\lambda_1}\frac{1}{\lambda_2}\frac{1}{\sqrt{1+\left(\frac{\sqrt{n}\,r}{\lambda_2}\right)^2}}\,, \tag{6.3.11}$$

which is solved by

$$P_1(r) = \frac{2}{\lambda_1}\cot^{-1}\left(\frac{\lambda_2^3}{4C\lambda_1\sqrt{n}^3}\left(\frac{\sqrt{n}\,r}{\lambda_2}+\sqrt{1+\frac{n\,r^2}{\lambda_2^2}}\right)^3\right)\,, \tag{6.3.12}$$

where C is an integration constant. Note that since $\sqrt{n}/\lambda_2$ is fiducial cell independent and λ_1 scales according to Eq. (6.3.3), C has to scale as $C \mapsto \alpha C$. Moreover, the argument of $\cot^{-1}(x)$ is always positive, i.e. there are no continuity issues here. The classical regime is given by $\sqrt{n}r/\lambda_2 \gg 1$ and $2r^3/C\lambda_1 \gg 1$, as Eq. (6.3.12) reduces to

$$P_1(r) \xrightarrow{\frac{\sqrt{n}r}{\lambda_2}\to\infty} \frac{2}{\lambda_1}\cot^{-1}\left(\frac{2r^3}{C\lambda_1}\right) \xrightarrow{\frac{2r^3}{C\lambda_1}\to\infty} \frac{C}{r^3}\,, \tag{6.3.13}$$

which is in agreement with the classical solution (6.2.17). Again, the physically relevant quantities are

$$\frac{\sin\left(\lambda_1 P_1\right)}{\lambda_1} = \frac{\lambda_2^3}{2C\lambda_1^2\sqrt{n}^3}\frac{\left(\frac{\sqrt{n}r}{\lambda_2}+\sqrt{1+\frac{nr^2}{\lambda_2^2}}\right)^3}{\frac{\lambda_2^6}{16C^2\lambda_1^2n^3}\left(\frac{\sqrt{n}r}{\lambda_2}+\sqrt{1+\frac{nr^2}{\lambda_2^2}}\right)^6+1}\,, \tag{6.3.14}$$

$$\cos\left(\lambda_1 P_1\right) = \frac{\frac{\lambda_2^6}{16C^2\lambda_1^2n^3}\left(\frac{\sqrt{n}r}{\lambda_2}+\sqrt{1+\frac{nr^2}{\lambda_2^2}}\right)^6-1}{\frac{\lambda_2^6}{16C^2\lambda_1^2n^3}\left(\frac{\sqrt{n}r}{\lambda_2}+\sqrt{1+\frac{nr^2}{\lambda_2^2}}\right)^6+1}\,. \tag{6.3.15}$$

Continuing by inserting Eqs. (6.3.9) and (6.3.14) into Eq. (6.3.5a) leads to

$$\frac{v_1'}{v_1} = 3\frac{\sqrt{n}}{\lambda_2}\frac{1}{\sqrt{1+\left(\frac{nr}{\lambda_2}\right)^2}}\frac{\frac{\lambda_2^6}{16C^2\lambda_1^2n^3}\left(\frac{\sqrt{n}r}{\lambda_2}+\sqrt{1+\frac{nr^2}{\lambda_2^2}}\right)^6-1}{\frac{\lambda_2^6}{16C^2\lambda_1^2n^3}\left(\frac{\sqrt{n}r}{\lambda_2}+\sqrt{1+\frac{nr^2}{\lambda_2^2}}\right)^6+1}\,, \tag{6.3.16}$$

which can be integrated to

$$v_1(r) = \frac{2C^2\lambda_1^2\sqrt{n}^3}{\lambda_2^3}D\frac{\frac{\lambda_2^6}{16C^2\lambda_1^2n^3}\left(\frac{\sqrt{n}r}{\lambda_2}+\sqrt{1+\frac{nr^2}{\lambda_2^2}}\right)^6+1}{\left(\frac{\sqrt{n}r}{\lambda_2}+\sqrt{1+\frac{nr^2}{\lambda_2^2}}\right)^3}\,, \tag{6.3.17}$$

where D is an integration constant. Again note that according to Eq. (6.2.13), D is fiducial cell independent. The classical behaviour (6.2.17) is recovered in the same limits as before, i.e.

$$v_1(r) \xrightarrow{\frac{\sqrt{n}r}{\lambda_2}\to\infty} D\frac{C^2\lambda_1^2}{4r^3}\left(\frac{4r^6}{C^2\lambda_1^2}+1\right) \xrightarrow{\frac{2r^3}{C\lambda_1}\to\infty} Dr^3\,. \tag{6.3.18}$$

Using these solutions and observing that

$$v_1\frac{\sin\left(\lambda_1 P_1\right)}{\lambda_1} = const. = CD\,, \tag{6.3.19}$$

the Hamiltonian constraint (6.3.5e) can be used to find the solution for $v_2(r)$ as

$$\begin{aligned} v_2(r) &= \frac{\lambda_2^2}{\sin\left(\lambda_2 P_2\right)^2}\left(2-3v_1\frac{\sin\left(\lambda_1 P_1\right)}{\lambda_1}\frac{\sin\left(\lambda_2 P_2\right)}{\lambda_2}\right) \\ &= 2n\left(\frac{\lambda_2}{\sqrt{n}}\right)^2\left(1+\frac{nr^2}{\lambda_2^2}\right)\left(1-\frac{3CD}{2\lambda_2}\frac{1}{\sqrt{1+\frac{nr^2}{\lambda_2^2}}}\right)\,, \end{aligned} \tag{6.3.20}$$

This has the desired scaling behaviour (cfr. Eq. (6.2.13)) as all the combinations $\lambda_2/\sqrt{n}$ and C/λ_2 are fiducial cell independent and only the overall n-factor scales with α^2. Again, the classical behaviour (6.2.18) is recovered in the limit $\sqrt{n}r/\lambda_2 \gg 1$, namely

$$v_2(r) \xrightarrow{\frac{\sqrt{n}r}{\lambda_2}\to\infty} 2nr^2\left(1-\frac{3CD}{2\sqrt{n}r}\right)\,. \tag{6.3.21}$$

To sum up, the solutions of the effective equations are given by

$$v_1(r) = \frac{2C^2\lambda_1^2\sqrt{n}^3}{\lambda_2^3} D \frac{\frac{\lambda_2^6}{16C^2\lambda_1^2 n^3}\left(\frac{\sqrt{n}r}{\lambda_2}+\sqrt{1+\frac{nr^2}{\lambda_2^2}}\right)^6+1}{\left(\frac{\sqrt{n}r}{\lambda_2}+\sqrt{1+\frac{nr^2}{\lambda_2^2}}\right)^3} \,, \tag{6.3.22a}$$

$$v_2(r) = 2n\left(\frac{\lambda_2}{\sqrt{n}}\right)^2\left(1+\frac{nr^2}{\lambda_2^2}\right)\left(1-\frac{3CD}{2\lambda_2}\frac{1}{\sqrt{1+\frac{nr^2}{\lambda_2^2}}}\right) \,, \tag{6.3.22b}$$

$$P_1(r) = \frac{2}{\lambda_1}\cot^{-1}\left(\frac{\lambda_2^3}{4C\lambda_1\sqrt{n}^3}\left(\frac{\sqrt{n}r}{\lambda_2}+\sqrt{1+\frac{nr^2}{\lambda_2^2}}\right)^3\right) \,, \tag{6.3.22c}$$

$$P_2(r) = \frac{1}{\lambda_2}\cot^{-1}\left(\frac{\sqrt{n}r}{\lambda_2}\right)+\frac{\pi}{\lambda_2}\theta\left(-\frac{\sqrt{n}\,r}{\lambda_2}\right) \,, \tag{6.3.22d}$$

which, according to the scaling behaviours Eq. (6.3.3) and

$$C \longmapsto \alpha C \quad , \quad D \longmapsto D \,, \tag{6.3.23}$$

all have the desired behaviour under fiducial cell rescaling, and agree with the classical solutions in the classical regime $\sqrt{n}r/\lambda_2 \gg 1$, $2r^3/C\lambda_1 \gg 1$[11].

As in the classical case, there are two integration constants C and D. It has to be checked how they can be fixed by means of physical input. Using the solutions (6.3.22a)-(6.3.22b) and the relations (6.2.12) allows to reconstruct the metric with line element

$$\mathrm{d}s^2 = -\frac{a(r)}{L_o^2}\mathrm{d}t^2+\frac{\mathscr{L}_o^2}{a(r)}\mathrm{d}r^2+b(r)^2\left(\mathrm{d}\theta^2+\sin(\theta)^2\,\mathrm{d}\phi^2\right) \,, \tag{6.3.24}$$

and metric components

$$b = \left(\frac{3v_1}{2}\right)^{\frac{1}{3}} = \frac{\sqrt{n}}{\lambda_2}\left(3DC^2\lambda_1^2\right)^{\frac{1}{3}}\frac{\left(\frac{\lambda_2^6}{16C^2\lambda_1^2n^3}\left(\frac{\sqrt{n}r}{\lambda_2}+\sqrt{1+\frac{nr^2}{\lambda_2^2}}\right)^6+1\right)^{\frac{1}{3}}}{\left(\frac{\sqrt{n}r}{\lambda_2}+\sqrt{1+\frac{nr^2}{\lambda_2^2}}\right)} \,, \tag{6.3.25}$$

$$a = \frac{v_2}{2b^2} = \frac{v_2}{2}\left(\frac{2}{3v_1}\right)^{\frac{2}{3}}$$

[11]Note that both limits commute.

$$= n\left(\frac{\lambda_2}{\sqrt{n}}\right)^4\left(1+\frac{nr^2}{\lambda_2^2}\right)\left(1-\frac{3CD}{2\lambda_2}\frac{1}{\sqrt{1+\frac{nr^2}{\lambda_2^2}}}\right)\frac{\left(\frac{1}{3DC^2\lambda_1^2}\right)^{\frac{2}{3}}\left(\frac{\sqrt{n}r}{\lambda_2}+\sqrt{1+\frac{nr^2}{\lambda_2^2}}\right)^2}{\left(\frac{\lambda_2^6}{16C^2\lambda_1^2n^3}\left(\frac{\sqrt{n}r}{\lambda_2}+\sqrt{1+\frac{nr^2}{\lambda_2^2}}\right)^6+1\right)^{\frac{2}{3}}}\,, \tag{6.3.26}$$

where $\bar{a} = a/L_o$ (cfr. Eq. (6.2.6)) and $\sqrt{n} = \mathscr{L}_o$ was used. All solutions (6.3.22a)-(6.3.22d), as well as the metric (6.3.24)-(6.3.26) are well-defined and smooth in the full range $r \in (-\infty, \infty)$. This will be important for determining the integration constants C and D in the next section.

6.3.2 Dirac Observables and Causal Structure

The next important step is to determine the integration constants C and D by means of physical input, meaning Dirac observables. In contrast to the classical case, the metric (6.3.24) does not allow to remove one of the integration constants by means of a residual diffeomorphism. Thus, their interpretation has to be clarified. For doing so, it is useful to analyse the asymptotic regimes $r \to \pm\infty$ as the metric becomes classical there. The result should again be rephrased in terms of the scalar b which means Eq. (6.3.25) has to be solved for r. The result is

$$\begin{aligned} r^{(\pm)}(b) &= \frac{\lambda_2}{2\sqrt{n}}\frac{z_\pm^2(b)-1}{z_\pm(b)}\,, \\ z_\pm(b) &= \left(\frac{8}{3D}\left(\frac{\sqrt{n}b}{\lambda_2}\right)^3 \pm \frac{4C\lambda_1\sqrt{n}^3}{\lambda_2^3}\sqrt{\frac{4b^6}{9\lambda_1^2D^2C^2}-1}\right)^{\frac{1}{3}} \end{aligned} \tag{6.3.27}$$

making explicit that $b(r)$ has two branches indicating the two asymptotic regions. The point $b_\mathcal{T} = (3\lambda_1 CD/2)^{\frac{1}{3}}$, where the two branches merge, i.e. $z_+(b_\mathcal{T}) = z_-(b_\mathcal{T})$, corresponds to the global minimum of $b(r)$. The surface $b(r_\mathcal{T}) = b_\mathcal{T}$ will be introduced below in more detail and is referred to as transition surface. In the limit $b \to \infty$, which corresponds to the classical limit as this implies both conditions, $\sqrt{n}|r|/\lambda_2 \gg 1$ and $2|r|^3/C\lambda_1 \gg 1$, this yields

$$z_\pm(b) \xrightarrow{b\to\infty} \begin{cases} z_+ \simeq \left(\frac{16}{3D}\right)^{\frac{1}{3}}\frac{\sqrt{n}b}{\lambda_2} \\ z_- \simeq (3DC^2\lambda_1^2)^{\frac{1}{3}}\frac{\sqrt{n}}{\lambda_2 b} \end{cases}\,, \tag{6.3.28}$$

and corresponds to $r^{(+)} \to +\infty$ and $r^{(-)} \to -\infty$. Inserting the expression (6.3.27) into

the expression for $a(r)$ (6.3.26) gives $a(b)$, which in the large b-limit reduces to

$$a_\pm(b) \xrightarrow{b\to\infty} \begin{cases} a_+ \simeq \frac{n}{4}\left(\frac{16}{3D}\right)^{\frac{2}{3}}\left(1-\left(\frac{3}{2}D\right)^{\frac{4}{3}}\frac{C}{\sqrt{n}}\frac{1}{b}\right) \\ a_- \simeq \frac{n}{4}\left(\frac{\lambda_2}{\sqrt{n}}\right)^4\left(\frac{1}{3DC^2\lambda_1^2}\right)^{\frac{2}{3}}\left(1-\frac{3CD\sqrt{n}}{\lambda_2^2}\left(3DC^2\lambda_1^2\right)^{\frac{1}{3}}\frac{1}{b}\right) \end{cases} . \tag{6.3.29}$$

As in the classical case, the time coordinate is changed to absorb the prefactor in $\bar{a}$ and instead of r the physical areal radius is used to parametrise the metric. On the $r\to+\infty$ side this coordinate redefinition is $t\mapsto\tau=\mathscr{L}_o(3D/2)^{-\frac{1}{3}}t/L_o$ and $r\mapsto b=(3D/2)^{\frac{1}{3}}r$, while for the $r\to-\infty$ branch it is $t\mapsto\tau=\mathscr{L}_o(24DC^2\lambda_1^2\mathscr{L}_o^6/\lambda_2^6)^{-\frac{1}{3}}t/L_o$, $r\mapsto b=(24DC^2\lambda_1^2\mathscr{L}_o^6/\lambda_2^6)^{\frac{1}{3}}(-r)$. The resulting line element is

$$\mathrm{d}s_+^2 \simeq -\left(1-\frac{2M_{BH}}{b}\right)\mathrm{d}\tau^2+\frac{1}{1-\frac{2M_{BH}}{b}}\mathrm{d}b^2+b^2\mathrm{d}\Omega_2^2 , \tag{6.3.30a}$$

$$\mathrm{d}s_-^2 \simeq -\left(1-\frac{2M_{WH}}{b}\right)\mathrm{d}\tau^2+\frac{1}{1-\frac{2M_{WH}}{b}}\mathrm{d}b^2+b^2\mathrm{d}\Omega_2^2 , \tag{6.3.30b}$$

where the abbreviations

$$M_{BH}=\left(\frac{3}{2}D\right)^{\frac{4}{3}}\frac{C}{2\sqrt{n}} \quad , \quad M_{WH}=\frac{3CD\sqrt{n}}{2\lambda_2^2}\left(3DC^2\lambda_1^2\right)^{\frac{1}{3}} , \tag{6.3.31}$$

are used. This shows that at large areal radii $b\to\infty$ the spacetime is well-approximated by a classical Schwarzschild metric of mass M_{BH} on the positive branch, and M_{WH} on the negative one. The effective spacetime Eq. (6.3.24) thus interpolates between two classical Schwarzschild spacetimes. The positive branch will from now on be referred to as black hole side, while the negative branch will be denoted as white hole side. These names will become more clear once the causal structure is discussed. Moreover, M_{BH} is the mass of the Schwarzschild spacetime on the black hole side, i.e. the black hole mass. Similarly, M_{WH} is the white hole mass. As the relations of M_{BH}, M_{WH} with C, D Eq. (6.3.31) are invertible, i.e.

$$C=\frac{\lambda_2^3}{4\lambda_1\sqrt{n}^3}\left(\frac{M_{WH}}{M_{BH}}\right)^{\frac{3}{2}} \quad , \quad D=\left(\frac{2\sqrt{n}}{\lambda_2}\right)^3\left(\frac{2}{3}\left(\frac{\lambda_1\lambda_2}{3}\right)^3 M_{BH}^3\left(\frac{M_{BH}}{M_{WH}}\right)^{\frac{9}{2}}\right)^{\frac{1}{4}} , \tag{6.3.32}$$

the integration constants can be uniquely fixed by providing the physical input data M_{BH} and M_{WH}. As in the classical case there are two independent Dirac observables, which

could be chosen to be

$$\mathcal{M}_{BH} = \frac{3v_1}{2}\frac{\sin(\lambda_1 P_1)}{\lambda_1}\frac{\left(\frac{3}{2}v_1\cos^2\left(\frac{\lambda_1 P_1}{2}\right)\right)^{\frac{1}{3}}}{\lambda_2\cot\left(\frac{\lambda_2 P_2}{2}\right)} \overset{\text{on-shell}}{=} M_{BH}\ , \tag{6.3.33a}$$

$$\mathcal{M}_{WH} = \frac{3v_1}{2}\frac{\sin(\lambda_1 P_1)}{\lambda_1}\left(\frac{3}{2}v_1\sin^2\left(\frac{\lambda_1 P_1}{2}\right)\right)^{\frac{1}{3}}\frac{\cot\left(\frac{\lambda_2 P_2}{2}\right)}{\lambda_2} \overset{\text{on-shell}}{=} M_{WH}\ . \tag{6.3.33b}$$

This construction of the observables guarantees that their on-shell evaluation correspond to the values of the black and white hole mass. Note that these observables do not scale under fiducial cell rescaling, indicating that they are proper gauge invariant quantities with physical relevance, as necessary for interpreting them as masses. A naïve consideration explaining the existence of two physically relevant Dirac observables can be done. In the classical case also two Dirac observables existed, one of them being fiducial cell dependent and thus not being physical. Contrary to this, in the polymer model there are two Dirac observables, which both do not scale and their both values change the physics of the metric. Naïvely, in the limit $\lambda_1, \lambda_2 \to 0$[12], $\mathcal{M}_{BH}$ reduces to the classical Dirac observable $\mathcal{M}$ of Eq. (6.2.24). This limit is not defined for $\mathcal{M}_{WH}$, which indicates that there is no classical counterpart. Nevertheless, there are observables that reduce to the classical observable $\mathcal{O}$ Eq. (6.2.25), which then are fiducial cell dependent. The following observation underlines this: Classically, it was not possible to make the fiducial cell dependent Dirac observable $\mathcal{O}$ independent. In the effective quantum theory, with a given fiducial cell dependent Dirac observable, it is possible to make it non-scaling by multiplying it with a suitable power of λ_1 or λ_2, as the polymerisation scales also scale with the fiducial cell. This is what is occurring in the present case. This requires of course polymerisation scales scaling with the fiducial cell. Counter examples, i.e. models where the polymerisation scales are both fiducial cell independent have been studied in [6] and indeed, in these models there is only one Dirac observable that is of physical relevance.

As the integration constants are determined by physical input, the system is fully solved. The required physical input to determine the integration constants C and D are the two values of black and white hole mass M_{BH}, M_{WH}. This determines the metric (6.3.24) and the spacetime. Note that one could rephrase this physical input in terms of e.g. curvature scalars. Measuring the Kretschmann scalar at a given areal radius b fixes the

[12]Note that this limit should not be taken. In quantum mechanics the classical regime is given by actions $\gg \hbar$, while $\hbar \neq 0$. To arrive at classical physics out of the quantum theory one should consider peaked states with large actions compared to $\hbar$, instead of performing the limit $\hbar \to 0$. The same is true in this case, where the classical regime is at low curvatures and large distances with respect to λ_1, λ_2. In the model presented here, this limit can be performed and it is instructive, while there are models where this is not the case (cfr. [78, 79, 88] and the discussion in [6]).

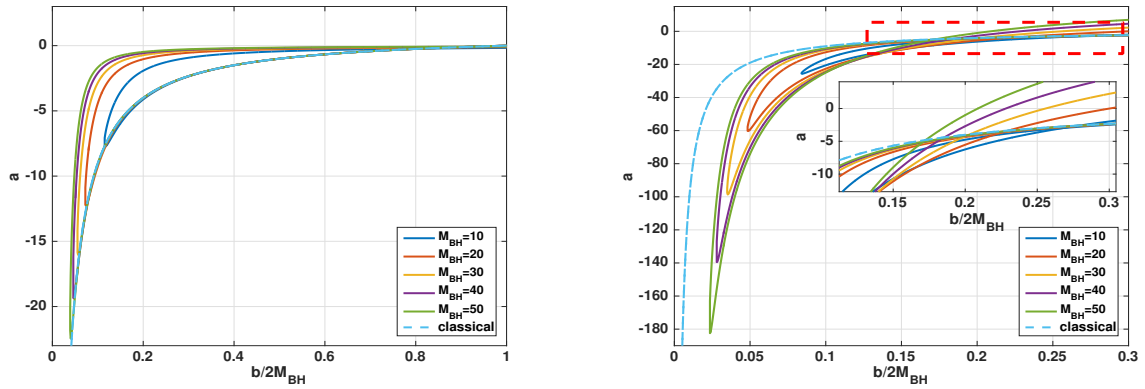

(a) (b)

FIGURE 6.1: *Plot of $a(b)$ as a function of b for different black hole masses for the parameters $\mathscr{L}_o\lambda_1 = \lambda_2/\mathscr{L}_o = 1$. The masses are related by $M_{WH} = M_{BH}\left(\frac{M_{BH}}{m}\right)^{\beta-1}$ for $m = 1$ and $\beta = 5/3$ in (a) as well as $\beta = 3/5$ in (b). In these plots, $a(b)$ takes only negative values indicating that the interior region of the black hole is depicted. Already there good agreement is reached with the classical solution for larger b. Furthermore, a minimal value for b, i.e. $b_\mathcal{T}$ is visible.*

black hole mass in first order of λ_1, λ_2. Additionally measuring the Ricci scalar at the same radius would vanish up to contributions suppressed by λ_i but allows to determine M_{WH}. This would be an equivalent point of view. In principle both masses are completely independent. According to the detailed discussion below in Sec. 6.3.3, it is necessary to relate the masses by means of $M_{WH} = M_{BH}\left(\frac{M_{BH}}{m}\right)^{\beta-1}$, with a constant m of dimension mass and $\beta = 5/3$ or $3/5$. The metric is visualised in terms of $a(b)$ and the given mass relation in Fig. 6.1. The solution visibly approaches the classical Schwarzschild spacetime.

As the spacetime and its observables are identified now, the focus shall be shifted to the global causal structure of that spacetime. As discussed above, there are two asymptotic regions $r \to \pm\infty$, which are approximated by Schwarzschild spacetimes. In a next step the horizon structure is analysed. The metric (6.3.24) admits a Killing horizon corresponding to the Killing vector field $\partial/\partial t$ whenever $a(r) = 0$. This proves to be the case if and only if $v_2(r) = 0$, as $v_1 > 0$ (cfr. Eq. (6.2.12)). Using the solution Eq. (6.3.22b), this condition becomes

$$v_2(r) = 0 \qquad \Leftrightarrow \qquad 1 - \frac{3CD}{2\lambda_2}\frac{1}{\sqrt{1+\frac{nr^2}{\lambda_2^2}}} = 0\,, \tag{6.3.34}$$

and is solved for

$$r_s^{(\pm)} = \pm\frac{3CD}{2\sqrt{n}}\sqrt{1-\left(\frac{2\lambda_2}{3CD}\right)^2}\,. \tag{6.3.35}$$

This shows the existence of two Killing horizons, one on the black hole and one on the white hole branch. The areal radius of the horizons is given by

$$b(r_s^{(\pm)}) = \left(\frac{3}{2}\,v_1(r_s^{(\pm)})\right)^{\frac{1}{3}}\,, \tag{6.3.36}$$

where, according to the expression (6.3.22a), this gives

$$\begin{aligned} v_1(r_s^{(\pm)}) &= \frac{2C^2\lambda_1^2\sqrt{n}^3}{\lambda_2^3}D\,\frac{\frac{\lambda_2^6}{16C^2\lambda_1^2n^3}\left(\pm\frac{3CD}{2\lambda_2}\sqrt{1-\left(\frac{2\lambda_2}{3CD}\right)^2}+\frac{3CD}{2\lambda_2}\right)^6+1}{\left(\pm\frac{3CD}{2\lambda_2}\sqrt{1-\left(\frac{2\lambda_2}{3CD}\right)^2}+\frac{3CD}{2\lambda_2}\right)^3} \\ &= \frac{\lambda_2^3}{8\sqrt{n}^3}Df^{(\pm)}(x)+\frac{2\lambda_1^2\sqrt{n}^3DC^2}{\lambda_2^3f^{(\pm)}(x)}\,, \end{aligned} \tag{6.3.37}$$

with

$$f^{(\pm)}(x) = \frac{1}{x^3}\left(1\pm\sqrt{1-x^2}\right)^3 \qquad , \qquad x = \frac{2\lambda_2}{3CD}\,. \tag{6.3.38}$$

Using the relations (6.3.32), this can be expressed in terms of the masses as

$$v_1(r_s^{(\pm)}) = \frac{1}{3}\left(2\left(\lambda_1\lambda_2\right)^3\left(M_{BH}M_{WH}\right)^{\frac{3}{2}}\right)^{\frac{1}{4}}\left[\left(\frac{M_{BH}}{M_{WH}}\right)^{\frac{3}{2}}f^{(\pm)}(x)+\left(\frac{M_{WH}}{M_{BH}}\right)^{\frac{3}{2}}\frac{1}{f^{(\pm)}(x)}\right]\,, \tag{6.3.39}$$

with

$$x = \left(\frac{\lambda_1\lambda_2}{2\left(M_{BH}M_{WH}\right)^{\frac{3}{2}}}\right)^{\frac{1}{4}}\,.$$

In the limit of large masses, i.e. $M_{BH}M_{WH} \gg 1$ with finite asymmetry $M_{BH}/M_{WH} \sim 1$,

the expansion of $f^{(\pm)}(x)$ is

$$f^{(\pm)}(x) = \left(\frac{1 \pm \sqrt{1-x^2}}{x}\right)^3 \simeq \begin{cases} \frac{8}{x^3} - \mathcal{O}\left(\frac{1}{x}\right) & \text{for } + \,, \\ \frac{x^3}{8} + \mathcal{O}\left(x^5\right) & \text{for } - \,. \end{cases} \tag{6.3.40}$$

For $v_1(r_s^{(\pm)})$ this implies

$$v_1(r_s^{(\pm)}) \simeq \begin{cases} \frac{2}{3}\left(2M_{BH}\right)^3 - \mathcal{O}\left(\left(\lambda_1\lambda_2\right)^{\frac{1}{2}}\left(M_{BH}M_{WH}\right)^{\frac{3}{4}}\left(\frac{M_{BH}}{M_{WH}}\right)^{\frac{3}{2}}\right) & \text{for } + \,, \\ \frac{2}{3}\left(2M_{WH}\right)^3 - \mathcal{O}\left(\left(\lambda_1\lambda_2\right)^{\frac{1}{2}}\left(M_{BH}M_{WH}\right)^{\frac{3}{4}}\left(\frac{M_{WH}}{M_{BH}}\right)^{\frac{3}{2}}\right) & \text{for } - \,, \end{cases} \tag{6.3.41}$$

which ensures that the classical result on the black and white hole side is recovered[13], i.e.

$$b(r_s^{(\pm)}) \simeq \begin{cases} 2M_{BH}\left(1 - \mathcal{O}\left(\frac{\left(\lambda_1\lambda_2\right)^{\frac{1}{2}}}{\left(M_{BH}M_{WH}\right)^{\frac{3}{4}}}\right)\right) & \text{for } + \,, \\ 2M_{WH}\left(1 - \mathcal{O}\left(\frac{\left(\lambda_1\lambda_2\right)^{\frac{1}{2}}}{\left(M_{BH}M_{WH}\right)^{\frac{3}{4}}}\right)\right) & \text{for } - \,. \end{cases} \tag{6.3.42}$$

Further note that the size of the classical horizon is reduced by quantum effects of Planck order.

Other than the horizons, another important surface of the spacetime is the transition surface. In Fig. 6.1 it is visible that $b > 0$ in contrast to the classical case, where $b = 0$ was the singularity. This curvature singularity is replaced by a regular bounce and $b(r)$ reaches its minimum. A detailed discussion of the curvature at the transition surface is provided in the next section 6.3.3. The transition surface is characterised my the minimal value that b can take, i.e. $b' = 0$. A quick computation shows that this minimum is reached at

$$r_{\mathcal{T}} = \frac{\lambda_2}{2\mathscr{L}_o}\left(\left(\frac{\lambda_2^3}{4C\lambda_1\mathscr{L}_o^3}\right)^{-\frac{1}{3}} - \left(\frac{\lambda_2^3}{4C\lambda_1\mathscr{L}_o^3}\right)^{\frac{1}{3}}\right) .$$

The areal radius becomes

$$b_{\mathcal{T}} := b(r_{\mathcal{T}}) = \left(\frac{3\lambda_1 CD}{2}\right)^{\frac{1}{3}} = 2^{1/12}(\lambda_1\lambda_2)^{1/4}(M_{BH}M_{WH})^{1/8} \,, \tag{6.3.43}$$

where again Eq. (6.3.32) was used. As mentioned, this value is finite and vanishes for

[13]This remains true for the mass relation discussed in Sec. 6.3.3, Eq. (6.3.70), although $M_{WH}/M_{BH} \sim M_{BH}^{\beta-1}$. The explicit computation is shown in [3]. The assumption $M_{BH}/M_{WH} \sim 1$ can be weakened by analysing the orders in the expansion more carefully.

λ_1, $\lambda_2 \to 0$. The transition surface interpolates between the singular regions of the two asymptotic Schwarzschild spacetimes. This bounce is a common feature in LQC related models as already seen in cosmology (cfr. Sec. 4.2 or e.g. [138, 139, 144, 165]) and also in the black hole context e.g. [78, 80, 88].

The question remains why this surface is called transition surface. The answer is that a transition between a trapped (black hole interior) and anti-trapped (white hole interior) takes place at $b_{\mathcal{T}}$. This can be seen by analysing the expansion coefficients $\theta_\pm$[14] (see e.g. [95] for an introduction). Consider the future pointing in- and out-going null normals $u_\pm$ to the $t = const.$ and $r = const.$ surfaces with $r_s^{(-)} < r < r_s^{(+)}$. They can be determined to be

$$u_\pm = u_\pm^a \frac{\partial}{\partial x^a} = \frac{1}{\sqrt{-2N}} \frac{\partial}{\partial r} \pm \frac{1}{\sqrt{-2a}} \frac{\partial}{\partial t} \,, \tag{6.3.44}$$

and are chosen to satisfy the normalisation conditions $g(u_\pm, u_\pm) = 0$ and $g(u_\pm, u_\mp) = -1$. The in- and outgoing expansions are defined as[15]

$$\theta_\pm = S^{ab} \nabla_a u_b^\pm = -\sqrt{-\frac{2}{N}} \frac{b'}{b} \,, \tag{6.3.45}$$

where $S^{ab} = g^{ab} + u_+^a u_-^b + u_-^a u_+^b$ is the projector on the $t = const.$, $r = const.$ 2-surface, which is simply a 2-sphere. For $r_{\mathcal{T}} < r < r_s^{(+)}$ both expansions are negative, meaning light rays are trapped and all meeting in a focal point. This is called a black hole interior. As $b' = 0$ changes its sign at the transition surface, both expansions are positive for $r_s^{(-)} < r < r_{\mathcal{T}}$ which is an anti-trapped region where everything has to exit. This region is exactly what is called the white hole interior. Thus, at the transition surface a transition from a black hole to a white hole region happens. Note that this justifies the names black and white hole sides. Jumping inside the horizon from the black hole side, one will find oneself first in the trapped black hole interior region, being blown out of the white hole region. The observer hence finds herself in the white hole exterior region. Nevertheless, these names are interchangeable as discussed below.

All these global and causal features can be represented in a conformally compactified Penrose diagram. In analogy to the classical black hole (cfr. Sec. 3.1) it is possible to

[14] Intuitively, $\theta_\pm$ describes the change of area of bundle of in- or outgoing light rays. In flat space, θ_- is negative, indicting that ingoing light rays are focussed. In contrast, θ_+ is positive, describing the de-focussing of outgoing light rays. The situation can change when spacetime is dynamic.

[15] This result is only true for the interior region. For the exterior one finds $\theta_\pm = \pm\sqrt{\frac{2}{N}}\frac{b'}{b}$.

define Kruskal-Szekeres coordinates (cfr. also [103]) as

$$T^2 - X^2 = \exp\left[\left(\left.\frac{\mathrm{d}\bar{a}}{\mathrm{d}r}\right|_{r=r_s^{(\pm)}}\right) r_*(r)\right] \quad , \quad \frac{T}{X} = \begin{cases} \tanh\left(\frac{t}{2}\left(\left.\frac{\mathrm{d}\bar{a}}{\mathrm{d}r}\right|_{r=r_s^{(\pm)}}\right)\right) & -1 < \frac{T}{X} < 1 \\ \coth\left(\frac{t}{2}\left(\left.\frac{\mathrm{d}\bar{a}}{\mathrm{d}r}\right|_{r=r_s^{(\pm)}}\right)\right) & -1 < \frac{X}{T} < 1 \end{cases} , \tag{6.3.46}$$

where the tortoise coordinate r_* is defined as

$$r_*(r) = \int_{b_0}^{b(r)} \mathrm{d}b \, \frac{\frac{\mathrm{d}r^{(\pm)}}{\mathrm{d}b}}{\bar{a}(b)} = \int_{r_\mathcal{T}}^{r} \mathrm{d}r \, \frac{L_o^2}{a(r)} \, . \tag{6.3.47}$$

In the definition of r_*, there is the freedom to choose a reference point b_0, in this case chosen to be the transition surface $b_\mathcal{T}$. Note further that the above definitions are two different charts for $r_s^{(+)}$ and $r_s^{(-)}$, respectively. It is possible to analyse how $r \to \pm\infty$, the horizons and the transition surface are represented in (T, X)-coordinates. This was elaborated in detail in [3] and as the computation is not instructive for this part, only the results are presented.

Consider first the +-chart, i.e. the derivative of a is evaluated at $r_s^{(+)}$ in Eq. (6.3.46). Due to the choice of $b_0 = b_\mathcal{T}$, it is $r_*(b_\mathcal{T}) = 0$ and $T^2 - X^2 = 1$. The detailed analysis shows further that $r_*(r \to r_s^{(+)}) \to -\infty$. By using residuum integration techniques, it can be shown that $r_*(r > r_s^{(+)})$ picks up the phase $-i\pi / \left.\frac{\mathrm{d}\bar{a}}{\mathrm{d}r}\right|_{r=r_s^{(+)}}$. Together with the factor $\left.\frac{\mathrm{d}\bar{a}}{\mathrm{d}r}\right|_{r=r_s^{(+)}}$ in Eq. (6.3.46), this adds a minus sign and indicates the exchange of time and space in the black hole interior. The coordinates (T, X) are thus well-defined in the exterior region. This reasoning fails for the white hole side $r_*(r \to r_s^{(-)}) \to +\infty$ and picks up the phase $-i\pi / \left.\frac{\mathrm{d}\bar{a}}{\mathrm{d}r}\right|_{r=r_s^{(-)}}$ for $r < r_s^{(-)}$, which does not cancel the prefactor $\left.\frac{\mathrm{d}\bar{a}}{\mathrm{d}r}\right|_{r=r_s^{(+)}}$. The +-chart is hence only defined for the black and white hole interior, as well as for the black hole exterior only. The coordinates are compactified by means of

$$\tilde{U} = \arctan\left(T - X\right) \quad , \quad \tilde{V} = \arctan\left(T + X\right) \qquad \left(-\frac{\pi}{2} < \tilde{U}, \tilde{V} < \frac{\pi}{2}\right) . \tag{6.3.48}$$

The results for the +-chart can be summarised as

- $b = b_\mathcal{T}$ corresponds to $T^2 - X^2 = 1$ and $\tilde{U} + \tilde{V} = \pm\frac{\pi}{2}$;
- $b = b(r_s^{(+)})$ corresponds to $T^2 - X^2 = 0$, i.e. $\tilde{U}\tilde{V} = 0$;
- $b = b(r_s^{(-)})$ corresponds to $T^2 - X^2 \to -\infty$, i.e. $\tilde{U} = \mp\frac{\pi}{2}$ or $\tilde{V} = \pm\frac{\pi}{2}$;
- $b \to \infty$ correspond to $T^2 - X^2 \to -\infty$ and hence $\tilde{U} = \mp\frac{\pi}{2}$ or $\tilde{V} = \pm\frac{\pi}{2}$.

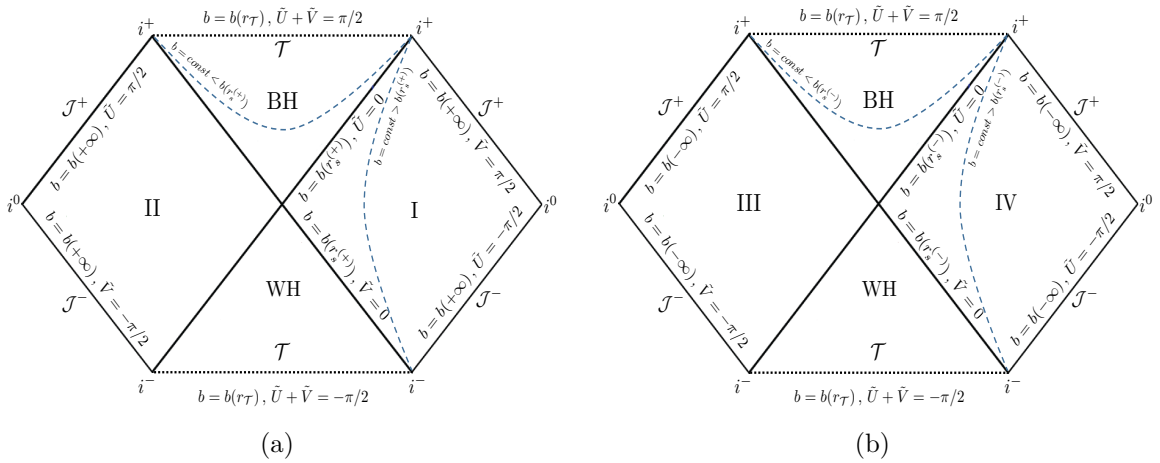

FIGURE 6.2: *Penrose diagrams for the $r > r_\mathcal{T}$ (a) and $r < r_\mathcal{T}$ (b) regions. Recall that, although the same notation is used for both regions, they are covered by different $(\tilde{U}, \tilde{V})$-coordinate charts. As usual, the angular coordinates are suppressed so that each point of the diagram can be thought of as representing a 2-sphere of radius b.*

The analogue reasoning is possible for the $-$-chart, qualitatively leading to the same result. Plotting $(\tilde{U}, \tilde{V})$ gives the Penrose diagram for both patches (see Fig. 6.2). The global structure looks similar to the classical Schwarzschild spacetime with the important difference that the spacetime does not end in the singularity at $b = 0$, but rather continues due to the quantum bounce. For joining both Penrose diagrams in Fig. 6.2 it is crucial to observe that the single charts (black hole and white hole sides) are valid in the full interior. As argued above the $+$-chart is well-defined up to $r_s^{(-)}$ and vice versa. Due to this smooth overlap it is possible to identify both diagrams in Fig. 6.2 at the transition surface. The result is depicted in Fig. 6.3. A remaining issue is the global topology. This is a particular choice and in the beginning of this section, $\mathbb{R} \times \mathbb{R} \times \mathbb{S}^2$ was chosen, i.e. non-compact in the time direction. This justifies Fig. 6.3, which consists of an infinite tower of alternating black and white hole patches. The opposite possibility would be to identify the upper transition surface of the white hole patch with the lower transition surface of the black hole patch. This would correspond to a cyclic topology and would permit closed timelike curves, which are physically not reasonable.

An important remaining issue concerns the masses of the spacetimes. The Penrose diagram shows an infinite tower of black hole and white hole spacetimes, while only the two masses M_{BH} and M_{WH} characterise the system. For better understanding, an observer 1 who lives in region `I` and jumps into the black hole exiting in region `III`. Observer 1 measures at a given areal radius $b \gg 2M_{BH}$ spacetime scalars and determines the initial conditions v_2^o, P_1^o and P_2^o. This process involves determining the values of the Dirac observables (6.3.33a), (6.3.33b), which are fixed by $M_{BH}^{(1)}$, $M_{WH}^{(1)}$ and inverting them to determine P_1 and P_2. Due to the involved trigonometric functions this is only unique

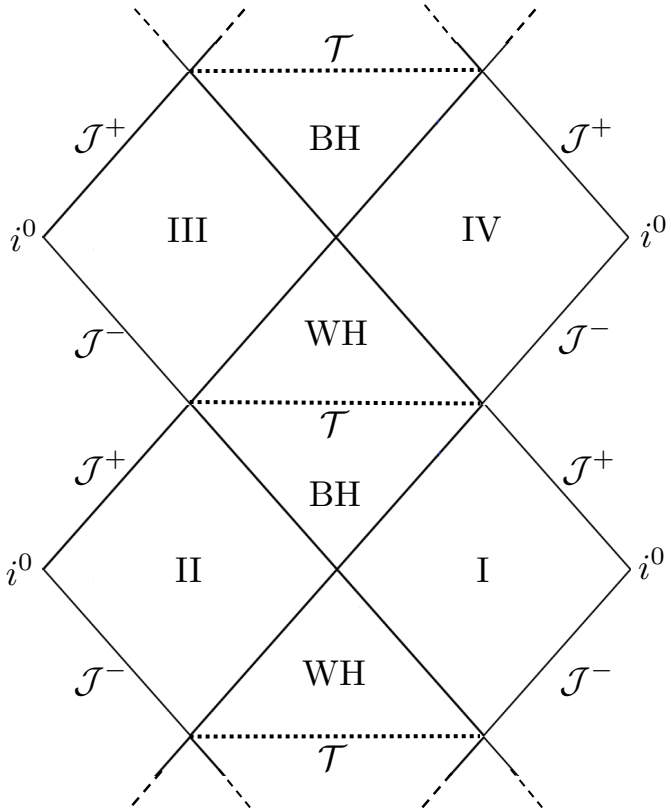

FIGURE 6.3: *Penrose diagram for the Kruskal extension of the full quantum corrected polymer Schwarzschild spacetime.*

up to choices of the branches. A second observer 2 is located in region `III` from the beginning and also measures spacetime scalars to determine v_2^o, P_1^o and P_2^o. When both observers meet, observer 1 thinks she is on the white hole side, and she will choose $P_1^o \sim 0$ and $P_2 \sim 0$ in region `I`. By doing so P_1 and P_2 evolve during the evolution and will become $P_1 \sim \pi/2\lambda_1$ and $P_2 \sim \pi/2\lambda_2$ (cfr. Eqs. (6.3.22c), (6.3.22d)) in region `III`. Observer 2 thinks she is on the black hole side as she originated there. In solving for her initial values for P_1 and P_2 she will choose the branch so that the initial values are close to 0. In fact the observers will notice that their masses are different by means of $M_{BH}^{(1)} = M_{WH}^{(2)}$ and vice versa. They further notice that their results differ by the following transformation

$$v_1 \longmapsto v_1 \quad , \quad P_1 \longmapsto \frac{\pi}{\lambda_1} - P_1 \quad , \quad P_2 \longmapsto \frac{\pi}{\lambda_2} - P_2 \quad , \quad v_2 \longmapsto v_2 \, . \tag{6.3.49}$$

This is in fact needed for consistency as the observables transform under this map according to

$$\mathcal{M}_{BH} \longmapsto \mathcal{M}_{WH} \quad , \quad \mathcal{M}_{WH} \longmapsto \mathcal{M}_{BH} \, , \tag{6.3.50}$$

which only swaps the notion of what the black hole and what the white hole mass are. This is in agreement with the results the two observers measured. On the one hand, this says that the names black and white hole are just names and non-physical as they can be interchanged without consequences. This is also related to the fact that the Hamiltonian is invariant[16] under the above transformation (6.3.49). On the other hand, this demonstrates that the initial value problem is well-defined. This is non-obvious as the Hamiltonian flow is spacelike for the exterior region and the masses were determined at different asymptotic regions in the construction of Sec. 6.3.2. Thus, the problem is rather a boundary value problem. Nevertheless, as also both masses can consistently be determined in region `I` only, this boundary value problem can be translated to an unique initial value problem. It is possible to conclude that going from region `III` to region `VI` the masses are exchanged again. In conclusion, the masses alternate between each patch of the Penrose diagram and the asymptotic regions will be characterised by M_{BH}, M_{WH} and then again M_{BH}. Note that this discussion is independent of any relation between the two masses.

6.3.3 Onset of Quantum Effects and Curvature Cutoff

The model is promising as the singularity is resolved and asymptotically it approaches the classical Schwarzschild metric. An important remaining issue is the onset of quantum effects, which should be controlled by curvature and length scales. This can be analysed by looking at when the approximation $\sin(\lambda_i P_i) \sim \lambda_i P_i$ fails, i.e. when the classical regime is left. More precisely, recalling e.g. Eqs. (6.3.12) and (6.3.13), the classical approximation holds whenever

$$\frac{\mathscr{L}_o r}{\lambda_2} \gg 1 \quad , \quad \frac{2r^3}{C\lambda_1} \gg 1 \, , \tag{6.3.51}$$

holds. The classical approximation is again valid for negative r, where these conditions become

$$\frac{\mathscr{L}_o |r|}{\lambda_2} \gg 1 \quad , \quad \frac{32C\lambda_1 \mathscr{L}_o^6 |r|^3}{\lambda_2^6} \gg 1 \, . \tag{6.3.52}$$

These expressions depend on the choice of the r-coordinate. To make it independent they should be re-expressed in terms of the areal radius b, which is straightforward in the classical regimes of the separate two branches. For the positive branch, the asymptotic behaviour is

[16] This is due to the choice of the sin-function for polymerising. Choosing e.g. a product of sin and cos would still be fine from the classical limit point of view, but would explicitly break this symmetry.

$$b(r\to\infty)\simeq\left(\frac{3D}{2}\right)^{\frac{1}{3}}r=:b_+\ ,$$

for which the conditions (6.3.51) read

$$\frac{\mathscr{L}_o}{\lambda_2}\left(\frac{2}{3D}\right)^{\frac{1}{3}}b_+\gg 1\quad,\quad\frac{1}{\mathscr{L}_o^2\lambda_1^2}\gg\frac{9C^2D^2}{16\mathscr{L}_o^2b_+^6}\ , \tag{6.3.53}$$

where the second condition was squared. According to the discussion in Sec. 6.2, $P_1/\mathscr{L}_o$ is only related to the Kretschmann scalar if the integration constant D is independent of the mass. As similar restriction is visible in Eq. (6.3.53), where the second equation is a curvature scale only when

$$\frac{9C^2D^2}{16\mathscr{L}_o^2}\propto M_{BH}^2\ , \tag{6.3.54}$$

which restricts the initial conditions as this relates M_{BH} to M_{WH}. As the guiding principle in building the model is an onset of quantum effects at a fixed curvature scale, this is a necessary condition. Assuming a simple relation of the form

$$M_{WH}=M_{BH}\left(\frac{M_{BH}}{\bar{m}_{(\beta)}}\right)^{\beta-1}\sim M_{BH}^{\beta}\ , \tag{6.3.55}$$

with an arbitrary constant of dimension mass $\bar{m}_{(\beta)}$, condition (6.3.54) is satisfied for $\beta=\frac{5}{3}$, i.e.

$$M_{WH}=M_{BH}\left(\frac{M_{BH}}{\bar{m}_{(\frac{5}{3})}}\right)^{\frac{2}{3}}\ , \tag{6.3.56}$$

which describes an amplification of the mass on the white hole side. For this given mass relation the integration constants C and D become (cfr. Eq. (6.3.32))

$$\begin{aligned}\frac{C}{\mathscr{L}_o}&=\frac{\lambda_2^3}{4\lambda_1\mathscr{L}_o^4}\frac{M_{BH}}{\bar{m}_{(\frac{5}{3})}}=2\frac{M_{BH}}{m_{(\frac{5}{3})}}\,,\\ D&=\frac{1}{3}\left(\frac{2\mathscr{L}_o}{\lambda_2}\right)^3\left[2(\bar{m}_{(\frac{5}{3})}\lambda_1\lambda_2)^3\right]^{\frac{1}{4}}=\frac{2}{3}\left(m_{(\frac{5}{3})}\right)^{\frac{3}{4}}\ ,\end{aligned} \tag{6.3.57}$$

with the redefined dimensionless constant $m_{(\beta)}=8\lambda_1\mathscr{L}_o^4\bar{m}_{(\beta)}/\lambda_2^3$. Note that as C and D remain finite in the limit $\lambda_1,\lambda_2\to 0$, $m_{(\beta)}$ remains finite as well. The conditions (6.3.53)

become

$$b_+ \gg \left(m_{\left(\frac{5}{3}\right)}\right)^{\frac{1}{4}} \frac{\lambda_2}{\mathscr{L}_o} \quad , \quad \frac{1}{\mathscr{L}_o^2\lambda_1^2} \gg \frac{M_{BH}^2}{\left(m_{\left(\frac{5}{3}\right)}\right)^{\frac{1}{2}} b_+^6} = \frac{1}{48\left(m_{\left(\frac{5}{3}\right)}\right)^{\frac{1}{2}}} \mathcal{K}_{BH}^{class} \, , \tag{6.3.58}$$

which defines a critical length and curvature scale at which quantum effects become non-negligible

$$\ell_{crit}^{\left(\frac{5}{3}\right)} = \left(m_{\left(\frac{5}{3}\right)}\right)^{\frac{1}{4}} \frac{\lambda_2}{\mathscr{L}_o} \quad , \quad \mathcal{K}_{crit}^{\left(\frac{5}{3}\right)} = \frac{48\left(m_{\left(\frac{5}{3}\right)}\right)^{\frac{1}{2}}}{\mathscr{L}_o^2\lambda_1^2} \, . \tag{6.3.59}$$

The mass relation (6.3.56) is consistent with interpreting $\sin(\lambda_1 P_1)/\mathscr{L}_o\lambda_1$ as proportional to the square root of the Kretschmann scalar in the classical limit as

$$\frac{\sin\left(\lambda_1 P_1\right)}{\mathscr{L}_o\lambda_1} \overset{r\gg 1}{\simeq} \frac{C}{\mathscr{L}_o r^3} = \frac{3CD}{2\mathscr{L}_o b_+^3} = 2\left(m_{\left(\frac{5}{3}\right)}\right)^{-\frac{1}{4}} \frac{M_{BH}}{b_+^3} \propto \sqrt{\mathcal{K}_{BH}^{class}} \, .$$

Fixing this mass relation (6.3.56), the question remains which onset of quantum effects is implied on the white hole side, i.e. re-expressing Eq. (6.3.52) in terms of $b_- := (24DC^2\lambda_1^2\mathscr{L}_o^6/\lambda_2^6)^{\frac{1}{3}}|r| \simeq b(r \to -\infty)$, which yields

$$b_- \gg \frac{\mathscr{L}_o}{\lambda_2}\left(24DC^2\lambda_1^2\right)^{\frac{1}{3}} \quad , \quad \frac{1}{\mathscr{L}_o^2\lambda_1^2} \gg \frac{9D^2C^2}{16\mathscr{L}_o b_-^6} \, . \tag{6.3.60}$$

Inserting Eqs. (6.3.56) and (6.3.57) leads to

$$b_- \gg \frac{M_{WH}}{M_{BH}}\ell_{crit}^{\left(\frac{5}{3}\right)} \quad , \quad \frac{M_{WH}^2}{M_{BH}^2}\mathcal{K}_{crit}^{\left(\frac{5}{3}\right)} \gg \mathcal{K}_{WH}^{class} \, . \tag{6.3.61}$$

As $M_{WH} > M_{BH}$ for $\beta = 5/3$, both scales are larger than the critical scales on the black hole side. Therefore, on the white hole side curvature effects become relevant only at higher curvatures while small length effects become relevant already at larger lengths.

The same discussion can be held for the negative branch. Again, re-expressing r in Eq. (6.3.52) by means of $b_- := (24DC^2\lambda_1^2\mathscr{L}_o^6/\lambda_2^6)^{\frac{1}{3}}|r|$ leads to the conditions (6.3.60). Following the same logic as above, the right equation is needs to be a curvature scale, which is equivalent to the condition

$$\frac{9C^2D^2}{16\mathscr{L}_o^2} \propto M_{WH}^2 \, . \tag{6.3.62}$$

With the same ansatz as in Eq. (6.3.55), the condition (6.3.62) is satisfied for $\beta = 3/5$, thus yielding

$$M_{WH} = M_{BH}\left(\frac{M_{BH}}{\bar{m}_{(\frac{3}{5})}}\right)^{-\frac{2}{5}} , \tag{6.3.63}$$

which describes a de-amplified white hole mass. For this value of β, Eq. (6.3.32) yields

$$\frac{C}{\mathscr{L}_o} = \frac{\lambda_2^3}{4\lambda_1\mathscr{L}_o^4}\frac{\bar{m}_{(\frac{3}{5})}}{M_{WH}} \quad , \quad D = \frac{2}{3}\left[\left(\bar{m}_{(\frac{3}{5})}\right)^{-5}\left(\frac{8\mathscr{L}_o^4\lambda_1}{\lambda_2}\right)^3\right]^{\frac{1}{4}} M_{WH}^2 . \tag{6.3.64}$$

Defining the dimensionless quantity $m_{(\beta)} = 8\lambda_1\mathscr{L}_o^4\bar{m}_{(\beta)}/\lambda_2^3$ leads to

$$b_- \gg \left(m_{(\frac{3}{5})}\right)^{\frac{1}{4}}\frac{\lambda_2}{\mathscr{L}_o} \quad , \quad \frac{48\left(m_{(\frac{3}{5})}\right)^{\frac{1}{2}}}{\mathscr{L}_o^2\lambda_1^2} \gg \frac{48M_{WH}^2}{b_-^6} = \mathcal{K}_{WH}^{class} , \tag{6.3.65}$$

and thus to the critical scales where quantum effects become relevant are given by

$$\ell_{crit}^{(\frac{3}{5})} = \left(m_{(\frac{3}{5})}\right)^{\frac{1}{4}}\frac{\lambda_2}{\mathscr{L}_o} \quad , \quad \mathcal{K}_{crit}^{(\frac{3}{5})} = \frac{48\left(m_{(\frac{3}{5})}\right)^{\frac{1}{2}}}{\mathscr{L}_o^2\lambda_1^2} . \tag{6.3.66}$$

The classical regime for $\beta = 3/5$ and (6.3.63) on the black hole side corresponds to

$$b_+ \gg \frac{M_{BH}}{M_{WH}}\ell_{crit}^{(\frac{3}{5})} \quad , \quad \frac{M_{BH}^2}{M_{WH}^2}\mathcal{K}_{crit}^{(\frac{3}{5})} \gg \mathcal{K}_{WH}^{class} , \tag{6.3.67}$$

which is perfectly consistent with Eq. (6.3.61). Thus, with $M_{BH} > M_{WH}$, both the scales (6.3.67) are shifted to higher values on the black hole side, leading to curvature effects relevant at higher curvatures and finite length effects relevant at larger lengths.

Eq. (6.3.63) allows to relate $\sin(\lambda_1 P_1)/\mathscr{L}_o\lambda_1$ with the square root of the Kretschmann scalar on the white hole side as

$$\frac{\sin(\lambda_1 P_1)}{\mathscr{L}_o\lambda_1} \overset{r\ll -1}{\simeq} \frac{\lambda_2^6}{16C\lambda_1^2\mathscr{L}_o^7}\frac{1}{|r|^3} = \frac{3CD}{2\mathscr{L}_o b_-^3} = 2\left(m_{(\frac{3}{5})}\right)^{-\frac{1}{4}}\frac{M_{WH}}{b_-^3} \propto \sqrt{\mathcal{K}_{WH}^{class}} . \tag{6.3.68}$$

As a last point of this analysis, it should be studied whether the amplification solution Eq. (6.3.56) is compatible with Eq. (6.3.63), as well as the exchangeability of black and

white hole sides according to the discussion at the end of Sec. 6.3.2. Inverting Eq. (6.3.63) yields

$$M_{BH} = M_{WH}\left(\frac{M_{WH}}{\bar{m}_{\left(\frac{3}{5}\right)}}\right)^{\frac{2}{3}} , \tag{6.3.69}$$

which is Eq. (6.3.56) with M_{BH} and M_{WH} exchanged and the identification $\bar{m}_{\left(\frac{3}{5}\right)} = \bar{m}_{\left(\frac{5}{3}\right)} =: \bar{m}$, i.e. $m_{\left(\frac{3}{5}\right)} = m_{\left(\frac{5}{3}\right)} =: m$. For this identification the amplification (6.3.56) describes exactly the inverse de-amplification (6.3.63). The amplification and de-amplification are of the same amount and the solutions are symmetric, which means both β-values are compatible with each other and also compatible with the discussion at the end of Sec. 6.3.2.

The discussion can be summarised as follows: To achieve an onset of quantum effects at a unique, mass-independent Kretschmann curvature scale $\mathcal{K}_{crit}$, it was necessary to fix a relation of the masses according to

$$M_{WH} = M_{BH}\left(\frac{M_{BH}}{\bar{m}}\right)^{\beta-1} \quad , \quad \beta \in \left\{\frac{5}{3}\,,\,\frac{3}{5}\right\} , \tag{6.3.70}$$

where one value of β describes exactly the inverse mass change as the other value. This relation allows to identify $\sin(\lambda_1 P_1)/\mathscr{L}_o\lambda_1$ as proportional to the square root of the Kretschmann scalar on the side with the smaller mass (respectively M_{BH}, M_{WH} for $\beta = 5/3\,,\, 3/5$). The onset of quantum effects is controlled by the mass independent critical length and curvature scales

$$\ell_{crit} = m^{\frac{1}{4}}\frac{\lambda_2}{\mathscr{L}_o} \quad , \quad \mathcal{K}_{crit} = \frac{48m^{\frac{1}{2}}}{\mathscr{L}_o^2\lambda_1^2} , \tag{6.3.71}$$

where m is a dimensionless number, which is related to $\bar{m}$ (and for $\beta = 5/3$ to D) according to

$$m = \frac{8\lambda_1\mathscr{L}_o^4}{\lambda_2^3}\bar{m} \overset{\beta=\frac{5}{3}}{=} \left(\frac{3}{2}D\right)^{\frac{4}{3}} . \tag{6.3.72}$$

On the side with the smaller mass (denoted by subscript 1), quantum effects become relevant whenever

$$b_1 \sim \ell_{crit} = m^{\frac{1}{4}}\frac{\lambda_2}{\mathscr{L}_o} \quad , \quad \mathcal{K}_1 \sim \mathcal{K}_{crit} = \frac{48m^{\frac{1}{2}}}{\mathscr{L}_o^2\lambda_1^2} . \tag{6.3.73}$$

The onset of quantum effects is at Planck curvature and Planck length, as long as $m \sim 1$.

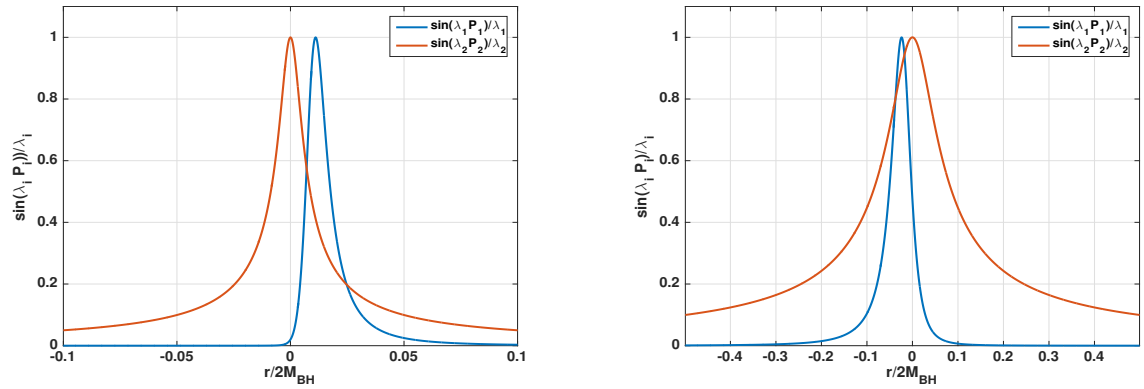

(a) (b)

FIGURE 6.4: *Plot of* $\sin(\lambda_1 P_1)/\mathscr{L}_o\lambda_1$ *and* $\sin(\lambda_2 P_2)\mathscr{L}_o/\lambda_2$ *for* $\beta = 5/3$ *in (a) and* $\beta = 3/5$ *in (b) for the parameters* $\mathscr{L}_o = \lambda_1 = \lambda_2 = \bar{m} = 1$ *and* $M_{BH} = 100$*. The plot shows that the order of high curvature corrections and finite volume corrections is exchanged coming from the other side or changing* β*.*

On the amplified side (subscript 2) the onset of quantum effects is at

$$b_2 \sim \frac{M_2}{M_1}\,\ell_{crit} \quad , \quad \mathcal{K}_2 \sim \frac{M_2^2}{M_1^2}\,\mathcal{K}_{crit}\,, \tag{6.3.74}$$

where $M_2 > M_1$. This finally justifies the interpretation at the beginning of Sec 6.3. As Eq. (6.3.71) shows, $\lambda_2/\mathscr{L}_o$ is related to the critical length ℓ_{crit} and leads to quantum corrections when the length scale becomes small. Further, $\mathscr{L}_o\lambda_1$ is indeed an inverse curvature scale related to $\mathcal{K}_{crit}$ and controls the quantum corrections in the high curvature regime.

A still remaining issue to be better understood the change of quantum scale on the amplified side. As $M_2 > M_1$, the curvature scale in Eq. (6.3.74) becomes larger and thus less relevant. In contrast, the length scale also grows, and finite length effects become relevant earlier. Nevertheless, these effects are always far away from the horizon as $b(r_s) \sim M_2$ for large masses, while $M_2/M_1 \sim M_2^{\frac{3}{5}}$, hence $b(r_s)$ grows faster than $M_2/M_1 \cdot \ell_{crit}$. This amplification of the quantum scales inverts the order of the kind of quantum effect to become relevant first. Consider an observer jumping into the black hole from the lower mass side (1). She will first encounter quantum effects due to high curvature and afterwards finite length effects. Falling into the black hole from the larger mass side (2), she would first see finite size effects and only afterwards the curvature effects. This is depicted in Fig. 6.4 were $\sin(\lambda_1 P_1)/\mathscr{L}_o\lambda_1$ and $\sin(\lambda_2 P_2)\mathscr{L}_o/\lambda_2$ is plotted for both values of β. Exchanging the value of β corresponds to a affecting P_1 or P_2 corrections becoming relevant first.

The discussion so far focussed on the classical regime and when it fails to hold. This was no statement about the deep quantum regime and if the curvature is really bounded. It is

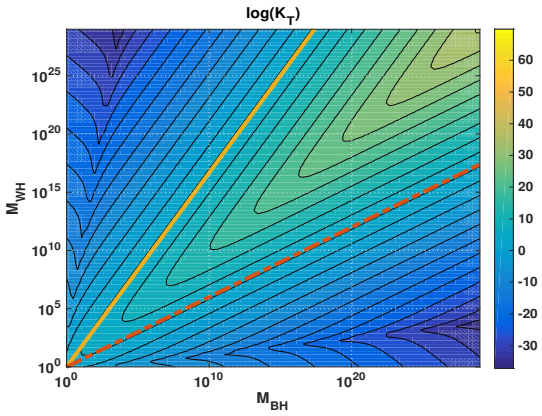

FIGURE 6.5: *The color scale encodes the value of the logarithm of the Kretschmann scalar at the transition surface as a function of the black hole M_{BH} and white hole mass M_{WH} for $\mathscr{L}_o\lambda_1 = \lambda_2/\mathscr{L}_o = 1$. Both axis are in logarithmic scale. Finite non-zero curvatures for large masses can only be achieved by following a level line asymptotically given by Eq. (6.3.55) for $\beta = 5/3$ and $\beta = 3/5$. Different values of $\bar{m}$ correspond to different choices of the level line. The yellow line corresponds to $\beta = 5/3$ and the red dashed line to $\beta = 3/5$.*

possible to analytically compute the Kretschmann scalar. The expression is involved and not particularly insightful. Instead, in Fig. 6.5 the Kretschmann scalar at the transition surface is depicted as function of the both masses. The Kretschmann scalar is almost at maximum at the transition surface and quantum effects are large. From Fig. 6.5, it is visible that the curvature can be made arbitrarily large by choosing suitable values for M_{BH} and M_{WH}. To keep a unique and mass independent upper bound for the curvature, the two masses have to be related so that they follow a level line. For masses larger than the Planck mass, this relation is given by $M_{WH} = M_{BH}\left(\frac{M_{BH}}{\bar{m}}\right)^{\beta-1} \sim M_{BH}^{\beta}$ for $\beta = 5/3$ and $\beta = 3/5$,[17] as can be seen from Fig. 6.5 and confirmed by analytic computations. The value of $\bar{m}$ determines which of the level lines is picked. This deep quantum regime argument is compatible with the above discussion.

In Fig. 6.6 the full Kretschmann scalar $\mathcal{K}$ as function of b is plotted for different masses and both values of β. As required, there is a unique upper bound[18] and the onset of quantum effects is always at the same scale. The exception is $M_{BH} = 1$, which corresponds to a Planck mass black hole. The critical value of the curvature $\mathcal{K}_{crit}$ is indicated by a vertical line and is close to the maximal reachable curvature. The plot shows further that at large radii b the classical behaviour is approached and only the masses are (de-)amplified. For $M_{BH}/m = 1$ the bounce is symmetric, which corresponds to a Planck sized black hole where the effective spacetime description most likely breaks down.

[17] Another possibility is $\beta = -1$, which is not considered here as this requires always one of the two masses to be sub-Planckian. This seems physically not reasonable, although there are ways to interpret such a scenario [79, 215]

[18] As can be easily checked this holds also true for other curvature invariants.

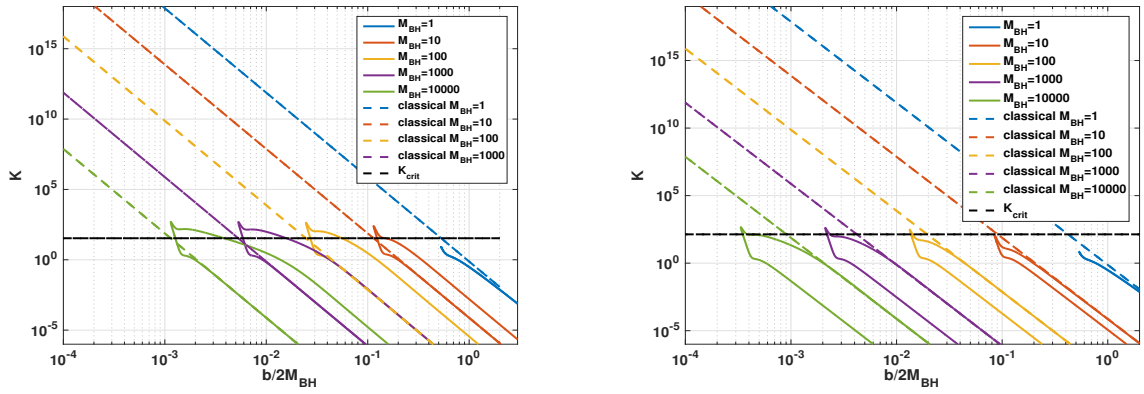

(a) (b)

FIGURE 6.6: *Kretschmann scalar $\mathcal{K}$ against b in a log-log plot for different masses. The dashed lines correspond to the classical result. The parameters are chosen to be $\mathscr{L}_o\lambda_1 = \lambda_2/\mathscr{L}_o = 1$, $\bar{m} = 1$ and $\beta = 5/3$ in (a) as well as $\beta = 3/5$ in (b). Quantum effects always become relevant at the same scale. The horizontal dashed line corresponds to $\mathcal{K}_{crit}$ given in Eq. (6.3.71). Differences occur only for Planck sized black holes ($M_{BH} = 1$), for which quantum effects due to the polymerisation of P_2 become relevant first.*

The present model has already desirable features, such as quantum effects occurring only in the high curvature regime and a unique upper curvature scale. A novel feature are the two mass observables, which were not noticed in previous approaches, although they were present [6]. This points towards the main drawback of this model: To reach an unique mass independent curvature scale, both masses have to be related in a very specific way restricting the initial conditions. This restriction is introduced by hand and is not an outcome of the Hamiltonian analysis. Implementing the mass relation in a quantum theory of this model would be technically challenging. This is why in the following section another model is discussed, where the relation of the masses is much broader and the unique curvature cut-off is reached without specifying any relation, besides subtleties discussed below.

6.4 POLYMERISATION 2: (v, b)-LIKE VARIABLES

The previous model led to the necessity to establish a relation between the masses in order to achieve an unique upper curvature bound. The heart of this problem are the used variables and thus the chosen polymerisation scheme. Recall the expression for the on-shell value of the momenta, which is (cfr. Eq. (6.2.28))

$$\frac{P_1(b)}{\mathscr{L}_o} = \frac{2M}{b^3}\left(\frac{2}{3D}\right)^{\frac{1}{3}} \quad , \quad P_2(b)\mathscr{L}_o = \frac{1}{b}\left(\frac{3D}{2}\right)^{\frac{1}{3}} . \tag{6.4.1}$$

It was argued that $P_1/\mathscr{L}_o$ can be related to the square root of the Kretschmann scalar and thus polymerising this momentum will lead to curvature quantum corrections. A necessary condition for this interpretation is that D is mass independent and thus the initial data is restricted. In the analysis of the onset of quantum effects (cfr. Sec. 6.3.3) this allows a unique curvature scale of quantum effects *only if* the initial conditions are related in a very precise way.

It is possible to introduce new variables, which can be interpreted as being related to the Kretschmann scalar without the need of restricting any initial data. To construct them, the metric ansatz (6.2.1) is taken and the Kretschmann scalar is computed. This curvature scalar is a function of the metric components a and b and of their first and second derivatives $\mathcal{K} = \mathcal{K}(a, b, a', b', a'', b'')$. Using the variable transformation Eq. (6.2.12) allows to express all a and b in terms of v_1 and v_2, and analogous for their derivatives. In the next step using the Hamiltonian equations of motion (6.2.15) and the Hamiltonian constraint allows to express the Kretschmann scalar in terms of phase space variables only, namely

$$\mathcal{K} \overset{\text{equations of motion, Hamiltonian constraint}}{=} 12 \left(\frac{3v_1}{2}\right)^{\frac{2}{3}} P_1^2 P_2^2 \,. \tag{6.4.2}$$

This is a phase space function, which has to reduce to the value of the Kretschmann scalar on-shell. Note that this phase space function is not the Kretschmann scalar in full generality and off-shell, as the equations of motion were used. Nevertheless, it is on-shell, without fixing any integration constant, and this is the closest what is achievable up to now. It is possible to define the following new canonical variables

$$v_k = \left(\frac{3}{2}v_1\right)^{\frac{2}{3}} \frac{1}{P_2} \quad , \quad v_j = v_2 - \frac{3v_1 P_1}{2P_2} \quad , \quad k = \left(\frac{3}{2}v_1\right)^{\frac{1}{3}} P_1 P_2 \quad , \quad j = P_2 \,, \tag{6.4.3}$$

satisfying the standard canonical Poisson brackets

$$\begin{aligned} &\{v_k, k\} = 1 \quad , \quad \{v_j, j\} = 1 \\ &\{k, j\} = \{v_k, v_j\} = \{k, v_j\} = \{j, v_k\} = 0 \,. \end{aligned} \tag{6.4.4}$$

The variable k is related to the Kretschmann scalar by means of

$$\mathcal{K} = 12k^2 \,.$$

This is a direct analogy to LQC (cfr. Sec. 4.2), where the Ricci scalar R is related to the

phase space function b by means of the same proportionality $R \propto b^2$ [19]. In this sense, the variables chosen here are the analogues of (v, b) variables in cosmology. There is another interpretation of k in terms of the so-called Misner-Sharp mass $M_{\text{Misner-Sharp}}$ (see [216] and [217] for an overview). Off-shell, or in fact using the Hamiltonian constraint only, it is

$$k \overset{\mathcal{H}\approx 0}{\approx} R_{\mu\nu\alpha\beta}\epsilon^{\mu\nu}\epsilon^{\alpha\beta} = b\left(1 - \frac{b'^2}{N}\right) = \frac{2M_{\text{Misner-Sharp}}(b)}{b^3} \,, \tag{6.4.5}$$

where $\epsilon^{\mu\nu} = g^{\mu\alpha}g^{\nu\beta}\epsilon_{\alpha\beta}$ with $\epsilon_{\alpha\beta}\mathrm{d}x^\alpha \wedge \mathrm{d}x^\beta = b^2 \sin\theta \mathrm{d}\theta \wedge \mathrm{d}\phi$ is the volume two-form of the $r, t = const.$ two-sphere. The Misner-Sharp mass $M_{\text{Misner-Sharp}}(b)$ is defined in spherically symmetric spacetimes and measures the gravitational energy enclosed in a sphere of areal radius b, and is a quasi-local measure of gravitational energy. This way k can off-shell partially be related to the full Riemann curvature tensor $R_{\mu\nu\alpha\beta}$.

As second momentum, $j = P_2$ is used, which is the same as before. This is a good choice as it is related to $1/b$, i.e. finite length corrections. It should be further improved as it is only proportional to inverse length when the integration constants are restricted. This will play a role in the later discussion of the onset of quantum effects in Sec. 6.4.2. There are variables for which this problem was solved (see [6]). Nevertheless, this model has other physical disadvantages, such as the need of sub-Planckian masses. Up to now, the choice of momenta (j, k) seems to be the best possible option, although there is room for improvements.

The scaling behaviour of (v_i, P_i) under rescaling the fiducial cell (cfr. Eq. (6.2.13)) transfers to the new variables via the transformation (6.4.3). This results in

$$v_k \longmapsto \alpha v_k \quad , \quad k \longmapsto k \quad , \quad v_j \longmapsto \alpha^2 v_j \quad , \quad j \longmapsto \alpha^{-1} j \,, \tag{6.4.6}$$

and shows that the product of momentum with a conjugate phase space variable is a density of weight 1 in t-direction. Again, physical quantities can only depend on $v_k/\mathscr{L}_o$, k, $v_j/\mathscr{L}_o^2$ and $\mathscr{L}_o j$, as they have to be independent of the fiducial structures. The fact that k does not scale with the fiducial cell (in contrast to P_1) is compatible with its interpretation as curvature scalar.

Performing the canonical transformation (6.4.3) leads to the classical Hamiltonian in the new variables

$$H_{\text{cl}} = \sqrt{n}\,\mathcal{H}_{\text{cl}} \qquad , \qquad \mathcal{H}_{\text{cl}} = 3v_k k j + v_j j^2 - 2 \approx 0 \,. \tag{6.4.7}$$

[19] Note that this is also only true on-shell in the same way as discussed above.

Remarkably, it has exactly the same functional structure as the previous Hamiltonian in (v_i, P_i)-variables Eq. (6.2.14). This structure is still simple and allows to solve the equations after polymerisation with the exact same strategy. What changes is the relation to the metric components a and b, which is given by

$$b(r) = \sqrt{v_k\, j}\ , \tag{6.4.8}$$

$$a(r) = \frac{j\, v_j + k\, v_k}{2 v_k\, j^2}\ . \tag{6.4.9}$$

Solving the classical equations of motion gives of course the classical Schwarzschild solution. The on-shell expression of k and j is interesting and for $\sqrt{n} = const. = \mathscr{L}_o$ it is given by

$$k(b) = \left(\frac{D}{\mathscr{L}_o}\right)^{\frac{3}{2}} \frac{C}{b^3} = \frac{2M_{BH}}{b^3} \quad , \quad \mathscr{L}_o\, j(b) = \left(\frac{D}{\mathscr{L}_o}\right)^{\frac{1}{2}} \frac{1}{b}\ , \tag{6.4.10}$$

where again two Dirac observables can be found. One of them is the black hole mass

$$2\mathcal{M}_{BH} = \mathcal{R}_{BH} = k\,(v_k j)^{\frac{3}{2}} \overset{\text{on-shell}}{=} C \left(\frac{D}{\sqrt{n}}\right)^{\frac{3}{2}}\ . \tag{6.4.11}$$

As discussed, the second Dirac observable

$$\mathcal{O} = \frac{2}{3} v_k k \overset{\text{on-shell}}{=} CD\ , \tag{6.4.12}$$

scales with the fiducial cell ($C \mapsto C$, $D \mapsto \alpha D$) and can be removed from the metric.

It is important that k is *exactly* proportional to the square root of the Kretschmann scalar without restricting the initial conditions. This is the main argument supporting these variables, as now the onset of quantum effects might be at a constant curvature scale, and it is independent of the choice of the initial conditions, which was the main restriction in the previous model. Nevertheless, $\mathscr{L}_o j$ is still dependent on D, which might in turn lead to the need of restricting the initial conditions (see below).

The effective quantum theory is again constructed by classical polymerisation, i.e. the replacement

$$k \longmapsto \frac{\sin(\lambda_k\, k)}{\lambda_k}\ , \tag{6.4.13}$$

$$j \longmapsto \frac{\sin(\lambda_j\, j)}{\lambda_j}\ , \tag{6.4.14}$$

where the polymerisation scales λ_j, λ_k are kept as pure constants proportional to the Planck length. Due to the interpretation of k and j, this is expected to lead to quantum corrections at high curvatures and small lengths, or equivalently small areas.

According to the scaling behaviour of k and j (Eq. (6.4.6)) the polymerisation scales transform as

$$\lambda_k \longmapsto \lambda_k \quad , \quad \lambda_j \longmapsto \alpha\lambda_j\ , \tag{6.4.15}$$

under fiducial cell rescaling. The physically relevant scales are thus λ_k and $\lambda_j/\mathscr{L}_o$. Recalling further the definitions (6.4.3), the new momenta have the dimensions

$$[k] = [bP_1P_2] = L^{-2} \quad , \quad [j] = [P_2] = L^{-2}\ , \tag{6.4.16}$$

where L denotes the dimension of length. As the products $\lambda_k k$, $\lambda_j j$ are dimensionless, this leads to the dimensions

$$[\lambda_k] = \left[\frac{1}{k}\right] = L^2 \quad , \quad \left[\frac{\lambda_j}{\mathscr{L}_o}\right] = \left[\frac{1}{\mathscr{L}_o j}\right] = L\ , \tag{6.4.17}$$

of the polymerisation scales. This is compatible with interpreting λ_k as inverse curvature scale and $\lambda_j/\mathscr{L}_o$ as length scale, controlling the onset of curvature and small length quantum effects, respectively.

6.4.1 Solutions and Causal Structure

The polymerised Hamiltonian becomes

$$H_{\text{eff}} = \sqrt{n}\,\mathcal{H}_{\text{eff}} \quad , \quad \mathcal{H}_{\text{eff}} = 3v_k\frac{\sin(\lambda_k\, k)}{\lambda_k}\frac{\sin(\lambda_j\, j)}{\lambda_j} + v_j\frac{\sin^2(\lambda_j\, j)}{\lambda_j^2} - 2 \approx 0\ , \tag{6.4.18}$$

with the corresponding equations of motion given by

$$\begin{aligned}
v_k' &= 3\sqrt{n}\, v_k\, \cos(\lambda_k k)\, \frac{\sin(\lambda_j j)}{\lambda_j}\,,\\
v_j' &= 3\sqrt{n}\, v_k\, \frac{\sin(\lambda_k k)}{\lambda_k}\, \cos(\lambda_j j) + 2v_j\, \sqrt{n}\, \frac{\sin(\lambda_j j)}{\lambda_j}\, \cos(\lambda_j j)\,,\\
k' &= -3\sqrt{n}\, \frac{\sin(\lambda_k k)}{\lambda_k}\, \frac{\sin(\lambda_j j)}{\lambda_j}\,,\\
j' &= -\sqrt{n}\, \frac{\sin^2(\lambda_j j)}{\lambda_j^2}\,,\\
H_{\text{eff}} &= 3v_k \frac{\sin(\lambda_k\, k)}{\lambda_k} \frac{\sin(\lambda_j\, j)}{\lambda_j} + v_j \frac{\sin^2(\lambda_j\, j)}{\lambda_j^2} - 2 \approx 0\,.
\end{aligned} \tag{6.4.19}$$

As the Hamiltonian has the same functional form as Eq. (6.3.5), the equations of motion are functionally equal. Hence for $\sqrt{n} = const. = \mathscr{L}_o$, not only the solution strategy is the same, but also the solutions are identical, identifying $v_1 \leftrightarrow v_k$, $v_2 \leftrightarrow v_j$, $P_1 \leftrightarrow k$ and $P_2 \leftrightarrow j$, leading to the solutions

$$v_k(r) = \frac{2DC^2\lambda_k^2\sqrt{n}^3}{\lambda_j^3} \frac{\frac{\lambda_j^6}{16C^2\lambda_k^2 n^3}\left(\frac{\sqrt{n}\,r}{\lambda_j} + \sqrt{1+\frac{nr^2}{\lambda_j^2}}\right)^6 + 1}{\left(\frac{\sqrt{n}\,r}{\lambda_j} + \sqrt{1+\frac{nr^2}{\lambda_j^2}}\right)^3}\,, \tag{6.4.20a}$$

$$v_j(r) = 2n\left(\frac{\lambda_j}{\sqrt{n}}\right)^2\left(1+\frac{nr^2}{\lambda_j^2}\right)\left(1 - \frac{3CD}{2\lambda_j}\frac{1}{\sqrt{1+\frac{nr^2}{\lambda_j^2}}}\right)\,, \tag{6.4.20b}$$

$$k(r) = \frac{2}{\lambda_k}\cot^{-1}\left(\frac{\lambda_j^3}{4C\lambda_k\sqrt{n}^3}\left(\frac{\sqrt{n}\,r}{\lambda_j} + \sqrt{1+\frac{nr^2}{\lambda_j^2}}\right)^3\right)\,, \tag{6.4.20c}$$

$$j(r) = \frac{1}{\lambda_j}\cot^{-1}\left(\frac{\sqrt{n}r}{\lambda_j}\right) + \frac{\pi}{\lambda_j}\theta\left(-\frac{\sqrt{n}r}{\lambda_j}\right)\,, \tag{6.4.20d}$$

where C, D are the integration constants, which, according to the scaling behaviours Eq. (6.4.6), transform as $C \mapsto C$ and $D \mapsto \alpha D$ under a fiducial cell rescaling.

The crucial difference to the previous model is the relation of these variables to the metric components a and b. Especially subtle is the fact that the metric components depend on configuration space variables and simultaneously on momenta (cfr. Eqs. (6.4.8) and (6.4.9)). As the momenta j and k have no physical meaning, but their trigonometric functions, these expressions have to be polymerised, too. Only if this is done, there will be a chance to construct an operator for the metric components on a polymer Hilbert space (cfr. Sec. 4.3). There are probably several choices in polymerising the expressions (6.4.8)

and (6.4.9), but to remain consistent with the polymerisation of the Hamiltonian, the sin-function is chosen. The metric components become

$$b^2(r) = v_k(r)\frac{\sin(\lambda_j j(r))}{\lambda_j} = \frac{2DC^2\lambda_k^2\sqrt{n}^3}{\lambda_j^4}\frac{1}{\sqrt{1+\frac{nr^2}{\lambda_j^2}}}\frac{\frac{\lambda_j^6}{16C^2\lambda_k^2 n^3}\left(\frac{\sqrt{n}\,r}{\lambda_j}+\sqrt{1+\frac{nr^2}{\lambda_j^2}}\right)^6+1}{\left(\frac{\sqrt{n}\,r}{\lambda_j}+\sqrt{1+\frac{nr^2}{\lambda_j^2}}\right)^3}\,, \tag{6.4.21}$$

$$\begin{aligned} a(r) &= \frac{1}{2v_k(r)}\frac{\lambda_j^2}{\sin^2(\lambda_j j(r))}\left(v_j(r)\frac{\sin(\lambda_j j(r))}{\lambda_j}+v_k(r)\frac{\sin(\lambda_k k(r))}{\lambda_k}\right) \\ &= \frac{\lambda_j^6}{2DC^2\lambda_k^2\sqrt{n}^3}\left(1+\frac{nr^2}{\lambda_j^2}\right)^{\frac{3}{2}}\left(1-\frac{CD}{\lambda_j\sqrt{1+\frac{nr^2}{\lambda_j^2}}}\right)\frac{\left(\frac{\sqrt{n}\,r}{\lambda_j}+\sqrt{1+\frac{nr^2}{\lambda_j^2}}\right)^3}{\frac{\lambda_j^6}{16C^2\lambda_k^2 n^3}\left(\frac{\sqrt{n}\,r}{\lambda_j}+\sqrt{1+\frac{nr^2}{\lambda_j^2}}\right)^6+1}\,, \end{aligned} \tag{6.4.22}$$

with the line element

$$\mathrm{d}s^2 = -\frac{a(r)}{L_o^2}\mathrm{d}t^2+\frac{\mathscr{L}_o^2}{a(r)}\mathrm{d}r^2+b^2(r)\left(\mathrm{d}\theta^2+\sin^2\theta\mathrm{d}\phi^2\right)\,. \tag{6.4.23}$$

Again, two integration constants C and D occur, and as stated above, $\sqrt{n}=\mathscr{L}_o$ was chosen. The integration constants are dependent on the fiducial cell by means of $C\mapsto C$ and $D\mapsto\alpha D$.

Again characteristic features of this spacetime can be examined. First of all, note that the line element is well-defined and smooth for the full r-domain $r\in(-\infty,\infty)$ and describes interior and exterior regions at the same time. The first important step is to determine the asymptotic behaviour at $r\to\pm\infty$. This also allows to determine the integration constants C and D in terms of physical scalars and corresponding Dirac observables.

6.4.1.1 Asymptotic Behaviour

Starting with the positive branch $r\to\infty$, the metric coefficients Eqs. (6.4.21) and (6.4.22) become

$$b_+^2 := b^2(r\to+\infty) = \frac{D}{\sqrt{n}}\,r^2 \qquad , \qquad a_+ := a(r\to+\infty) = \frac{n\sqrt{n}}{D}\left(1-\frac{CD}{\sqrt{n}\,r}\right) \tag{6.4.24}$$

from which follows

$$a\Big(b(r\to+\infty)\Big)=\frac{n\sqrt{n}}{D}\left(1-\left(\frac{D}{\sqrt{n}}\right)^{\frac{3}{2}}\frac{C}{b}\right)\ . \tag{6.4.25}$$

This expression is independent of the choice of the r coordinate as it is expressed in terms of the effective scalar b. Similar to the previous cases, it is possible to rescale the t and r coordinate to absorb the prefactor in front of a. Choosing $t\mapsto\tau=\sqrt{\frac{\mathscr{L}_o^3}{DL_o^2}}\,t$ and $r\mapsto b=\sqrt{\frac{D}{\mathscr{L}_o}}\,r$ for $\sqrt{n}=\mathscr{L}_o$ yields the line element

$$\mathrm{d}s_+^2\simeq-\left(1-\left(\frac{D}{\sqrt{n}}\right)^{\frac{3}{2}}\frac{C}{b}\right)\mathrm{d}\tau^2+\frac{\mathrm{d}b^2}{1-\left(\frac{D}{\sqrt{n}}\right)^{\frac{3}{2}}\frac{C}{b}}+b^2\mathrm{d}\Omega_2^2\ . \tag{6.4.26}$$

This is a classical Schwarzschild spacetime of mass

$$2M_{BH}=C\left(\frac{D}{\sqrt{n}}\right)^{\frac{3}{2}}\ . \tag{6.4.27}$$

The same analysis can be done for the $r\to-\infty$ limit. The results are

$$b_-^2:=b^2(r\to-\infty)=\frac{16DC^2\lambda_k^2}{\sqrt{n}}\left(\frac{\sqrt{n}}{\lambda_j}\right)^6|r|^2\ , \tag{6.4.28}$$

$$a_-:=a(r\to-\infty)=\frac{n\sqrt{n}}{16DC^2\lambda_k^2}\left(\frac{\lambda_j}{\sqrt{n}}\right)^6\left(1-\frac{CD}{\sqrt{n}|r|}\right)\ , \tag{6.4.29}$$

from which follows

$$a\Big(b(r\to-\infty)\Big)=\frac{n\sqrt{n}}{16DC^2\lambda_k^2}\left(\frac{\lambda_j}{\sqrt{n}}\right)^6\left(1-\frac{4nDC^2\lambda_k}{\lambda_j^3}\sqrt{\frac{D}{\sqrt{n}}}\,\frac{1}{b}\right)\ . \tag{6.4.30}$$

Using the same strategy as before and rescaling the coordinates by means of $t\mapsto\tau=\sqrt{\frac{\mathscr{L}_o^3}{DL_o^2}}\,\frac{\lambda_j^3}{4C\lambda_k\mathscr{L}_o^3}\,t$ and $r\mapsto b=4C\lambda_k\left(\frac{\mathscr{L}_o}{\lambda_j}\right)^3\sqrt{\frac{D}{\mathscr{L}_o}}(-r)$, gives the line element

$$\mathrm{d}s_-^2\simeq-\left(1-\frac{4nDC^2\lambda_k}{\lambda_j^3}\sqrt{\frac{D}{\sqrt{n}}}\,\frac{1}{b}\right)\mathrm{d}\tau^2+\frac{\mathrm{d}b^2}{1-\frac{4nDC^2\lambda_k}{\lambda_j^3}\sqrt{\frac{D}{\sqrt{n}}}\,\frac{1}{b}}+b^2\mathrm{d}\Omega_2^2\ , \tag{6.4.31}$$

which is again a classical Schwarzschild spacetime. The mass in this asymptotic region is

given by

$$2M_{WH} = \frac{4\lambda_k C^2 \sqrt{n}^3}{\lambda_j^3}\left(\frac{D}{\sqrt{n}}\right)^{\frac{3}{2}} = 8C\lambda_k\left(\frac{\sqrt{n}}{\lambda_j}\right)^3 M_{BH}\ . \tag{6.4.32}$$

This observation leads to the following two important consequences: First, in both limits $b(r \to \pm\infty)$, spacetime is well-approximated by classical Schwarzschild regions and approaching the classical behaviour before and after the bounce. The two Schwarzschild regions are characterised by the masses M_{BH} and M_{WH}, respectively. Second, this allows to fix the integration constants C and D by means of the (gauge independent) physical input of the masses M_{BH} and M_{WH}. Inverting Eqs. (6.4.27) and (6.4.32) leads to

$$C = \frac{\lambda_j^3}{4\lambda_k\sqrt{n}^3}\frac{M_{WH}}{M_{BH}} \qquad , \qquad D = \sqrt{n}\left(\frac{8\lambda_k\sqrt{n}^3}{\lambda_j^3}\frac{M_{BH}^2}{M_{WH}}\right)^{\frac{2}{3}}\ . \tag{6.4.33}$$

Using the solutions (6.4.20a)-(6.4.20d) for the effective dynamics allows to construct phase space functions for C, D and also for the two masses. In this way it is possbile to construct the black and white hole mass Dirac observables as

$$2\mathcal{M}_{BH} = \frac{\sin(\lambda_k k)}{\lambda_k}\cos\left(\frac{\lambda_k k}{2}\right)\left(\frac{2v_k}{\lambda_j\cot\left(\frac{\lambda_j j}{2}\right)}\right)^{\frac{3}{2}}\ , \tag{6.4.34a}$$

$$2\mathcal{M}_{WH} = \frac{\sin(\lambda_k k)}{\lambda_k}\sin\left(\frac{\lambda_k k}{2}\right)\left(\frac{2v_k}{\lambda_j}\cot\left(\frac{\lambda_j j}{2}\right)\right)^{\frac{3}{2}}\ , \tag{6.4.34b}$$

which yield the values M_{BH} and M_{WH}, when evaluated on the solutions. In contrast to the classical case, they both are fiducial cell independent and have physical relevance, as they both appear in the line element and the asymptotic spacetimes.

It is instructive to insert the expressions for C and D into the expression for the final metric (6.4.23) and the components (6.4.21) and (6.4.22). Performing a further coordinate change to $x = {}^{\mathscr{L}_o r}/_{\lambda_j}$ and $\tau = {}^{\lambda_j t}/_{L_o}$, results in the line element

$$\mathrm{d}s^2 = -\frac{a(x)}{\lambda_j}\mathrm{d}\tau^2 + \frac{\lambda_j^2}{a(x)}\mathrm{d}x^2 + b(x)^2\mathrm{d}\Omega_2^2\ , \tag{6.4.35}$$

with components

$$b^2(x) = \frac{1}{2}\left(\frac{\lambda_k}{M_{BH}M_{WH}}\right)^{\frac{2}{3}} \frac{1}{\sqrt{1+x^2}} \frac{M_{BH}^2\left(x+\sqrt{1+x^2}\right)^6 + M_{WH}^2}{\left(x+\sqrt{1+x^2}\right)^3} \,, \tag{6.4.36}$$

$$\frac{a(x)}{\lambda_j^2} = 2\left(\frac{M_{BH}M_{WH}}{\lambda_k}\right)^{\frac{2}{3}} \left(1 - \left(\frac{M_{BH}M_{WH}}{\lambda_k}\right)^{\frac{1}{3}} \frac{1}{\sqrt{1+x^2}}\right) \frac{(1+x^2)^{\frac{3}{2}}\left(x+\sqrt{1+x^2}\right)^3}{M_{BH}^2\left(x+\sqrt{1+x^2}\right)^6 + M_{WH}^2} \,. \tag{6.4.37}$$

Note that λ_j does not appear in the metric any more. The precise value of $\lambda_j/\mathscr{L}_o$ does not affect the physics and this scale turns out to be fiducial.

As discussed at the end of Sec. 6.3.2, the metric can be analysed for symmetry of both sides. Changing the point of view from being on the black hole side to the white hole side corresponds to the transformation

$$v_j \mapsto v_j \quad , \quad v_k \mapsto v_k \quad , \quad k \mapsto \frac{\pi}{\lambda_k} - k \quad , \quad j \mapsto \frac{\pi}{\lambda_j} - j \,. \tag{6.4.38}$$

This describes the evolution of the phase space variables from one side to the other (see the discussion in Sec. 6.3.2 around Eq. (6.3.49) for more details). The mass Dirac observables (6.4.34a) and (6.4.34b) transform according to

$$2\mathcal{M}_{BH} \longmapsto 2\mathcal{M}_{WH} \quad , \quad 2\mathcal{M}_{WH} \longmapsto 2\mathcal{M}_{BH} \,. \tag{6.4.39}$$

An observer, who specified a value for M_{BH} and M_{WH}, travelling from the black hole side to the white hole side would observe that her M_{BH} coincides with the value of M_{WH} of an observer living on the white hole side and vice versa. Again, this shows that the names black hole and white hole side are completely interchangeable. The reason for this symmetry is again the polymerisation scheme using the sin-function. Other schemes could break this symmetry. On the level of the metric (6.4.35) this symmetry manifests in invariance under the transformation[20]

$$x \longmapsto -x \quad , \quad \mathcal{M}_{BH} \longmapsto \mathcal{M}_{WH} \quad , \quad \mathcal{M}_{WH} \longmapsto \mathcal{M}_{BH} \,.$$

[20]This can be easily checked by re-writing $x + \sqrt{1+x^2} = \exp\left(\sinh^{-1}(x)\right)$.

6.4.1.2 Horizons

As a next step the horizon structure is to be analysed. The Killing horizons can be determined by the condition

$$a(r_s^{(\pm)}) \stackrel{!}{=} 0 \quad \Leftrightarrow$$
$$\frac{\lambda_j^6}{2DC^2\lambda_k^2\sqrt{n}^3}\left(1+\frac{nr^2}{\lambda_j^2}\right)^{\frac{3}{2}}\left(1-\frac{CD}{\lambda_j\sqrt{1+\frac{nr^2}{\lambda_j^2}}}\right)\frac{\left(\frac{\sqrt{n}\,r}{\lambda_j}+\sqrt{1+\frac{nr^2}{\lambda_j^2}}\right)^3}{\frac{\lambda_j^6}{16C^2\lambda_k^2n^3}\left(\frac{\sqrt{n}\,r}{\lambda_j}+\sqrt{1+\frac{nr^2}{\lambda_j^2}}\right)^6+1}\Bigg|_{r=r_s^{(\pm)}} \stackrel{!}{=} 0\,. \tag{6.4.40}$$

The only term that can vanish is

$$1-\frac{CD}{\lambda_j\sqrt{1+\frac{nr^2}{\lambda_j^2}}}=0\,,$$

which leads to

$$r_s^{(\pm)}=\pm\sqrt{\frac{C^2D^2}{\mathscr{L}_o^2}-\frac{\lambda_j^2}{\mathscr{L}_o^2}}=\frac{\lambda_j}{\mathscr{L}_o}\sqrt{\left(\frac{M_{BH}M_{WH}}{\lambda_k}\right)^{\frac{2}{3}}-1}\,. \tag{6.4.41}$$

As expected, there are exactly two horizons with areal radius $b(r_s^{(\pm)})$, which are

$$\begin{aligned} b\left(r_s^{(\pm)}\right)^2 &= \frac{M_{BH}}{2M_{WH}}\left((M_{BH}M_{WH})^{\frac{1}{3}}\pm\sqrt{(M_{BH}M_{WH})^{\frac{2}{3}}-\lambda_k^{\frac{2}{3}}}\right)^3 \\ &\quad+\frac{M_{WH}}{2M_{BH}}\frac{\lambda_k^2}{\left((M_{BH}M_{WH})^{\frac{1}{3}}\pm\sqrt{(M_{BH}M_{WH})^{\frac{2}{3}}-\lambda_k^{\frac{2}{3}}}\right)^3}\,. \end{aligned} \tag{6.4.42}$$

For large masses, i.e. $M_{BH}M_{WH}\gg\lambda_k$, this becomes

$$b(r_s^{(+)})^2\simeq 4M_{BH}^2\left(1-\frac{3}{4}\left(\frac{\lambda_k}{M_{BH}M_{WH}}\right)^{\frac{2}{3}}-\mathcal{O}\left(\frac{\lambda_k^2}{M_{BH}^2M_{WH}^2}\right)\right)\,, \tag{6.4.43}$$

$$b(r_s^{(-)})^2\simeq 4M_{WH}^2\left(1-\frac{3}{4}\left(\frac{\lambda_k}{M_{BH}M_{WH}}\right)^{\frac{2}{3}}-\mathcal{O}\left(\frac{\lambda_k^2}{M_{BH}^2M_{WH}^2}\right)\right)\,, \tag{6.4.44}$$

which is in agreement with the classical result on both sides. The leading corrections are suppressed by λ_k and negative. Hence, the quantum corrected horizon is sightly smaller than classical expectation.

6.4.1.3 Transition Surface

Another important surface in the effective quantum corrected spacetime is the transition replacing the classical singularity. Analysing the expression (6.4.21) for $b(r)$ shows that it is larger than zero throughout the evolution. The transition surface is characterised by the minimal value that $b(r)$ can reach. The minimum is reached when $b' = 0$, which is equivalent to $(b^2)' = 0$ as $b \neq 0$ everywhere. Computations can be simplified further by introducing the new coordinate

$$z = \frac{\mathscr{L}_o r}{\lambda_j} + \sqrt{1 + \frac{\mathscr{L}_o^2 r^2}{\lambda_j^2}} \quad , \quad z \in (0, \infty) \, . \tag{6.4.45}$$

As $\mathrm{d}z/\mathrm{d}r \neq 0$, the transition surface is equally described by the condition $\mathrm{d}(b^2)/\mathrm{d}z = 0$. Inserting z in Eq. (6.4.21) yields

$$b^2(z) = \frac{2C^2\lambda_k^2\mathscr{L}_o^3 D}{\lambda_j^4} \, \frac{2z}{z^2+1} \, \frac{\frac{\lambda_j^6}{16C^2\lambda_k^2\mathscr{L}_o^6} z^6 + 1}{z^3} \, .$$

After a number of manipulations the transition surface satisfies the condition

$$\frac{\mathrm{d}b^2}{\mathrm{d}z} = 0 \quad \Leftrightarrow \quad -\frac{2z^4+z^2}{z^4+z^2}\left(\frac{\lambda_j^6 z^6}{\mathscr{L}_o^6} + 16C^2\lambda_k^2\right) + \frac{3\lambda_j^6 z^6}{\mathscr{L}_o^6} = 0 \, , \tag{6.4.46}$$

which for $y = z^2$ and $y > 0$ simplifies to (recall Eq. (6.4.33))

$$y^4 + 2y^3 = \frac{16C^2\lambda_k^2\mathscr{L}_o^6}{\lambda_j^6}(2y+1) = \frac{M_{WH}^2}{M_{BH}^2}(2y+1) \, , \tag{6.4.47}$$

and is a fourth order polynomial equation in y with the restriction $y > 0$. The crucial point is that this equation has only one unique solution for $y > 0$, which can easily be demonstrated graphically (cfr. Fig. 6.7). This solution is given by

$$\begin{aligned} y_{\mathcal{T}} = &-\frac{1}{2} + \frac{1}{2}\sqrt{1 + 2^{2/3}\left(-B + B^2\right)^{1/3}} \\ &+ \frac{1}{2}\sqrt{2 - 2^{2/3}\left(-B+B^2\right)^{1/3} + \frac{-8+16B}{4\sqrt{1+2^{2/3}\left(-B+B^2\right)^{1/3}}}} \, , \end{aligned} \tag{6.4.48}$$

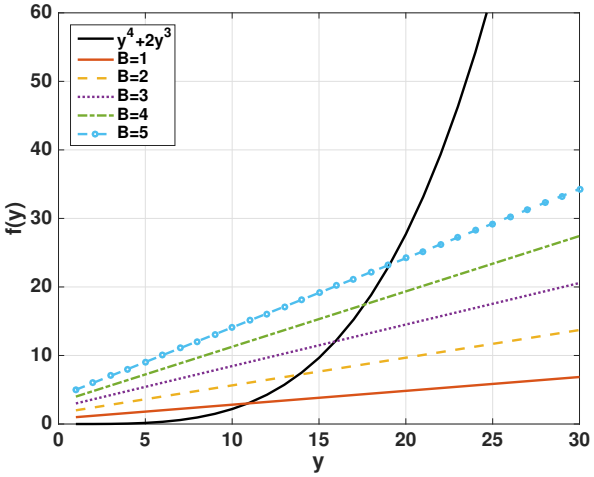

FIGURE 6.7: *Graphical solutions of Eq. (6.4.47). The black line corresponds to the left hand side of Eq. (6.4.47), the coloured lines to the right hand side for different values of* $B = {}^{M^2_{WH}}/_{M^2_{BH}}$. *For* $y > 0$, *there exists exactly one solution.*

with $B = \frac{16C^2\lambda_k^2\mathscr{L}_o^6}{\lambda_j^6} = {}^{M^2_{WH}}/_{M^2_{BH}}$. Areal radius $b_\mathcal{T} = b(r_\mathcal{T})$ of the transition surface can be directly computed on this basis. As this expression is complicated and not insightful, it is not reported here.

With the computation in Sec. 6.3.2, it is straightforward to show that this point is indeed a transition from a trapped to anti-trapped region, i.e. a black-to-white hole transition. The expansions $\theta_\pm$ for $t = const.$, $r = const.$ surfaces for $r_s^{(-)} < r < r_s^{(+)}$ are given by (cfr. Eq. (6.3.45))

$$\theta_\pm = -\sqrt{-\frac{2}{N}\frac{b'(r)}{b(r)}}\,. \tag{6.4.49}$$

Both expansions are negative as $b'(r) > 0$ in the black hole interior region $r_\mathcal{T} < r < r_s^{(+)}$, which shows that this region is trapped. In contrast, both expansions are positive in the white hole interior region $r_s^{(-)} < r < r_\mathcal{T}$ as $b'(r) < 0$ there. This shows that this region is anti-trapped. The smooth transition happens at the transition surface $b'(r) = 0$ where both expansions vanish.

On the basis of this analysis, the Penrose diagram of the spacetime can be constructed without much additional effort. This procedure follows the argumentation presented in Sec. 6.3.2. The qualitative behaviour is exactly the same, i.e. one transition surface, two horizons, asymptotically Schwarzschild in both regions $r \to \pm\infty$. To ensure that the steps presented in Sec. 6.3.2 work, the derivative of a at the horizon has to be checked. It is easy to verify that $a'(r_s^{(\pm)}) \neq 0$ and $\mathrm{sign}(a'(r_s^{(\pm)})) = \pm 1$, which is again qualitatively the same as in the previous case and guarantees that the construction works exactly the

same[21]. The final Penrose diagram of the effective spacetime is the same as in Fig. 6.3.

6.4.2 Onset of Quantum Effects and Curvature Cutoff

The crucial and still missing part is the onset of quantum effects. The motivation of these variables was to achieve quantum effects at a unique mass independent curvature scale, without fixing a relation between the two masses as in the previous model. To investigate this, the afore used strategy can be applied. Again, the classical regime is reached in both limits $r \to +\infty$ and $r \to -\infty$. First, the positive branch is discussed. Looking at the solutions Eqs. (6.4.20a)-(6.4.20d), shows that they reduce to the corresponding classical expressions when the conditions

$$\frac{\mathscr{L}_o\, r}{\lambda_j} \gg 1 \qquad , \qquad \frac{2r^3}{C\lambda_k} \gg 1 \tag{6.4.50}$$

are satisfied. These conditions represent the classical regime on the black hole side. Expressing this in terms of b by using Eq. (6.4.24) and re-phrasing it in terms of the two masses using Eq. (6.4.33) leads to

$$b_+ \gg \left(8\lambda_k \frac{(M_{BH})^2}{M_{WH}}\right)^{\frac{1}{3}} \quad , \quad \frac{M_{BH}}{b_+^3} \ll \frac{1}{\lambda_k}\,. \tag{6.4.51}$$

Of special interest is the second condition, which can be related to the classical Kretschmann scalar on the black hole side by means of

$$\mathcal{K}_{cl}^{BH} = \frac{48M_{BH}^2}{b_+^6} \ll \frac{48}{\lambda_k^2}\,. \tag{6.4.52}$$

This gives a unique mass independent curvature scale at which quantum effects become relevant. Moreover, in contrast to the previous model, this scale is independent of any relation of the black and white hole mass. The problem is not entirely solved as the fist condition in Eq. (6.4.51) does depend on the masses. Due to the construction of the variable j, it is expected that this is a length scale, depending on the masses in this case. It is possible to rearrange this condition, allowing to view this as a curvature scale, i.e.

$$\mathcal{K}_{cl}^{BH} = \frac{48M_{BH}^2}{b_+^6} \ll \frac{M_{WH}^2}{M_{BH}^2}\frac{3}{4\lambda_k^2}\,, \tag{6.4.53}$$

[21]The Penrose diagram is only sensitive to the causal and global structure of the spacetime and neglects all quantitative details. This is also due to the fact that the conformal embedding is at most unique up to conformal transformations, allowing to rearrange e.g. the spacing of different $t = const.$ lines.

which is sensitive to the asymmetry of both sides.

The same discussion applies to the white hole side, where the classical regime is given whenever

$$\frac{\mathscr{L}_o|r|}{\lambda_j} \gg 1 \qquad , \qquad \frac{32C\lambda_k\mathscr{L}_o^6|r|^3}{\lambda_j^6} \gg 1 \tag{6.4.54}$$

holds. This expression can be made coordinate independent by replacing r by b_- according to Eq. (6.4.28). Further inserting the expressions (6.4.33) for C and D yields

$$b_- \gg \left(8\lambda_k\frac{M_{BH}^2}{M_{WH}}\right)^{\frac{1}{3}}\frac{M_{WH}}{M_{BH}} = \left(8\lambda_k\frac{M_{WH}^2}{M_{BH}}\right)^{\frac{1}{3}} \quad , \quad \frac{M_{WH}}{b_-^3} \ll \frac{1}{\lambda_k} \, . \tag{6.4.55}$$

The second condition can be re-written in terms of the classical Kretschmann scalar of the white hole side, i.e.

$$\mathcal{K}_{cl}^{WH} = \frac{48M_{WH}^2}{b_-^6} \ll \frac{48}{\lambda_k^2} \, , \tag{6.4.56}$$

which defines a unique mass independent curvature scale, at which quantum effects become relevant. Indeed, together with Eq. (6.4.52) the polymerisation scale λ_k can be interpreted as an inverse curvature scale defining the scale at which quantum effects become relevant. In turn, there are no quantum effects in the low curvature regime, as it was required. The first condition in Eq. (6.4.55) could be interpreted as length scale, which is mass dependent. It is again possible to rewrite this condition in terms of a asymmetry dependent curvature scale

$$\mathcal{K}_{cl}^{WH} = \frac{48M_{WH}^2}{b_+^6} \ll \frac{M_{BH}^2}{M_{WH}^2}\frac{3}{4\lambda_k^2} \, . \tag{6.4.57}$$

Before this property is analysed further, some cross checks are done.

It is important that quantum effects become negligible at the horizon of astrophysical black holes (large masses). The following consideration is analogous for both sides, only the black hole side is discussed in detail. The first condition of Eq. (6.4.51) can also be rewritten as

$$b_+ \gg 2M_{BH}\left(\frac{\lambda_k}{M_{BH}M_{WH}}\right)^{\frac{1}{3}} \, .$$

In the limit $M_{BH}M_{WH} \gg \lambda_k$, the horizon is always larger as this scale, as (cfr. Eq. (6.4.43))

$$b(r_s^{(+)})^2 \simeq 4M_{BH}^2\left(1-\frac{3}{4}\left(\frac{\lambda_k}{M_{BH}M_{WH}}\right)^{\frac{2}{3}}-\mathcal{O}\left(\frac{\lambda_k^2}{M_{BH}^2M_{WH}^2}\right)\right)$$
$$\gg 4M_{BH}^2\left(\frac{\lambda_k}{M_{BH}M_{WH}}\right)^{\frac{2}{3}} . \tag{6.4.58}$$

This is a restriction on the product of both masses, which means that for an astrophysical black hole where, M_{BH} is large, the corresponding white hole mass needs to be much above λ_k/M_{WH}, i.e. has to be much bigger than the Plank mass. The second condition of Eq. (6.4.51) can be written as

$$(\lambda_k M_{BH})^{\frac{2}{3}} \ll b_+^2 .$$

This is always satisfied at the horizon

$$(\lambda_k M_{BH})^{\frac{2}{3}} \ll b(r_s^{(+)})^2 \simeq 4M_{BH}^2\left(1-\frac{3}{4}\left(\frac{\lambda_k}{M_{BH}M_{WH}}\right)^{\frac{2}{3}}-\mathcal{O}\left(\frac{\lambda_k^2}{M_{BH}^2M_{WH}^2}\right)\right) , \tag{6.4.59}$$

for $M_{BH}M_{WH} \gg \lambda_k$ and black hole masses above the Planck mass ($M_{BH}^2 \gg \lambda_k/8$). The same analysis holds for the white hole side. Due to this, quantum effects are negligible at the horizon for black and white hole masses above the Planck mass.

Another question is: For which mass relation do the finite length effects (first condition in Eq. (6.4.51)) become relevant earlier than the curvature effects Eq. (6.4.52)? For the black hole side these conditions can be written as

$$b_+ \gg \left(8\lambda_k\frac{M_{BH}^2}{M_{WH}}\right)^{\frac{1}{3}} \quad , \quad b_+ \gg (M_{BH}\lambda_k)^{\frac{1}{3}} . \tag{6.4.60}$$

The first length scale is larger than the second one, i.e.

$$\left(8\lambda_k\frac{M_{BH}^2}{M_{WH}}\right)^{\frac{1}{3}} > (M_{BH}\lambda_k)^{\frac{1}{3}} ,$$

when

$$\frac{M_{WH}}{M_{BH}} < 8 . \tag{6.4.61}$$

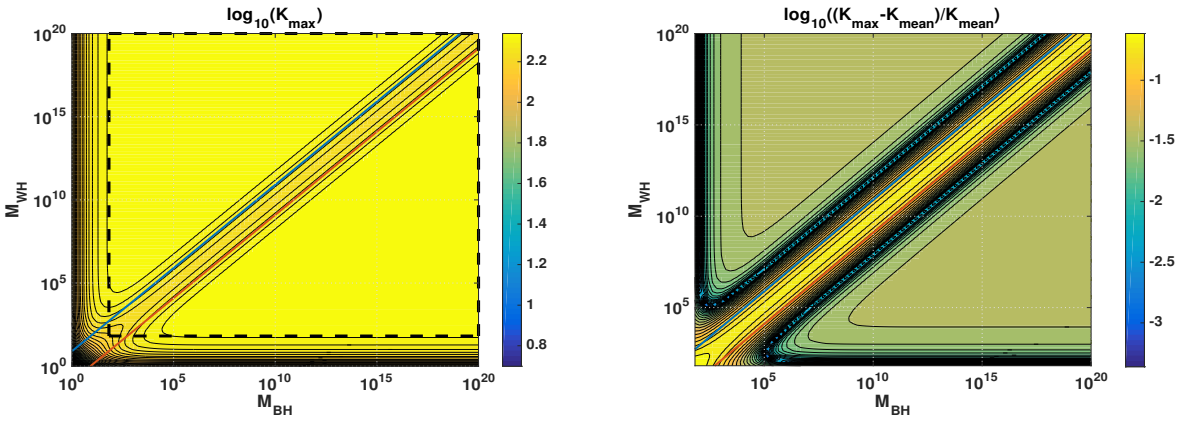

(a) (b)

FIGURE 6.8: *Logarithm of the maximal value of the Kretschmann scalar (a) and the deviation of the Kretschmann scalar from its mean value (average over all masses in the black dashed box) (b) as a function of M_{BH} and M_{WH} in logarithmic axis. The maximal value of the Kretschmann scalar remains largely independent of the masses. The two colour lines represent the boundaries of Eqs. (6.4.61) and (6.4.62). For the plot the maximal value of the Kretschmann scalar is computed numerically. The parameters are set to $\lambda_j = \lambda_k = \mathscr{L}_o = 1$.*

In other words, if the asymmetry M_{WH}/M_{BH} is small than 8, the curvature scale Eq. (6.4.53) is smaller than the scale Eq. (6.4.52). The same argument leads to

$$\frac{M_{WH}}{M_{BH}} < \frac{1}{8}\,, \tag{6.4.62}$$

on the white hole side to Thus, the regime $1/8 < M_{WH}/M_{BH} < 8$ is particular in the way that the quantum corrections, coming from the j polymerisation, are dominant against the k effects on both sides. Nevertheless, both polymerisations yield a curvature scale as onset of quantum effects.

The arguments so far were in the classical regime, and the questions asked were targeted at the validity of the classical approximation. However, this does not reveal anything about the quantum regime. It is possible to evaluate the Kretschmann scalar at its maximum value, which characterises the deep quantum regime. The maximum value is again close to the transition surface. In Fig. 6.8, the maximal value of the Kretschmann scalar as a function of the two masses M_{BH} and M_{BH} is reported. Consistent with the previous analysis, there is a unique upper bound for the Kretschmann curvature. This bound is, in contrast to the previous model (cfr. Fig. 6.5), almost independent of the masses. The maximal value changes in the regime where one of the masses becomes of Planck order. Furthermore, the central region $1/8 < M_{WH}/M_{BH} < 8$ is particular. The curvature is still approximately constant there, but the absolute value differs from the approximately constant value outside this region. The special behaviour of this central region is understood,

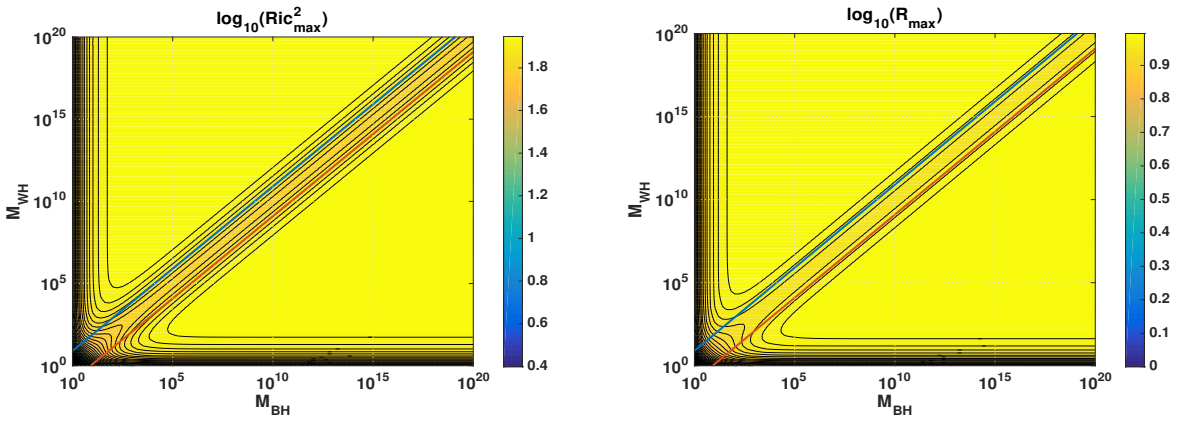

(a) (b)

FIGURE 6.9: *Other curvature invariants as* $Ric^2 = R_{\mu\nu}R^{\mu\nu}$ *in (a) and the Ricci-scalar* R *show the same behaviour as* $\mathcal{K}$ *at the transition surface and remain bounded. Due to* $\mathcal{K} = \mathcal{K}_{cl} + \mathcal{O}(\lambda_k^2)$, $R_{\mu\nu}R^{\mu\nu} = \mathcal{O}(\lambda_k^4)$, $R^2 = \mathcal{O}(\lambda_k^4)$, *also the Weyl scalar* $C_{\mu\nu\alpha\beta}C^{\mu\nu\alpha\beta} = \mathcal{K} - 2R_{\mu\nu}R^{\mu\nu} + {}^1\!/_3 R^2 = \mathcal{K}_{cl} + \mathcal{O}(\lambda_k^2)$ *admits the same behaviour at the transition surface and reduces to the classical expression in the classical regime. The parameters are set to* $\lambda_j = \lambda_k = \mathscr{L}_o = 1$.

because this is exactly the region where the j-quantum effects dominate the k-effects, while the opposite is true outside this regime. The same argument can be made for other curvature invariants as R^2, $R_{\mu\nu}R^{\mu\nu}$ or $C_{\mu\nu\alpha\beta}C^{\mu\nu\alpha\beta}$ (Weyl scalar), which leads to the same conclusion (see Fig. 6.9).

Both classical and deep-quantum region arguments lead to the conclusion that up to mild restrictions, the model has a unique upper curvature bound independent of how a relation between the masses is chosen. Deviations are related to the asymmetry of the two masses. Nevertheless, there are specific preferred choices.

Of particular interest is a linear mass relation

$$M_{WH} = mM_{BH} \ , \tag{6.4.63}$$

where m is a dimensionless constant. For this relation the conditions (6.4.53) and (6.4.57) become

$$\mathcal{K}_{cl}^{BH} = \frac{48M_{BH}^2}{b_+^2} \ll \frac{3m^2}{4\lambda_k^2} \quad \Leftrightarrow \quad \mathcal{K}_{cl}^{WH} = \frac{48M_{WH}^2}{b_+^2} \ll \frac{3}{4\lambda_k^2 m^2} \ . \tag{6.4.64}$$

Checking the classical limit for

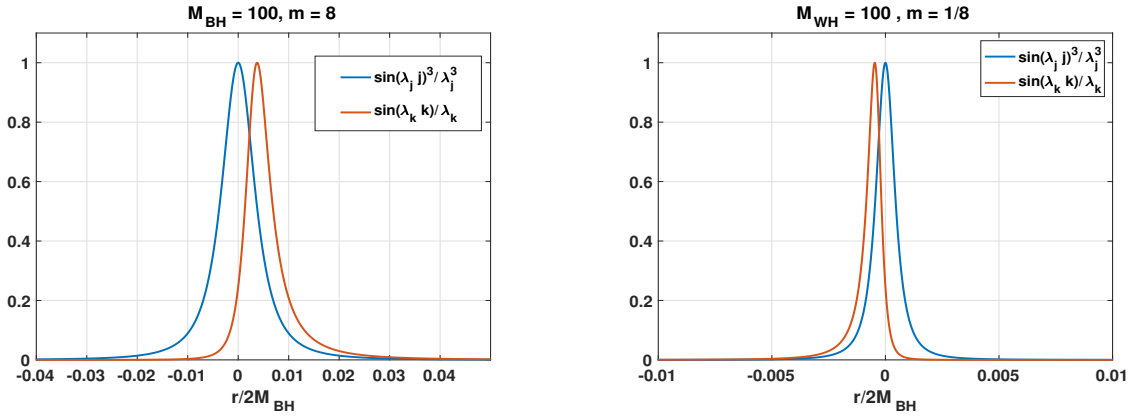

(a) (b)

FIGURE 6.10: $\sin(\lambda_j j)^3/\lambda_j^3$ *compared to* $\sin(\lambda_k k)/\lambda_k$ *for* $m = 8$ *(a) and* $m = 1/8$ *(b). The parameters are* $\lambda_j = \lambda_k = \mathscr{L}_o = 1$.

$$\mathscr{L}_o^3 \frac{\sin(\lambda_j j)^3}{\lambda_j^3} \simeq \frac{4\lambda_k \mathscr{L}_o^3}{\lambda_j^3} \begin{cases} \frac{1}{m}\frac{2M_{BH}}{b_+^3} & , \ r \to +\infty \\ m\frac{2M_{WH}}{b_-^3} & , \ r \to -\infty \end{cases} ,$$

shows that it is up to a m-dependent numerical factor proportional to $\sin(\lambda_k k)/\lambda_k$, i.e. the square root of the Kretschmann scalar. As discussed in Sec. 6.3, $\mathscr{L}_o P_2 = \mathscr{L}_o j$ is proportional to D/b, i.e. depends on the integration constant D. For mass independent D, this was interpreted as inverse length, leading to finite length quantum corrections in the polymerised theory. Nevertheless, a valid possibility is also to chose $D \propto M_{BH}^{\frac{1}{3}}$, which would make j proportional to a power of the Kretschmann scalar. This is achieved by choosing the linear mass relation Eq. (6.4.63). In agreement with the above computation for $m = 8$ the new curvature scale at the black hole side (6.4.64) agrees with the curvature scale of the k-sector (6.4.52). For this value the curvature scale (6.4.64) on the white hole side is smaller than Eq. (6.4.56). Hence, coming from the white hole side, quantum effects of the j-sector are relevant first. The same result can be found for $m = 1/8$, where the quantum effects coincide on the white hole side. Fig. 6.10 shows this graphically. Of particular interest is the case $m = 1$, which means the value of the masses is the same. In this case, quantum effects of the j-sector become first relevant at the Kretschmann curvature scale $3/4\lambda_k^2$, coming from both sides. Effects of the k-sector become relevant afterwards at higher curvatures $(48/\lambda_k^2)$. Fig. 6.11 shows that quantum effects become relevant at the same curvature scale from both sides and are caused by the j-sector. The k-sector plays a sub-dominant role.

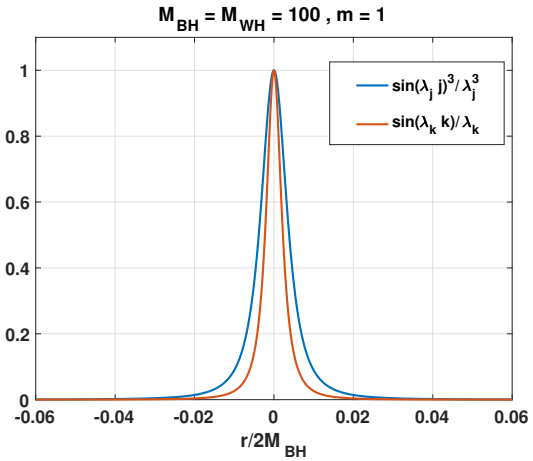

FIGURE 6.11: $\sin(\lambda_j j)^3/\lambda_j^3$ *compared to* $\sin(\lambda_k k)/\lambda_k$ *for* $m = 1$. *The curve of* j *encloses* k *completely, i.e. the dominant contribution for quantum effects comes from* j. *Coming from both sides, the onset of quantum effects is at the Kretschmann curvature scale* $3/4\lambda_k^2$. *Parameters are* $\lambda_j = \lambda_k = \mathscr{L}_o = 1$

Other possibilities are

$$M_{WH} = \frac{M_{BH}^2}{m} \ , \tag{6.4.65}$$

and the corresponding inverse relation

$$M_{BH} = \frac{M_{WH}^2}{m} \ . \tag{6.4.66}$$

where m is a constant of dimension mass. This corresponds to selecting D in order for j to asymptotically describe an inverse length. Indeed, the first scale of quantum effects in Eq. (6.4.51) becomes

$$b_+ \gg (8\lambda_k m)^{\frac{1}{3}} \ , \tag{6.4.67}$$

for the relation (6.4.65), and hence the onset of Eq. (6.4.67) is a proper length scale. For large black hole masses, coming from the black hole side, one would first observe quantum effects coming from the k-polymerisation at the Kretschmann curvature scale $48/\lambda_k^2$ and afterwards effects coming from small 2-sphere areal radii (j-polymerisation) at the length scale $(8m\lambda_k)^{\frac{1}{3}}$. For the inverse relation (6.4.66), the same is true for Eq. (6.4.55), which becomes a proper length sacle. Therefore, the same observation of first curvature effects, then length effects, applies for coming from the white hole side.

From the onset of quantum effects perspective, the model is adequate for a large class of black and white hole masses (cfr. Fig. 6.8). In principle, there is no need to fix a

relation between the two masses, although the results are not completely independent of it. The model is slightly restricted as one curvature scale depends on the asymmetry of the two masses M_{BH}/M_{WH}. Thus, there is again room for optimisation and further elaborate models. Of particular interest is that there are the two special mass relations singled out. The relation Eq. (6.4.65) (and the symmetric counterpart Eq. (6.4.66)) ensure quantum effects at a unique curvature and length scale. On the contrary, the symmetric solution given by Eq. (6.4.63) for $m = 1$ is preferred as for this relation there is only one curvature scale at which quantum effects become relevant.

6.5 Conclusions and Further Directions

In this chapter, new effective models of polymer black holes were introduced. As discussed, polymerisation is a way to include quantum effects motivated by LQG. Based on this technique, the two presented models improve the current status of the literature as 1) they are independent of fiducial structures, 2) only have quantum effects in the high curvature regime and 3) the curvature is bounded by a unique upper scale related to Planck curvature. As also discussed, the models describe the full black hole spacetime and the classical Schwarzschild solution is already approached at the horizon. This was not achieved in previous models [18, 78, 87, 88].

A further novel observation was the existence of two physically relevant and independent Dirac observables corresponding to black and white hole mass. A detailed discussion of these observables and the relation to previous models can be found in [6]. As both masses are independent, the models do in principle not determine any relation between them.

The first model, in terms of (v_i, P_i) variables, achieves a unique upper curvature bound only if the initial conditions, i.e. the two masses are restricted in a very specific way. One of these possibilities is an amplification of the mass, the other a de-amplification of the same amount. Furthermore, the value of the masses oscillates between the two values M_{BH} and M_{WH} each time the transition surface is passed. In contrast to this, the second model, for which new variables j, k were introduced, tries to overcome this limitation. Indeed, the bound for the curvature scalars is fine for a large range of black and white hole masses. Nevertheless, it depends on the asymmetry of both sides. Special relations, namely $M_{WH} \propto M_{BH}^2$ or $\propto M_{BH}^{\frac{1}{2}}$, as well as the symmetric case $M_{WH} = M_{BH}$ are preferred.

The models have the further advantage that the Hamiltonian is simple, as only positive and at most quadratic powers of the phase space variables occur. An important next step is to leave the effective approximation and construct the quantum theory explicitly. This was already sketched in [3] and follows the lines of LQC (cfr. Sec. 4.3), due to the

simplicity of the Hamiltonian. Once a quantum theory is present, coherent states should be studied which are peaked on classical geometries. This allows to understand for which quantum numbers and in which regime the effective approximation can be trusted.

The work presented in this chapter opens further research directions related to pure black hole physics. As such, in future work it might be interesting to study quantum fields on these effective backgrounds or to study the thermodynamics of these quantum black holes. The phenomenology of the models as the quasi-normal modes [218] are also of particular interest. Further the models are eternal and do not take matter into account. To understand the life cycle of a black hole better, an inclusion of the formation process would be of interest.

In conformity with this thesis, these models provide physically sensible spacetimes for quantum black holes taking LQG corrections into account. To further elaborate on the approach of Chpt. 5, the models need to be generalised to D dimensions and a negative cosmological constant has to be included. An outlook discussing the possible obstructions of this generalisation is presented in the following chapter.

7

Outlook: AdS-Black Holes

The previously discussed black hole models are in four spacetime dimensions and without any cosmological constant. To study the holographic aspects of these polymer black holes, the models have to be generalised. Setting both the work on holographic signatures of cosmological singularities and on the black hole models on the same footing, the black holes need to be generalised to arbitrary dimensions and a negative cosmological constant has to be included. This way the black hole is asymptotically described by AdS spacetime. There are preliminary attempts to do these generalisations in (v_i, P_i)-variables, which are presented here.

Starting point is the $D = d + 1$ dimensional Einstein-Hilbert action with negative cosmological constant $\Lambda < 0$

$$S_{EH} = \frac{1}{16\pi} \int d^D x \, \sqrt{-g} \left(R^{(D)} - 2\Lambda \right) \, . \tag{7.1.1}$$

The spherically symmetric and static ansatz in D dimensions is

$$\mathrm{d}s^2 = -\bar{a}(r)\mathrm{d}t^2 + N(r)\mathrm{d}r^2 + 2\bar{B}(r)\mathrm{d}t\mathrm{d}r + \bar{b}^2(r)\mathrm{d}\Omega^2_{D-2} \, . \tag{7.1.2}$$

Inserting this into Eq. (7.1.1) leads to the symmetry reduced action

$$S_{EH} = \frac{1}{4}\int \mathrm{d}r\; L(\bar{a},\bar{b},\bar{n})\;, \tag{7.1.3}$$

with the Lagrangian

$$L(\bar{a},\bar{b},\bar{n}) = L_o\sqrt{\bar{n}}\,\bar{b}^{D-4}\left[(D-2)\left(\frac{\bar{a}'\bar{b}\bar{b}'}{\bar{n}} + (D-3)\frac{\bar{a}\bar{b}'^2}{\bar{n}} + (D-3)\right) - 2\bar{b}^2\Lambda\right] \tag{7.1.4}$$

and Lagrange multiplier

$$\bar{n}(r) = \bar{a}(r)N(r) + \bar{B}^2(r)\;. \tag{7.1.5}$$

In the same way as in Sec. 6.2, the fiducial cell L_o and the physical size of the fiducial cell $\mathscr{L}_o$ are defined. Again, the fiducial cell is absorbed in the variable redefinition

$$\begin{aligned}
&\sqrt{n} = \int_0^{L_o}\mathrm{d}t\sqrt{\bar{n}} = L_o\sqrt{\bar{n}} \quad , \quad \sqrt{a} = \int_0^{L_o}\mathrm{d}t\sqrt{\bar{a}} = L_o\sqrt{\bar{a}}\;,\\
&b = \bar{b} \quad , \quad B = \int_0^{L_o}\mathrm{d}t\bar{B} = L_o\,\bar{B}\;.
\end{aligned}$$

This leads to the final Lagrangian

$$L(a,b,n) = \sqrt{n}\,b^{D-4}\left[(D-2)\left(\frac{a'bb'}{n} + (D-3)\frac{ab'^2}{n} + (D-3)\right) - 2b^2\Lambda\right]\;. \tag{7.1.6}$$

The structure of the Lagrangian is exactly the same as in the 4-dimensional case Eq. (6.2.4). The main difference is the cosmological constant term and the overall b^{D-4} factor. Nevertheless, this additional overall factor b^{D-4} can be absorbed into the lapse $\sqrt{n}$ later on. The canonical momenta are consequently defined as

$$\begin{aligned}
&p_a = \frac{\partial L}{\partial a'} = (D-2)b^{D-4}\frac{2bb'}{\sqrt{n}} \quad , \quad p_b = \frac{\partial L}{\partial b'} = (D-2)b^{D-4}\,\frac{2(D-3)ab' + a'b}{\sqrt{n}}\;,\\
&p_n = \frac{\partial L}{\partial n'} \approx 0\;,
\end{aligned} \tag{7.1.7}$$

where $p_n \approx 0$ is again the primary constraint, which induces the Hamiltonian constraint.

As before, p_n and n can be removed from the phase space interpreting n as Lagrange multiplier. The Hamiltonian takes the form

$$H_{cl} = \sqrt{n}\mathcal{H}_{cl} \quad , \quad \mathcal{H}_{cl} = \frac{p_a p_b}{(D-2)b^{D-3}} - \frac{D-3}{D-2}\frac{a p_a^2}{b^{D-2}} - (D-3)(D-2)b^{D-4} + 2b^{D-2}\Lambda \approx 0 \, . \tag{7.1.8}$$

It is possible to find the D-dimensional generalisation of the (v_i, P_i)-variables. They can be defined as

$$\begin{aligned} v_1 &= \frac{D-2}{D-1}\, b^{D-1} \qquad , \qquad P_1 = \frac{a'}{\sqrt{n}\, b} = \frac{1}{(D-2)b^{D-2}} \left(\frac{p_b}{b^2} - (D-3)\frac{2ap_a}{b^3} \right) , \\ v_2 &= (D-2)ab^{2(D-2)} \qquad , \qquad P_2 = \frac{b'}{\sqrt{n}\, b^{D-3}} = \frac{p_a}{(D-2)b^{2(D-3)}} , \end{aligned} \tag{7.1.9}$$

and satisfy the standard Poisson brackets. For $D = 4$ they reduce to the previous variables defined in Eq. (6.2.12). The Hamiltonian becomes in these variables

$$\begin{aligned} H_{cl} &= \sqrt{n}\mathcal{H}_{cl} \, , \\ \mathcal{H}_{cl} &= b^{D-4} \left[(D-1)v_1 P_1 P_2 + (D-3)v_2 P_2^2 - (D-2)(D-3) + 2\Lambda \left(\frac{D-1}{D-2} v_1 \right)^{\frac{2}{D-1}} \right] , \end{aligned} \tag{7.1.10}$$

where $b = \left({}^{(D-1)v_1}/_{D-2} \right)^{\frac{1}{D-1}}$. Again, the Hamiltonian becomes a simple form, where all quantities have positive powers. These equations are solvable in the classical case. This might get harder and impossible after the polymerisation. It is instructive to have a look at the classical equations where differences with respect to the 4-dimensional case occur. A suitable gauge is $\sqrt{n} = \mathscr{L}_o / b^{D-4}$. The equations of motion become

$$v_1' = (D-1)\mathscr{L}_o v_1 P_2 \, , \tag{7.1.11a}$$

$$v_2' = (D-1)\mathscr{L}_o v_1 P_1 + 2(D-3)\mathscr{L}_o v_2 P_2 \, , \tag{7.1.11b}$$

$$P_1' = -(D-1)\mathscr{L}_o P_1 P_2 - \frac{4\mathscr{L}_o}{D-2}\Lambda \left(\frac{D-1}{D-2} v_1 \right)^{-\frac{D-3}{D-2}} , \tag{7.1.11c}$$

$$P_2' = -(D-3)\mathscr{L}_o P_2^2 \tag{7.1.11d}$$

$$\mathcal{H}_{cl} = (D-1)v_1P_1P_2 + (D-3)v_2P_2^2 - (D-2)(D-3) + 2\Lambda\left(\frac{D-1}{D-2}v_1\right)^{\frac{2}{D-1}} \approx 0\ . \tag{7.1.11e}$$

Due to the choice of $\sqrt{n}$, these equations have the same structure as the 4-dimensional ones of Eq. (6.2.15) up to the Λ terms. For $\Lambda = 0$ these equations are still nested and can be solved analogously to before. Even polymerising does not change the structure compared to the 4-dimensional effective equations, which allows analytic solutions for the polymerised case in D-dimensions. In contrast, the additional terms for $\Lambda \neq 0$ couple the equation for v_1 Eq. (7.1.11a) with the equation for P_1 Eq. (7.1.11c), which could become a problem once the system is polymerised. Classically, the equation for P_2 Eq. (7.1.11d) is still decoupled and can be integrated without complications. The result can be inserted into the equation of v_1 Eq. (7.1.11a), which allows to also integrate it. Both results can be inserted into the equation for P_1 Eq. (7.1.11d), which can also be integrated. The solution for v_2 follows from the Hamiltonian constraint Eq. (7.1.11e). If the system is polymerised according to the scheme discussed in Sec. 6.3, Eq. (7.1.11a) becomes P_1 dependent with an additional $\cos(\lambda_1 P_1)$ factor (cfr. Eq. (6.3.5a)). In the case $\Lambda = 0$, the equation for P_1 Eq. (7.1.11c) can be solved first and inserted there. Previously, this allowed to decouple and solve the equation for v_1 Eq. (7.1.11a). For $\Lambda \neq 0$, this is not possible any more, as the P_1 equation (7.1.11c) also depends on v_1. This will be a computational challenge, but there might be possibilities to circumvent this problem. In general, one can say that the generalisation to D-dimensions is straightforward and analytic solutions still exist. However, the generalisation to $\Lambda \neq 0$ is more difficult. While it is conceptually feasible, a new solution strategy has to be found for the final polymerised effective quantum equations.

Another difficulty comes from the interpretation of P_1, which was interpreted as proportional to the square root of the Kretschmann scalar for $\Lambda = 0$. For non-zero cosmological constants, the Kretschmann scalar is given by

$$\mathcal{K}_{cl} = const. \cdot \frac{\mu^2}{b^{2(D-1)}} + const. \cdot \Lambda^2\ , \tag{7.1.12}$$

where $\mu = 8\pi M/\Big((D-2)\mathrm{Vol}(S^{D-2})\Big)$ (see [89]) with the mass M of the AdS-Schwarzschild black hole. The Kretschmann scalar is a sum of the gravitational part of the curvature and the curvature induced by the cosmological constant. Solving the classical equations of motion leads to the solution

$$\frac{P_1}{\mathscr{L}_o} = const. \cdot \frac{\mu}{b^{D-1}} + const. \cdot \Lambda$$

for P_1. Also, this is a sum of the part induced by the mass M and the part induced by the cosmological constant. Squaring P_1 leads to the two squared terms present in the expression for the Kretschmann scalar (7.1.12), and to a mixed term, which is not present and does not allow to interpret P_1 in the same way. Although the single squared terms fit, the mixed terms cause a problem in this interpretation and might influence the onset of quantum effects.

To solve this, there are several options. One possibility is to ignore this fact. This might work out as P_1^2 will have at least the same order of magnitude as the Kretschmann scalar, which is sufficient to constrain the quantum effects in the high curvature regime. It might further be true that P_1 controls some other measure of curvature, i.e. a sum of several curvature invariants. Neither of them are special, i.e. achieving a unique upper curvature bound in one of them would be enough, as long as the others also remain finite everywhere. This needs to be studied after solving the effective equations and it might still lead to sensible quantum effects, even if the previous interpretation P_1 loses its validity. The second option is new variables. The generalisations of the jk-variables presented in Sec. 6.4, could be chosen as such. The variable k could be constructed in the in Sec. 6.4 presented manner. Further, there was an off-shell interpretation of k as $2M_{\text{Minser-Sharp}}/b^3$, which also measures the curvature. As this interpretation is off-shell, it should not be changed by including a cosmological constant. Nevertheless, this is part of current and future research and has to be identified in detail.

Summarising, the generalisation to D-dimensions is technically straightforward. The inclusion of a cosmological constant is more problematic, as this changes the interpretation of the variables and makes solving the equations of motion analytically harder. Nevertheless, it might be possible to find a new solution strategy, which has to be discussed once the precise equations are derived. Furthermore, it is likely that the newly introduced jk-variables can be generalised to arbitrary dimensions. Due to the off-shell interpretation of k, an inclusion of a cosmological constant would not be problematic and the interpretation as in Sec. 6.4 could be kept. While this analysis points towards possible problems, it also hints at potential solutions. This leaves space for future research. It is important that this is a suitable framework to go beyond the limitations of the Kasner-singularities, discussed in Sec. 5.6. A further advantage is the simplicity of the Hamiltonian, which in the $D = 4$ theory allows to construct the quantum theory (as sketched in [3]). This allows to go even beyond the setting discussed in Chpt. 5.

8

Conclusions and Outlook

In this thesis the foundations for studying the relation of Loop Quantum Gravity (LQG) with holography, more precisely the Anti-de Sitter / Conformal Field Theory (AdS/CFT) correspondence, was laid. A central role is taken by singularities occurring in cosmology and black hole models, which are resolved by the non-perturbative LQG techniques. It was investigated if non-perturbative techniques inspired by LQG can be meaningfully embedded into the holography and the AdS/CFT correspondence, and further, in which framework this embedding can be tested. This chapter summarises first the content of the thesis. Afterwards, the results are pointed out and it is discussed to which extent initial question, how LQG can be embedded into the AdS/CFT framework, can be answered. As a last point, an outlook to future research directions is given.

8.1 Summary

In the first part of the thesis introductory material is presented, which sets the grounds for the later parts. As a first step in chapter 2, Anti-de Sitter (AdS) space and its boundary was discussed. A definition and different viewpoints on this particular spacetime was given. In addition it was worked out why this space is a natural candidate for holographic considerations. These are two central properties, which were worked out in detail: First one is that AdS space behaves naturally as a box and particles behave as captured in a

harmonic oscillator potential. Secondly, massless particles as light are infinitely redshifted towards the boundary of AdS space. On top of that it was discussed that the conformal boundary of AdS is a timelike spacetime with conformal symmetry. As the boundary is timelike and reduced by one spatial dimension, it behaves naturally as holographic screen and can be interpreted as the background of a holographically dual theory. This leads to chapter 3, where the foundations of the holographic principle were discussed on the example of black holes. Due to this, properties of classical black holes as the spacetime around the horizon and the occurrence of a curvature singularity were reviewed. Besides the relevance for the holographic principle, these foundations were central for the last part of the thesis, chapter 6 and 7. In addition central theorems as the Hawking area theorem and the no-hair theorem were reviewed and put into context to the development of black hole thermodynamics. The latter was introduced in section 3.2, which discusses the semi-classical properties of black holes. The holographic principle was motivated on the basis of these semi-classical considerations. It states that a gravitating system can be described by a number of degrees of freedom proportional to its enclosing area rather than the system's volume. The holographic principle can be realised in string theory within the AdS/CFT correspondence, which was introduced in section 3.3. A general overview of the AdS/CFT correspondence was given and different approximations and regimes were related to each other. It was shown in this chapter that the string theory realisation of holography allows to formulate the holographic principle mathematically precise. On top of that, in section 3.4 an outlook on the idea of gauge/gravity duality was given. It was argued that the holographic principle might also be realised in other theories of quantum gravity. An alternative to string theory is LQG, a non-perturbative approach to quantum gravity where progress has been made in the context of symmetry reduced models, in particular in cosmology. The LQG approach to cosmology, Loop Quantum Cosmology (LQC), is the basis for the second part of the thesis and was reviewed in chapter 4. In a first step, the classical cosmological framework was worked out in section 4.1. Moreover, the problem of the big bang singularity as well as general solution strategies of constrained systems were studied. The second part of the chapter, section 4.2, discusses the effective treatment of cosmology by applying polymerisation, which is the replacement of certain phase space variables by means of their complex exponentials. This technique played a central role in the third part of the thesis and sets the grounds for a full quantum theory of cosmology based on LQG ideas. The dynamics of the effective polymerised Hamiltonian, which is classical but takes non-perturbative quantum corrections into account are discussed, and the central result of LQC, the singularity resolution, was worked out. The need for polymerisation becomes clear as the full quantum theory of LQC was studied in section 4.3. It was shown how the quantum theory can be construed. On top of this, it was discussed how the quantum theory can be related to the effective dynamics using coherent states. Lastly, the symmetry reduced LQC was put in the context of LQG in section 4.4. Due

to this, the principles of LQG and holonomy corrections were reviewed. It was presented how polymerisation can be motivated in terms of holonomy corrections and contact to the previous LQC discussions was made. A discussion of how LQC can possibly be extracted from LQG closes the introductory first part of this thesis.

New research was first presented in the second part of the thesis, which includes chapter 5. Based on previous work [71, 72] and a companion paper [73], a first check was done on how the non-perturbative effects of LQG are compatible with the holographic principle and in particular the AdS/CFT correspondence. As a first step in section 5.1, the basic setup and the previous work [71–73] was reviewed. It was argued that the length of spacelike geodesics can be related to equal-time two-point correlators of the dual field theory using the AdS/CFT correspondence, which was introduced in section 3.3. Following the strategy of [71, 72] it was motivated that anisotropic cosmological spacetimes, also called Kasner spacetimes, are a suitable framework to analyse the signatures of cosmological singularities. Further it was discussed that the classical singularity causes a finite distance pole in the dual field theory. On top of that, in section 5.2 it was reviewed that quantum corrections motivated by LQC resolve this finite distance pole, which was the result of [73]. The limitations and simplifying assumptions of this preceding work were discussed and possibilities for loosening them in two steps were established in section 5.3. In a first step the onset of quantum effects was tuned to the proper 5d instead of the 4d scale, which was used due to simplification in the previous work. It was discussed that this can be achieved by replacing the polymerisation scales according to $\lambda_{4d} \to z\lambda_{5d}$. Moreover, the second step includes Kasner transitions, allowing the model to mimic the proper anisotropic LQC behaviour [17, 189]. These two steps make the model more complicated and analytical computations were not possible any more. Hence, the numerical solution strategy was discussed in section 5.4, where it was explained how the numerical boundary value problem can be rephrased in terms of an initial value problem. The results of both steps of loosening the simplifications were presented in section 5.5. It was shown that the two-point correlator is still resolved when the onset of quantum effects is at the 5d scale. This result was non-trivial as the modification of the bulk metric resolved the singularity there, but did not change the singular boundary metric, which classically caused the finite distance pole. Nevertheless, although the singular boundary is not modified, the singularity is resolved in the bulk, sufficing to improve the two-point correlator behaviour. On top of that, the same analysis was done for a model of Kasner transitions in section 5.5.2. Nevertheless, as was discussed in detail in section 5.5.2.1, the approximate description due to an extension of 4d mimetic gravity [33] to the 5d Planck scale by again replacing $\lambda_{4d} \to z\lambda_{5d}$ is not directly possible. Two different models of Kasner transitions, which have quantum effects on the 5d Planck scale were discussed in section 5.5.2.1, and neither fulfilled the given requirements. Yet, the numerical computation was presented

for the mimetic gravity model with the replacement $\lambda_{4d} \to z\lambda_{5d}$ in section 5.5.2.2. It was shown that, even if the qualitative behaviour around the resolved singularity changed, the result of a resolution of the two-point correlator pole remained unaltered. A conclusion and detailed discussion of the results and limitations of the framework was given in section 5.6. The therein discussed technical difficulties with the anisotropic cosmological setting motivated a shift of the framework to black holes.

The change of framework led to the third and last part of the thesis, which discusses effective polymer black holes in 4d without cosmological constant in chapter 6. The holographic setting needs higher-dimensional black hole models with negative cosmological constants. Therefore, in section 6.1 the current status of polymer black holes is discussed and it is argued that there is no consensus about black holes in LQG in 4d and without cosmological constant. Further criteria, which should be satisfied by an effective quantum black hole model, were formulated and it was argued that especially the requirement of an unique upper curvature bound was not achieved in previous work. As a first step, the canonical description of static and spherically symmetric black holes in terms of new variables was introduced in section 6.2. Having the classical solutions derived, it was possible to interpret the new introduced momenta P_1 and P_2 as related to the square root of the Kretschmann scalar and inverse areal radii. Because of this interpretation, and the considerations presented already in section 4.2, the variables are suitable for polymerisation and for achieving an unique upper curvature bound. In section 6.3, details of the polymerisation and the effective description in terms of the new (v_i, P_i)-variables were worked out. On top of the construction of the effective quantum model, the model was solved and properties of the quantum corrected spacetime and the causal structure were analysed. It was argued that the classical singularity is replaced by a regular transition surface, where a transition from a black hole interior region to a white hole region takes place. A further central observation was the appearance of two independent physical Dirac observables, namely the mass of the black and white hole asymptotic Schwarzschild regions. Further, this asymptotic behaviour shows that the classical regime is approached consistently with General Relativity (GR). As a last step, in section 6.3.3 the onset of quantum effects and the curvature bound are analysed. It was found that the onset of quantum effects as well as the curvature bound of the Kretschmann scalar are only unique if a particular relation of the masses, i.e. $M_{WH} \propto M_{BH}^{\beta}$ with $\beta = 5/3$ or $3/5$ is satisfied. It was argued that this leads to an amplification or de-amplification of the masses, where both exponents are compatible as they describe the inverse mass change of the same amount. On the one hand, this allows to meet the criterion on an unique upper curvature bound, while on the other hand it restricts the initial condition and a fixing of M_{WH} in terms of M_{BH} has to be done by hand. It is discussed that this by hand fixing of the two system parameters M_{BH} and M_{WH} is a drawback of the model and its origin is the choice of polymerisa-

tion scheme. As polymerisation strategy a constant scale was used and possible phase space dependences were transferred into the choice of particular variables. Therefore, a change of the polymerisation scheme can be achieved by keeping the scales constant, but changing the variables to be polymerised. Consequently, in section 6.4, new variables, especially the momenta k and j were introduced to overcome the previous limitations. It was argued that k is related to the square root of Kretschmann scalar on-shell without fixing remaining integration constants, which was needed for the interpretation of P_1. Further, k could be related to the Riemann tensor off-shell (but on the constraint surface) via the Misner-Sharp mass. As such, k can be interpreted as the black hole analogue to the cosmological (v, b)-variables, which are used in LQC (chapter 4). The new model was solved in section 6.4.1, and the spacetime properties were worked out. Qualitatively, the model is similar to the previous one, i.e. it asymptotically reduces to Schwarzschild spacetime with mass M_{BH} and M_{WH}, respectively, the singularity is replaced by a transition surface, and there are two horizons. Further, in section 6.4.2, the onset of quantum effects and the curvature bound were discussed. It is revealed that the curvature remains bounded for any mass relation and thus the previous limitations are overcome, although not completely. The limitation comes from the fact that the Kretschmann curvature at the transition surface, as well as the scales of quantum effects are dependent on the mass asymmetry M_{BH}/M_{WH}. It was examined that the symmetric solution $M_{BH} = M_{WH}$ and $M_{WH} \propto M_{BH}^{\beta}$ for $\beta = 2$ or $1/2$ are favoured. On top of that, it was argued that in the symmetric situation only one unique curvature scale is relevant, and that in the second asymmetric possibility, quantum effects can be properly interpreted as finite length and high curvature effects. A detailed discussion of the achievements of the models and their drawbacks as well as further research directions were given in the conclusions 6.5 of this chapter.

Finally, an outlook on the generalisation of the previous presented models to higher dimensions and negative cosmological constant was given in chapter 7. In particular the generalisation of (v_i, P_i) to arbitrary dimensions was presented and the classical equation of motion with non-zero cosmological constant was derived. From this, the limitations of the previously applied solution strategy were discussed. It was argued that in the polymerised case, the generalisation to D-dimensions is straightforward, while the additional cosmological constant terms couple the equations, which requires a new solution strategy. It was further discussed that the interpretation of P_1 as the square root of the Kretschmann scalar fails due to the cosmological constant terms. Possible solutions to this problem were discussed, such as the interpretation via other curvature invariants or the possibility to construct new variables related to k and j.

8.2 Discussion of Results

In this thesis the foundations for studying holographic aspects of LQG with asymptotic boundaries were laid. As discussed, LQG is constructed a priori as non-holographic theory. Nevertheless, the non-perturbative techniques and the resulting singularity resolution in different models could supplement string theory, which is non-perturbatively defined only holographically via the AdS/CFT correspondence. Even if singularities were studied in string theory and AdS/CFT [23, 177–185], it is not clear how singularity resolution fits into the picture of holography. Therefore, the question how LQG and singularity resolution can be meaningfully placed in the framework of AdS/CFT was already addressed in the second part of the thesis. Of central importance is the result of chapter 5, which can be interpreted as a proof of principle. It demonstrates that it is in principle possible to apply non-perturbative quantum effects motivated by LQG to the AdS/CFT framework. In particular the resolution of the cosmological singularity by means of limiting curvature effects was shown to be dual to a resolution of the finite distance pole in the equal-time two-point correlator of the dual field theory. Moreover, the same qualitative result was found in the preceding work [73] and in the two cosmological models discussed in chapter 5, which can be interpreted as a certain robustness of this result for different qualitative quantum gravity models. The conclusion is that these quantum gravity effects, although not motivated by string theory, improve the dual field theory behaviour. This adds the perspective of non-perturbative quantum gravity as LQG to the discussion singularity resolution within AdS/CFT, and a No Transmission Principle (NTP), analysed in [27, 28]. Nevertheless, this statement and framework are limited as a simplified computation could be done only on the gravitational side. Because of the lack of an independent Conformal Field Theory (CFT) computation, it is not clear what the quantum effects leading to the singularity resolution is dual to, in terms of the field theory. For example, it is not clear if the resolution of the finite distance pole is due to the change of a non-renormalisable state to a renormalisable one, which was already discussed in [71, 72]. Another possible explanation would be the necessity to include finite N effects on the field theory side, as on the gravitational side also quantum effects were introduced. To investigate this further, a dual computation in the CFT would be needed. Unfortunately, the framework does not allow these computations as the dual CFT is formulated on time dependent Kasner background. Because of this time-dependence, common non-perturbative treatments via lattice techniques are technically not reachable in the near future. On top of this, the model is limited by the analytical control over the quantum effects in the bulk. It was analysed in detail that the models of Kasner transitions do not satisfy the phenomenological requirements. This would be overcome by setting up the full 5d quantum equations and polymerising the resulting midi-super-space model. Even if the principle techniques are available [186–188], the application to this cosmological setting is out of scope. Another

possibility would be to continue with the ideologically similar mimetic gravity [33, 193], which turned out to be equivalent to LQC in the homogeneous and isotropic sector [194]. As further investigations showed, this is not true for the anisotropic regime [2]. Hence, to proceed with the holographic analysis of LQG, the framework has to be changed. As the analysis of chapter 5 showed, singularities are a suitable framework to test the compatibility of LQG with the ideas of AdS/CFT, despite the framework having to be generalised. Exactly this was the focus of the third part of the thesis in chapter 6 and 7. The setting of black holes, which classically carry a singularity and approach proper AdS space asymptotically, is promising. On the one hand, the singularity allows to test non-perturbative quantum effects and on the other hand the boundary space, i.e. the background of the dual field theory, is the boundary of proper AdS space and hence can be brought in the form of flat Minkowski space. This could make complementary dual computations with lattice techniques possible. Moreover, there was a lot of recent effort in LQG on black holes [18, 78, 80, 87, 88, 197, 219]. Nevertheless, there is no consensus about black holes in 4d and without cosmological constant within the LQG community. Hence, a step back was taken and new models of effective polymer black holes were discussed in this thesis. The first polymerisation scheme, based on constant polymerisation scales and a new introduced set of variables, already improves the behaviour of previous models. On the one hand, the solution is valid in the whole spacetime and not restricted to the interior as previous models. Further it has the correct classical behaviour, as the classical Schwarzschild spacetime is asymptotically approached. On the other hand, the onset of quantum effects is at an unique curvature scale and the curvature invariants have a unique upper bound. This could be achieved by the novel observation that there are two, instead of previously assumed one (see the detailed analysis [6]), system parameters M_{BH} and M_{WH}, which are the masses of the Schwarzschild spacetimes in the two distinct asymptotic regions. The unique upper curvature bound was achieved by fixing by hand a relation between these a priori independent masses. Thus additional input has to be given to the model. The other set of variables with momenta k and j allowed to overcome this limitation to a certain extend. Indeed, the curvature is bounded for all mass relations, although this bound depends on the asymmetry of both sides. This favours the symmetric case where only one unique curvature scale is relevant. The qualitative characteristics of the effective spacetime are not changed with respect to the previous model. As the curvature bound is still not completely unique, there is further space for improvements and the development of other polymerisation schemes. Another feature of the presented models is the simplicity of the Hamiltonian, which contains only positive and at most quadratic powers of the phase space variables. As sketched in [3], this allows the construction of the full quantum theory. This is a necessary step to better understand the limitations of the effective approximation. A last important result is the fact that the model in (v_i, P_i) variables can be extended to arbitrary dimensions and negative cosmo-

logical constant. This allows to bring the model, even with discussed existing limitations, back to the framework of holography and AdS/CFT.

8.3 Further Research Directions

The results of this thesis open up to least two further research directions to follow. The first direction is further investigating the holographic properties of non-perturbative LQG corrections. As the discussion in chapter 5 shows, there is a proof of principle that LQG quantum corrections are meaningful in the holographic context, as the behaviour of the dual theory is improved. Nevertheless, to better understand the features of the dual theory, a different framework has to be chosen in which independent computations on both sides are possible. This framework is possibly given by black holes, and it has to be worked out in detail how the here developed models can be generalised to arbitrary dimensions and negative cosmological constants. To do so, the an important step would be to verify that the D-dimensional (v_i, P_i) variables lead to a curvature bound and the correct onset of quantum effects. Alternatively, a construction of the jk-variables in D-dimensions could be developed in future. On top of that, as a quantum theory of the black hole models might be available, it is possible to go beyond more simplifications and proceed going towards the full (symmetry reduced) quantum gravitational regime. These details can be worked out in future research. Besides, to make this line of research meaningful and testable, further improvements and computations have to be done on the field theory side. In the discussed framework of black holes, the background of the dual CFT is the static boundary of AdS space, and thus there is a chance for explicit dual computations. Indeed, investigations of the entanglement entropy exist for several N [220], which are suitable for holographic considerations. This way the holographic properties of LQG might be better understood and relations to other approaches as string theory might be found. Moreover, in the long term perspective, this might allow to put string theory and LQG in context and techniques could be exchanged to improve the understanding and intuition about both approaches. Apart from this, the holographic dual to LQG might be used to perform "experiments" and tests of LQG predictions [69, 70]. Therefore, a gravitational problem or predictions as singularity resolution might be tested by well-developed Quantum Field Theory (QFT) techniques. This might help to support or rule out certain models and to gain insight and intuition about quantum gravity. Nevertheless, even if a quantitative comparison fails and it transpires that LQG is non-holographic, it has to be understood why this is the case. As argued, the holographic principle is a priori motivated by consideration of semi-classical black holes and as such it is independent of the approach. In this case, a lot can be learned about quantum gravity and the different approaches itself by understanding why certain approaches respect the

holographic principle and others not.

The second line of research is black hole physics, which is interesting and promising for the understanding of quantum gravity on its own. A possible first step is the full and detailed construction of the black hole quantum theory. Already sketched for (v_i, P_i) variables in [3], the Hamiltonian constraint can explicitly be solved and observables were constructed. The construction of the quantum theory could be finished by explicitly defining the physical scalar product by following the lines of LQC [138, 144]. Besides, the same construction is also possible for jk-variables, in which the Hamiltonian constraint has the exact same form and only the structure of observables change. Moreover, once the quantum theory is constructed, it should be checked if there are coherent states remaining peaked on the effective dynamics. This way it can also be studied in which regime and for which quantum numbers (e.g. large masses) the effective approximation is reliable. On top of that, it could be investigated if the quantum states remain peaked on an effective geometry after the bounce, as it is the case in cosmology. Further, it would be possible to do transition amplitude computations for the transition of certain black hole masses to white hole masses and the results might be compared to spin foam computations [77, 221]. Especially interesting is also the quantisation of mass and the non-commutativity of both observables. The physical consequences of this non-commutativity and the implication on the transition of a black hole into a white hole could be worked out in future. Having a quantum theory at hand, the mass spectrum could be computed and compared to predictions of other approaches [222–225]. Besides, quantum fields might be studied on this quantum background in the framework of [226] to possibly gain insights into Hawking radiation. In addition to that, Hawking radiation might be effectively modelled by defining operators, increasing or decreasing the black hole mass by one quantum. In such a construction, Hawking emission would correspond to the action of the mass decreasing operator. Therefore, this model is an explicit realisation of the ideas discussed in [227, 228] and information theory aspects can be examined in future. Apart from the quantum theory, an interesting direction would also be the phenomenology of the models. So far, only eternal black holes without matter couplings can be described. The formation process and the matter dynamics are completely ignored, which points towards a generalisation of the models in future work. The strategy, which was worked out in [229–231], could be applied to the models presented here, in order to understand the formation process and the fate of the collapsing matter at the transition surface. Additionally, by allowing the model to be time-dependent via the masses only, also the evaporation process could be studied. A fundamental question is what happens for small masses at the end of the evaporation process, which could be compared to black-to-white hole transition models, such as [77, 196, 219]. Beside this, other features like the quasi-normal mode spectra are of phenomenological interest [218] and it could be further studied if there are

possible measurable effects.

In conclusion, in this thesis the question was examined, how LQG can be placed meaningfully in the context of holography and the AdS/CFT correspondence. The analysis of holographic signatures of classical singularities and their resolved counter-parts in the symmetry reduced effective quantum theory were of central importance. As a result, a proof of principle was given, showing that the singularity resolution in the cosmological setting improves the dual field theory behaviour in the holographic context. As the discussion showed, the cosmological setting is limited, but the basis for extending the framework to black holes was built. Consequently, the presented research can on the one hand be extended in the direction of holographic aspects of LQG and its relation to string theory. On the other hand, research in the direction of black hole physics can be continued by examining the quantum theory and phenomenology of the presented black hole models.

Appendices

A Conventions and Notations

In this appendix general conventions and notations are collected.

According to standard notation, it is used

G as gravitational constant,

c as the speed of light,

k_B as the Boltzmann constant, and

$\hbar$ as the reduced Planck constant.

In additions denotes $\ell_p = \sqrt{\hbar G/c^3}$ the Planck length. Throughout this thesis, unless specified differently, Planck units with

$$G = c = k_B = \hbar = 1$$

are used. Further it is $\kappa = 16\pi G$ defined. The Einstein summation rules are always applied.

The metric signature is always chosen to be "mostly plus", i.e.

$$\eta_{\mu\nu} = \mathrm{diag}\,(-1, +1, +1, \ldots)$$

where $\eta = \eta_{\mu\nu} \mathrm{d}x^\mu \mathrm{d}x^\nu$ is the Minkowski metric. A vector $V \in TM$ is then called timelike,

spacelike or lightlike, when

$$g(V,V) = \begin{cases} -1 & \text{timelike} \\ +1 & \text{spacelike} \\ 0 & \text{lightlike / null} \end{cases} . \tag{A.1}$$

Here vector fields are defined as sections over the tangent bundle TM, and the set of all these sections is denoted $\Gamma(TM)$.

The Riemann tensor is defined according to the following sign convention

$$R^{\lambda}{}_{\alpha\beta\mu} = \frac{\partial \Gamma^{\lambda}{}_{\alpha\beta}}{\partial x^{\mu}} - \frac{\partial \Gamma^{\lambda}{}_{\alpha\mu}}{\partial x^{\beta}} + \Gamma^{\kappa}{}_{\alpha\beta}\Gamma^{\lambda}{}_{\kappa\mu} - \Gamma^{\kappa}{}_{\alpha\mu}\Gamma^{\lambda}{}_{\kappa\beta} = \mathrm{d}x^{\lambda}\left([\nabla_{\mu}, \nabla_{\beta}]\,\frac{\partial}{\partial x^{\alpha}}\right) , \tag{A.2}$$

and the Ricci-tensor and -scalar follow as

$$R_{\mu\nu} = R^{\lambda}{}_{\mu\nu\lambda} = g^{\lambda\beta}R_{\lambda\mu\nu\beta} \tag{A.3}$$

and

$$R = R^{\mu}{}_{\mu} = g^{\mu\nu}R_{\mu\nu} . \tag{A.4}$$

In this definition $\Gamma^{\lambda}{}_{\alpha\beta}$ are the metric compatible and torsion-free Christoffel-symbols defined by

$$\Gamma^{\lambda}{}_{\alpha\beta} = \frac{1}{2}g^{\lambda\kappa}\left(\frac{\partial g_{\alpha\kappa}}{\partial x^{\beta}} + \frac{\partial g_{\beta\kappa}}{\partial x^{\alpha}} - \frac{\partial g_{\alpha\beta}}{\partial x^{\kappa}}\right) . \tag{A.5}$$

The Kretschmann scalar is defined as

$$\mathcal{K} = R_{\alpha\beta\mu\nu}R^{\alpha\beta\mu\nu} . \tag{A.6}$$

Further the Einstein tensor is defined as

$$G_{\mu\nu} = R_{\mu\nu} - \frac{R}{2}g_{\mu\nu} . \tag{A.7}$$

The Einstein equations take the form

$$G_{\mu\nu} = \kappa T_{\mu\nu} \,, \tag{A.8}$$

which follow from the Einstein-Hilbert action

$$S_{EH} = \frac{1}{\kappa} \int_M \mathrm{d}^D x \, R\sqrt{-g} + S_M \tag{A.9}$$

where $S_M = \int_M \mathrm{d}^D x \, \mathcal{L}_M \sqrt{-g}$ is the matter action and

$$T^{\mu\nu} = -\frac{1}{\sqrt{-g}} \frac{\delta S_M}{\delta g_{\mu\nu}} \,,$$

symmetric energy-momentum tensor.

In Dirac's constraint theory [142], *weak equalities* play an important role. In this thesis the symbol $\approx$ denotes this *weak equality* in contrast to $=$ which is a strong equality. Assuming the system is constraint, the constraint has to be satisfied only on the level of solutions to the equations of motion, but not on the phase space in general. Hence, a weak equality holds only on-shell, i.e. along the solutions of the equations of motions and constraints, but not on the phase space in general. This is important, because for a constraint $\phi \approx 0$ and a generic phase space function $\mathcal{O}$, it is $\{\mathcal{O}, \phi\} \neq 0$. Demanding $\phi = 0$ *strongly*, i.e. on the level of phase space, would instead imply $\{\mathcal{O}, \phi\} \equiv 0$, which is generically not true.

B Collection of Basic Definitions

In this appendix further definitions used in the main part are collected.

Definition B.1 (Orbit [232])**:**
Given an action $\triangleright$ of a Lie-group G and a topological manifold M, the *orbit* $\mathcal{O}_p$ *of a point* $p \in M$ is defined as

$$\mathcal{O}_p := \{q \in M \mid \exists g \in G : \ q = g \triangleright p\} .$$

Definition B.2 (Hyperbolic space [90])**:**
d-dimensional *Hyperbolic space* $\mathbb{H}^d$ of hyperbolic radius L is defined as a sub-manifold of $d+1$-dimensional Minkowski $\mathcal{M}_{1,d}$ ($\mathbb{R}^{d+1}$ equipped with the Minkowski metric) as

$$\mathbb{H}^d := \left\{ x \in \mathcal{M}_{1,d} \mid \ -(x^0)^2 + \sum_{i=1}^{d} (x^i)^2 = -L^2 \ , \ x^0 > 0 \right\} .$$

A metric is induced on $\mathbb{H}^d$ via the pull-back of the Minkowski metric. It follows that $\mathbb{H}^d$ is a d-dimensional spacelike Riemannian manifold, which corresponds to the upper sheet of the two-sheeted hyperboloid.

Definition B.3 (Killing vector field [91])**:**
A vector field $V \in \Gamma(TM)$ on a metric manifold (M, g) is a *Killing vector field*, if it satisfies the Killing equation

$$\mathcal{L}_V g = 0 \quad \Leftrightarrow \quad V^\alpha \partial_\alpha g_{\mu\nu} - g_{\mu\alpha} \partial_\nu V^\alpha - g_{\alpha\nu} \partial_\mu V^\alpha = 0 \ ,$$

where $\mathcal{L}$ denotes the Lie-derivative. Killing vector fields denote generators of spacetime symmetries.

Definition B.4 (Killing horizon [98])**:**
Assume $K \in \Gamma(TM)$ is a Killing vector field. Then a co-dim -1 surface satisfying

$$g(K, K) = 0$$

is called *Killing horizon*.

Definition B.5 (Lambert-W-function)**:**
The *Lambert-W-function* is implicitly defined via

$$W(x) \cdot e^{W(x)} = x \ ,$$

and thus is the inverse Function of $f(x) = x \cdot e^x$. It has two branches, which coincide at $W_0(-1/e) = W_{-1}(-1/e) = -1$.

Different points in spacetime are causally related to each other. It is possible to define first causal curves as

Definition B.6 (Causal curve [95])**:**
On a spacetime (manifold M equipped with a Lorentzian metric g) a curve $\gamma : I \subseteq \mathbb{R} \longrightarrow M$ is called causal if

$$\forall \lambda \in I : \; g(\mathcal{V}_\gamma(\lambda), \mathcal{V}_\gamma(\lambda)) \leq 1 \; ,$$

where $\mathcal{V}_\gamma(\lambda)$ is the tangent of γ in the point $\gamma(\lambda)$.

Distinction is made between future and past directed curves, which intuitively means that for all λ $\mathcal{V}_\gamma(\lambda)$ points towards the future/past. This definition can be made precise, see e.g. [95].

Further it can be defined

Definition B.7 (Causal future/past [95])**:**
For a spacetime region $A \subset M$ the *causal future/past of* A is defined as

$$J^{\pm}(A) := \left\{ p \in M \;\middle|\; \exists q \in A, \exists \gamma : [0,1] \to M : \begin{array}{c} \gamma(0) = q,\ \gamma(1) = p, \\ \gamma \text{ is future/past directed and causal.} \end{array} \right\} .$$

The plus sign denotes the causal future, while the minus sign the causal past.

List of Acronyms

ADM Arnowitt-Deser-Misner

AdS Anti-de Sitter

AdS/CFT Anti-de Sitter / Conformal Field Theory

CCR Canonical Commutation Relations

CDT Causal Dynamical Triangulation

CFT Conformal Field Theory

EE Einstein Equations

FLRW Friedmann-Lemaítre-Robertson-Walker

GR General Relativity

LQC Loop Quantum Cosmology

LQG Loop Quantum Gravity

NCG Non-Commutative Geometry

NTP No Transmission Principle

ODE Ordinary Differential Equation

QCD Quantum Chromo Dynamics

QFT Quantum Field Theory

SYM Super Yang-Mills

WdW Wheeler-de Witt

YM Yang-Mills

List of Figures

List of Tables

Bibliography

[1] N. Bodendorfer, F. M. Mele, and J. Münch, "Holographic signatures of resolved cosmological singularities II: numerical investigations", *Classical and Quantum Gravity* **36** (2019) 245013, arXiv:1804.01387 [hep-th].

[2] N. Bodendorfer, F. M. Mele, and J. Münch, "Is limiting curvature mimetic gravity an effective polymer quantum gravity?", *Classical and Quantum Gravity* **35** (2018) 225001, arXiv:1806.02052 [gr-qc].

[3] N. Bodendorfer, F. M. Mele, and J. Münch, "Effective quantum extended spacetime of polymer Schwarzschild black hole", *Classical and Quantum Gravity* **36** (2019) 195015, arXiv:1902.04542 [gr-qc].

[4] N. Bodendorfer, F. M. Mele, and J. Münch, "A note on the Hamiltonian as a polymerisation parameter", *Classical and Quantum Gravity* **36** (2019) 187001, arXiv:1902.04032 [gr-qc].

[5] N. Bodendorfer, F. M. Mele, and J. Münch, "(b,v)-type variables for black to white hole transitions in effective loop quantum gravity", arXiv:1911.12646 [gr-qc].

[6] N. Bodendorfer, F. M. Mele, and J. Münch, "Mass and Horizon Dirac Observables in Effective Models of Quantum Black-to-White Hole Transition", arXiv:1912.00774 [gr-qc].

[7] A. Einstein, "Die Feldgleichungen der Gavitation", *Sitzungsberichte der Preussischen Akademie der Wissenschaften* (1915) 844–847.

[8] A. Einstein, "Die Grundlage der allgemeinen Relativitätstheorie", *Annalen der Physik* **354** (1916) 769–822.

[9] B. P. Abbott et al. (LIGO Collaboration Virgo Collaboration), "Observation of Gravitational Waves from a Binary Black Hole Merger", *Physical Review Letters* **116** (2016) 061102.

[10] K. Akiyama et al. (EHT collaboration), "First M87 Event Horizon Telescope Results. I. The Shadow of the Supermassive Black Hole", *The Astrophysical Journal* **875** (2019) L1.

[11] R. Penrose, "Gravitational Collapse and Space-Time Singularities", *Physical Review Letters* **14** (1965) 57–59.

[12] S. Hawking, *Properties of expanding universes*. PhD thesis, Cambridge University, 1966.

[13] M. Natsuume, "The singularity problem in string theory", *QFT 2001 Workshop Kyoto,*

Japan, July 16-19, 2001 (2001) arXiv:gr-qc/0108059.

[14] M. Bojowald, "Singularities and Quantum Gravity", in *AIP Conference Proceedings*, vol. 910, pp. 294–333, AIP, 2007. arXiv:gr-qc/0702144.

[15] M. Bojowald, "Absence of a Singularity in Loop Quantum Cosmology", *Physical Review Letters* **86** (2001) 5227–5230, arXiv:gr-qc/0102069.

[16] A. Ashtekar and P. Singh, "Loop quantum cosmology: a status report", *Classical and Quantum Gravity* **28** (2011) 213001, arXiv:1108.0893 [gr-qc].

[17] E. Wilson-Ewing, "The loop quantum cosmology bounce as a Kasner transition", *Classical and Quantum Gravity* **35** (2018) 065005, arXiv:1711.10943 [gr-qc].

[18] J. Olmedo, S. Saini, and P. Singh, "From black holes to white holes: a quantum gravitational, symmetric bounce", arXiv:1707.07333 [gr-qc].

[19] V. Balasubramanian, S. F. Hassan, E. Keski-Vakkuri, and A. Naqvi, "Space-time orbifold: A toy model for a cosmological singularity", *Physical Review D* **67** (2003) 026003, arXiv:hep-th/0202187.

[20] L. Cornalba and M. S. Costa, "A new cosmological scenario in string theory", *Physical Review D* **66** (2002) 066001, arXiv:hep-th/0203031.

[21] L. Cornalba, M. Costa, and C. Kounnas, "A resolution of the cosmological singularity with orientifolds", *Nuclear Physics B* **637** (2002) 378–394, arXiv:hep-th/0204261.

[22] M. Berkooz, B. Craps, D. Kutasov, and G. Rajesh, "Comments on cosmological singularities in string theory", *Journal of High Energy Physics* **2003** (2003) 031–031, arXiv:hep-th/0212215.

[23] B. Craps, T. Hertog, and N. Turok, "Quantum resolution of cosmological singularities using AdS/CFT correspondence", *Physical Review D* **86** (2012) 43513, arXiv:0712.4180 [hep-th].

[24] L. Fidkowski, V. Hubeny, M. Kleban, and S. Shenker, "The Black Hole Singularity in AdS/CFT", *Journal of High Energy Physics* **2004** (2004) 14, arXiv:hep-th/0306170.

[25] J. Maldacena, "Eternal black holes in anti-de Sitter", *Journal of High Energy Physics* **2003** (2003) 021–021, arXiv:hep-th/0106112.

[26] M. Hanada, Y. Hyakutake, G. Ishiki, and J. Nishimura, "Holographic description of a quantum black hole on a computer", *Science* **344** (2014) 882–885, arXiv:1311.5607 [hep-th].

[27] N. Engelhardt and G. T. Horowitz, "Holographic consequences of a no transmission principle", *Physical Review D* **93** (2016) 026005, arXiv:1509.07509 [hep-th].

[28] N. Engelhardt and G. T. Horowitz, "New insights into quantum gravity from gauge/gravity duality", *International Journal of Modern Physics D* **25** (2016) 1643002, arXiv:1605.04335 [hep-th].

[29] J. Madore, "On the resolution of space-time singularities", in *Noncommutative geometry and Hopf algebras in field theory and particle physics* (L. Castellani, F. Lizzi, and G. Landi, eds.), (Torino), pp. 2419–2425, Int. J. Mod. Phys. B 14 no. 22-23, World Scientific Publishing, 2000, 1999.

[30] M. Maceda and J. Madore, "On the Resolution of Space-Time Singularities II", *Journal of Nonlinear Mathematical Physics* **11** (2004) 21–36.

[31] M. Maceda, J. Madore, P. Manousselis, and G. Zoupanos, "Can non-commutativity resolve the big-bang singularity?", *The European Physical Journal C* **36** (2004) 529–534, arXiv:hep-th/0306136.

[32] M. A. Gorji, K. Nozari, and B. Vakili, "Spacetime singularity resolution in Snyder noncommutative space", *Physical Review D* **89** (2014) 084072, arXiv:1403.2623 [gr-qc].

[33] A. H. Chamseddine and V. Mukhanov, "Resolving cosmological singularities", *Journal of Cosmology and Astroparticle Physics* **2017** (2017) 009–009, arXiv:1612.05860 [gr-qc].

[34] A. H. Chamseddine and V. Mukhanov, "Nonsingular Black Hole", *European Physical Journal C* **77** (2017) 183, https://arxiv.org/abs/1612.05861.

[35] P. Nicolini, A. Smailagic, and E. Spallucci, "Noncommutative geometry inspired Schwarzschild black hole", *Physics Letters B* **632** (2006) 547–551, arXiv:gr-qc/0510112.

[36] J. B. Achour, F. Lamy, H. Liu, and K. Noui, "Non-singular black holes and the limiting curvature mechanism: a Hamiltonian perspective", *Journal of Cosmology and Astroparticle Physics* **2018** (2018) 072–072, arXiv:1712.03876 [gr-qc].

[37] S. W. Hawking, "Black hole explosions?", *Nature* **248** (1974) 30–31.

[38] S. W. Hawking, "Particle creation by black holes", *Communications In Mathematical Physics* **43** (1975) 199–220.

[39] J. D. Bekenstein, "Black holes and the second law", *Lettere Al Nuovo Cimento Series 2* **4** (1972) 737–740.

[40] J. D. Bekenstein, "Black Holes and Entropy", *Physical Review D* **7** (1973) 2333–2346.

[41] J. D. Bekenstein, "Generalized second law of thermodynamics in black-hole physics", *Physical Review D* **9** (1974) 3292–3300.

[42] L. Susskind, "The world as a hologram", *Journal of Mathematical Physics* **36** (1995) 6377–6396, arXiv:hep-th/9409089.

[43] G. t. Hooft, "Dimensional Reduction in Quantum Gravity", arXiv:gr-qc/9310026.

[44] J. Maldacena, "The Large N Limit of Superconformal Field Theories and Supergravity", *Advances in Theoretical and Mathematical Physics* **2** (1998) 231–252, arXiv:hep-th/9711200.

[45] R. Bousso, "The holographic principle", *Reviews of Modern Physics* **74** (2002) 825–874, arXiv:hep-th/0203101.

[46] S. S. Gubser, I. R. Klebanov, and A. M. Polyakov, "Gauge theory correlators from noncritical string theory", *Physics Letters B* **428** (1998) 105–114, arXiv:hep-th/9802109.

[47] E. Witten, "Anti De Sitter Space And Holography", *Advances in Theoretical and Mathematical Physics* **2** (1998) 253–291, arXiv:hep-th/9802150.

[48] T. Thiemann, *Modern Canonical Quantum General Relativity.* Cambridge University Press, Cambridge, 2007.

[49] J. Pullin and R. Gambini, *A First Course in Loop Quantum Gravity.* Oxford University Press, USA, 2011.

[50] C. Rovelli and F. Vidotto, *Covariant Loop Quantum Gravity: An Elementary Introduction to Quantum Gravity and Spinfoam Theory.* Cambridge University Press, 2014.

[51] D. Oriti, "Group field theory as the second quantization of loop quantum gravity", *Classical and Quantum Gravity* **33** (2016) 85005, arXiv:1310.7786 [gr-qc].

[52] E. Alesci and F. Cianfrani, "A new perspective on cosmology in Loop Quantum Gravity", *Europhysics Letters* **104** (2013) 10001, arXiv:1210.4504 [gr-qc].

[53] E. Alesci, F. Cianfrani, and C. Rovelli, "Quantum-reduced loop gravity: Relation with the full theory", *Physical Review D* **88** (2013) 104001, arXiv:1309.6304 [gr-qc].

[54] S. Gielen, D. Oriti, and L. Sindoni, "Homogeneous cosmologies as group field theory condensates", *Journal of High Energy Physics* **2014** (2014) 13, arXiv:1311.1238 [gr-qc].

[55] D. Oriti, L. Sindoni, and E. Wilson-Ewing, "Emergent Friedmann dynamics with a quantum bounce from quantum gravity condensates", *Classical and Quantum Gravity* **33** (2016) 224001, arXiv:1602.05881 [gr-qc].

[56] C. Beetle, J. S. Engle, M. E. Hogan, and P. Mendonça, "Diffeomorphism invariant cosmological symmetry in full quantum gravity", *International Journal of Modern Physics D* **25** (2016) 1642012, arXiv:1603.01128 [gr-qc].

[57] M. Bojowald, "Spherically symmetric quantum geometry: states and basic operators", *Classical and Quantum Gravity* **21** (2004) 3733–3753, arXiv:gr-qc/0407017.

[58] M. Bojowald and R. Swiderski, "Spherically symmetric quantum geometry: Hamiltonian constraint", *Classical and Quantum Gravity* **23** (2006), no. 6 2129–2154, arXiv:gr-qc/0511108.

[59] A. Dapor and K. Liegener, "Cosmological effective Hamiltonian from full loop quantum gravity dynamics", *Physics Letters B* **785** (2018) 506–510, arXiv:1706.09833 [gr-qc].

[60] N. Bodendorfer, "Quantum reduction to Bianchi I models in loop quantum gravity", *Physical Review D* **91** (2015) 081502, arXiv:1410.5608 [gr-qc].

[61] N. Bodendorfer, J. Lewandowski, and J. Swiezewski, "A quantum reduction to spherical symmetry in loop quantum gravity", *Physics Letters B* **747** (2015) 18–21, arXiv:1410.5609 [gr-qc].

[62] N. Bodendorfer, "An embedding of loop quantum cosmology in (b, v) variables into a full theory context", *Classical and Quantum Gravity* **33** (2016) 125014, arXiv:gr-qc/1512.00713.

[63] N. Bodendorfer and A. Zipfel, "On the relation between reduced quantisation and quantum reduction for spherical symmetry in loop quantum gravity", *Classical and Quantum Gravity* **33** (2016) 155014, arXiv:1512.00221 [gr-qc].

[64] B. Baytas, M. Bojowald, and S. Crowe, "Equivalence of Models in Loop Quantum Cosmology and Group Field Theory", *Universe* **5** (2019) 41, arXiv:1811.11156 [gr-qc].

[65] A. Ijjas and P. J. Steinhardt, "Bouncing Cosmology made simple", arXiv:1803.01961

[astro-ph.CO].

[66] Y.-F. Cai, "Exploring bouncing cosmologies with cosmological surveys", *Science China Physics, Mechanics & Astronomy* **57** (2014) 1414–1430, arXiv:1405.1369 [hep-th].

[67] A. Ashtekar and A. Barrau, "Loop quantum cosmology: from pre-inflationary dynamics to observations", *Classical and Quantum Gravity* **32** (2015), no. 23 234001, arXiv:1504.07559 [gr-qc].

[68] M. Bojowald, "Critical Evaluation of Common Claims in Loop Quantum Cosmology", *Universe* **6** (2020) 36, arXiv:2002.05703 [gr-qc].

[69] N. Bodendorfer, "A note on quantum supergravity and AdS/CFT", arXiv:1509.02036 [hep-th].

[70] N. Bodendorfer, "Strings meet Loops via AdS/CFT". [video file], (2016), Accessed 5 June 2020, Available from: https://www.youtube.com/watch?v=AN6oQMNmu3k&t=1s.

[71] N. Engelhardt, T. Hertog, and G. T. Horowitz, "Holographic Signatures of Cosmological Singularities", *Physical Review Letters* **113** (2014) 121602, arXiv:1404.2309 [hep-th].

[72] N. Engelhardt, T. Hertog, and G. T. Horowitz, "Further holographic investigations of big bang singularities", *Journal of High Energy Physics* **2015** (2015) 44, arXiv:1503.08838 [hep-th].

[73] N. Bodendorfer, A. Schäfer, and J. Schliemann, "Holographic signatures of resolved cosmological singularities", *Journal of High Energy Physics* **2019** (2016) 43, arXiv:1612.06679 [hep-th].

[74] A. Ashtekar and M. Bojowald, "Quantum geometry and the Schwarzschild singularity", *Classical and Quantum Gravity* **23** (2006) 391–411, arXiv:gr-qc/0509075.

[75] L. Modesto, "Loop quantum black hole", *Classical and Quantum Gravity* **23** (2006) 5587–5601, arXiv:gr-qc/0509078.

[76] R. Gambini, J. Olmedo, and J. Pullin, "Quantum black holes in loop quantum gravity", *Classical and Quantum Gravity* **31** (2014) 095009, arXiv:1310.5996 [gr-qc].

[77] E. Bianchi, M. Christodoulou, F. D'Ambrosio, H. M. Haggard, and C. Rovelli, "White holes as remnants: a surprising scenario for the end of a black hole", *Classical and Quantum Gravity* **35** (2018) 225003, arXiv:1802.04264 [gr-qc].

[78] A. Corichi and P. Singh, "Loop quantization of the Schwarzschild interior revisited", *Classical and Quantum Gravity* **33** (2016) 055006, arXiv:1506.08015 [gr-qc].

[79] L. Modesto, "Semiclassical Loop Quantum Black Hole", *International Journal of Theoretical Physics* **49** (2010) 1649–1683, arXiv:0811.2196 [gr-qc].

[80] C. G. Böhmer and K. Vandersloot, "Loop quantum dynamics of the Schwarzschild interior", *Physical Review D* **76** (2007) 104030, arXiv:0709.2129 [gr-qc].

[81] D.-W. Chiou, "Phenomenological loop quantum geometry of the Schwarzschild black hole", *Physical Review D* **78** (2008) 064040, arXiv:0807.0665 [gr-qc].

[82] D. Oriti, D. Pranzetti, and L. Sindoni, "Black holes as quantum gravity condensates",

Physical Review D **97** (2018) 066017, arXiv:1801.01479 [gr-qc].

[83] J. Ben Achour, F. Lamy, H. Liu, and K. Noui, "Polymer Schwarzschild black hole: An effective metric", *EPL (Europhysics Letters)* **123** (2018) 20006, arXiv:1803.01152 [gr-qc].

[84] M. Bojowald, S. Brahma, and D.-h. Yeom, "Effective line elements and black-hole models in canonical loop quantum gravity", *Physical Review D* **98** (2018) 046015, arXiv:1803.01119 [gr-qc].

[85] I. P. Lobo and M. Ronco, "Rainbow-Like Black-Hole Metric from Loop Quantum Gravity", *Universe* **4** (2018) 139, arXiv:1812.02136 [gr-qc].

[86] H. A. Morales-Técotl, S. Rastgoo, and J. C. Ruelas, "Effective dynamics of the Schwarzschild black hole interior with inverse triad corrections", arXiv:1806.05795 [gr-qc].

[87] A. Ashtekar, J. Olmedo, and P. Singh, "Quantum Transfiguration of Kruskal Black Holes", *Physical Review Letters* **121** (2018) 241301, arXiv:1806.00648 [gr-qc].

[88] A. Ashtekar, J. Olmedo, and P. Singh, "Quantum extension of the Kruskal spacetime", *Physical Review D* **98** (2018) 126003, arXiv:1806.02406 [gr-qc].

[89] M. Ammon and J. Erdmenger, *Gauge/Gravity Duality*. Cambridge University Press, Cambridge, 2015.

[90] J. W. Cannon, W. J. Floyd, R. Kenyon, and W. R. Parry, "Hyperbolic Geometry", in *Flavors of Geomerty* (S. Levy, ed.), ch. MSRI Publi. Cambridge University Press, Cambridge, 1997.

[91] S. M. Carroll, *Spacetime and Geometry An Introduction to General Relativity*. Pearson Education, publishing as Addison-Wesley, San Francisco, 2004.

[92] J. L. Petersen, "Introduction to the Maldacena Conjecture on AdS/CFT", *International Journal of Modern Physics A* **14** (1999) 3597–3672, arXiv:hep-th/9902131.

[93] T. Fließbach, *Allgemeine Relativitätstheorie*. Springer Spektrum, Heidelberg, 6. ed., 2012.

[94] R. Penrose, "Relativistic Symmetry Groups", in *Group Theory in Non-Linear Problems*, pp. 1–58. Springer Netherlands, Dordrecht, 1974.

[95] R. M. Wald, *General Relativity*. University Of Chicago Press, 1984.

[96] S. W. Hawking and G. F. R. Ellis, *The Large Scale Structure of Space-Time*. Cambridge University Press, Cambridge, 1973.

[97] T. Jacobson, "Introductory Lectures on Black Hole Thermodynamics". [pdf-file], (1996), Accessed 5 June 2020, Available from: http://www.physics.umd.edu/grt/taj/776b/lectures.pdf.

[98] F. Dowker, "Black Holes". [pdf-file], (2014), Accessed 5 June 2020, Available from: http://sns.ias.edu/~bkocsis/Assets/Teaching/BH2015/dowker.pdf.

[99] R. Arnowitt, S. Deser, and C. W. Misner, "Coordinate Invariance and Energy Expressions in General Relativity", *Physical Review* **122** (1961) 997–1006.

[100] M. D. Kruskal, "Maximal Extension of Schwarzschild Metric", *Physical Review* **119** (1960)

1743–1745.

[101] G. Szekeres, "On the singularities of a Riemannian manifold", *Mathematicae Debrecen* **7** (1960) 285–301.

[102] C. W. Misner, K. S. Thorne, and J. A. Wheeler, *Gravitation*. W. H. Freeman and Company, New York, 1973.

[103] T. Klösch and T. Strobl, "Classical and quantum gravity in 1 + 1 dimensions. II: The universal coverings", *Classical and Quantum Gravity* **13** (1996) 2395–2421, `arXiv:gr-qc/9511081`.

[104] G. D. Birkhoff, *Relativity and Modern Physics*. Harvard University Press, Cambridge, 1927.

[105] J. T. Jebsen, "On the general spherically symmetric solutions of Einstein's gravitational equations in vacuo", *General Relativity and Gravitation* **37** (2005) 2253–2259.

[106] S. W. Hawking, "Gravitational Radiation from Colliding Black Holes", *Physical Review Letters* **26** (1971) 1344–1346.

[107] R. Penrose, ""Golden Oldie": Gravitational Collapse: The Role of General Relativity", *General Relativity and Gravitation* **34** (2002) 1141–1165.

[108] W. Israel, "Event Horizons in Static Vacuum Space-Times", *Physical Review* **164** (1967) 1776–1779.

[109] W. Israel, "Event horizons in static electrovac space-times", *Communications in Mathematical Physics* **8** (1968) 245–260.

[110] B. Carter, "Axisymmetric Black Hole Has Only Two Degrees of Freedom", *Physical Review Letters* **26** (1971) 331–333.

[111] S. W. Hawking, "Black holes in general relativity", *Communications in Mathematical Physics* **25** (1972) 152–166.

[112] E. T. Newman, E. Couch, K. Chinnapared, A. Exton, A. Prakash, and R. Torrence, "Metric of a Rotating, Charged Mass", *Journal of Mathematical Physics* **6** (1965) 918–919.

[113] E. T. Newman and A. I. Janis, "Note on the Kerr Spinning-Particle Metric", *Journal of Mathematical Physics* **6** (1965) 915–917.

[114] J. M. Bardeen, B. Carter, and S. W. Hawking, "The four laws of black hole mechanics", *Communications in Mathematical Physics* **31** (1973) 161–170.

[115] X. Calmet, ed., *Quantum Aspects of Black Holes*. Springer International Publishing, Cham, 2015.

[116] T. Jacobson, "Introduction to Quantum Fields in Curved Spacetime and the Hawking Effect", `arXiv:gr-qc/0308048`.

[117] L. Susskind and J. Lindesay, *An Introduction to Black Holes, Information and the String Theory Revolution*. WORLD SCIENTIFIC, 2004.

[118] J. Bekenstein, "Universal upper bound on the entropy-to-energy ratio for bounded systems", *Physical Review D* **23** (1981) 287–298.

[119] R. Bousso, "A covariant entropy conjecture", *Journal of High Energy Physics* **1999** (1999) 4, arXiv:hep-th/9905177.

[120] G. 't Hooft, "A planar diagram theory for strong interactions", *Nuclear Physics B* **72** (1974) 461–473.

[121] R. Blumenhagen, D. Lüst, and S. Theisen, *Basic concepts of string theory*. Springer, 2012.

[122] M. Rangamani, A. Bernamonti, and X. Dong, "AdS/CFT Correspondence". [video files], (2016), Accessed 5 June 2020, Available from: https://www.perimeterinstitute.ca/it-qubit-summer-school/resources/ads/cft-correspondence.

[123] D. Harlow, "TASI Lectures on the Emergence of the Bulk in AdS/CFT", arXiv:1802.01040 [hep-th].

[124] N. Kajuri, "Lectures on Bulk Reconstruction", arXiv:2003.00587 [hep-th].

[125] S. Ryu and T. Takayanagi, "Holographic Derivation of Entanglement Entropy from the anti-de Sitter Space/Conformal Field Theory Correspondence", *Physical Review Letters* **96** (2006) 181602, arXiv:hep-th/0603001.

[126] D. V. Fursaev, "Proof of the holographic formula for entanglement entropy", *Journal of High Energy Physics* **2006** (2006) 018–018, arXiv:hep-th/0606184.

[127] V. Balasubramanian and S. F. Ross, "Holographic particle detection", *Physical Review D* **61** (2000) 044007, arXiv:hep-th/9906226.

[128] J. de Boer and S. N. Solodukhin, "A holographic reduction of Minkowski space–time", *Nuclear Physics B* **665** (2003) 545–593, arXiv:hep-th/0303006.

[129] A. Strominger, "The dS/CFT correspondence", *Journal of High Energy Physics* **2001** (2001) 034–034, arXiv:hep-th/0106113.

[130] B. Dittrich, C. Goeller, E. R. Livine, and A. Riello, "Quasi-local holographic dualities in non-perturbative 3d quantum gravity I - Convergence of multiple approaches and examples of Ponzano-Regge statistical duals", *Nuclear Physics B* **938** (2019) 807–877, arXiv:1710.04202 [hep-th].

[131] B. Dittrich, C. Goeller, E. R. Livine, and A. Riello, "Quasi-local holographic dualities in non-perturbative 3d quantum gravity II – From coherent quantum boundaries to BMS3 characters", *Nuclear Physics B* **938** (2019) 878–934, arXiv:1710.04237 [hep-th].

[132] B. Dittrich, C. Goeller, E. R. Livine, and A. Riello, "Quasi-local holographic dualities in non-perturbative 3D quantum gravity", *Classical and Quantum Gravity* **35** (2018) 13LT01, arXiv:1803.02759 [hep-th].

[133] A. Ashtekar and J. Pullin, *Loop Quantum Gravity: The first 30 years*, vol. 4 of *100 Years of General Relativity*. World Scientific, 2017.

[134] C. Rovelli, *Quantum Gravity*. Cambridge University Press, Cambridge, 2004.

[135] N. Bodendorfer, "Introduction to Quantum Gravity I+II". [pdf-file], (2020), Accessed 5 June 2020, Available from: https://homepages.uni-regensburg.de/~bon39708/lectures/2020_ss/skript_ss_2020.pdf.

[136] N. Bodendorfer, "An elementary introduction to loop quantum gravity", arXiv:gr-qc/1607.05129.

[137] A. Ashtekar, "An Introduction to Loop Quantum Gravity Through Cosmology", *Nuovo Cim.* **122B** (2007) arXiv:gr-qc/0702030.

[138] A. Ashtekar, M. Bojowald, and J. Lewandowski, "Mathematical structure of loop quantum cosmology", *Adv.Theor.Math.Phys.* **7** (2003) 233–268, arXiv:gr-qc/0304074.

[139] I. Agullo and P. Singh, "Loop Quantum Cosmology", *Loop Quantum Gravity: The first 30 years* (2017) 183–240, arXiv:1612.01236 [gr-qc].

[140] M. Bojowald, "Quantum cosmology: a review", *Reports on Progress in Physics* **78** (2015) 023901, arXiv:1501.04899 [gr-qc].

[141] M. Bojowald, "Loop Quantum Cosmology", *Living Reviews in Relativity* **8** (2005) 11.

[142] P. A. M. Dirac, *Lectures on Quantum Mechanics*. Belfer Graduate School of Science, Yeshiva University Press, New York, 1964.

[143] G. Date, "Lectures on Constrained Systems", arXiv:1010.2062 [gr-qc].

[144] A. Ashtekar, T. Pawlowski, and P. Singh, "Quantum nature of the big bang: Improved dynamics", *Physical Review D* **74** (2006) 084003, arXiv:gr-qc/0607039.

[145] A. Ashtekar, T. Pawlowski, and P. Singh, "Quantum nature of the big bang: An analytical and numerical investigation", *Physical Review D* **73** (2006) 124038, arXiv:gr-qc/0604013.

[146] A. Ashtekar, T. Pawlowski, and P. Singh, "Quantum Nature of the Big Bang", *Physical Review Letters* **96** (2006) 141301, arXiv:gr-qc/0602086.

[147] M. Han and H. Liu, "Effective dynamics from coherent state path integral of full loop quantum gravity", *Physical Review D* **101** (2020) 046003, arXiv:1910.03763 [gr-qc].

[148] M. Han and H. Liu, "Improved ($\bar{\mu}$-Scheme) Effective Dynamics of Full Loop Quantum Gravity", 1912.08668.

[149] J. Ben Achour and E. R. Livine, "Thiemann complexifier in classical and quantum FLRW cosmology", *Physical Review D* **96** (2017) 066025, arXiv:1705.03772 [gr-qc].

[150] J. Ben Achour and E. R. Livine, "Polymer Quantum Cosmology: Lifting quantization ambiguities using a $SL(2,\mathbb{R})$ conformal symmetry", *Physical Review D* **99** (2019) 126013, arXiv:1806.09290 [gr-qc].

[151] J. Ben Achour and E. Livine, "Protected $SL(2,\mathbb{R})$ symmetry in quantum cosmology", *Journal of Cosmology and Astroparticle Physics* **2019** (2019) 012–012, arXiv:1904.06149 [gr-qc].

[152] N. Bodendorfer and F. Haneder, "Coarse graining as a representation change", *Physics Letters B* **792** (2019) 69–73, arXiv:1811.02792 [gr-qc].

[153] N. Bodendorfer and D. Wuhrer, "Renormalisation with SU(1, 1) coherent states on the LQC Hilbert space", arXiv:1904.13269 [gr-qc].

[154] C. Kiefer, *Quantum Gravity: Third Edition*. Oxford University Press, 2012.

[155] D. Atkatz, "Quantum cosmology for pedestrians", *American Journal of Physics* **62** (1994) 619–627.

[156] D. L. Wiltshire, "An introduction to quantum cosmology", arXiv:gr-qc/0101003.

[157] C. Kiefer, N. Kwidzinski, and D. Piontek, "Singularity avoidance in Bianchi I quantum cosmology", *The European Physical Journal C* **79** (2019) 686, arXiv:1903.04391 [gr-qc].

[158] A. Ashtekar, A. Corichi, and P. Singh, "Robustness of key features of loop quantum cosmology", *Physical Review D* **77** (2008) 024046, arXiv:0710.3565 [gr-qc].

[159] D. A. Craig and P. Singh, "Consistent probabilities in Wheeler-DeWitt quantum cosmology", *Physical Review D* **82** (2010), no. 12 123526, arXiv:1006.3837 [gr-qc].

[160] D. A. Craig and P. Singh, "Consistent probabilities in loop quantum cosmology", *Classical and Quantum Gravity* **30** (2013), no. 20 205008, arXiv:1306.6142 [gr-qc].

[161] A. Corichi, T. Vukašinac, and J. Zapata, "Polymer quantum mechanics and its continuum limit", *Physical Review D* **76** (2007) 44016, arXiv:0704.0007 [gr-qc].

[162] J. Berra-Montiel and A. Molgado, "Polymer quantum mechanics as a deformation quantization", *Classical and Quantum Gravity* **36** (2019) 025001, arXiv:1805.05943 [gr-qc].

[163] M. Martín-Benito, G. A. Mena Marugán, and J. Olmedo, "Further improvements in the understanding of isotropic loop quantum cosmology", *Physical Review D* **80** (2009) 104015, arXiv:0909.2829 [gr-qc].

[164] G. A. Mena Marugaán, F. Etayo, M. Fioravanti, and R. Santamaría, "A brief introduction to Loop Quantum Cosmology", in *AIP Conference Proceedings*, pp. 89–100, AIP, 2009.

[165] P. Diener, A. Joe, M. Megevand, and P. Singh, "Numerical simulations of loop quantum Bianchi-I spacetimes", *Classical and Quantum Gravity* **34** (2017), no. 9 94004, arXiv:1701.05824 [gr-qc].

[166] C. Rovelli and E. Wilson-Ewing, "Why are the effective equations of loop quantum cosmology so accurate?", *Physical Review D* **90** (2014) 23538, arXiv:1310.8654 [gr-qc].

[167] V. Taveras, "Corrections to the Friedmann equations from loop quantum gravity for a universe with a free scalar field", *Physical Review D* **78** (2008) 064072, arXiv:0807.3325 [gr-qc].

[168] M. Bojowald and S. Brahma, "Minisuperspace models as infrared contributions", *Physical Review D* **93** (2016) 125001, arXiv:1509.00640 [hep-th].

[169] N. Bodendorfer, "A note on the scalar products in sLQC", *Classical and Quantum Gravity* **36** (2019) 087003, arXiv:1810.12087 [gr-qc].

[170] T. Thiemann, "Introduction to Modern Canonical Quantum General Relativity", gr-qc/0110034.

[171] T. Thiemann, "Lectures on loop quantum gravity", *Lecture Notes in Physics* **631** (2002) 41–135, arXiv:gr-qc/0210094.

[172] H. Haber, "Parallel Transport and Curvature." [pdf-file], (2015), Accessed 5 June 2020, Available from: http://scipp.ucsc.edu/~haber/ph171/parallel_transport15.pdf.

[173] T. Lang, K. Liegener, and T. Thiemann, "Hamiltonian renormalisation I: derivation from Osterwalder–Schrader reconstruction", *Classical and Quantum Gravity* **35** (2018) 245011, arXiv:1711.05685 [gr-qc].

[174] T. Lang, K. Liegener, and T. Thiemann, "Hamiltonian renormalisation II. Renormalisation flow of 1+1 dimensional free scalar fields: derivation", *Classical and Quantum Gravity* **35** (2018) 245012, arXiv:1711.06727 [gr-qc].

[175] T. Lang, K. Liegener, and T. Thiemann, "Hamiltonian renormalization III. Renormalisation flow of 1 + 1 dimensional free scalar fields: properties", *Classical and Quantum Gravity* **35** (2018) 245013, arXiv:1711.05688 [gr-qc].

[176] T. Lang, K. Liegener, and T. Thiemann, "Hamiltonian renormalisation IV. Renormalisation flow of D + 1 dimensional free scalar fields and rotation invariance", *Classical and Quantum Gravity* **35** (2018) 245014, arXiv:1711.05695 [gr-qc].

[177] T. Hertog and G. T. Horowitz, "Towards a Big Crunch Dual", *Journal of High Energy Physics* **2004** (2004) 73, arXiv:hep-th/0406134.

[178] T. Hertog and G. T. Horowitz, "Holographic description of AdS cosmologies", *Journal of High Energy Physics* **2005** (2005) 5, arXiv:hep-th/0503071.

[179] S. R. Das, J. Michelson, K. Narayan, and S. P. Trivedi, "Time-dependent cosmologies and their duals", *Physical Review D* **74** (2006) 26002, arXiv:hep-th/0602107.

[180] N. Turok, B. Craps, and T. Hertog, "From Big Crunch to Big Bang with AdS/CFT", arXiv:0711.1824 [hep-th].

[181] S. R. Das, J. Michelson, K. Narayan, and S. P. Trivedi, "Cosmologies with null singularities and their gauge theory duals", *Physical Review D* **75** (2007) 26002, arXiv:hep-th/0610053.

[182] A. Awad, S. R. Das, K. Narayan, and S. P. Trivedi, "Gauge theory duals of cosmological backgrounds and their energy momentum tensors", *Physical Review D* **77** (2008) 46008, arXiv:0711.2994 [hep-th].

[183] A. Awad, S. R. Das, S. Nampuri, K. Narayan, and S. P. Trivedi, "Gauge theories with time dependent couplings and their cosmological duals", *Physical Review D* **79** (2009) 46004, arXiv:0807.1517 [hep-th].

[184] J. L. F. Barbón and E. Rabinovici, "AdS crunches, CFT falls and cosmological complementarity", *Journal of High Energy Physics* **2011** (2011) 44, arXiv:1102.3015 [hep-th].

[185] M. Smolkin and N. Turok, "Dual description of a 4d cosmology", arXiv:1211.1322 [hep-th].

[186] N. Bodendorfer, T. Thiemann, and A. Thurn, "New variables for classical and quantum gravity in all dimensions: I. Hamiltonian analysis", *Classical and Quantum Gravity* **30** (2013) 45001, arXiv:1105.3703 [gr-qc].

[187] N. Bodendorfer, T. Thiemann, and A. Thurn, "New variables for classical and quantum gravity in all dimensions: II. Lagrangian analysis", *Classical and Quantum Gravity* **30** (2013) 45002, arXiv:1105.3704 [gr-qc].

[188] N. Bodendorfer, T. Thiemann, and A. Thurn, "New variables for classical and quantum gravity in all dimensions: III. Quantum theory", *Classical and Quantum Gravity* **30** (2013) 45003, arXiv:1105.3705 [gr-qc].

[189] B. Gupt and P. Singh, "Quantum gravitational Kasner transitions in Bianchi-I spacetime", *Physical Review D* **86** (2012) 024034, arXiv:1205.6763 [gr-qc].

[190] C. Ecker, D. Grumiller, and S. A. Stricker, "Evolution of holographic entanglement entropy in an anisotropic system", *Journal of High Energy Physics* **2015** (2015) 146, arXiv:1506.02658 [hep-th].

[191] C. Ecker, D. Grumiller, P. Stanzer, S. A. Stricker, and W. van der Schee, "Exploring nonlocal observables in shock wave collisions", *Journal of High Energy Physics* **2016** (2016) 54, arXiv:1609.03676 [hep-th].

[192] H. W. Press, S. A. Teukolsky, W. T. Vetterling, and B. P. Flannery, *Numerical Recipes 3rd Edition: The Art of Scientific Computing*. Cambridge University Press, New York, USA, 2007.

[193] A. H. Chamseddine and V. Mukhanov, "Mimetic dark matter", *Journal of High Energy Physics* **2013** (2013) 135, arXiv:1308.5410 [astro-ph.CO].

[194] N. Bodendorfer, A. Schäfer, and J. Schliemann, "On the canonical structure of general relativity with a limiting curvature and its relation to loop quantum gravity", arXiv:1703.10670 [gr-qc].

[195] D. Langlois, H. Liu, K. Noui, and E. Wilson-Ewing, "Effective loop quantum cosmology as a higher-derivative scalar-tensor theory", *Classical and Quantum Gravity* **34** (2017) 225004, arXiv:1703.10812 [gr-qc].

[196] H. M. Haggard and C. Rovelli, "Quantum-gravity effects outside the horizon spark black to white hole tunneling", *Physical Review D* **92** (2015) 104020, arXiv:1407.0989 [gr-qc].

[197] T. De Lorenzo and A. Perez, "Improved black hole fireworks: Asymmetric black-hole-to-white-hole tunneling scenario", *Physical Review D* **93** (2016) 124018, arXiv:1512.04566 [gr-qc].

[198] D.-W. Chiou, "Phenomenological dynamics of loop quantum cosmology in Kantowski-Sachs spacetime", *Physical Review D* **78** (2008) 044019, arXiv:0803.3659 [gr-qc].

[199] A. Joe and P. Singh, "Kantowski-Sachs spacetime in loop quantum cosmology: bounds on expansion and shear scalars and the viability of quantization prescriptions", *Classical and Quantum Gravity* **32** (2015) 015009, arXiv:1407.2428 [gr-qc].

[200] K. Schwarzschild, "Über das Gravitationsfeld eines Massenpunktes nach der Einsteinschen Theorie", *Sitzungsberichte der Königlich-Preussischen Akademie der Wissenschaften* (1916) 189–196.

[201] M. Assanioussi, A. Dapor, and K. Liegener, "Perspectives on the dynamics in loop effective black hole interior", arXiv:1908.05756 [gr-qc].

[202] M. Bojowald, S. Brahma, and J. D. Reyes, "Covariance in models of loop quantum gravity: Spherical symmetry", *Physical Review D* **92** (2015) 045043, arXiv:1507.00329 [gr-qc].

[203] M. Campiglia, R. Gambini, and J. Pullin, "Loop quantization of spherically symmetric midi-superspaces", *Classical and Quantum Gravity* **24** (2007) 3649–3672, arXiv:gr-qc/0703135.

[204] L. Modesto, "Black Hole Interior from Loop Quantum Gravity", *Advances in High Energy Physics* **2008** (2008) 1–12, arXiv:gr-qc/0611043.

[205] C. Rovelli and F. Vidotto, "Planck stars", *International Journal of Modern Physics D* **23** (2014), no. 12 1442026, arXiv:1401.6562 [gr-qc].

[206] M. Bouhmadi-López, S. Brahma, C.-Y. Chen, P. Chen, and D.-h. Yeom, "Comment on "Quantum Transfiguration of Kruskal Black Holes"", arXiv:1902.07874 [gr-qc].

[207] A. Ashtekar and J. Olmedo, "Properties of a recent quantum extension of the Kruskal geometry", arXiv:2005.02309 [gr-qc].

[208] M. Cavaglia', V. de Alfaro, and A. T. Filippov, "Hamiltonian Formalism for Black Holes and Quantization", *International Journal of Modern Physics D* **04** (1994) 661–672, arXiv:gr-qc/9411070.

[209] B. Vakili, "Classical Polymerization of the Schwarzschild Metric", *Advances in High Energy Physics* **2018** (2018) 1–10, arXiv:1806.01837 [hep-th].

[210] E. Alesci and F. Cianfrani, "Loop quantum cosmology from quantum reduced loop gravity", *Europhysics Letters* **111** (2015) 40002, arXiv:1410.4788 [gr-qc].

[211] M. Bojowald and S. Brahma, "Signature change in two-dimensional black-hole models of loop quantum gravity", *Physical Review D* **98** (2018) 026012, arXiv:1610.08850 [gr-qc].

[212] A. Laddha and M. Varadarajan, "The diffeomorphism constraint operator in loop quantum gravity", *Classical and Quantum Gravity* **28** (2011) 195010, arXiv:1105.0636 [gr-qc].

[213] A. Laddha, "Hamiltonian constraint in Euclidean LQG revisited: First hints of off-shell Closure", arXiv:1401.0931 [gr-qc].

[214] R. Helling, "Higher curvature counter terms cause the bounce in loop cosmology", arXiv:0912.3011 [gr-qc].

[215] L. Modesto and I. Prémont-Schwarz, "Self-dual black holes in loop quantum gravity: Theory and phenomenology", *Physical Review D* **80** (2009) 064041, arXiv:0905.3170 [hep-th].

[216] C. W. Misner and D. H. Sharp, "Relativistic Equations for Adiabatic, Spherically Symmetric Gravitational Collapse", *Physical Review* **136** (1964) B571–B576.

[217] L. B. Szabados, "Quasi-Local Energy-Momentum and Angular Momentum in GR: A Review Article", *Living Reviews in Relativity* **7** (2004) 4.

[218] M. Bouhmadi-López, S. Brahma, C.-Y. Chen, P. Chen, and D.-h. Yeom, "A consistent model of non-singular Schwarzschild black hole in loop quantum gravity and its quasinormal modes", arXiv:2004.13061 [gr-qc].

[219] P. Martin-Dussaud and C. Rovelli, "Evaporating black-to-white hole", arXiv:1905.07251 [gr-qc].

[220] A. Rabenstein, N. Bodendorfer, A. Schäfer, and P. Buividovich, "Lattice study of Rényi entanglement entropy in $SU(N_c)$-lattice Yang-Mills theory with $N_c = 2, 3, 4$", *Physical Review D* **100** (2019) 034504, arXiv:1812.04279 [hep-lat].

[221] C. Rovelli and F. Vidotto, "Small Black/White Hole Stability and Dark Matter", *Universe* **4** (2018) 127, arXiv:1805.03872 [gr-qc].

[222] V. A. Berezin and A. M. B. A. Y. Neronov, "Towards the mass spectrum of quantum black holes and wormholes", arXiv:gr-qc/9710067.

[223] V. V. Kiselev, "A quantum mass-spectrum of Kerr black hole: superstrings", arXiv:gr-qc/0412117.

[224] J. D. Bekenstein and V. Mukhanov, "Spectroscopy of the quantum black hole", *Physics Letters B* **360** (1995) 7–12, arXiv:gr-qc/9505012.

[225] J. D. Bekenstein, "The Quantum Mass Spectrum of the Kerr Black Hole", in *Jacob Bekenstein*, pp. 331–334. WORLD SCIENTIFIC, 2019.

[226] A. Ashtekar, W. Kaminski, and J. Lewandowski, "Quantum field theory on a cosmological, quantum space-time", *Physical Review D* **79** (2009) 064030, arXiv:0901.0933 [gr-qc].

[227] S. Leutheusser and M. Van Raamsdonk, "Tensor network models of unitary black hole evaporation", *Journal of High Energy Physics* **2017** (2017) 141, arXiv:1611.08613 [hep-th].

[228] J. Oppenheim, "Spectrum of quantum black holes and quasinormal modes", *Physical Review D* **69** (2004) 044012, arXiv:gr-qc/0307089.

[229] J. Ben Achour, S. Brahma, and J.-P. Uzan, "Bouncing compact objects. Part I. Quantum extension of the Oppenheimer-Snyder collapse", *Journal of Cosmology and Astroparticle Physics* **2020** (2020) 041–041, arXiv:2001.06148 [gr-qc].

[230] J. Ben Achour and J.-P. Uzan, "Bouncing compact objects II: Effective theory of a pulsating Planck star", arXiv:2001.06153 [gr-qc].

[231] J. Ben Achour, S. Brahma, S. Mukohyama, and J.-P. Uzan, "Consistent black-to-white hole bounces from matter collapse", arXiv:2004.12977 [gr-qc].

[232] F. P. Schuller, "Geometric Anatomy of Theoretical Physics - Online Lecture". [video file], (2015), Accessed 5 June 2020, Available from: https://www.youtube.com/watch?v=vYAXjTGr_eM&list=PLPH7f_7ZlzxTi6kS4vCmv4ZKm9u8g5yic&index=19.